

**Modeling, Reaction Schemes
and Kinetic Parameter Estimation
in Automotive Catalytic Converters
and Diesel Particulate Filters**

THESIS

submitted in partial fulfillment of the requirements
for the degree of Doctor of Philosophy in Mechanical Engineering
of the Department of Mechanical and Industrial Engineering
University of Thessaly

BY

GEORGIOS N. PONTIKAKIS

Dipl. Mechanical Engineer,
Aristotle University Thessaloniki

Born on 17th May 1975
in Thessaloniki

Supervising Committee

Assoc. Prof. A. M. Stamatelos, supervisor
Assoc. Prof. C. Papadimitriou
Asst. Prof. D. Valougeorgis

Volos, June 2003

© Γιώργος Ποντικάκης

Η έγκριση της διδακτορικής διατριβής από το Τμήμα Μηχανολόγων Μηχανικών Βιομηχανίας της Πολυτεχνικής Σχολής του Πανεπιστημίου Θεσσαλίας δεν υποδηλώνει αποδοχή των απόψεων του συγγραφέα (Ν. 5343/32 Αρθρ. 202 παρ. 2).

*Κεφάλι μου γεμάτο όνειρα,
χέρια μου γεμάτα λάσπη*

— ΜΙΛΤΟΣ ΣΑΧΤΟΥΡΗΣ

Πολυμαθίη νόον ἔχειν οὐ διδάσκει

— ΗΡΑΚΛΕΙΤΟΣ

Contents

Acknowledgements	ix
Abstract	xi
Ευρεία Περίληψη	xiii
1 Introduction	1
1.1 Trends in automotive pollution control	2
1.2 Modeling Background	4
1.3 Starting point and objectives of this thesis	6
2 Monolithic Catalytic Converters	9
2.1 Operation of the monolithic catalytic converter	10
2.1.1 Overview	10
2.1.2 Heat and mass transfer	11
2.1.3 Chemical phenomena	12
2.1.4 Washcoats	13
2.2 Overview of the modeling problem	16
2.2.1 Navigation in the modeling landscape	16
2.2.2 Kinetics level modeling	17
2.2.3 Washcoat level modeling	19
2.2.4 Channel level modeling	19
2.2.5 Reactor level modeling	20
2.3 Kinetics level modeling	20
2.3.1 Three-way catalytic converter	21
2.3.2 Diesel oxidation catalyst	22
2.4 Washcoat level modeling	26
2.4.1 Mathematical model formulation	26
2.4.2 Calculation of stored oxygen in the 3WCC washcoat	29
2.4.3 Calculation of stored hydrocarbon in the DOC washcoat	30
2.4.4 Diffusion in the washcoat	31
2.5 Channel model	33
2.6 Reactor model	35
2.7 Tunable parameters of the model	35
2.8 Conclusions	37
2.9 Summary	37

3 Wall Flow Diesel Particulate Filters	47
3.1 Operation of wall flow and deep-bed filters	48
3.1.1 Overview	48
3.1.2 Filtration and loading	50
3.1.3 Regeneration	53
3.2 Overview of the DPF modeling problem	56
3.2.1 Loading-regeneration level	56
3.2.2 Channel level	57
3.2.3 Reactor level	57
3.3 Loading and pressure drop model	58
3.3.1 Loading	58
3.3.2 Pressure drop	59
3.4 Regeneration model	61
3.4.1 Geometry of the channels and the soot layer	62
3.4.2 Reaction Scheme	63
3.4.3 Balance equations	67
3.4.4 Analytical spatial integration of balances	71
3.5 Channel model	74
3.6 Reactor model	76
3.6.1 1D reactor model	77
3.6.2 3D reactor model	78
3.6.3 3D heat transfer calculation by CATWALL-ANSYS interfacing	80
3.7 Conclusions	87
3.8 Summary	87
4 Parameter estimation	95
4.1 Previous tuning practice	95
4.2 Formulation of the optimization problem	96
4.2.1 Performance measure	96
4.2.2 Optimization method	97
4.3 Performance measure formulation	99
4.3.1 Requirements for the performance measure	99
4.3.2 Measurements exploitation	100
4.3.3 Error positiveness	100
4.3.4 Error definition	102
4.3.5 Performance measure definition for single-response tests . . .	103
4.3.6 Performance measure definition for multi-response measurements	105
4.4 Optimization with Conjugate Gradients	105
4.4.1 Constraints	107
4.5 Optimization with Genetic Algorithms	108
4.5.1 General	108
4.5.2 The Genetic Algorithm operation concept	109
4.5.3 Encoding	112
4.5.4 Fitness and Selection	113
4.5.5 Genetic operators	115
4.5.6 Deletion	117
4.6 Conclusions	118
4.7 Summary	118

5 Catalytic Converter Case studies	125
5.1 The ULEV case study	125
5.1.1 TLEV-vehicle results	128
5.1.2 LEV-vehicle results	128
5.2 Variable Precious Metal Loading case study	135
5.2.1 Measurements set	135
5.2.2 Model tuning for the 50 g/ft ³ catalyst	136
5.2.3 Model tuning for the 100 g/ft ³ catalyst	147
5.2.4 Model validation for the reduced size 50 g/ft ³ catalyst	158
5.2.5 First steps towards the prediction of PML effect	164
5.3 Variable cell density/wall thickness case study	164
5.3.1 Measurements set	164
5.3.2 Icat – model tuning	166
5.3.3 Prediction of the effect of variable cell density/wall thickness	166
5.4 Conclusions – Future perspectives of 3WCC modeling	166
5.5 Summary	174
6 Diesel Particulate Filter Case Studies	177
6.1 1D DPF model validation	177
6.1.1 Experimental	177
6.1.2 Validation Results	181
6.1.3 Discussion	184
6.1.4 1D modeling conclusions	195
6.2 3D DPF model assessment	196
6.2.1 Modeling results	196
6.2.2 Discussion	204
6.2.3 3D modeling conclusions	205
6.3 Summary	206
7 From computational cores to engineering tools	209
7.1 Industry requirements	210
7.2 Comparative discussion of various modeling levels	210
7.3 Design concepts and requirements	216
7.4 From computational cores to engineering tools	218
A The problem of diffusion–reaction in the washcoat	225
A.1 General	225
A.2 Reaction rates	225
A.3 CO oxidation by O ₂ in stoichiometric conditions	226
A.3.1 Neglecting G_1	228
A.3.2 Taking into account G_1	230
A.3.3 Results	232
A.4 Simultaneous oxidation of CO and HC by O ₂	232
A.5 Conclusions	236

Acknowledgements

During the period I have been working for this thesis, a lot of people helped me and supported me in a variety of ways. I am indebted to all of them. Here, I would like to distinguish and express my special thanks to the following:

— My advisor Dr. Tassos Stamatelos for his invaluable support in every aspect of this work. Through the years, he guided me, contributed in every bit of this work and offered his thoughtful advice and knowledge that extend far beyond mechanical engineering. Furthermore, he patiently tolerated the quirks of my character, kept my morale high in every difficulty, shielded me against any external interferences, and granted generous financial support.

Above all, Tassos has been an unequalled Teacher ever since the time I was a student, providing *inspiration* for this work and *meaning* to the role and mentality of the engineer. I consider these as the greatest benefits that I have received during our collaboration. It has been my honour to be his student and a member of his research team and I deeply hope that our collaboration and friendship continues in the future.

— The other members of my supervising committee — Dr. Costas Papadimitriou for his help and motivation with the field of optimization and genetic algorithms and Dr. Dimitrios Valougeorgis for fruitful discussions.

— Dr. Nikolaos Aravas and Dr. Vassilios Bontozoglou, of the Mechanical Engineering Faculty in Volos, for their valuable advice and rewarding discussions.

— Dr. Christos Vassilikos, of Imperial College, for his significant contributions in the study of diffusion in the washcoat. I am indebted for the many hours we spent together the respective mathematical investigations and I hope that the material we developed will soon be capitalized in a joint publication.

— Sungtae Hong, IBIDEN Co. Ltd, for his important feedback in the validation of CATWALL DPF code, fruitful cooperation during the development of the ANSYS–CATWALL interface and hospitality during my stay in Japan for the latter project.

— Dr. Philippe Versaevel, of PSA, for his contributions in the development of the MATLAB/SIMULINK versions of the CATRAN and CATWALL codes, and the valuable suggestions for code improvements.

— Ms. Christelle Bourgeois, of PSA, for her useful suggestions regarding the chemistry of the CATWALL code.

- Dr. Jürgen Gieshoff, of dmc² division of OMG, for his suggestions and feedback regarding diesel catalyst modeling.
- Dr. Martin Votsmeier, of dmc² division of OMG, for useful discussions and suggestions regarding the oxygen storage modeling.
- Dr. Hans van den Tillaart, former employee of Degussa–Hüls A.G., for discussions and insight about the role of diffusion and kinetic modeling in catalytic converters.
- Dr. Stan Kolaczkowski, of the University of Bath, for providing insight in the role of diffusion in the washcoat and for the many friendly discussions we had.
- Dr. Josef Hoebink, of the Technical University of Eindhoven, who offered me intuition on the essence of kinetic modeling.
- Dr. Bob Hayes, of the University of Alberta, for his advice in the field of scientific computing, benchmarking and his feedback on the feasibility of higher dimension modeling in conjunction with parallel processing.
- Dr. Tony Smith, of S&C Thermofluids, for his feedback regarding the use of commercial solvers for comparison purposes.
- Dr. Marcus Frey and Dr. Günter Wenninger, of DaimlerChrysler, Stuttgart, for useful discussions regarding the kinetic modeling of the DPF.
- Dr. Yoshihide Watanabe, Toyota Central R&D Labs, for his important suggestions regarding the interaction of NO with Ceria in 3WCC washcoats.
- My former senior colleagues in Aristotle University, Dr. Grigorios Koltsakis and Dr. Panagiotis Konstantinidis for their valuable help and advice since I was a student.
- My current colleagues in the University of Thessaly, Georgios Stratakis, Georgios Konstantas and Olympia Zogou, for the smooth collaboration, fruitful discussions and valuable feedback in every aspect of development and validation of modeling tools for the gasoline and diesel exhaust aftertreatment devices and systems.

I would like to emphasize that this work is not—and could not have ever been—a product of isolated effort. *This is a part of a team work.* From my viewpoint, it is a presentation of some contributions that have been realised through collaborative work, exchange of ideas and mutual help within the research activities of the Laboratory of Thermodynamics and Thermal Engines. I gratefully acknowledge the significant support that I have always received and I hope that this mentality is embraced by any newcomers to our Laboratory.

Financial support for this study was provided by the European Commission, PSA Peugeot Citroën, dmc² division of Degussa–Hüls A.G., and Ibiden Co. Ltd.

Abstract

This thesis is concerned with the modeling of catalytic converters (CC) and diesel particulate filters (DPF) employed in automotive exhaust lines for the reduction of gasoline and diesel engines emissions.

Two engineering models are developed in this work, for the CC and DPF respectively. The models incorporate phenomenological reaction schemes and semi-empirical rate expressions. The objective of the models is to incorporate all necessary degrees of freedom for the accurate prediction of the CC and DPF operation and, at the same time, to eliminate superfluous complexity.

The most important part of such models is the formulation of an appropriate reaction scheme that includes the primary chemical phenomena occurring in the wash-coat of the catalytic converters and the soot deposit of the DPF. A new reaction scheme is developed for each aftertreatment device to align with this fundamental modeling requirement. These reaction schemes and the corresponding balance equations that are developed form the modeling cores for the respective devices. Analytical solutions of the balance equations are obtained to enhance modeling accuracy and computational efficiency.

Additionally, interfaces to two commercial FEM software suites are developed for the DPF model, in order to enable the 3D computation of temperature and stress fields. This allows the detailed study of the DPF operation as regards partial regenerations and cracks formation which endanger the integrity of the filter.

A computer-aided optimization procedure is also developed for the estimation of the kinetic parameters introduced by the rate expressions of the models. The optimization procedure is based on a genetic algorithm and a properly defined performance measure.

The validity of the models and the kinetic parameter estimation procedure is checked by applying them to real world case studies. It is demonstrated that the models are capable of predicting the operating behaviour of the CC and the DPF under realistic conditions and are thus well suited for use within the frame of computer-aided engineering design and optimization of automotive exhaust lines.

Finally, the modeling levels in the field of automotive powertrain applications is discussed and it is attempted to identify the requirements of the industry. It is claimed that the current modeling paradigm of the industry may not be directly applied to the exhaust aftertreatment devices modeling while, in the same time, modeling efforts often do not recognize industrial needs. It is argued that the emergence of a new modeling paradigm, accompanied by models aligned with the industry's requirements, will eventually transform the current models from computational cores into robust engineering tools. This evolution is a long-term goal of the research activities of the Laboratory of Thermodynamics and Thermal Engines, among which this work is placed.

Μαθηματική Μοντελοποίηση, Σχήματα Αντιδράσεων
και Εκτίμηση Κινητικών Παραμέτρων
σε Καταλυτικούς Μετατροπείς Αυτοκινήτων
και Φίλτρα Αιθάλης Κινητήρων Diesel

Ευρεία Περίληψη

Αυτή η διδακτορική διατριβή ασχολείται με την μοντελοποίηση καταλυτικών μετατροπέων και φίλτρων αιθάλης που χρησιμοποιούνται σε γραμμές καυσαερίων αυτοκινήτων, για την μείωση των εκπομπών ρύπων από κινητήρες βενζίνης και πετρελαίου.

Δύο μοντέλα ανταπτύσσονται σε αυτή την εργασία, για τον καταλυτικό μετατροπέα και το φίλτρο αιθάλης αντιστοίχως. Τα μοντέλα χρησιμοποιούν φαινομενολογικά σχήματα αντιδράσεων και ημιεμπειρικούς ρυθμούς αντιδρασης. Ο στόχος των μοντέλων είναι να ενσωματώσουν όλους τους απαραίτητους βαθμούς ελευθερίας για την ακριβή πρόβλεψη της λειτουργίας του καταλυτικού μετατροπέα και του φίλτρου αιθάλης και, ταυτοχρόνως, να παραμείνουν όσο το δυνατόν πιο απλά.

Το πιο σημαντικό κομμάτι αυτής της κατηγορίας μοντέλων είναι η διατύπωση ενός κατάλληλου σχήματος αντιδράσεων που περιέχει τα χυριότερα χημικά φαινόμενα που συμβαίνουν στην καταλυτική επίστρωση των καταλυτικών μετατροπέων και στο εναπόθεμα καπνού του φίλτρου αιθάλης. Για να εκπληρωθεί αυτή η θεμελιώδης απαίτηση, ένα νέο κινητικό σχήμα αναπτύσσεται για κάθε μία από αυτές τις συσκευές αντιρρύπανσης. Αυτά τα σχήματα αντιδράσεων και οι εξισώσεις ισοζυγίων στις οποίες ενσωματώνονται, αποτελούν τους πυρήνες για τη μοντελοποίηση αυτών των συσκευών αντιρρύπανσης.

Επίσης αναπτύσσεται μια διαδικασία βελτιστοποίησης υποβοηθούμενη από υπολογιστή για την εκτίμηση των κινητικών παραμέτρων που εισάγονται στο μοντέλο από τους ρυθμούς αντιδράσεων. Η διαδικασία βελτιστοποίησης αυτή βασίζεται σε ένα γενετικό αλγόριθμο και σε ένα κατάλληλα ορισμένο μέτρο απόδοσης του μοντέλου.

Η ορθότητα της λειτουργίας των μοντέλων και της διαδικασίας εκτίμησης των κινητικών παραμέτρων των αντιδράσεων ελέγχεται εφαρμόζοντάς τα σε πραγματικές μελέτες. Δείχνεται ότι τα μοντέλα μπορούν να προβλέψουν την λειτουργία του καταλυτικού μετατροπέα και του φίλτρου αιθάλης κάτω από ρεαλιστικές συνθήκες λειτουργίας, και γι' αυτό μπορούν να χρησιμοποιηθούν στα πλαίσια μιας διαδικασίας σχεδιασμού και βελτιστοποίησης γραμμών καυσαερίου.

Η πρωτοτυπία της εργασίας αυτής όσον αφορά τη μοντελοποίηση του τριοδικού καταλυτικού μετατροπέα έγκειται στα εξής σημεία:

- Αναπτύχθηκε και επαληθεύθηκε μια μεθοδολογία για την εκτίμηση των κινητικών παραμέτρων του σχήματος αντιδράσεων του καταλυτικού μετατροπέα, η οποία χρησιμοποιεί ένα κατάλληλα προσαρμοσμένο γενετικό αλγόριθμο και ένα κατάλληλο μέτρο απόδοσης.
- Η μεθοδολογία εκτίμησης των κινητικών παραμέτρων εφαρμόστηκε για ανα-

τυχθεί ένα καινούργιο σχήμα αντιδράσεων για το μοντέλο του τριοδικού καταλυτικό μετατροπέα. Το μοντέλο έχει συνολικά πέντε φαινομενολογικές αντιδράσεις για την περιγραφή των οξειδο-αναγωγικών αντιδράσεων ετερογενούς κατάλυσης που γίνονται στα Πολύτιμα Μέταλλα της καταλυτικής επίστρωσης, και ακόμη πέντε αντιδράσεις για την περιγραφή των φαινομένων αποθήκευσης και αντίδρασης οξυγόνου στα οξειδια Δημητρίου, Ζιρκονίου κ.λ.π. της καταλυτικής επίστρωσης. Το βελτιωμένο σχήμα αντιδράσεων απεδείχθη ικανό να αποδώσει τη μεταβατική συμπεριφορά των σύγχρονων καταλυτικών επιστρώσεων στις νομοθετημένες δοκιμές επί του κινητήρα-οχήματος με αξιόλογη ακρίβεια.

- Ειδικά για την περίπτωση των οξειδωτικών καταλυτικών μετατροπέων για ντηζελοκινητήρες, ανεπτύχθη κατάλληλο σχήμα αντιδράσεων που αντιμετωπίζει και τη μοντελοποίηση της αποθήκευσης υδρογονανθράκων στο ζεόλιθο που εμπεριέχεται στις σύγχρονες επιστρώσεις. Το συγκεκριμένο σχήμα αύξησε σημαντικά την ακρίβεια μοντελοποίησης του συγκεκριμένου τύπου καταλυτικών μετατροπέων.
- Αναπτύχθηκε μια βελτιωμένη έκδοση του υπομοντέλου καναλιού του καταλυτικού μετατροπέα. Εδώ ξεκαθαρίστηκε ο ρόλος της διάχυσης στο εσωτερικό της καταλυτικής επίστρωσης, ο οποίος ενθεωρείτο σημαντικός από ορισμένους ερευνητές, οι οποίοι εισηγούντο την μοντελοποίηση σε περισσότερες διαστάσεις εντός της επιστρώσεως. Το βελτιωμένο μοντέλο που προέκυψε από αυτή την εργασία, σε συνδυασμό με τη διαδικασία προσδιορισμού των ελεύθερων κινητικών παραμέτρων, απεδείχθη ικανό να προσεγγίσει την πειραματικά μετρημένη συμπεριφορά σε ποικιλία μελετών περιπτώσεων με ακρίβεια που ποτέ άλλοτε δεν έχει παρουσιαστεί στη βιβλιογραφία. Επομένως εκ του αποτελέσματος καταπίπτει η ανάγκη μοντελοποίησης με επιπλέον διάσταση εντός της επίστρωσης, η οποία θα απαιτούσε τη χρήση παραλλήλων επεξεργαστών για λογικούς χρόνους εκτέλεσης.

Επιπλέον, το μοντέλο του φίλτρου αιθαλής συνδέεται με δύο εμπορικούς κώδικες πεπερασμένων στοιχείων, ώστε να επιτευχθεί ο υπολογισμός τρισδιάστατων πεδίων θερμοκρασίας και τάσεων. Αυτό επιτρέπει την λεπτομερή μελέτη της λειτουργίας του φίλτρου αιθαλής όσον αφορά τις μερικές αναγεννήσεις και τον σχηματισμό ρωγμών που βάζουν σε κίνδυνο την ακεραιότητα του φίλτρου. Όμως, αποδεικνύεται ότι οι διογκωμένες απαιτήσεις μετεπεξεργασίας των αποτελεσμάτων και πειραματικής επαλήθευσης των τρισδιάστατων μοντέλων απαιτούν την εισαγωγή εντελώς νέων μεθοδολογιών για την αξιοποίησή τους στο σχεδιασμό, που οπωσδήποτε θα αποτελέσουν αντικείμενο μελλοντικών εργασιών.

Η πρωτοτυπία της εργασίας αυτής όσον αφορά τη μοντελοποίηση του φίλτρου αιθαλής έγκειται στα εξής σημεία:

- Το σχήμα αντιδράσεων του μοντέλου αναγέννησης της φίλτρου αιθαλής αναπτύχθηκε ώστε να περιλάβει συνολικά εννέα αντιδράσεις: Δύο αντιδράσεις για τη θερμική οξειδωση του εναποθέματος αιθαλής, δύο αντιδράσεις για την οξειδωση της αιθαλής από NO₂, τρεις αντιδράσεις για την καταλυτική οξειδωση της αιθαλής, και ακόμη δύο αντιδράσεις για την προσρόφηση, εκρόφηση και οξειδωση του υδρογονανθρακα της αιθαλής.
- Έγινε επαλήθευση του βελτιωμένου μοντέλου θερμικής και καταλυτικής αναγέννησης του φίλτρου αιθαλής σε μια σειρά από πειράματα επί της δυναμομετρικής πέδης. Παρόλο που η διαδικασία της επαλήθευσης του μοντέλου

είναι ακόμη στα πρώτα στάδια, η ακρίβεια που επιτυγχάνεται είναι αξιόλογη και επιτρέπει τη χρήση του μοντέλου ως εργαλείου σχεδιασμού (concept design stage).

- Η ολοκλήρωση της επαλήθευσης του μοντέλου που αποτελεί αντικείμενο μελλοντικών εργασιών αναμένεται να εστιάσει στο ρόλο των προσροφημένων υδρογονανθράκων της αιθάλης καθώς και το μηχανισμό οξείδωσης της αιθάλης με NO₂ (μηχανισμός CRT).
- Το μονοδιάστατο μοντέλο του φίλτρου αιθάλης επεκτάθηκε σε τρισδιάστατο μοντέλο, συνδέοντάς το με εμπορικά προγράμματα πεπερασμένων στοιχείων, για τον τρισδιάστατο υπολογισμό του θερμοκρασιακού πεδίου του φίλτρου. Το τρισδιάστατο μοντέλο ενισχύεται και από ένα υπομοντέλο για τον υπολογισμό της ανομοιομορφίας της ροής στην είσοδο του φίλτρου, λόγω του τρισδιάστατου πεδίου ροϊκών αντιστάσεων που υπάρχει στο εσωτερικό του φίλτρου.

Τέλος, συζητούνται τα διάφορα επίπεδα της μοντελοποίησης στον τομέα των συγκροτημάτων ισχύος αυτοκινήτων και γίνεται απόπειρα να προσδιοριστούν οι ανάγκες της βιομηχανίας αυτοκινήτου. Αξιώνεται ότι το τρέχον Παράδειγμα της βιομηχανίας δεν μπορεί να εφαρμοστεί στη μοντελοποίηση συσκευών αντιρρύπανσης ενώ, ταυτοχρόνως, οι προσπάθειες μοντελοποίησης δεν λαμβάνουν υπ' όψιν τις ανάγκες της βιομηχανίας. Υποστηρίζεται ότι η ανάδυση ενός νέου Παραδείγματος μοντελοποίησης, συνοδευόμενη από μοντέλα που ευθυγραμμίζονται προς τις ανάγκες της βιομηχανίας, θα μετασχηματίσει τελικά τα τρέχοντα μοντέλα από υπολογιστικούς πυρήνες σε αξιόπιστα εργαλεία για τον μηχανικό. Αυτή η εξέλιξη είναι ένας μακροπρόθεσμος στόχος της ερευνητικής δραστηριότητας του Εργαστηρίου Θερμοδυναμικής και Θερμικών Μηχανών, στις οποίες εντάσσεται και αυτή η εργασία.

Chapter 1

Introduction

The automotive monolithic catalytic converter is by far the largest market for chemical reactors. Since the first federal legislation regarding emission limits in the United States in 1975, the market that was created has been expanding rapidly and attracting interest due to environmental, economical and scientific reasons. The moving force behind it is the social pressure for environmentally friendly engineering and pollution reduction and it is reflected in the gradually more stringent automotive emissions legislation of most developed countries, especially the United States and European countries.

The automotive industry responded to the legislation by introducing exhaust gas aftertreatment systems, whose heart is the catalytic converter. The catalytic converter is a remarkable chemical reactor, in the sense that:

- it is designed under dimensional, pressure-drop and cost-of-production constraints,
- it is required to operate with maximum conversion efficiency under fully transient conditions of temperature, input gas flow rate and input gas composition, and
- it is subject to a chemically hostile environment—as the exhaust gas contains various substances potentially poisonous for its activity—and yet it is supposed to perform for at least 5 years, unattended.

The above requirements for the converter's operation posed significant and fascinating challenges for the engineer and the scientist. These challenges, combined with the sums of money that the automotive and chemical engineering industry expended for the research and development of automotive catalysts, resulted in a very active field of research. Research and development in the field of catalytic converters and exhaust aftertreatment in general is still growing today and is not expected to settle until the internal combustion engines become obsolete in favour of another, more promising technology—most probably fuel cells.

This thesis belongs to this field of research. It presents modeling tools and methodologies that have been developed for the study of the two key devices for exhaust aftertreatment: the catalytic converter and the diesel particulate filter. The purpose of these tools is to support computer-aided engineering (CAE) of automotive exhaust systems.

In what follows in this introduction, we first attempt to briefly sketch the trends in automotive emissions legislation and pollution control. Our aim is to clarify

why computer modeling and CAE of exhaust-gas aftertreatment systems are being rendered necessary in the field of automotive pollution control.

Then, we discuss in brief some ideas that are the cornerstones of our modeling approach. This is necessary background in order to give a clear view of the character of the models that were our starting point and justify the directions we subsequently followed.

Finally, the starting point and the objectives of the present thesis are given. The models and methodologies described herein are engineering tools, oriented to the needs of the automotive industry, in order to enable it deliver to the market more efficient products, rapidly and cost-effectively. The cores of the tools for this purpose were already available before this work. This work seeks to enhance their usability and broaden their scope.

1.1 Trends in automotive pollution control

The exhaust gas from the internal combustion engines (both gasoline and diesel) contains small concentrations of carbon monoxide (CO), hydrocarbons (HCs), nitrogen oxides (NO_x), sulfur oxides (SO_x) and particulate matter. CO, HCs, SO_x and particulate matter are generated from incomplete combustion of fuel and small quantities of lubricant oil. The source of NO_x emissions is the nitrogen (N_2) oxidation to NO and NO_2 due to the high temperatures in the combustion chamber of the engine [1].

Automotive emissions have been identified as a major source of air pollution, especially in urban areas. United States first established maximum permissible emission levels of CO, HC and NO_x for automobiles in 1975. Later, Europe, Japan, Australia and other countries followed. U.S. and European Union standards are the most important and are becoming increasingly stringent, aligning with the social demand for environmentally friendly development and overall abatement of pollution.

According to all legislations, emissions are measured over an engine or vehicle test procedure in order to verify and ensure compliance with the maximum permitted values of the regulated pollutants. These test cycles are supposed to create repeatable emission measurement conditions and, at the same time, simulate a real driving condition of a given application. The legislation standards also regulated the methods that must be used to measure the pollutants.

The regulated pollutants according to the U.S. and European legislation are:

- Carbon monoxide (CO).
- Hydrocarbons (HCs). The total hydrocarbon content is measured in the European Union while the non-methane hydrocarbon content is measured in the U.S.
- Nitrogen oxides (NO_x), composed of NO and NO_2 . Other oxides of nitrogen that may be present in exhaust gases, such as N_2O , are not regulated.
- Particulate matter (PM).

In the U.S. the limits for both diesel- and gasoline-engined light-duty vehicles are the same, with the exception of the NO_x limits, which are more relaxed for diesel cars. In the European Union, the gasoline engines are exempt from the particulate

matter standards, while, depending on vehicle type and engine, there are different standards for each pollutant.

In general, all emission legislations are fairly complicated: Different emission limits and test procedures exist, depending on the pollutant, engine type and vehicle type. Emission standards are established by the Environmental Protection Agency (EPA) in the U.S. and by Directives of the European Union in Europe. A detailed description of the legislation will not be given here as it can be readily found elsewhere; consult e.g. [2]. We shall focus, though, on two aspects of legislation: (a) gradually decreasing emission limits, and (b) oncoming introduction of on-board diagnostics, coupled with periodical vehicle tests, to ensure efficient operation of exhaust aftertreatment systems.

In the early '70s, it was possible for manufacturers to build cars conforming with the legislation by simply adjusting the engine settings, but this became unfeasible shortly after. Therefore, the automotive industry, following the legislation trends, examined and developed a large number of catalytic exhaust aftertreatment systems, of increasing complexity. The monolithic catalytic converter has been the crucial component in the majority of such systems. Being the most efficient and economical way to reduce gaseous pollutants from engine exhaust, the monolithic catalytic converter has been commercially exploited as three-way catalytic converter (3WCC) in conjunction with spark-ignition engines and as diesel oxidation catalyst (DOC), used for the oxidation of CO and HC of diesel exhaust.

Today, the technology is pushed to its limits, as ultra low emitting vehicles are required by the legislation. Apart from the three-way catalytic converters and diesel oxidation catalysts, many other devices are under study and are gradually being applied in modern commercial vehicles, such as:

- diesel particulate filters (DPFs) for diesel particulate emissions reduction,
- lean- NO_x diesel catalysts (de NO_x catalysts) for diesel NO_x emissions, and
- NO_x adsorbers (NO_x traps), for both diesel and gasoline lean-burn (GDI) engines.

Furthermore, a vehicle's exhaust line nowdays may contain more than one aftertreatment device—e.g. a 3WCC in a close-coupled position may be combined with a usual underfloor 3WCC; or a catalytic converter may be followed by a particulate filter. In order to conform to the legislation, exhaust aftertreatment engineers must carefully tune the performance of a system that contains the whole exhaust line and engine management. Special engine management according to the needs of the exhaust aftertreatment devices has become feasible with the widespread use of electronic management units and it is absolutely necessary for the efficient operation of all aftertreatment devices.

Moreover, until today, catalytic converters were rarely evaluated after their installation in the automobiles; this has recently changed. The oncoming EURO IV standard includes, apart from emission limits, a requirement for an on-board emission diagnostics systems (OBD). U.S. emission standards also define emission limits for 50,000 miles/5 years and 100,000–120,000 miles/10 years. This poses the extra issue of the catalytic converter durability.

Thus, we observe a trend towards more complicated exhaust lines and the need to consider not only the catalytic converter but the exhaust line as a system. This progressively makes the experimental testing of the exhaust line difficult and more

expensive, requiring more time and experimental data to tune such complicated systems appropriately so as to attain the imposed emission limits.

In order to decrease cost and design time for exhaust line development, modeling of the whole exhaust line as a system would be extremely helpful. If fast, reliable models were available to the industry, new exhaust line configurations could be tested rapidly and inexpensively; additionally, optimization of the exhaust line components could be aided by numerical optimization procedures to achieve improved configurations and lower overall emissions.

Consequently, the targets for the exhaust line models are set by the requirements of the industry. Currently, they can be summarized as follows:

1. Modeling of short-term behaviour of aftertreatment devices
 - For catalytic converters: accurate instantaneous prediction of CO, HC and NO_x emissions.
 - For diesel particulate filters: regeneration modeling, stress modeling.
2. Modeling of long-term behaviour of aftertreatment devices
 - For catalytic converters: catalyst ageing and deactivation modeling.
 - For diesel particulate filters: ash accumulation modeling, crack initiation and propagation, material ageing.
3. Integration of the aftertreatment devices models with models for the piping of the exhaust line to build tools for the prediction of the whole exhaust line behaviour regarding emissions (and stresses, mostly in the case of the DPF).

The underlying notion is the full incorporation of computer-aided engineering (CAE) practices in the design of exhaust aftertreatment systems and exhaust lines.

Traditionally, modeling tools and CAE procedures in general are used in many areas of automobile design [3]. Accordingly, catalytic converter models appeared in the literature shortly after the application of the first automotive catalysts. The scope and success of these models was diverse. The modeling of the exhaust line proved to be a very complex problem and resisted the extensive application of modeling. As of today, modeling tools are not fully accepted in the field of catalytic converter optimization, let alone the CAE-driven design of the whole exhaust line. Although much information about the operation of the catalytic converters has been acquired, the above requirements are not fulfilled. Progress is being made, though, and this thesis is a part of continuous work to this direction.

1.2 Modeling Background

The most crucial part of the exhaust line design is the modeling of the aftertreatment devices, either catalytic converters or particulate filters. The design of the rest of the exhaust line is tuned so as to enhance their performance and reliability. Some modeling background is given here to clarify the character of the models that were the starting point of this work.

In all types of aftertreatment devices, there is strong interaction between physical and chemical processes. The first models that appeared were mainly dealing with

the physical processes in the catalytic converter, namely heat and mass transfer. Engineering practice first attacked the most prominent factors that influence converter performance. This approach was adequate for the design engineer in order to identify major directions for performance improvement. Since the legislation limits were more relaxed at that time, bigger prediction errors were acceptable.

Thus, the chemical description of the catalytic converters was initially simplistic and took account of very few phenomena. Gradually, the composition of catalytic converter washcoats became more elaborate, and the actual chemical phenomena more complicated. At the same time, heat and mass transfer in the converters were already well studied. Hence, focus shifted to the exploration of the catalytic chemical processes in the converter, which are fundamentally more difficult but comprise the core of the problem.

Generally, heterogeneous catalytic reactions occurring in the converter are extremely complicated [4]. They proceed in multiple reaction paths —usually unknown to the reactions engineer—, they are very sensitive to impurities and their reaction rates usually do not obey simple power-law rate expressions. Due to these difficulties, it is not obvious how to proceed with the chemical description of the catalyst. Two different approaches have appeared: we may call them, the ‘fundamental’ approach and the ‘engineering’ approach.

On the one hand, the fundamental approach focuses to the actual chemical phenomena involved in the operation of the catalytic converter and investigates them in detail. This is normally a controversial and time-consuming work, but can give valuable insight for the understanding of the catalytic system’s operation. A disadvantage of this approach is that detailed measurements and data are needed in order to support modeling. Furthermore, conclusions drawn for one catalytic system are not necessarily valid for a different system, albeit similar.

On the other hand, the essence of the engineering approach is that the model explicitly takes into account all phenomena that are well defined and studied, i.e. most of the physical phenomena. All other phenomena—including primarily chemical phenomena, which are inherently more obscure—are *lumped* into overall expressions, such as effective reaction rates of overall reactions. In their turn, these expressions contain effective properties (such as activation energies and pre-exponential factors for chemical reactions).

The lumped parameters models must be first ‘tuned’ against one or more experiments in order to determine the tunable parameters of the model. Afterwards, the model may be used to predict, under any inlet conditions, the behaviour of the same or modified converter configuration. Modifications in the catalytic converter’s configuration are accounted for by the model to the extent they influence phenomena that are taken into account *explicitly* and are *not* lumped in any tunable parameters. That is, lumped parameters models simplify the modeling of the catalytic converter but introduce the need for the determination of the model’s parameters.

A lot of fundamental studies regarding reaction paths and corresponding kinetics have appeared in the literature. Nevertheless, no complete fundamental model has appeared to allow prediction of the behaviour of the catalytic converter under realistic conditions. Therefore, engineering lumped parameters models are generally preferred for real-world problems. They mainly offer simplicity, restricted requirements of experimental data and emphasis to the most influential factors of the system being modeled. Owing to these advantages, such models are already in use to aid design of new aftertreatment technologies [5]. From now on, we shall be

exclusively occupied with this modeling approach.

1.3 Starting point and objectives of this thesis

The starting point of this work was a set of two engineering models for the basic aftertreatment devices of a modern exhaust line of an automobile:

1. A two-dimensional monolithic catalytic converter model.
2. A one-dimensional model for the thermal and catalytic regeneration of the wall-flow diesel particulate filter (DPF).

The catalytic converter model was a two-dimensional lumped parameters model, which featured a kinetic scheme with ‘overall’ reactions as well as adsorption, desorption and storage of chemical species. Depending on the choice of the reaction scheme, it was applicable to a wide variety of exhaust aftertreatment devices but had been mainly used for three-way catalytic converters and diesel oxidation catalysts. The wall-flow diesel particulate filter model was a one-dimensional thermal and catalytic regeneration model. The approach of these two models had already been validated and tested in practice (see e.g. [6, 7, 8, 9, 10]). Nevertheless, they suffered from some restrictions, which provided the motivation for this work:

- Primarily, the catalytic converter model lacked a systematic way to adjust the tunable parameters of the reaction scheme. Tuning was performed manually, a fact that reduced model’s validity, accuracy and usability in the frame of a CAE design process.
- The validity and application range of the reaction kinetics submodel was questionable, especially as regards oxygen storage modeling.
- The DPF model’s main limitation was that it was a 1D model. The regeneration process is a strongly 3D phenomenon; moreover, 3D calculations temperature field are necessary for satisfactory stress analysis of the filter. Coupled thermal and stress analysis is of ultimate importance in the case of the DPF, because the most common reason that leads to DPF failure is crack formation due to thermal dilatations.
- DPF modeling had to be extended to account for the effect of the presence of volatile organic fraction (VOF) in the accumulated soot.

This thesis is addresses the main shortcomings of both the original catalytic converter and the DPF model and promote their accuracy and applicability, without losing the main advantages of this class of engineering models—simplicity and focus to what is most important. According to the above discussion, the main objectives of this thesis are the following:

- to develop and validate a computer-aided tuning procedure for the tuning of the catalytic converter kinetics model,
- to apply the computer-aided tuning procedure in order to update the three-way catalytic converter kinetics scheme and improve predictions quality,

- to apply and validate the new channel model using data from last generation catalytic converters,
- to extend the diesel oxidation catalyst kinetics model in order to allow for hydrocarbon adsorption–storage–desorption in zeolite diesel oxidation catalysts, and
- to improve the DPF kinetics submodel in order to correct the underlying kinetics scheme and include a mechanism for the effect of the VOF,
- to extend the DPF model in order to allow for 3D heat transfer calculations.

This work intentionally tries to be aligned with the main requirements set by the automotive industry and discussed in Section 1.1, specifically with the first items of the list: The necessity for reliable modeling tools for the accurate prediction of catalytic converter efficiency and DPF regeneration characteristics and stress analysis. The remainder of this thesis is organized as follows:

- Chapter 2 initially provides background on the operation and modeling of the catalytic converters, which is followed by the formulation of an engineering model for the three-way catalytic converter and the diesel oxidation catalyst. Similarly, in Chapter 3 we discuss the operating concept and develop a model for the operation of the wall-flow diesel particulate filter.
- Chapter 4 describes the optimization methodology that has been developed to enable the computer-aided estimation of tunable parameters that are introduced by the kinetic expressions of the catalytic converter model. A custom performance measure is defined, which is coupled with a genetic algorithm optimization procedure. The resulting methodology enables model fitting against any set of full-scale measurements.
- Chapters 5 and 6 present the validation of the catalytic converter and diesel filter models respectively. The models are applied to full-scale measurements and their predictive power and application range is discussed. It is confirmed that the developed models are capable of predicting the behaviour of catalytic converters and diesel particulate filters with great accuracy, which indicates that the models are useful tools of the aftertreatment systems design engineer.
- In conclusion, Chapter 7 attempts to present an overview of the role of modeling in the design and analysis of exhaust aftertreatment systems. The automotive industry requirements and the current modeling paradigm are discussed, and the connection to the underlying concepts of engineering tools for exhaust aftertreatment devices is investigated. Finally, perspectives and future paths for research and development are examined.

References

- [1] Jan Kašpar, Paolo Fornasiero, and Heal Hickey. Automotive catalytic converters: current status and some perspectives. *Catalysis Today*, 77:419–449, 2003.
- [2] Emission standards (summary of worldwide emission standards). <http://www.dieselnets.com/standards.html>.
- [3] M. H. Sandford and R. D. Jones. Powerplant systems and the role of cae – part 1 exhaust systems. *SAE paper 920396*, 1992.
- [4] Lanny D. Schmidt. *The Engineering of Chemical Reactions*. Oxford University Press, 1998.
- [5] R. Domesle, D. Lindner, W. Mueller, L. Mussmann, M. Votsmeier, E. S. Lox, T. Kreuzer, M. Makino, and C. D. Vogt. Application of advanced three-way catalyst technologies on high cell density ultra thinwall ceramic substrates for future emission legislations. *SAE paper 2001-01-0924*, 2001.
- [6] G. C. Koltsakis and A. M. Stamatelos. Modeling catalytic regeneration of diesel particulate traps. *Industrial & Engineering Chemistry Research*, 35:2–13, 1996.
- [7] G. C. Koltsakis and A. M. Stamatelos. Modes of catalytic regeneration in diesel particulate filters. *Industrial & Engineering Chemistry Research*, 36:4155–4165, 1997.
- [8] G. C. Koltsakis, P. A. Konstantinidis, and A. M. Stamatelos. Development and application range of mathematical models for automotive 3-way catalytic converters. *Applied Catalysis B (Environmental)*, 12(2–3):161–191, 1997.
- [9] G. C. Koltsakis, P. A. Konstantinidis, and A. M. Stamatelos. Three-way catalytic converter modeling and applications. *Chemical Engineering Communications*, 164:153, 1998.
- [10] I. P. Kandylas, G. C. Koltsakis, and A. M. Stamatelos. Mathematical modelling of precious metal catalytic converters for diesel NO_x reduction. *Proc Instn Mech Engrs, Part D: J. Automobile Engineering*, 213:279–292, 1999.

Chapter 2

Monolithic Catalytic Converters

Entia non sunt multiplicanda praeter necessitatem.

— WILLIAM OF OCKHAM

Monolithic catalytic converters are flow-through chemical reactors located in the exhaust line of the majority of modern vehicles. Their purpose is to convert gaseous-phase pollutants of the exhaust gas into harmless products. Catalytic converters have been the great success of the automotive industry in the field of pollution control; their introduction reduced emissions to levels previously unconceivable.

The success of the monolithic catalytic converters enabled the enforcement of increasingly stringent legislated emission limits. This trend has brought the catalytic converters technology to its limit and has necessitated the use of modeling for the design and optimization of modern exhaust lines [1]. Since the chemical and physical phenomena occurring during converter operation are extremely complicated and, to a great extent, not well understood, their modeling has not been an easy task. Nevertheless, research is active and promising.

Here, we formulate an engineering model for catalytic converter operation. A brief description of the monolithic catalytic converters' structure and operation is initially provided and the dominant physical (heat and mass transfer) and chemical (reactions, chemisorption) phenomena involved in their operation are discussed. The structure of the catalytic converter dictates splitting the modeling problem into four distinct and connected levels [2]: (a) the reactor level, (b) the channel level, (c) the washcoat level and (d) the kinetics level. A submodel is formulated for each of the levels of the problem and the novel features of the proposed model and the various alternative approaches are discussed.

The modeling approach described herein is an extension of the approach developed by Koltsakis and Stamatelos [3, 4]. The primary contributions introduced by this thesis are the following:

- An improved kinetic model of storage phenomena has been developed for the washcoats of both three-way catalytic converters (oxygen storage) [2] and diesel oxidation catalysts (hydrocarbon storage) [5]. The reaction scheme and the kinetic expressions for the storage reactions have been updated, and a rigorous mathematical treatment has been formulated. The improvements regarding storage modeling resulted in significant increase of the accuracy and reliability of the catalytic converter model, as illustrated in Chapter 5
- The effect of diffusion in the washcoat of the catalytic converters has been in-

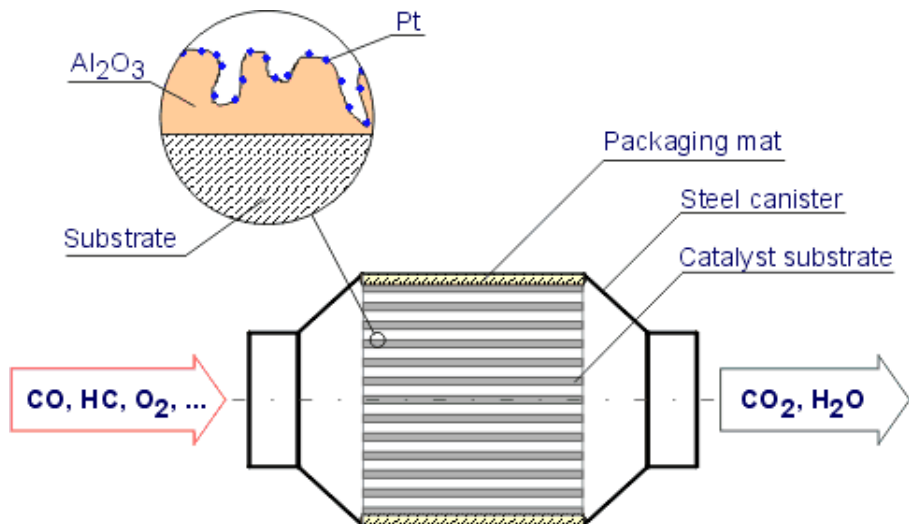


Figure 2.1: Structure of monolithic catalytic converter

vestigated. A diffusion mechanism employing an effectiveness factor approach has been inserted in the washcoat model, and its impact on the results of the catalytic converter model has been examined. Diffusion effects were further investigated in a more detailed level, using a separate code (Appendix A). The results indicated that the effect of diffusion is not observable in the overall efficiency of the 3WCC under the conditions met in the legislation tests.

2.1 Operation of the monolithic catalytic converter

2.1.1 Overview

The most common catalytic converter design is illustrated in Figure 2.1. It utilizes a ceramic honeycomb monolithic substrate, featuring many small parallel channels running in the axial direction. An alternative design utilizes a metallic substrate, made of thin metal foil formed into a honeycomb structure which provides the same functionality [1]. The two alternative designs are compared in Figure 2.2. Since both designs feature qualitatively the same operation behaviour—though the ceramic monolith is more widely employed in commercial applications of the catalytic converter—, we will hereafter refer to both designs with the term (monolithic) catalytic converter without further discrimination.

Parts that have been commercially used for automotive applications typically have a cell density of 400 cells per square inch (cpsi), with 600 cpsi parts becoming increasingly popular in converters for gasoline fueled cars. Substrates of cell densities as high as 1200 cpsi are under development [6, 7].

The ceramic or metallic substrate of the monolithic catalytic converter does not have any catalytic activity of its own. The function of the monolith substrate is to provide high geometric surface area for contacting the gas phase, which flows through the channels, with the catalyst, which is coated on the channel walls. The active catalyst layer has to be coated on the monolith walls. That coating, called the washcoat, is composed of porous, high surface area inorganic oxides such as $\gamma\text{-Al}_2\text{O}_3$, CeO_2 and ZrO_2 . Noble metal catalysts, such as platinum (Pt), palladium



Figure 2.2: Comparison of ceramic vs. metallic substrate

(Pd) and Rhodium (Rh), are deposited on the surface and within the pores of the washcoat [1, 8, 9, 10]. Exhaust gas flowing in a catalytic converter diffuses through the washcoat pore structure to the catalytic sites where heterogeneous catalytic reactions occur.

In the following, we briefly describe the most important phenomena involved in the catalytic operation, in order to facilitate the formulation of the model that follows.

2.1.2 Heat and mass transfer

The flow in the channels of the monolith is laminar for the whole range of exhaust gas velocities that are induced by the engine. Reynolds numbers typically range from 10 (engine at idle) to 200 (engine at full load). The development of the flow is completed near the entrance of the monolith and a laminar boundary layer is thus formed for the greatest part of the reactor.

Since the flow boundary layer is laminar, the exhaust gas is transported via molecular diffusion from the main flow of the exhaust gas to the catalyst washcoat through the laminar boundary layer. The gas diffuses further into the porous washcoat, where it simultaneously gets adsorbed (stored) or reacts at the active sites of the catalyst. Products and desorbing species diffuse back to the main flow.

Reactions in the monolith's washcoat are strongly dependent on the prevailing temperature. Consequently, the converter has very low activity during warmup operation, when the monolith is still cold, and the converter operation is then called *kinetically controlled*. As monolith temperature rises, reaction rates become higher. After a certain temperature, the actual reaction rates increase abruptly. Species in the washcoat vanish or form at such high rates that significant concentrations gradients are established between the bulk flow of the exhaust gas and the gas in the washcoat. In that case, the converter operation is *mass transfer controlled*, because mass transfer is the limiting factor of the conversion efficiency [11]. The temperature where the transition from the kinetically controlled regime to the mass transfer controlled regime is observed is called the *light-off temperature*.

Chemical or physical phenomena in the washcoat are accompanied with heat absorption or release, thus the mass diffusion is coupled with heat transport. Convection is the main mechanism of heat exchange between the monolith and the exhaust gas. Radiation is usually considered negligible. On the other hand, convec-

tion and radiation are the mechanisms responsible for the heat exchange between the catalytic converter and the surrounding air. In order to reduce heat losses to the ambient air (which may cause the cooling of the converter and efficiency deterioration), the monolith is normally insulated. The insulation mat is located between the metallic canning and the monolith itself (Figure 2.1).

During the warmup phase of the catalyst, when the catalytic converter is still practically inactive, significant amounts of pollutants may be emitted. Hence, primarily heat transfer to the converter should be enhanced and its thermal capacity should be minimized, in order to attain light-off temperature as rapidly as possible. Several *fast light-off techniques* [12], targeted to attain these goals, are under consideration, such as:

- heating air at the catalyst's inlet [13]
- electrically heating the catalyst [14]
- positioning the main catalyst close to the manifold (close-coupled catalyst)
- employing a precatalyst (start catalyst or light-off catalyst) also featuring thin-wall substrates [15, 16]

During the mass-transfer controlled operation of the catalyst after light-off, the diffusion resistances in the boundary layer and the washcoat have to be as low as possible to achieve maximum efficiency and reduce emission breakthroughs. Such diffusion resistances are connected with monolith and washcoat geometry (e.g. hydraulic diameter of monolith channels, monolith wall thickness, washcoat thickness and porosity).

Apart from the above techniques, which are related to heat and mass transfer, washcoat improvements are also under intensive study. They are related to the chemical phenomena in the catalytic converter and are discussed below.

2.1.3 Chemical phenomena

As the purpose of the catalytic converter is to cause undesired pollutants contained in the exhaust gas to react to harmless—or, at least, less undesired—products, the prevailing phenomena are heterogeneous catalytic reactions between species of the exhaust gas that diffuse in the washcoat. These heterogeneous reactions proceed via a multitude of reaction paths, which may be dependent on the local conditions in the washcoat (temperature, chemical composition of the washcoat and concentrations of the species at the gaseous phase) [17].

Apart from chemical reactions, other significant phenomena that may be observed in the washcoat of a catalytic converter are storage phenomena. These phenomena involve physical or chemical adsorption (physisorption or chemisorption) of species in the washcoat, where they are stored [8, 18]. Stored molecules may subsequently react (if they formed chemical bonds when they were stored) or desorb again (if they were stored due to physical adsorption or condensation).

To reduce emissions when the catalyst is operating at low temperature, washcoats are under intensive study. The objective of washcoat developments is usually either to make the catalyst active in low temperatures (i.e. to lower light-off temperature), or to employ washcoat components to adsorb pollutants before light-off temperatures (or, in general, when conditions in the washcoat do not favour conversion of

pollutants) [19]. Adsorbed pollutants should be released at higher temperatures, when they are able to react and be converted.

Exactly which chemical phenomena occur in the washcoat of a catalytic converter depends on the washcoat composition. There is presently a big variety of washcoat compositions which, nevertheless, share some common characteristics depending on the application that the converter is destined. Monolithic catalytic converters applications in the area of automotive exhaust aftertreatment may be roughly divided in the following categories [1]:

- Three-way catalytic converters, applied in the case of spark-ignition engine exhaust lines.
- Diesel Oxidation Catalysts, suitable for the conversion of CO and HC diesel engine exhaust.
- Lean NO_x catalysts and NO_x traps (recently in production: [20]), for the abatement of NO_x emissions of diesel exhaust.

Each converter category corresponds to a different family of washcoats.

The prevailing phenomena for the three-way catalytic converters and the diesel oxidation catalysts are presented in Sections 2.3.1 and 2.3.2, for the purpose of kinetic modeling of the respective devices. It must be noted, though, that details on the chemical behaviour of the washcoat (a) may be pursued to varying levels of detail—which is usually a matter of one's scientific discipline—and (b) are matters of ongoing research that will not settle easily, since the involved phenomena are very complex and different types of washcoats continue to appear.

2.1.4 Washcoats

The washcoat is a porous, high surface area layer bonded to the surface of the ceramic monolith. Its exact role, which is certainly very complex, is not clearly understood or explained. The main function of the washcoat is to provide very high surface area, which is needed for the dispersion of catalytic metals.

Washcoat materials include inorganic base metal oxides such as Al₂O₃ (aluminum oxide or alumina), SiO₂, TiO₂, CeO₂, ZrO₂, V₂O₅, La₂O₃ and zeolites [21, 22]. Some of them are used as catalyst carriers, others are added to the washcoat as promoters or stabilizers, still others (such as V₂O₅ or CeO₂) exhibit catalytic activity of their own [23]. Good washcoat materials are characterized by high specific surface area and thermal stability [9].

Precious metal catalysts are usually applied in a second step called impregnation. During the impregnation, the washcoated monolith is exposed to a water-based solution containing catalytic precursors. The supported catalyst is then dried and calcined to its final form [8]. During the calcination, the catalyst precursors decompose to form the final catalyst, usually a metal or a metal oxide. The most common catalysts are precious metals such as platinum (Pt), palladium (Pd) and rhodium (Rh).

The BET (Brunauer, Emmet, and Teller, [8, pp. 102–105]) specific surface area of the catalyst washcoat materials is typically higher than 100 m²/g. The washcoat layer on a metallic foil and on a ceramic substrate is illustrated in Figure 2.3. The thickness of the washcoat layer is typically 20–100 μm. Much thicker washcoat deposits (“fillets”) are formed in the cell corners, especially in the sinusoidal channels of metallic substrates.

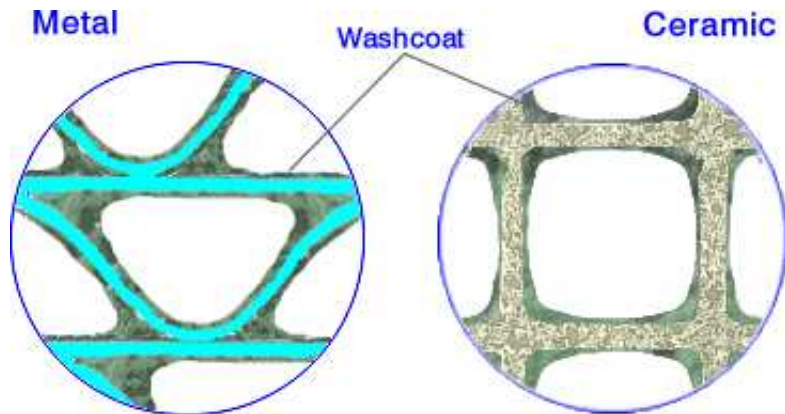


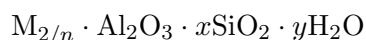
Figure 2.3: Washcoats on metallic and ceramic substrates

There is a significant diversity concerning the washcoats being used in commercial catalytic converters today. Pt/Rh washcoats continue to be in use today, utilizing Pt for the CO and HC oxidation and Rh for the NO_x reduction [9]. They are usually composed of 0.10–0.15% Pt and Rh at a ratio of 5:1. Together with CeO₂ and ZrO₂ as oxygen storage components [23], they have been used very successfully in γ -Al₂O₃ washcoats.

On the other hand, Pd has also become popular in the case of the trimetallic catalyst [24], where Pt, Pd and Rh are all combined in the washcoat, usually with Pt and Rh in smaller amounts. A typical formulation of a trimetallic catalyst is with Pt:Pd:Rh weight ratio 1:13:1. Pd/Rh and Pd-only washcoats are also employed [25]. Such advanced washcoat formulations are prepared in multiple layers (*layered washcoats*). In Pd/Rh washcoats, Pd and Rh are separated to avoid deactivation by alloy formation. In Pd-only washcoats, a layer of Pd deposited on the OSC enhances O₂ oxidation function, while a layer of Pd promoted with metal oxides results in better HC and NO_x conversion [9]. In Figure 2.4, the view taken into the corner of a single channel of the monolith shows an alumina-rich underlayer and a Ceria-Zirconia overlayer.

The oxygen storage component, incorporated in every washcoat, takes advantage of the oscillatory nature of the air-to-fuel ratio in the exhaust [27], which exposes the catalyst to alternating rich and lean conditions. The OSC adsorbs O₂ during the lean operation of the converter, and subsequently releases O₂ under rich operating conditions. Thus, when the catalyst is operating rich, O₂ is provided to consume the unreacted CO and HC, increasing the overall efficiency of the converter. Usually, CeO₂, possibly combined with ZrO₂, is used as the oxygen storage component in modern three-way catalytic converters.

Adsorbing components such as zeolites have also been tested in washcoat formulations. Zeolites are hydrated crystals of alumina (Al₂O₃) and silica (SiO₂) [28]. They are represented by the empirical formula [8]:



The metal cation M produces electrical neutrality. When zeolites are dehydrated, they develop a uniform pore structure having minimum channel diameters of 0.3 to 1.0 μ m. Owing to this fine-pore structure, they exhibit unusual adsorption and catalytic characteristics, the most important being shape-selectivity: bulky molecules

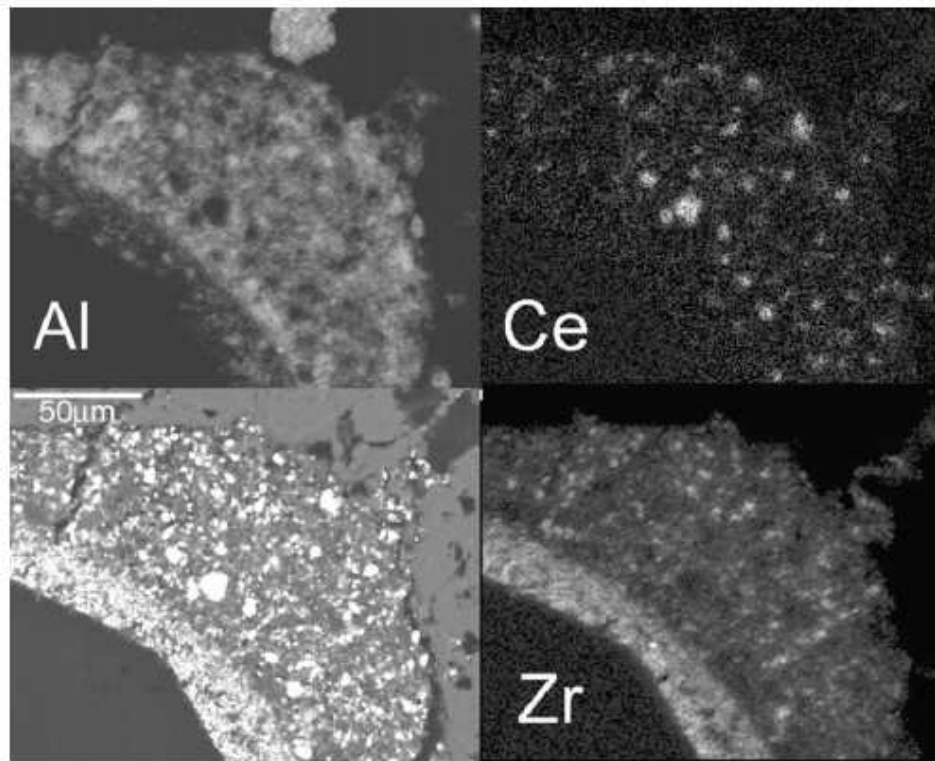


Figure 2.4: Typical layered washcoat structure of current three-way catalyst (reproduced from [26]). The lower left-hand panel is a backscattered electron image and the other panels are chemical maps obtained with an electron microprobe.

may not diffuse into the pore structure of the zeolite. Therefore they are sometimes characterized as *molecular sieves*.

Zeolites have been under intense study from the chemical industry for a long time [28]. In connection with catalytic converter washcoats, they are important for the HC emissions adsorption, especially for the diesel engines. The idea is to adsorb and retain HCs during the warmup phase of catalytic converter operation and until the latter lights-off. Subsequently, they released from the zeolite and oxidized as normal. This has been used with some success [] but the performance of adsorbing materials found until today is still far from ideal.

The concept of storage has also been applied in the case of the NO_x adsorbers or NO_x traps, which are now applied in the case of the new lean-burn gasoline engines, which generate much more nitrogen oxides than their stoichiometric counterparts. The washcoat of a NO_x trap is a 3WCC washcoat, to which a NO_x storage component has been added—usually Barium oxide (BaO). During lean burn operation of the engine, NO_x are chemisorbed onto BaO . Periodically, the engine switches to short rich operation, and CO reacts with stored NO_x to CO_2 . This also empties the storage component, and the process is called *regeneration*. The frequency and duration of the rich operation intervals should be carefully adjusted and requires advanced integration with engine management.

In general, washcoats are under intensive study because of the significant precious metal loading concentrations and their inevitable cost. Work is concentrated on finding the most economic washcoat formulation required to comply with the emissions standards, which may be notably different between different applications

(vehicle–engine–exhaust system–legislated cycle combinations) [29]. Modeling tools are therefore needed: Engineering 3WCC models able to accurately predict the behaviour of the catalyst for different configurations—especially for different precious metal and washcoat loadings—would be very important for the design of economic as well as efficient exhaust lines.

2.2 Overview of the modeling problem

Having identified the dominant phenomena occurring in a catalytic converter, we may proceed with the formulation of the model. In this section, we first give an outline of the catalytic converter modeling problem. Four distinct levels of modeling are identified: The reactor, channel, washcoat and kinetics level. We attempt to clarify what is modeled at each level and discuss which are the primary choices that one has to make when developing a catalytic converter model.

2.2.1 Navigation in the modeling landscape

A great number of models have been presented until today, featuring a multitude of approaches and levels of modeling detail [2, 3, 30, 31, 32, 33, 34, 35, 36, 37, 38]. The diversity of published works on the field indicates that no definite answers have been given to the catalytic converter modeling problem. There are several reasons for this situation:

- *Modeling objectives and application range.* Not all published works share common objectives and application range, varying from fast, approximate models to very detailed, computationally intensive models. Fundamental research models typically attempt to describe phenomena as accurately as possible, require a lot of input data and usually can be tested only in extremely simplified catalyst behaviour scenarios [17]. For application-oriented models, formulation depends on the system or device where modeling is applied as well as the design parameters under investigation [4, 5, 2]. In this case, accuracy may be sacrificed because of constraints such as simplicity or flexibility.
- *Problem complexity.* Catalytic converter operation involves heterogeneous catalytic chemical reactions, which are coupled with simultaneous heat and mass transfer and take place under highly transient conditions. Under such conditions, it is difficult to describe chemical phenomena quantitatively or even qualitatively [39]. Each set of inevitable approximations and simplifying assumptions that are included essentially defines a different modeling approach, and no one can a priori be considered better or worse than any other one.
- *Rapidly changing washcoat technology.* Catalytic converter manufacturers continuously improve the chemical characteristics of the catalytic converter washcoats, in an effort to produce efficient as well as low-cost designs. Thus, chemical kinetics research has to keep track of most modern washcoat developments, which inhibits the acquisition of in-depth knowledge about the washcoats chemical behaviour and may lead to system-specific conclusions and results.
- *Performance assessment difficulty.* Finally, there is no consensus on how to assess model performance, so that models with similar scope can be compared.

The introduction of such a methodological tool should help towards identifying the weaknesses and advantages of different approaches and provide with a quantitative criterion for model comparison [40]. This issue is addressed in Chapter 4.

The variety of modeling approaches that have been proposed and tested until today can be largely attributed to the above points. Nevertheless, similarities may be noticed among many different models and the majority of them share a common structure, which is dictated by the structure and operating concept of the catalytic converter itself.

Specifically, the catalytic converter is essentially a batch of parallel channels, which have been covered in their interior by a chemically active washcoat layer. The structure of most published models follows the structure of the converter itself so that each model can be divided into four distinct levels: The kinetics level, the washcoat level, the channel level and the reactor level. Below, we attempt to clarify what is modelled at each level and discuss which are the most common choices that one has to make when developing a catalytic converter model.

2.2.2 Kinetics level modeling

At the kinetics level, the mission of catalytic converter modeling is twofold:

1. Qualitative description: To identify the *prevailing* physical and chemical phenomena occurring in the washcoat at the various conditions that are characteristic of the catalytic converter operation.
2. Quantitative description: To find appropriate mathematical expressions that enable calculation of the rates at which the identified phenomena proceed, as well as calculation of characteristic physical quantities—concentrations, temperatures, heat fluxes etc—with sufficient accuracy.

That is, the modeling must decide *which* phenomena dominate and, if possible, the *rates* that they proceed. Both of the above aspects are influenced by the local conditions prevailing in the washcoat.

The efforts of the first objective usually concentrate on the identification of the reactions, which take place in the active sites of the catalyst particles dispersed in the washcoat. The study of physical or chemical adsorption and storage also falls in this task. When building the reaction scheme, the primary choice is between elementary or overall reactions. Elementary reactions describe in detail the actual steps that the heterogeneous catalysis follows. On the other hand, overall reactions view heterogeneous catalysis phenomenologically as an one-step reaction between reactants and final products, and no intermediate steps are considered.

The second objective of the modeling at the kinetics level is the mathematical description of the rates that the physical and chemical processes proceed, as functions of the local conditions in the washcoat. Regardless of the reaction scheme, a reaction rate must be determined for each reaction introduced in the model. Elementary reactions usually employ simple Arrhenius-type rate expressions. Overall reactions use more complicated rate expressions, which are either totally empirical or they are based on the Langmuir–Hinshelwood formalism and containing some empirical terms, e.g. [35, 41, 42]. Essentially, the overall reaction approach favours the simplification of the reaction scheme, at the expense of using more complicated

and highly empirical rate expressions; in a sense, the complexity of the reaction scheme details is hidden into the mathematical formulation of the rate expressions.

Because of the extreme complexity of the heterogeneous reactions and the usually insufficient knowledge of the composition and structure of the washcoat, this is the most obscure and controversial part of the catalytic converter modeling. In fact, neither the reaction scheme nor the corresponding reaction rates are usually known. This is due to several reasons [39]:

- First, all reactions occurring in a catalytic converter proceed heterogeneously on the noble metal surface. The exact reaction path involves multiple reactions and intermediate steps, thus the exact reaction path is not known. Besides, the reaction path depends on the possible presence of species in the real exhaust gas that are not present in an special experimental setup designed for reaction identification.
- Second, the reactions kinetics are very sensitive to the washcoat formulation. Noble metal loading and its dispersion in the washcoat, washcoat porosity etc may affect the reaction rates. Possible impurities that may be present may promote one rate over the others.
- Last but not least, catalytic processes suffer from ageing and deactivation, and these depend on the conditions under which the catalyst is aged. Two catalytic converters with identical washcoat formulations behave significantly differently after ageing under different operating conditions.

To summarize, reaction kinetics in a catalytic converter are very sensitive to the input gas composition, the washcoat formulation and its history. Thus, the reaction rates cannot be a priori determined for each washcoat formulation.

To circumvent the above difficulties, most modeling efforts resorted to the use of overall reaction schemes together with empirical rate expressions. Such rate expressions may be viewed as fitting laws: they are semi-empirical functions of some bulk quantities that are characteristic of the converter operation, such as temperature and species concentrations [33, 4]. They contain parameters that must be estimated (*tuned*) by fitting the model to a set of experimental data, which represent the behavior of the catalyst under a typical operating cycle. The corresponding models are called *lumped parameters models*, because all phenomena that are not explicitly accounted for by the model are lumped into the values of their tunable parameters.

Thus, in a lumped parameters model, the chemical activity of the catalyst is lumped into the *form* of the rate expressions and the *values* of their tunable parameters. If both the form of the reaction rates and the determination of the tunable parameters values are successful, such a model is supposed to predict of the converter's behaviour for different geometrical configurations and inlet conditions. It may not be used for different *chemical* configurations of the washcoat, because the models does not account for chemical phenomena directly.

It has been shown that this approach gives satisfactory results in practice [2, 3, 4, 5]. The most questionable part of this procedure was the tuning of the model, which was traditionally manual. To address this problem, a computer-aided tuning procedure is developed in Chapter 4.

2.2.3 Washcoat level modeling

Washcoat modeling is local in nature. At this level, local phenomena at each point of the washcoat along the channel axis are considered. The objective at the washcoat level modeling is to define how the simultaneous phenomena of diffusion and reaction in the washcoat will be taken into account.

Heat transfer through the washcoat is normally omitted, since the washcoat is approximately isothermal [43, 11]. Several approaches exist for the modeling of mass transport: from completely neglecting washcoat diffusion to detailed calculation of species profiles diffusing-reacting in the washcoat solving the corresponding balance equations. The former can be viewed as a zero-dimensional approach, while the latter is one- or two- dimensional and implies significant added computational cost.

As of today, the approach of diffusion neglection has been usually preferred for its simplicity, although there was evidence that diffusion may become important [11, 43, 44]. Tunable parameter models essentially lump the diffusion effects into the tunable kinetic parameters. This approximation gives good predictions of catalyst behaviour under different configurations, provided that the washcoat loading and composition is fixed.

Nowadays, diffusion gradually receives more focus and it is suggested that the models be enhanced with some mechanism to provide diffusion effects calculations. The straightforward approach is to consider mass transport balances along a direction transverse to the channel wall and compute concentration profiles of species diffusing in the washcoat. This approach essentially makes the channel level calculations two-dimensional, thus imposing significant computational burden to the model. Moreover, it leads to models that go too deep in details and, typically, experimental data of the same quality and detail to support them are not available

What we have chosen is to use an alternative solution. We extent the model towards the inclusion of diffusion effects using an effectiveness factor approach, so that we keep the model simple and its needs in computational power low. The effectiveness factor employs approximate analytical solutions to compute total consumption or production of species depending on washcoat loading and intrinsic kinetics. The details are given in Section 2.4.4.

2.2.4 Channel level modeling

At the channel level, the local information provided by the washcoat model is exploited. The objectives of the model are the following:

1. To determine the mass and heat transfer between the exhaust gas and the solid phase of the converter (substrate and washcoat), and
2. To determine the exhaust gas characteristics (temperature and species concentrations) along the channel.

At this level, chemical and physical phenomena in the washcoat are viewed as mass sinks or sources. Profiles of concentration and convective heat transfer between the channel wall and the gas are computed along the channel axis.

Since the exhaust gas flow through the channel is laminar, it is approximated with plug flow in the vast majority of models, although 3D channel models have also appeared [36]. Thus, one-dimensional heat and mass balance equations for the exhaust gas are formulated at this level of modeling.

The second option here is between a transient and a quasi-steady approach. If transient (time-dependent) terms of the equations are omitted, steady state balances remain. The quasi-steady approach implies that these steady state balances are solved for each time step as solution proceeds in time for different boundary conditions. The boundary conditions are imposed by the transient reactor model.

By omitting transient terms, the steady-state approach essentially assumes that there is no accumulation of heat or mass in the gas flow, which is a realistic assumption [30, 45]. The objective of this approximation is to simplify the balance equations and reduce the computational cost that is involved in their solution and it is used by essentially all engineering models. Fully transient channel models are usually employed for more detailed kinetic studies [46].

2.2.5 Reactor level modeling

Only one problem is tackled at the reactor level: Heat transfer in the solid phase, i.e. conductive heat transfer in the monolith and convection and radiation to the surrounding air. At this level, the heat sources computed for each channel at the kinetics and channel level calculations are used to estimate the temperature field of the monolith.

Heat transfer calculations may be one, two or three-dimensional, depending on the desired level of accuracy. 1D reactor level models treat all the channels of the monolith identically (i.e. subject to identical boundary conditions), thus requiring the channel level computations to be performed only once. On the other hand, 2D or 3D computations divide the monolith into sectors (clusters of channels) and the channel level computations are done for each one of the distinct sectors [34, 3, 47, 48].

The 2D or 3D modeling at the reactor level is not critical in the case of the catalytic converter. As regards heat transfer, the catalytic converter is usually well insulated and allows the use of 1D models, which are advantageous in terms of computation time. 2D or 3D modeling can be used for accuracy improvement in the case of severe inlet flow maldistributions at the converter's inlet. Such computations necessitate the detailed measurements of exhaust gas flow distribution, which are not always available. Therefore, 2D and 3D effects are usually lumped into the tunable parameter of the model and the 1D approach is employed [2, 33, 38, 49].

So far, we have decided for the primary assumptions at each modeling level. These reflect the design concept of the model, which is the minimization of degrees of freedom and the elimination of any superfluous complexity in general. Subsequently, we present the details of the model formulation.

2.3 Kinetics level modeling

Two kinetics models are formulated in this section, for the three-way catalytic converter and the diesel oxidation catalyst respectively. For the 3WCC case, our purpose is to formulate a new reaction scheme with emphasis to the oxygen storage phenomena. For the DOC case, a submodel will be formulated for the adsorption–desorption of hydrocarbons in the zeolite-containing washcoats.

The kinetic model for the three-way catalytic converter has evolved from that of Koltsakis et al [3]. The reduction and oxidation reactions and their corresponding rate expressions have been kept intact. The steam-reforming reactions have been removed since it has been found that they unnecessarily complicate the overall

reaction scheme without significant contribution to the model's predictive ability. Finally, the oxygen storage reactions set has been updated and extended and the corresponding reaction rates have been improved. This has led to a significant improvement of the 3WCCC model's results [2, 38].

The diesel oxidation catalyst kinetic model that has been formulated in this work is pertinent to zeolite DOC washcoats and it is a variation of the 3WCC kinetic model. It includes the oxidation reactions used in the latter model, plus a novel submodel for the adsorption and desorption of heavy hydrocarbon molecules on the zeolite content of the washcoat. The model has been tested against realistic case studies with good results [5].

2.3.1 Three-way catalytic converter

There are two primary categories of heterogeneous catalytic reactions that occur in the 3WCC washcoat: Reduction-oxidation (redox) reactions and oxygen storage reactions. The model used in this work attempts to account for both categories, based on explicit kinetic rate expressions of the Langmuir-Hinselwood or simple Arrhenius type.

Several efforts have appeared in the literature regarding the study of automotive exhaust gas reactivity over a catalytically active washcoat and the formulation of suitable rate expressions.

Probably the most acclaimed kinetics are those determined by Voltz et al [41] for the oxidation of CO and HC on pellet-type Pt catalysts. They have been successfully used for the modeling of monolith catalytic converters with more complicated washcoat formulations, such as Pt:Rh, Pd-only, Pd:Rh and even tri-metal washcoats.

Generally, CO oxidation reactions have been more thoroughly studied for the 3WCC; a comparative study of rate expressions for CO oxidation is given by Boehman [50]. The HC oxidation is more complicated, because the real exhaust gas contains a very complex mixture of several hundreds of different hydrocarbon species. In practice, analyzers measure only the total hydrocarbon content of the exhaust gas and make no distinction of the separate hydrocarbon species. Therefore, for modeling purposes, the total hydrocarbon content of the exhaust gas is usually divided into two broad categories: easily oxidizing hydrocarbons ('fast' HC), and less-easily oxidizing hydrocarbons ('slow' HC).

For the CO-NO reaction, Subramanian and Varma [42] were the first to provide a rate expression. Pattas et al. [51] also reported an empirical rate expression for the CO-NO reaction, with variable order of reaction. The most extended reaction scheme was presented by Montreuil et al [35] for the modeling of Pt-Rh and Pd-Rh catalysts and also included a custom rate expression for CO-NO reduction. The effect of Cerium on the CO-NO reaction kinetics was also investigated from Oh [52] for Alumina supported Rhodium catalysts and from Granger et al. [53] for Platinum catalysts and power-law kinetic rate expressions were derived. The rate expressions are not usable for realistic modeling, because of the simplicity of tested washcoats and precious metal loadings.

For the present model, the complete reaction scheme, along with the rate expression for each reaction, is summarized in Table 2.1. The rates of the oxidation reactions of CO, H₂ and HC are based on the expressions by Voltz et al. The rates of the reactions are given in Table 2.1 and the inhibition factor G_1 is given in Table 2.2.

Both 'fast' and 'slow' HC species are accounted for in the reaction scheme, each being oxidized in different temperature. Throughout this work, it is assumed that

the exhaust hydrocarbon consisted of 85% ‘fast’ HC and 15% ‘slow’ HC. This is a rough approximation introduced in lack of more accurate data but, according to our experience, it gives satisfactory result. Both fast and slow hydrocarbons are represented as CH_{1.8}, since the measured average ratio of hydrogen to carbon atoms in the exhaust gas is 1.8. Thus, the two hydrocarbons are distinguished in the model only by the difference in their kinetic parameters.

The reduction of NO is mainly accomplished via reaction with CO, although other species may contribute to NO conversion (e.g. H₂ or HCs) [42]. In this work, for the reaction between CO and NO we employ the plain Langmuir–Hinshelwood reaction rate, without addition of any empirical inhibition terms.

Oxygen storage submodel Apart from the above reactions, the oxygen storage phenomena play a significant role in the efficiency of the 3WCC. Oxygen storage reactions are caused by the large quantities of Cerium (Ce) in the catalyst’s wash-coat. The 3-valent Ce oxide (Ce₂O₃) may react with O₂ or NO and oxidize to its 4-valent state (CeO₂). Under net reducing conditions, CeO₂ may function as an oxidizing agent for CO, HC and H₂. This function of Cerium has been originally investigated in the work of Herz et al. [54, 55]. The reduction of CeO₂ by O₂, CO and hydrocarbons was also studied by Theis et al. [56].

Elementary kinetic modeling of the oxygen storage phenomena has been investigated by Zhdanov and Kasemo [57], while phenomenological models, better suited for engineering reactor modeling have been presented by Herz et al. [55], Koltsakis and Stamatelos [3], and Aimard and Sorine [58].

These phenomena are taken into account by the model by five reactions for (a) Ce₂O₃ oxidation by O₂ and NO, and (b) CeO₂ reduction by CO and fast/slow hydrocarbons [2]. The model uses the auxiliary quantity ψ to express the fractional extent of oxidation of the oxygen storage component. It is defined as:

$$\psi = \frac{\text{moles CeO}_2}{\text{moles CeO}_2 + 2 \times \text{moles Ce}_2\text{O}_3} \quad (2.1)$$

The extent of oxidation ψ is continuously changing during transient converter operation. Its value is affected by the relative reaction rates of reactions. Under steady-state conditions, ψ tends asymptotically towards an ‘equilibrium’ value, where the ‘forces’ from the reactions that compete for Ceria reduction and oxidation are equalized. The system is shifted from the equilibrium point constantly, because of the rapidly changing conditions that prevail in the exhaust gas.

The rates of reactions, given in Table 2.1, are expected to be linear functions of ψ . Specifically, the oxidation rate of the oxygen storage component is assumed proportional to the active sites of Ce₂O₃, i.e. to $1 - \psi$. On the other hand, the oxidation rate of CO and HC by CeO₂ is assumed proportional to ψ . Moreover, the rates of these reactions are assumed to be linearly dependent on the local concentration of the corresponding gaseous phase reactant.

2.3.2 Diesel oxidation catalyst

For the case of the Diesel Oxidation Catalyst (DOC), only oxidation reactions will be considered in this work. NO_x conversion is not considered and generally remains an open problem, because it is a major pollutant of diesel exhaust (due to the lean burn conditions in the engine).

Reaction	Rate expression
<i>Oxidation reactions</i>	
1 $2\text{CO} + \text{O}_2 \longrightarrow 2\text{CO}_2$	$r_1 = \frac{A_1 e^{-E_1/R_g T} c_{\text{CO}} c_{\text{O}_2}}{G_1}$
2 $2\text{H}_2 + \text{O}_2 \longrightarrow 2\text{H}_2\text{O}$	$r_2 = \frac{A_2 e^{-E_2/R_g T} c_{\text{H}_2} c_{\text{O}_2}}{G_1}$
3 $\text{CH}_{1.8}(\text{fast}) + 1.4\text{O}_2 \longrightarrow$ $\longrightarrow \text{CO}_2 + 0.9\text{H}_2\text{O}$	$r_3 = \frac{A_3 e^{-E_3/R_g T} c_{\text{HCf}} c_{\text{O}_2}}{G_1}$
4 $\text{CH}_{1.8}(\text{slow}) + 1.4\text{O}_2 \longrightarrow$ $\longrightarrow \text{CO}_2 + 0.9\text{H}_2\text{O}$	$r_4 = \frac{A_4 e^{-E_4/R_g T} c_{\text{HCS}} c_{\text{O}_2}}{G_1}$
<i>NO reduction</i>	
5 $2\text{CO} + 2\text{NO} \longrightarrow 2\text{CO}_2 + \text{N}_2$	$r_5 = A_5 e^{-E_5/R_g T} c_{\text{CO}} c_{\text{NO}}$
<i>Oxygen storage</i>	
6 $2\text{Ce}_2\text{O}_3 + \text{O}_2 \longrightarrow 4\text{CeO}_2$	$r_6 = A_6 e^{-E_6/R_g T} c_{\text{O}_2} (1 - \psi)$
7 $2\text{Ce}_2\text{O}_3 + 2\text{NO} \longrightarrow 4\text{CeO}_2 + \text{N}_2$	$r_7 = A_7 e^{-E_7/R_g T} c_{\text{NO}} (1 - \psi)$
8 $\text{CO} + 2\text{CeO}_2 \longrightarrow \text{Ce}_2\text{O}_3 + \text{CO}_2$	$r_8 = A_8 e^{-E_8/R_g T} c_{\text{CO}} \psi$
9 $\text{CH}_{1.8}(\text{fast}) + 3.8\text{CeO}_2 \longrightarrow$ $\longrightarrow 1.9\text{Ce}_2\text{O}_3 + \text{CO}_2 + 0.9\text{H}_2\text{O}$	$r_9 = A_9 e^{-E_9/R_g T} c_{\text{HCf}} \psi$
10 $\text{CH}_{1.8}(\text{slow}) + 3.8\text{CeO}_2 \longrightarrow$ $\longrightarrow 1.9\text{Ce}_2\text{O}_3 + \text{CO}_2 + 0.9\text{H}_2\text{O}$	$r_{10} = A_{10} e^{-E_{10}/R_g T} c_{\text{HCS}} \psi$

Table 2.1: Reactions and rate expressions in the three-way catalytic converter

$$G_1 = T(1 + K_1 c_{\text{CO}} + K_2 c_{\text{THC}})^2 (1 + K_3 c_{\text{CO}}^2 c_{\text{THC}}^2) (1 + K_4 c_{\text{NO}}^{0.7})$$

$$K_i = k_i e^{-E_i/RT}, \quad i = 1 \dots 4$$

where :

$$k_1 = 65.5 \quad k_2 = 2080 \quad k_3 = 3.98 \quad k_4 = 4.79 \cdot 10^5$$

$$E_1 = -7990 \quad E_2 = -3000 \quad E_3 = -96534 \quad E_4 = 31036$$

Table 2.2: Inhibition term of rate expressions

Reaction	Rate expression
<i>Oxidation reactions</i>	
1 $\text{CO} + \frac{1}{2}\text{O}_2 \longrightarrow \text{CO}_2$	$r = \frac{A_1 e^{-E_1/RT} c_{\text{CO}} c_{\text{O}_2}}{G_1}$
2 $\text{H}_2 + \frac{1}{2}\text{O}_2 \longrightarrow \text{H}_2\text{O}$	$r = \frac{A_2 e^{-E_2/RT} c_{\text{H}_2} c_{\text{O}_2}}{G_1}$
3 $\text{CH}_{1.8}(\text{fast}) + 1.4\text{O}_2 \longrightarrow$ $\longrightarrow \text{CO}_2 + 0.9\beta\text{H}_2\text{O}$	$r_3 = \frac{A_3 e^{-E_3/RT} c_{\text{HCf}} c_{\text{O}_2}}{G_1}$
4 $\text{CH}_{1.8}(\text{fast}) + 1.4\text{O}_2 \longrightarrow$ $\longrightarrow \text{CO}_2 + 0.9\beta\text{H}_2\text{O}$	$r_4 = \frac{A_4 e^{-E_4/RT} c_{\text{HCf}} c_{\text{O}_2}}{G_1}$
<i>DR sorption model</i>	
Equilibrium	$\ln \vartheta_{eq} = \ln(W_0\rho) - A \left(\frac{R_g T}{\beta} \right)^2 \left(\ln \frac{p_0}{p} \right)^2$
5 HC adsorption	$r_5 = -\frac{A_5(\vartheta - \vartheta_{eq})}{M_{\text{HC}}}$
6 HC desorption	$r_6 = -\frac{A_6 e^{-E_6/R_g T} (\vartheta - \vartheta_{eq})}{M_{\text{HC}}}$

Table 2.3: Reactions and rate expressions in the diesel oxidation catalyst

For the CO and HC conversion, the rate expressions given in Table 2.3 are used. Evidently, the oxidation reactions in the DOC are assumed to have the same reaction rates expressions with the corresponding reactions of the 3WCC (Table 2.1), although the values of kinetic constants are different. The use of the same rate expressions is justified since the washcoats of the DOC contains Pt and Pd for the oxidation reactions. Thus, the active sites available for reactions in the DOC washcoat are the same with the 3WCC waschoat.

Of course, the DOC and 3WCC washcoats are not the same and, in principle, the differences in other washcoat components may influence the oxidation reactions. Nevertheless, there is empirical evidence that the oxidation rates used for the 3WCC reactions are sufficient to describe conversion efficiency in the DOC washcoat. We also include a H₂ oxidation reaction, for which the same inhibition factor for the reaction rate is used, due to lack of further data.

Finally, lean conditions (excess of oxygen) prevail in the diesel exhaust and, thus, the oxygen storage reactions are also not significant.

Diesel oxidation catalysts operate at lower tempratures than gasoline vehicle catalysts. For passenger cars, inlet temperatures at the inlet of a DOC catalyst are below 200 °C for almost all the urban part of the European Driving Cycle. For effective HC conversion, DOCs must either exhibit HC light-off temperatures below 200 °C or store hydrocarbons until light-off conditions have been reached [59].

Hydrocarbon storage is usually considered a more feasible solution and HC storage components are nowdays incorporated in the DOC washcoats. Such components are usually ZSM-5 zeolites. Hydrocarbons (especially heavier molecules) are adsorbed in the zeolite when the temperature of the converter is low and are released in higher temperatures. The objective is to release HCs at light-off temperatures, as they are subsequently burned.

The modeling complications due to the diversity of HC mixture in the exhaust gas, discussed in Section 2.3.1 for the case of the 3WCC, apply here as well. The situation complicates further because of the adsorbing properties of the washcoat's zeolite. Heavier hydrocarbon species tend to adsorb in the zeolite while lighter HC species may not adsorb. To approximate the situation, we introduce one more HC category, the adsorbable hydrocarbon. Thus, the mixture of exhaust HCs is lumped into the following three categories:

- Fast oxidizing hydrocarbons (e.g. propene), $\simeq 20\%$ of the mixture,
- Slow oxidizing hydrocarbons (e.g. propane), $\simeq 10\%$ of the mixture, and
- Adsorbable hydrocarbons (e.g. decane), $\simeq 70\%$ of the mixture.

The percentages of each HC category are due to reliable measurements [5].

No modeling attempts had been presented in the literature before this work. In this work, we formulate and test a model for HC adsorption in the zeolitic content of the DOC washcoat. It will be referred to as the Dubinin–Radushkevich adsorption model, because it employs the Dubinin–Radushkevich isotherm for the calculation of the sorption equilibrium. We initially tested this model against data from SGB tests and we finally evaluated it with data from driving cycle tests [5]. The model is illustrated below.

Dubinin–Radushkevich sorption model This model is an application of the principles of the Polanyi adsorption theory for adsorption in microporous zeolites, extended by Dubinin and Radushkevich [18]. According to this model, the adsorbate in intimate contact with the solid is in liquid form. The equation of the Dubinin–Radushkevich isotherm gives the adsorbed mass of a species when equilibrium conditions between gas phase and liquid (adsorbed) phase have been established. The equilibrium adsorbed mass ϑ_{eq} is given as a function of temperature and partial pressure of the species at gas phase:

$$\ln \vartheta_{eq} = \ln(W_0\rho) - D \left(\ln \frac{p_0}{p} \right)^2, \quad D = A \left(\frac{R_g T}{\beta} \right)^2 \quad (2.2)$$

where W_0 is the zeolite's volume fraction (i.e. the total volume of all zeolite micropores per washcoat volume); A is a constant characteristic of the pore size distribution (both depend on the zeolite only); β is the affinity coefficient, which depends on the adsorbate; ρ is the liquid phase density; p_0 is the saturation pressure; and p is the partial pressure of the adsorbate at the gas–solid interface. The dependence of the saturation pressure p_0 on the temperature is given by the Antoine equation:

$$\ln p_0 = C_1 - \ln \frac{C_2}{T + C_3} \quad (2.3)$$

where C_1 , C_2 and C_3 are constants, different for each hydrocarbon. These constants were taken from the related literature [60].

The mass of hydrocarbon ϑ that is adsorbed at each time instance in the washcoat may, or may not be equal to the equilibrium adsorbed mass ϑ_{eq} . Normally, ϑ and ϑ_{eq} are different because of the continuous variation of the exhaust gas conditions. Therefore, adsorption or desorption occurs as the washcoat–exhaust gas system tends to move towards the equilibrium point. We assume that the rate towards equilibrium is proportional to the ‘distance’ between the current point and the equilibrium (dictated by temperature and gas-phase conditions).

Then, the HC sorption rate per washcoat volume is:

$$r_{srp} = -\frac{k_{srp}(\vartheta - \vartheta_{eq})}{M_{HC}} \quad (2.4)$$

It is noted that, according to the Dubinin–Radushkevich approach, the ϑ rate of change is expressed in [mol/(m³washcoat·s)], i.e. per unit washcoat volume and *not* per unit catalytic area, as with the rest heterogeneous reactions. This is because of the assumption that the adsorbed HC is in liquid form in the whole zeolite volume.

The proportionality factor k_{srp} is a sorption rate which is constant in the case of adsorption:

$$k_{srp} = A_5 (= const), \quad \vartheta < \vartheta_{eq} \quad (2.5)$$

but exhibits an exponential temperature dependence in case of desorption:

$$k_{srp} = A_6 e^{-E_6/R_g T}, \quad \vartheta > \vartheta_{eq} \quad (2.6)$$

since desorption is an activated process but adsorption is not [28]. The rate expressions of adsorption–desorption according to the DR model are summarized in Table 2.3.

2.4 Washcoat level modeling

The task of washcoat modeling is to define how the simultaneous phenomena of diffusion and reactions in the washcoat will be accounted for by the model. As previously stated, the detailed calculations of mass transfer through the washcoat are avoided. Instead, the “film model” approximation is employed, which is essentially a zero-dimensional approach.

The film model approach to the problem has been used in several engineering models that have appeared in the literature. In this work, it has been modified to include an effectiveness factor, aiming at the investigation of the diffusion phenomena in the washcoat. More importantly, the modeling of storage phenomena in the washcoat of both the 3WCC and the DOC has been significantly advanced. The original approach, which was based on the work of Koltakis and Stamatelos [3, 4], has been thoroughly improved and corrected. This has enabled us to obtain analytical solutions to the respective equations, therefore enhancing the stability and accuracy of the resulting model.

2.4.1 Mathematical model formulation

The film model approximation assumes that species from each channel’s bulk gas flow diffuse down to a hypothetical catalyst solid–gas interface, through the boundary layer of the gas flow. At the chemically active solid–gas interface, chemical

species may react or be stored/released. This approximation essentially neglects the concentration gradients due to diffusion resistance in the washcoat, taking into account only the mass transport resistance of the boundary layer.

This has been questioned by Zygourakis & Aris [43] and Hayes & Kolaszowski [11]. They provide evidence that concentration gradients in the washcoat are present and may significantly affect the operation of the monolithic converter, especially in high temperatures. Nevertheless, significant complexity is introduced in the models in order to explicitly consider diffusion in the washcoat. Therefore, the phenomenon is usually lumped into the kinetics of the model.

In our model, information about concentration profiles through the washcoat is extracted with approximate analytical calculations. The results are incorporated in the model using an effectiveness factor approach.

Specifically, the mass balance that expresses the film model approximation for the solid–gas interface states that all *gaseous-phase* species that diffuse to it are removed from the gas phase due to reactions:

$$\frac{\rho_g}{M_g} k_{m,j} S(c_j - c_{s,j}) = R_j \quad (2.7)$$

The above equation for the film model approximation is only valid for the species of the gaseous phase. For the species in the *solid-phase*, notably Ceria or adsorbed hydrocarbon, a second mass balance is required. For the 3WCC washcoat, the extra mass balance should state that the total mass of CeO₂ (or Ce₂O₃) component in the washcoat changes according to the rate that Ceria is oxidized or reduced.

$$R_{\text{CeO}_2} = \delta S \Psi_{cap} \frac{d\psi}{dt} \quad (2.8a)$$

$$R_{\text{Ce}_2\text{O}_3} = 0.5 \delta S \Psi_{cap} \frac{d(1 - \psi)}{dt} \quad (2.8b)$$

The above two balances are equivalent because the total amount of Ceria in the washcoat remains constant and thus:

$$R_{\text{CeO}_2} + 2R_{\text{Ce}_2\text{O}_3} = 0 \quad (2.9)$$

The quantity Ψ_{cap} is defined as [mol Ce/m³washcoat] and is commonly referred to as the the total oxygen storage capacity. Its value may be estimated by the content of Ceria in the washcoat.

The respective mass balance for the adsorbed hydrocarbon of the DOC washcoat should similarly state that the adsorbed mass should change according to the balance between adsorption and desorption reactions.

$$R_{\text{HCads}} = \delta S \frac{W_0}{M_{HC}} \frac{d\vartheta}{dt} \quad (2.10)$$

The *species* rate R_j of the above equations is the rate that some species j is produced or consumed because of reactions, storage/release or adsorption/desorption phenomena at the solid–gas interface. It is expressed per channel volume [mol/(m³washcoat·s)], in order to facilitate its use by the channel model (see Section 2.5). The product δS that appears in equations (2.8) and (2.10) has dimensions of [m³washcoat/m³channel]. Thus, δS converts between quantities expressed per washcoat volume and quantities expressed per channel volume (see also below).

The calculation of the species rate R_j is connected with (but different from) the reaction rate r_k . For N_R reactions, each taking place with a rate r_k , the rate R_j of consumption/production of some species j is:

$$R_j = \delta S \gamma \sum_{k=1}^N a_{j,k} \eta_k r_k \quad (2.11)$$

In the above equation:

- η_k is an effectiveness factor, which accounts for diffusion in the washcoat. Its calculation is discussed in Section 2.4.4.
- $a_{j,k}$ is the stoichiometric coefficient of species j in reaction k .
- γ is the specific catalyst area, i.e. catalytically active area per washcoat volume.
- δ is the washcoat thickness, which should be more accurately interpreted as ratio between the washcoat volume to channel wall (film) area [$\text{m}^3\text{washcoat}/\text{m}^2\text{film}$].
- S is the geometrical surface area of the washcoat, i.e. channel wall (film) area per channel volume [$\text{m}^2\text{film}/\text{m}^3\text{channel}$]. For a channel with hydraulic diameter d_h , we readily find: $S = 4/d_h$.

The essence of the washcoat submodel is the solution of the system of equations defined by (2.7) plus one of the equations (2.8) or (2.10). Reactions are assumed to occur in the washcoat under steady-state conditions, namely, under steady temperature T and concentrations $c_{s,j}$ at the solid–gas interface. The steady state conditions prevail for a small time period Δt . (This time period is equal to the temporal discretization interval dt which is imposed by the channel and reactor model.) The goal is to calculate the gaseous-phase concentrations $c_{s,j}$ as well as the quantities ψ and ϑ , which may be viewed as the solid-phase concentrations and indicate the status of the respective storage components of the washcoat.

A significant difficulty in this problem is that the rates of the storage reactions (the oxygen storage reactions of the 3WCC or the hydrocarbon sorption reactions of the DOC) are time-dependent. Transient terms are introduced because the reaction rates for the oxygen storage submodel and the hydrocarbon sorption model are functions of the quantities ψ and ϑ respectively, which indicate the ‘status’ of the storage component. Under steady-state conditions, these quantities tend asymptotically towards an equilibrium value. Therefore, the storage reaction rates vary as the system moves towards the equilibrium point.

Thus, the total consumption of each species that is involved in these reactions depends on both the starting and the final conditions of the system, i.e. on the starting and final value of ψ or ϑ . The dependence of storage reactions rates on time t should be contrasted with the reaction rates of the gaseous-phase species, which depend solely on the final conditions of the system (calculated by (2.7)) and, thus, are *not* a function of time.

To tackle the problem numerically, one could exploit the fact that the small time Δt (for which the steady-state conditions are assumed and the solution is pursued) is essentially the discretization interval used by the channel and reactor level modeling. Then, the straightforward solution would be to discretize (2.8) and proceed with the

numerical computation. This proves unsatisfactory, though, because the storage phenomena are faster than the heat and mass transfer phenomena accounted for by the channel and reactor level models. Therefore, a very small time step would be required, slowing down the solution process.

A workable practice to avoid slow calculation speed would be to use a second time scale and separately solve the initial value problem defined by one of the equations (2.8). This would yield a solution for ψ that could be inserted in the storage rates used in (2.11). Indeed, this has been the initial solution given to the problem [3, 4].

Nevertheless, it was realized in the process of this work that an analytical solution for the temporal profile of ψ over the time scale defined by Δt may be obtained from (2.8). The details of the analytical solution for the 3WCC and the DOC cases are given in the Sections 2.4.2 and 2.4.3 that follow. Assuming that we are able to analytically calculate the profiles for ψ , an effective (averaged) rate \bar{r}_k may be defined:

$$\bar{r}_k = \frac{1}{\Delta t} \int_{t_0}^t r_k dt, \quad \Delta t = t - t_0 \quad (2.12)$$

Then, the calculation of the rate for species production/depletion may be modified as follows:

$$R_j = \delta S \gamma \sum_{k=1}^N a_{j,k} \eta_k r_k + \delta S \sum_{k=1}^N a_{j,k} \bar{r}_k \quad (2.13)$$

The second sum of the right-hand side represents the rate of production or depletion of some species j because of storage reactions. The averaged rates \bar{r}_k are employed, while the terms γ and $\eta_{j,k}$ have been omitted. As mentioned in Section 2.3.1 the rates of oxygen storage reactions are expressed directly per volume washcoat and the specific catalyst area γ is not significant. The same is true for the adsorption/desorption rates of the Dubinin–Radushkevich sorption model (cf. Section 2.3.2). Further more, diffusion effects are also not included in the storage submodels and the effectiveness factors are not present in the second sum of (2.13).

The above analysis has reduced the problem so that only the solution of (2.7) is required, where the species rates are calculated from (2.13) instead of (2.11). Equation (2.7) expresses the balance between diffusion and reaction of the gaseous-phase species. It defines a system of equations that are non-linear functions of the concentrations c_j . This system is solved for c_j using the Newton-Raphson method for nonlinear systems of equations [61]. Finally, the details for the analytical calculation of ψ , which is needed for the calculation of \bar{r}_k in (2.13) are detailed below.

2.4.2 Calculation of stored oxygen in the 3WCC washcoat

The analytical solution for the calculation of the fractional extent of Ceria oxidation ψ may be developed from either (2.8a) or (2.8b). Using (2.8a), the rate for CeO_2 may be written as a function of the rates of the oxygen storage reactions:

$$R_{\text{CeO}_2} = \delta S \Psi_{cap} \frac{d\psi}{dt} = \delta S \sum_{k=1}^{N_R} a_{\text{CeO}_2,k} r_k$$

When the reaction rates r_k are substituted, the above equation is written as:

$$\Psi_{cap} \frac{d\psi}{dt} = a_{ox}(1 - \psi) - a_{red}\psi \quad (2.14)$$

where a_{ox} and a_{red} are defined as:

$$\begin{aligned} a_{ox} &= +4k_6c_{O_2}(1 - \psi) + 4k_7c_{NO}(1 - \psi) \\ a_{red} &= -2k_8c_{CO}\psi - 3.8k_9c_{HCF}\psi - 3.8k_{10}c_{HCS}\psi \end{aligned}$$

Equation (2.14) is an ordinary differential equation that may be solved easily with the initial condition that at $t = t_0$, $\psi = \psi_0$, to yield the profile of ψ over a time period $\Delta t = t - t_0$:

$$\psi = \frac{a_{ox}}{a_{ox} + a_{red}} - \frac{a_{ox} - (a_{ox} + a_{red})\psi_0}{a_{ox} + a_{red}} e^{-(a_{ox} + a_{red})\Delta t} \quad (2.15)$$

The above solution is not used directly in the model. Instead, it is employed to compute the reaction rates involved in the oxygen storage reactions. Specifically, having solved for ψ , the following integrals may be calculated:

$$\begin{aligned} \int_{t_0}^t \psi dt &= \frac{1}{a_{ox} + a_{red}} \\ &\times \left[a_{ox}\Delta t - \left(\frac{a_{ox}}{a_{ox} + a_{red}} - \psi_0 \right) \Psi_{cap} \left(1 - e^{-\frac{(a_{ox} + a_{red})\Delta t}{\Psi_{cap}}} \right) \right] \end{aligned} \quad (2.16a)$$

$$\begin{aligned} \int_{t_0}^t (1 - \psi) dt &= \frac{1}{a_{ox} + a_{red}} \\ &\times \left[a_{red}\Delta t + \left(\frac{a_{ox}}{a_{ox} + a_{red}} - \psi_0 \right) \Psi_{cap} \left(1 - e^{-\frac{(a_{ox} + a_{red})\Delta t}{\Psi_{cap}}} \right) \right] \end{aligned} \quad (2.16b)$$

The above integrals are subsequently used to calculate the averaged rates \bar{r}_k . For reactions 6 and 7 of Table 2.1, which involve Ce_2O_3 oxidation, these rates are:

$$\bar{r}_6 = A_6 e^{E_6/R_g T} c_{O_2} \int_{t_0}^t (1 - \psi) dt \quad (2.17)$$

$$\bar{r}_7 = A_7 e^{E_7/R_g T} c_{NO} \int_{t_0}^t (1 - \psi) dt \quad (2.18)$$

while the corresponding rates for the reactions 8–10 of the same table, which account for CeO_2 reduction, become:

$$\bar{r}_8 = A_8 e^{E_8/R_g T} c_{CO} \int_{t_0}^t \psi dt \quad (2.19)$$

$$\bar{r}_9 = A_9 e^{E_9/R_g T} c_{HCF} \int_{t_0}^t \psi dt \quad (2.20)$$

$$\bar{r}_{10} = A_{10} e^{E_{10}/R_g T} c_{HCS} \int_{t_0}^t \psi dt \quad (2.21)$$

2.4.3 Calculation of stored hydrocarbon in the DOC washcoat

The analytical calculation of the adsorbed hydrocarbon content of the DOC washcoat may be obtained analogously with the analytical calculations for the oxygen storage of the 3WCC. The mass balance to be solved for ϑ is:

$$\frac{\partial \vartheta}{\partial t} = -k_{srp}(\vartheta - \vartheta_{eq}) \quad (2.22)$$

which is solved for the initial condition: $\vartheta = \vartheta_0$ for $t = t_0$ to yield:

$$\vartheta = \vartheta_{eq} + (\vartheta - \vartheta_{eq})e^{-k_{srp}\Delta t} \quad (2.23)$$

The averaged sorption rates, \bar{r}_5 and \bar{r}_6 , may be subsequently obtained by integrating the above profile of ϑ over Δt .

2.4.4 Diffusion in the washcoat

Coupled diffusion and reaction in porous catalysts is an old problem in the chemical engineering science. The diffusion–reaction problem was first studied for porous catalyst particles, where a chemical reaction process occurred within the pores of the particle. It was understood that, in many cases, the observed reaction rates were less than the intrinsic reaction rates, because the interior surfaces were exposed to lower reactant concentrations than the bulk concentrations. Such mass transfer limitations were due to slow diffusion of reactants to the catalytically active sites.

In general, the subject has attracted much interest, because, as stated by Satterfield [62]:

... When gradients caused by diffusion are significant, a “falsification of kinetics occurs in the sense that the rate and selectivity of reaction change with bulk concentration and temperature in a different manner than they would in the absence of such gradients.

Furthermore:

... The scientist or engineer engaged in research or development needs to be able to conduct chemical kinetics studies free of physical transport limitations, if possible, in order to interpret his results correctly. [...] The engineer concerned with development, design and operation of reactors needs to be aware of what changes in conversion and selectivity may occur as he changes scale or alters operation parameters.

The problem of quantitative prediction of the overall reaction rate of a catalytic particle as a function of the intrinsic reaction rate was first solved by Thiele [63], for isothermal flat plates and spherical particles. He analytically computed the ratio of observed kinetics (at the particle’s surface) to intrinsic kinetics:

$$\eta(\phi) = \frac{r}{r_{intrinsic}}. \quad (2.24)$$

η has been termed the *effectiveness factor* or *utilization factor* and ϕ is a dimensionless number, now called the *Thiele modulus*; ϕ is a function of intrinsic reaction rate and diffusivity of the reactant in the particle. Later, Weisz and Hicks [64] numerically solved the same problem for *non-isothermal* catalyst particles and Aris [65] extended Thiele’s solution for isothermal particles of irregular shape.

The above investigations concern the steady-state chemical reactor operation. They managed to fully take into account the effect of diffusion on

- the sizing of the reactor
- the computation of the effect of operating parameters of the reactor.

An extension to the transient reactor of our case with the multitude of reacting species would be overwhelming. A simplified first step was realized by Zygourakis and Aris [43] who studied the Voltz oxidation reactions on steady-state conditions in a small part of the channel (zero-dimensional approach).

Our initial objective was to investigate the possibility to extract approximate analytical solutions that would take into account this type of effects in quasi-steady state. This was supposed to produce solutions closer to the experimental behaviour, without significantly increasing the computation time.

The results of these investigations are summarized in the Appendix A. In the final stages of this work, the significant improvements in the reaction scheme and oxygen storage submodel, in conjunction and synergy with the genetic algorithm tuning methodology, produced results of remarkable quality. The demonstration of such accuracy in the prediction of the behaviour of the 3WCC invalidated the hypothesis that diffusion was the primary cause of the observed discrepancies between predictions and measurements.

However, there exists one more reason to include certain aspects of diffusion effects in the model, that is, the incorporation in the model of some capability to assess the effect of precious metal loading on the kinetics parameters. Therefore, the well-known approach of Thiele is adopted, with certain additional assumptions as presented below.

We concentrate to one point in the axial direction of the channel (z direction) and we consider one chemical species that diffuses from the exhaust gas into the washcoat. The species is assumed to diffuse along an axis x perpendicular to the monolith's side and to react following a first-order law. Thus, a concentration profile is established in the washcoat. We are not interested in the details of the profile but only in the rate of production or depletion of the species from the gas at the gas–solid interface, which is:

$$W_s = \frac{R}{S} = -D_{\text{eff}} \frac{dc}{dx} \Big|_{x=0} \quad (2.25)$$

In the case that the diffusion is isothermal, it is trivial to compute W_s , solving the mass transport balance equation:

$$D_{\text{eff}} \frac{d^2c}{dx^2} - rca = 0 \quad (2.26)$$

subject to the boundary conditions $c(x = 0) = c_s$ (where c_s is the concentration of the species at the washcoat–gas interface) and $dc/dx|_{x=\delta}=0$ (adiabatic washcoat–substrate interface). We find that:

$$\frac{dc}{dx} \Big|_{x=0} = -c_s \phi \delta^{-1} \tanh \phi, \quad (2.27)$$

$$\phi = \sqrt{\frac{r\alpha}{D_{\text{eff}}}} \delta \quad \text{being the Thiele modulus.} \quad (2.28)$$

Thus, the real rate of production or depletion of the species from the gas–solid interface is:

$$W_s = D_{\text{eff}} c_s \phi \delta^{-1} \tanh \phi \quad (2.29)$$

If all the catalyst active sites were available at the washcoat–gas interface (or, equivalently, if there were no diffusion resistances in the washcoat), the ideal rate of production or depletion of the species from the gas flow would be calculated as:

$$W_{s0} = rc_s \alpha \delta \quad (2.30)$$

W_{s0} is the maximum feasible rate. This is also the rate calculated by the models based on the gas–solid interface assumption. In order to correct W_{s0} to its real value W_s , we use the effectiveness factor, defined as the ratio of the two rates. We arrive then at the classical result:

$$\eta = \frac{W_s}{W_{s0}} = \frac{\tanh \phi}{\phi} \quad (2.31)$$

which gives for the correct production/depletion rate:

$$W_s = \frac{\tanh \phi}{\phi} W_{s0} \quad (2.32)$$

If we assume that the area of the precious metal particles per unit washcoat volume α is proportional to the PM loading w , (which corresponds to similar dispersion patterns of the precious metal), we may note from (2.29) or (2.32) that W_s is approximately proportional to the square root of the PM loading (if the term $\tanh \phi$ is neglected, which is usually justifiable). This may be contrasted to the direct proportionality dependence that is implied by the direct application of (2.30).

The above also lead to a rule of thumb for 3WCC models based on the on the gas–solid interface assumption. If such a model were tuned against data from a catalytic converter with PM loading w_0 , in order to predict a catalytic converter with a different PM loading w , its apparent kinetics should be roughly modified by a factor $\sqrt{w/w_0}$.

The above analysis is exact for a single species that dissociates isothermally in the catalytic washcoat, following a first order reaction rate. Zygourakis & Aris [43] have observed that the validity of isothermal washcoat assumption is suggested by the Prater relationship:

$$T - T_s = -\frac{\Delta H D_{\text{eff}}}{\lambda} (c - c_s) . \quad (2.33)$$

For reactant concentrations encountered in the automotive exhaust, the temperature change in the washcoat is less than 1 °C. Using finite-element analysis, also Hayes & Kolaczkowski [11] have concluded that the 3WCC washcoat can be considered as isothermal.

However, in the case of the catalytic converter washcoats, we have many different species simultaneously diffusing in the washcoat and participating in more than one reaction. Moreover, the rate expressions are not exactly of the first order, because of the inhibition term G_1 . Thus, the application of (2.32) is not rigorous for catalytic converter washcoats and must be considered as just a rough approximation.

2.5 Channel model

The channel model presented here is a transient, one-dimensional model, based on the models of Koltsakis et al [3] and Koltsakis & Stamatelos [4]. It is the same

regardless of the catalytic converter type (3WCC, DOC or any other converter), because no washcoat-level information is explicitly required by the channel model.. The assumptions involved in the model are given first and their validity is discussed. The model is then formulated as a system of balance equations for heat and mass transport along the channel.

As summarized by Keren & Sheintuch [46] and Siemund et al [33], the most usual simplifications employed for the formulation of channel models are the following:

1. The axial diffusion of mass and heat in the gas phase is negligible.
2. The mass and heat accumulation in the gas phase is negligible.
3. The transient response of exhaust gas flow and of mass in the washcoat is negligible. (This comprises the assumption for the quasi-steady state nature of the problem.)

The first two assumptions are generally accepted and are employed in most models, e.g. those of Chen et al. [34] and Siemund et al. [33]. The applicability of the quasi-steady state assumption has been discussed by Young & Finlayson [45] and Oh & Cavendish [30]. It is justified since the ratio of thermal to mass time constants is large—in other words, mass transfer phenomena are much faster than thermal phenomena.

In order to write the mass balance for the exhaust gas, a mean bulk value c_j is employed for the gas-phase concentration of each species. Likewise, a value $c_{s,j}$ is considered for the concentration of each species at the active interface. Using the quasi-steady state approximation and neglecting accumulation and axial diffusion terms, the mass balance for the gas phase becomes:

$$\rho_g u_z \frac{\partial c_j}{\partial z} = \rho_g k_{m,j} S(c_j - c_{s,j}) \quad (2.34)$$

The mass transfer coefficient $k_{m,j}$ above is employed for the species diffusion through the flow boundary layer and the washcoat. The mass transfer coefficient for each species is given as a function of the Nusselt and Sherwood dimensionless numbers for the channel of the monolith.

For the energy balance in the catalytic converter channels, similarly to the above, a mean bulk value T_g is used for the exhaust gas temperature, and a solid phase temperature T_s is introduced for the monolith and the solid–gas interface. Energy is transferred to and from the exhaust gas only due to convection with the channel walls. Thus, the energy balance for the gas phase becomes:

$$\rho_s c_p u_z \frac{\partial T_g}{\partial z} = h S(T_s - T_g) \quad (2.35)$$

All the above equations are subject to the following boundary condition at the inlet of the channel:

$$u_z(t) = u_z^{in}(t) \quad (2.36)$$

$$T_g(z = 0, t) = T_g^{in}(t) \quad (2.37)$$

$$c_j(z = 0, t) = c_j^{in}(t) \quad (2.38)$$

2.6 Reactor model

The reactor model described in this work is an one-dimensional heat transfer model for the transient heat conduction in the monolith. The primary assumptions for the formulation of the reactor models concern the heat losses to the ambient air and the inlet gas distribution:

- Heat losses from the front and the rear face of the monolith are neglected in all models that have appeared in the literature.
- Heat losses from the monolith's side face are sometimes neglected in simpler models. In more sophisticated models they are taken into account. In 1D models, heat losses are inevitably distributed uniformly in each monolith's cross-section.
- The flow rate and temperature profiles of the exhaust gas at the inlet of the filter are usually considered uniform unless they are measured.

Many two- and three- dimensional reactor models have appeared in the literature, e.g. the models of Heck et al. [66]; Chen et al. [34]; Zygourakis [47]; Jahn et al. [67]; Taylor [68]. These models are indispensable if the exhaust gas at the converter inlet exhibits a severely nonuniform flow profile. In most of the cases, though, the one-dimensional approach is usually adequate and is therefore preferred for simplicity and low computational cost, especially since 3D effects may be also lumped inside the tunable kinetics parameters.

The one-dimensional temperature field in the converter is described by the equation of transient heat conduction in the solid phase, with heat sources being convection from the exhaust gas, convection to ambient air and the enthalpy released/absorbed by chemical reactions and sorption phenomena.

$$\rho_s c_{ps} \frac{\partial T_s}{\partial t} = k_{s,z} \frac{\partial^2 T_s}{\partial z^2} + hS(T_g - T_s) + \sum_{k=1}^{N_R} (-\Delta H_k \gamma r_k) + \sum_{k=1}^{N_R} (-\Delta H_k \bar{r}_k) + \dot{Q}_{amb} \quad (2.39)$$

where \dot{Q}_{amb} represents the heat losses to ambient air, which are distributed uniformly across the filter because the model is one-dimensional.

$$\dot{Q}_{amb} = h_{amb} (T_s - T_{amb}) + \epsilon \sigma (T_s^4 - T_{amb}^4) \quad (2.40)$$

2.7 Tunable parameters of the model

It is evident from the description of the monolithic catalytic converter model that the equations of the channel and reactor model do not contain many tunable parameters. Almost all tunable parameters are introduced by the chemical description of the catalyst, because this type of modeling relies on simplified rate expressions for apparent chemical kinetics.

Kinetics model Although the kinetics model contains a lot of tunable parameters, not all of them are tuned. Previous experience suggests that it is sufficient to tune only a subset of the tunable parameters of the model. Specifically:

1. Every reaction j introduces two tunable parameters, its pre-exponential factor A_j and its activation energy E_j . It must be noted that the H₂ oxidation parameters are not tuned. H₂ is contained in the exhaust gas in small quantities and its conversion is not measured. The H₂ oxidation reaction is included in the model, though, in order to account for its exothermy. Due to lack of data, we may not tune H₂ oxidation kinetics reliably, and we assume that its kinetics are approximately equal to the CO oxidation kinetics.
2. In principle, the parameters k_i and E_i ($i = 1 \dots 4$) of the inhibition term G_1 are also tunable. The expression for G_1 and its coefficients were determined originally in the work of Voltz et al. [41], which was performed on a Pt-Al₂O₃ pelleted catalyst. Nevertheless, they have been successfully used to model oxidation reactions on very different catalyst systems. Therefore, the parameters of the inhibition term G_1 are also not allowed to vary, to keep complexity at reasonable levels. Instead, the values specified in the original work of Voltz et al. are retained. They are given in Table 2.2.
3. In the oxygen storage submodel of the 3WCC, apart from the corresponding reaction kinetics, the oxygen storage capacity of the washcoat Ψ_{cap} is tuned.
4. In the Dubinin–Radushkevich sorption model, the equilibrium equation (2.2) introduces only one tunable parameter: The ratio A/β^2 . In practice, A is held constant at a value of $A = 10^{-9}$ and the value of β is tuned.
5. Again in the Dubinin–Radushkevich submodel, the rates towards equilibrium are tunable parameters. Adsorption introduces only one parameter: A_{ads} . Desorption introduces the corresponding A_{des} as well as the activation energy of desorption E_{des} , since this is an activated process.

Channel model If the diffusion in the washcoat is totally neglected, the channel model does not introduce any tunable parameters. In the case we include diffusion calculations, the effective diffusivity D_{eff} of the exhaust gas in the washcoat is needed. D_{eff} is usually an empirical function of temperature, which is determined experimentally. As we the case of the inhibition factor G_1 , we do not tune the parameters of the expression but rely on information from the literature.

Reactor model The 1D reactor model contains only one tunable parameter: the coefficient of convection between the catalyst and the ambient air h_{amb} . The value of h_{amb} is adjusted from the thermal response of the converter but, practically, the catalytic converters in automotive applications are well insulated and therefore the model is not very sensitive to this parameter.

What we seek for is to take into account all important phenomena that influence the operation of the monolithic catalytic converter while, in the same time, we avoid tuning every parameter that is incorporated in the model. We keep the number of tunable parameters to a minimum that is capable of demonstrating the degrees of freedom recognized in real world catalytic converter operation.

This is a vital point in good modeling practice. The excessive increase of the tuned system's degrees of freedom does not necessarily guarantee improved model performance. On the contrary, focus to the most important influences is lost, which is the essence of the engineering models.

Therefore, we only tune the parameters to which the model exhibits high sensitivity. For the rest, we include the influence in the model but we rely on standard literature values. Lack of accurate tuning cannot be compensated with the increase of tunable parameters. This provided the motivation to investigate ways to tune the model accurately and robustly. The methodologies that we developed are presented in Chapter 4.

2.8 Conclusions

Summarizing the model development, the kinetics, washcoat, channel and reactor level models of the catalytic converters are four well-defined and cooperating modules that form CATRAN, a complete model for the operation of catalytic converters for both spark-ignition and compression-ignition engine exhaust. CATRAN has become a commercial product of the Laboratory of Thermodynamics and Thermal Engines (LTTE), University of Thessaly [69] and is currently in use by several industrial partners as an engineering tool for the optimization of exhaust aftertreatment systems.

The model may be employed as a stand-alone command-line program, or may be used through a graphical Matlab/Simulink front-end. The latter has been developed in cooperation with an industrial partner to facilitate communication with models of the other components of the engine-piping-aftertreatment devices system and allow for computer-aided engineering.

The model is complemented by a second code for the estimation of its tunable parameters employing full-scale reference measurements. The parameter estimation code, which is based on a custom genetic algorithm optimization procedure and a suitable performance measure definition, was a separate aspect of this thesis, and it is developed in Chapter 4.

Further support to the model is provided by a set of tools for the pre- and post-processing and, most importantly, for the quality assurance of the measured (input) data, which is currently under development by other workers in LTTE [70]. These tools are implemented as Visual Basic for Applications (VBA) code under the Microsoft Excel development environment and are expected to further increase the quality of the whole modeling methodology, and provide directions for further improvements of the model.

2.9 Summary

- An engineering model has been formulated for the operation of the monolithic catalytic converter. The model is based on the principle of minimization of the degrees of freedom and the elimination of any superfluous complexity in general.
- The model consists of four major modules, that are suggested by the structure

and operating principles of the catalytic converter. The modules deal with kinetic modeling, washcoat modeling, channel modeling and reactor modeling.

- Two different kinetic models have been presented, for the three-way catalytic converter and the diesel oxidation catalyst respectively. The corresponding reaction schemes employ overall reactions and phenomenological rate expressions that are based on the Langmuir–Hinshelwood formalism. Moreover, each kinetics model includes a storage mechanism, which accounts for the oxygen storage on the 3WCC washcoats and the hydrocarbon storage in the zeolite-containing DOCs. The storage submodel rate expressions have been improved and new storage reactions have been introduced.
- Modeling at the washcoat level features several advances in regard to the storage phenomena of both the 3WCC and the DOC. The balance equations of the stored species have been clarified and corrected. Analytical solutions to the respective equations have been subsequently obtained, which enhance the stability and accuracy of the resulting storage models.
- An effectiveness factor approach has been introduced in the model for the investigation of the diffusion phenomena in the washcoat of the monolithic catalytic converter. As a first approximation, simplified analytical solutions have been incorporated in the model. The incorporation of the effectiveness factor allowed the estimation of the influence of diffusion phenomena in the overall performance of the catalytic converter model.
- The resulting model contains a number of tunable parameters, which primarily stem from the phenomenological rate expressions of the kinetics submodel. The most important tunable parameters have been identified and the need to develop a computer-aided procedure for their estimation has been recognized.

List of symbols

Roman Letters

a	Stoichiometric coefficient, [–]
A	Pre-exponential factor of reaction rate expression, [mol·K/(m ² s)]
c	Concentration in the gas phase, [–]
c_s	Concentration in the gas phase at the solid–gas interface, [–]
c_p	Specific heat capacity, [J/(kgK)]
d_h	Hydraulic diameter, [m]
D_{eff}	Effective diffusivity [mol/(m·s)]
E	Activation energy of reaction rate expression, [J]
G	Inhibition term (Table 2.2), [K]
ΔH	Molar heat of reaction, [J/mol]
h	Convection coefficient, [W/(m ² s)]
k_m	Mass transfer coefficient, [m/s]
k_{srp}	Sorption rate factor, [mol/(m ³ washcoat·s)]
K	Factor in the inhibition term (Table 2.2)
M	Molecular mass, [kg/mol]
N	Number of reactions, [–]
p	Pressure, [Pa]
\dot{Q}_{amb}	Heat convected to/from the ambient air, [J/(m ³ s)]
r	Reaction rate, [mol/(m ³ washcoat·s)]
\bar{r}	Averaged reaction rate, [mol/(m ³ washcoat·s)]
R_g	Universal gas constant, 8.314 [J/(mol·K)]
R	Rate of species production/depletion, [mol/(m ³ s)]
S	Geometric surface area per unit reactor volume, [m ² /m ³]
t	Time, [s]
T	Temperature, [K]
u_z	Exhaust gas velocity, [m/s]
w	Precious metal loading, [–]
W_s	Rate of species production/depletion per unit area (at the solid–gas interface), [mol/(m ² s)]
W_0	Zeolite volume fraction (m ³ zeolite pores/m ³ washcoat), [–]
x	transverse direction (perpendicular to channel's side), [m]
z	axial direction, [m]

Greek Letters

γ	Catalytic surface area per unit washcoat volume, [m ² catalytic area/m ³ washcoat]
β	Affinity coefficient, [–]
δ	Washcoat thickness, [m]
ε	Emissivity factor (radiation), [m ⁻¹]
η	Effectiveness factor, [–]
ϑ	Mass of adsorbed hydrocarbon at the DOC washcoat, [kg/m ³ washcoat]
λ	Thermal conductivity, [W/(m·K)]
ρ	Density [kg/m ³]
σ	Stefan–Boltzmann constant, [W/(m ² ·T ⁴)]

ϕ	Thiele modulus, [–]
ψ	Fractional extent of the oxygen storage component oxidation, [–]
Ψ_{cap}	Washcoat capacity of the oxygen storage component, [mol/m ³]

Subscripts/superscripts

<i>ads</i>	adsorption
<i>amb</i>	ambient
<i>des</i>	desorption
<i>eq</i>	equilibrium
<i>g</i>	gas
<i>in</i>	inlet
<i>j</i>	species index
<i>k</i>	reaction index
<i>s</i>	solid–gas interface
<i>srp</i>	sorption

Abbreviations

3WCC	Three-way catalytic converter
DOC	Diesel oxidation catalyst
HC	Hydrocarbon

References

- [1] G. C. Koltsakis and A. M. Stamatelos. Catalytic automotive exhaust aftertreatment. *Prog. Energy Combust. Sci.*, 23:1–39, 1997.
- [2] G. N. Pontikakis and A. M. Stamatelos. Three-way catalytic converter modelling as a modern engineering design tool. *ASME Transactions: Journal of Engineering for Gas Turbines and Power*, 2003. (*Submitted*).
- [3] G. C. Koltsakis, P. A. Konstantinidis, and A. M. Stamatelos. Development and application range of mathematical models for automotive 3-way catalytic converters. *Applied Catalysis B (Environmental)*, 12(2–3):161–191, 1997.
- [4] G. C. Koltsakis, P. A. Konstantinidis, and A. M. Stamatelos. Three-way catalytic converter modeling and applications. *Chemical Engineering Communications*, 164:153, 1998.
- [5] G. Pontikakis, G. Koltsakis, A. Stamatelos, R. Noirot, Y. Aglianay, H. Colas, and P. Versaevel. Experimental and modeling study on zeolite catalysts for diesel engines. In *CAPOC V, Fifth International Congress on Catalysis and Automotive Pollution Control*, Brussels, 2000.
- [6] J. Schmidt, A. Waltner, G. Loose, A. Hirschmann, A. Wirth, W. Mueller, J. van den Tillaart, L. Mussmann, D. Lindner, J. Gieshoff, K. Umehara, M. Makino, K. P. Biehn, and A. Kunz. The impact of high cell density ceramic substrates and washcoat properties on the catalytic activity of three way catalysts. *SAE paper 1999-01-0272*, 1999.
- [7] R. Domesle, D. Lindner, W. Mueller, L. Mussmann, M. Votsmeier, E. S. Lox, T. Kreuzer, M. Makino, and C. D. Vogt. Application of advanced three-way catalyst technologies on high cell density ultra thinwall ceramic substrates for future emission legislations. *SAE paper 2001-01-0924*, 2001.
- [8] C. N. Satterfield. *Heterogeneous Catalysis in Practice*. McGraw-Hill, 1980.
- [9] R. J. Farrauto and R. M. Heck. Catalytic converters: State of the art and perspectives. *Catalysis Today*, 51:351–360, 1999.
- [10] D. Lindner, L. Mußmann, J. A. A. van den Tillaart, E. S. Lox, A. Roshan, G. Garr, and R. Beason. Comparison of pd-only, pd/rh and pt/rh catalysts in tlev, lev vehicle applications – real vehicle data versus computer modeling results. *SAE paper 2000-01-0501*, 2000.
- [11] R. E. Hayes and S. T. Kolaczkowski. Mass and heat transfer effects in catalytic monolith reactors. *Chemical Engineering Science*, 46(21):3587–3599, 1994.
- [12] P. A. Konstantinidis, G. C. Koltsakis, and A. M. Stamatelos. Computer-aided assessment and optimization of catalyst fast light-off techniques. *Proc Instn Mech Engrs, Part D: J. Automobile Engineering*, 211:21–37, 1997.
- [13] H. Katashiba, R. Nishiyama, Y. Nishimura, Y. Hosoya, H. Arai, and S. Washino. Development of an effective air-injection system with heated air for lev/ulev. *SAE paper 950411*, 1995.

- [14] E. J. Bissett and Se H. Oh. Electrically heated converters for automotive emission control: determination of the best size regime for the heated element. *Chemical Engineering Science*, 54:3957–3966, 1999.
- [15] P. Ehmann, N. Rippert, K. Umehara, and C. D. Vogt. The development of a BMW catalyst concept for LEV/EU3 legislation for an 8 cylinder engine by using thin wall ceramic substrates. *SAE paper 1999-01-0767*, 1999.
- [16] C. C. Webb, B. B. Bykowski, and P. A. Weber. Using advanced emission control systems to demonstrate LEV II ULEV on light-duty gasoline vehicles. *SAE paper 1999-01-0774*, 1999.
- [17] J. Hoebink, R. A. Gemert, H. van den Tillaart, and G. B. Marin. Competing reactions in three-way catalytic converters: modeling of the nox conversion maximum in the light-off curves under net oxidizing conditions. *Chemical Engineering Science*, 55:1573–1581, 2001.
- [18] J. M. Thomas and W. J. Thomas. *Principles and Practice of Heterogeneous Catalysis*. VCH, 1997.
- [19] H. Lüders, P. Stommel, and S. Geckler. Diesel exhaust treatment – new approaches to ultra low emission diesel vehicles. *SAE paper 1999-01-0108*, 1999.
- [20] Martin Winterkorn, Peter Bohne, Leo Spiegel, and Günter Söhlke. Der Lupo FSI von Volkswagen – so sparsam ist sportlich (teil 2). *ATZ Automobiltechnische Zeitschrift*, 102(11):964–974, 2000.
- [21] Jan Kašpar, Paolo Fornasiero, and Heal Hickey. Automotive catalytic converters: current status and some perspectives. *Catalysis Today*, 77:419–449, 2003.
- [22] H. S. Gandhi, G. W. Graham, and R. W. McCabe. Automotive exhaust catalysis. *Journal of Catalysis*, 216:433–442, 2003.
- [23] L. Mußmann, D. Lindner, E. S. Lox, R. van Yperen, T. P. Kreuzer, I. Mitsushima, S. Taniguchi, and G. Garr. The role of Zirconium in Novel Three-Way Catalysts. *SAE paper 970465*, 1997.
- [24] B. H. Engler, E. S. Lox, K. Ostgathe, T. Ohata, K. Tsuchitani, S. Ichihara, H. Onoda, G. T. Garr, and D. Psaras. Recent trends in the application of tri-metal emission control catalysts. *SAE paper 940928*, 1994.
- [25] D. Lindner, E. S. Lox, R. van Yperen, K. Ostgathe, and T. Kreuzer. Reduction of exhaust gase emissions by using Pd-based three-way catalysts. *SAE paper 960802*, 1996.
- [26] M. Shelef, G. W. Graham, and R. W. McGabe. In A. Trovarelli, editor, *Catalysis by Ceria and related materials*, page 343. Imperial College Press, 2002.
- [27] P. L. Silveston. Automotive exhaust catalysis: Is periodic operation beneficial? *Chemical Engineering Science*, 51(10):2419–2426, 1996.
- [28] J. Kaerger and D. M. Ruthven. *Diffusion in Zeolites and Other Microporous Solids*. John Wiley & Sons, 1992.

- [29] L. Mussmann, D. Lindner, M. Votsmeier, E. Lox, and T. Kreuzer. Single layer high performance catalyst. *US patent 6,524,992*, 2001.
- [30] S. H. Oh and J. C. Cavendish. Transients of monolithic catalytic converter: response to step changes in feedstream temperature as related to controlling automobile emissions. *Industrial and Engineering Chemistry — Product Research and Development*, 21:29–37, 1982.
- [31] S. H. Oh and J. C. Cavendish. Mathematical modeling of catalytic converter light-off - part ii: Model verification by engine-dynamometer experiments. *American Institute of Chemical Engineers Journal*, 31(6), 1982.
- [32] S. H. Oh and J. C. Cavendish. Mathematical modeling of catalytic converter light-off - part iii: Prediction of vehicle exhaust emissions and parametric analysis. *American Institute of Chemical Engineers Journal*, 31(6), 1982.
- [33] S. Siemund, J. P. Leclerc, D. Schweich, M. Prigent, and F. Castagna. Three-way monolithic converter: simulations versus experiments. *Chemical Engineering Science*, 51(15):3709–3720, 1996.
- [34] D. K. S. Chen, E. J. Bisset, S. H. Oh, and D. L. Van Ostrom. A three-dimensional model for the analysis of transient thermal and conversion characteristics of monolithic catalytic converters. *SAE paper 880282*, 1988.
- [35] C. N. Montreuil, S. C. Williams, and A. A. Adamczyk. Modeling current generation catalytic converters: Laboratory experiments and kinetic parameter optimization — steady state kinetics. *SAE paper 920096*, 1992.
- [36] S. Tischer, C. Correa, and O. Deutshmann. Transient three-dimensional simulation of a catalytic combustion monolith using detailed models for heterogeneous and homogeneous reactions and transport phenomena. *Catalysis Today*, 69:57–62, 2001.
- [37] T. Shamim, H. Shen, S. Sengupta, S. Son, and A. A. Adamczyk. A comprehensive model to predict three-way catalytic converter performance. *Transactions of the ASME, Journal of Engineering for Gas Turbines and Power*, 124(421–428), 2002.
- [38] G. N. Pontikakis and A. M. Stamatelos. Mathematical modelling of catalytic exhaust systems for EURO-3 and EURO-4 emissions standards. *Proc Instn Mech Engrs, Part D: J. Automobile Engineering*, 215:1005–1015, 2001.
- [39] Lanny D. Schmidt. *The Engineering of Chemical Reactions*. Oxford University Press, 1998.
- [40] G.N. Pontikakis and A.M. Stamatelos. Identification of catalytic converter kinetic model using a genetic algorithm approa. *ASME Transactions, Journal of Dynamic Systems, Measurement & Control*, 2003. (*Submitted*).
- [41] S. E. Voltz, C. R. Morgan, D. Liederman, and S. M. Jacob. Kinetic study of carbon monoxide and propylene oxidation on platinum catalysts. *Industrial Engineering Chemistry — Product Research and Development*, 12:294, 1973.

- [42] B. Subramanian and A. Varma. Reaction kinetics on a commercial three-way catalyst: the CO–NO–O₂–H₂O system. *Industrial Engineering Chemistry — Product Research and Development*, 24:512–516, 1985.
- [43] K. Zygourakis and R. Aris. Multiple oxidation reactions and diffusion in the catalytic layer of monolith reactors. *Chemical Engineering Science*, 38(5):733–744, 1983.
- [44] E. Massing, J. F. Brilhac, A. Brillard, P. Gilot, and G. Prado. Modelling of the behaviour of a three way catalytic converter at steady state. influence of the propene diffusion inside the catalytic layer. *Chemical Engineering Science*, 55:1707–1716, 2000.
- [45] L. C. Young and B. A. Finlayson. Mathematical models of the monolithic catalytic converter: Part i. development of model and application of orthogonal collocation. *American Institute of Chemical Engineers Journal*, 22(2):31–343, 1976.
- [46] I. Keren and M. Sheintuch. Modeling and analysis of spatiotemporal oscillatory patterns during CO oxidation in the catalytic converter. *Chemical Engineering Science*, 55:1461–1475, 2000.
- [47] K. Zygourakis. Transient operation of monolith catalytic converters: a two-dimensional reactor model and the effects of radially nonuniform flow distributions. *Chemical Engineering Science*, 44:2075–2086, 1989.
- [48] J. Braun, T. Hauber, H. Többen, J. Windmann, P. Zacke, D. Chatterjee, C. Correa, O. Deutchmann, L. Maier, S. Tischer, and J. Warnatz. Three-dimensional simulation of the transient behaviour of a three-way catalytic converter. *SAE paper 2002-01-0065*, 2002.
- [49] C. Dubien, D. Schweich, G. Mabilon, B. Martin, and M. Prigent. Three way catalytic converter modeling: Fast and slow oxidizing hydrocarbons, inhibiting species and steam-reforming reaction. *Chemical Engineering Science*, 53(3):471–481, 1998.
- [50] L. A. Boehman, S. Niksa, and R. J. Moffatt. A comparison of rate laws for CO oxidation over Pt on alumina. *SAE paper 930252*, 1993.
- [51] K. N. Pattas, A. M. Stamatelos, P. K. Pistikopoulos, G. C. Koltsakis, P. A. Konstantinidis, E. Volpi, and E. Leveroni. Transient modeling of 3-way catalytic converters. *SAE paper 940934. SAE Transactions, Journal of Fuels and Lubricants*, 103:565–578, 1994.
- [52] Se H. Oh. Effects of Cerium addition on the CO–NO reaction kinetics over Alumina-supported Rhodium catalysts. *Journal of Catalysis*, 124:477–487, 1990.
- [53] P. Granger, C. Dathy, J. J. Lecomte, M. Prigent, G. Mabilon, and G. Leclercq. Kinetics of the NO and CO reaction over Platinum catalysts. *Journal of Catalysis*, 173:304–314, 1998.
- [54] R. Herz. Dynamic behavior of automotive catalysts: 1. catalyst oxidation and reduction. *Ind. Eng. Chem. Prod. Res. Dev.*, 20:451–457, 1981.

- [55] R. Herz, J. B. Klela, and J. A. Sell. Dynamic behavior of automotive catalysts: 2. carbon monoxide conversion under transient air/fuel ration conditions. *Ind. Eng. Chem. Prod. Res. Dev.*, 22:387–396, 1983.
- [56] J. R. Theis and W. J. LaBarge. The effects of catalyst volume and Ceria content on the emission performance and Oxygen storage capacity of automotive catalysts. *SAE paper 932666*, 1993.
- [57] V. P. Zhdanov and B. Kasemo. Kinetic models of oxygen supply from CeO_x to active nanometer particles of three-way catalysts. *Applied Surface Science*, 135:297–306, 1998.
- [58] F. Aimard, S. Li, and M. Sorine. Mathematical modeling of automotive three-way catalytic converters with oxygen storage capacity. *Control Eng. Practice*, 4(8):1119–1124, 1996.
- [59] Karen M. Adams, John V. Cavataio, Timothy Sale, William A. Rimkus, and Robert H. Hammerle. Laboratory screening of diesel oxidation catalysts and validation with vehicle testing: the importance of hydrocarbon storage. *SAE paper 962049*, 1996.
- [60] Robert H. Perry (Editor), Don W. Green (Editor), and James O. Maloney (Editor). *Perry's Chemical Engineers' Handbook*. McGraw-Hill Professional, 7th edition, 1997.
- [61] Press W. H., B. P. Flannery, S. A. Teukolsky, and W. T. Vetterling. *Numerical Recipes in FORTRAN-77. The Art of Scientific Computing*. Cambridge University Press, England, 1988. Also freely available online at <http://www.nr.com>.
- [62] C. N. Satterfield. *Mass Transfer in Heterogeneous Catalysis*. MIT Press, 1970.
- [63] E. W Thiele. Relation between catalytic activity and size of particle. *Ind. Eng. Chem*, 31(11):916, 1939. [Citation Classic. *Current Contents/Engineering, Technology & Applied Sciences*, 10(2):10, 1979.]
- [64] P. B. Weisz and J. S. Hicks. The behaviour of porous catalyst particles in view of internal mass and heat diffusion effects. *Chemical Engineering Science*, 17:265–275, 1962.
- [65] P. B. Weisz and J. S. Hicks. On the shape factors for irregular particles—i. the steady-state problem. diffusion and reaction. *Chemical Engineering Science*, 6:262–268, 1957.
- [66] R. H. Heck, J. Wei, and J. R. Katzer. Mathematical modeling of monolithic catalysts. *American Institute of Chemical Engineers Journal*, 22(3):477–484, 1976.
- [67] R. Jahn, D. Snita, M. Kubicek, and M. Marek. 3D modeling of monolith reactors. *Catalysis Today*, 38:39–46, 1997.
- [68] William Taylor III. CFD prediction and experimental validation of high-temperature thermal behavior of catalytic converters. *SAE paper 1999-01-0454*, 1999.

- [69] Laboratory of Thermodynamics and Thermal Engines. *CATRAN Catalytic Converter Modeling Software, Version V4R3*. University of Thessaly, Volos, April 2003.
- [70] G. Konstantas and A. M. Stamatelos. Quality assurance of exhaust emissions test data. *Proc. Instn Mech Engrs, Part D*, 2003. (*Submitted*).

Chapter 3

Wall Flow Diesel Particulate Filters

While monolithic catalytic converters are employed in automotive exhaust lines in order to control gaseous pollutants, they are not suitable for the abatement of particulate pollutants. The latter are mainly emitted by diesel engines (spark-ignition engines particulate emissions are negligible), hence the special filters that have been devised for this purpose are called *Diesel Particulate Filters* (DPFs). Currently, only one manufacturer equips its automobiles with diesel particulate filters [1, 2], despite that the DPF has been under study for about 20 years. Among the reasons responsible for this situation is certainly the fact that the operation of the DPF is coupled with serious problems that have not been fully solved yet.

Because of these problems, and because the DPF should be used in the diesel exhaust lines in combination with a diesel catalytic converter for the abatement of gaseous emissions, modeling is strongly needed in the area of DPF design. Modeling can provide insight to the DPF's operation and enable its use in catalyst–DPF diesel exhaust aftertreatment systems.

In the following, we first review the structure and operation of the various types of diesel particulate filters. We then isolate the main physical (filtration and heat transfer) and chemical (thermal and catalytic combustion of soot) phenomena pertaining to the specific case of a wall-flow filter with fuel-additive assisted regeneration. Similarly to the monolithic catalytic converter, we split the modeling problem into three levels, with which we deal separately: (a) the reactor level, (b) the channel level and (c) the loading–regeneration level. We introduce the submodels appropriate for each level and discuss the novel features, validity and usability of the approach.

The modeling approach described herein is an extension of the approach developed by Bissett and Shadmann [3, 3] and enhanced by Koltsakis and Stamatellos [4, 5]. The primary contributions introduced by this thesis are the following:

- The reaction scheme of the model regarding the thermal and catalytic regeneration has been refined and the solution procedure has been improved. The reaction scheme has also been extended in order to include soot oxidation with NO_2 (CRT mechanism) and the effect of the volatile organic fraction of the soot. These extensions have been smoothly integrated into the mathematical framework used for the thermal and catalytic regeneration mechanisms.
- The 1D model for the diesel filter has been interfaced with commercial finite element software to build a three-dimensional model of the filter. Furthermore, a module for the prediction of the inlet flow non-uniformity induced by the 3D flow resistance field of the filter has been developed to complement the

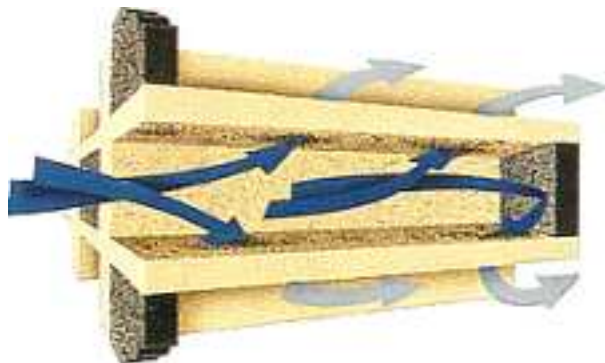


Figure 3.1: Schematic of a wall-flow diesel particulate filter

3D version of the model. Although the development of the 3D model may be viewed as a technological rather than a scientific innovation, it is a valuable engineering tool that enables the detailed study of the DPF operation and is expected to suggest directions for the improvement of the fundamental phenomena involved in the DPF operation.

3.1 Operation of wall flow and deep-bed filters

3.1.1 Overview

The diesel particulate filter is a device designed to collect diesel particulate matter from the diesel exhaust. The collection is being done by physical means, i.e. by mechanical filtration due to several mechanisms. To prevent filter clogging, particulate matter filtration must be periodically interrupted by a process to clean the filter and dispose of the collected matter, namely a *regeneration* process. Effectively, the operation of the filter consists of successive collection (*loading*) – regeneration cycles.

The filtration mechanisms in a DPF depend on filter material and design. The most widespread filter design is the wall-flow monolith, which is derived from the flow-through support used for catalytic converters by plugging channels as shown in Figure 3.1. Adjacent channels are alternatively plugged at each end in order to force the diesel aerosol through the porous substrate walls which act as a mechanical filter. Thus, diesel particulate matter (commonly referred to as *soot*) is deposited on the four sides of the inlet channels. The monolith can be made of cordierite or silicon carbide (SiC) [6, 7, 8].

Many other configurations have been presented as alternatives for DPF design. These include radial-flow fibrous filters as well as foam filters [9]. A typical design of fiber filters involves ceramic fibers woven around a perforated metal tube (Figure 3.2). Ceramic foams, illustrated in Figure 3.3, are open-pore structures. The elements of the structure—the *struts*—form a dodecahedral ceramic mesh where particles are deposited [9, 10, 11]. Modeling of the filtration and regeneration behaviour has been done in the past [10, 11]. Ceramic foam filters can be used in axial- or radial-flow filter configurations. Both fibrous and foam filters feature higher specific surface area, which is advantageous if they are used as catalyzed filters. Unfortunately, compared to wall flow filters with equal pressure drop, they are characterized by lower filtration efficiencies. However, it seems that their advantage in catalyzed

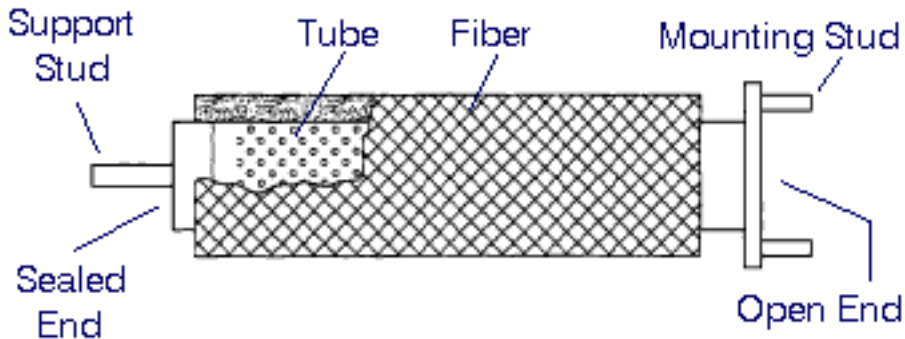


Figure 3.2: Schematic of radial-flow fiber DPF filter

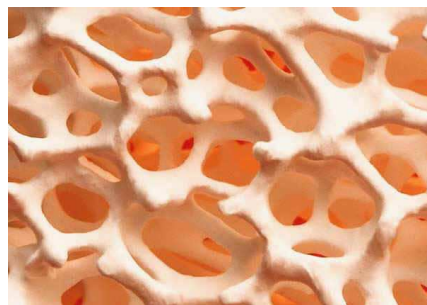


Figure 3.3: Ceramic foam

filter operation could lead to a workable catalyzed filter of hybrid construction (wall-flow with higher pore size). Washcoating of the standard wall-flow diesel filter is not yet successful in significantly enhancing regeneration potential [12, 13]. Modeling will be essential in the design optimization of such filter designs, and is currently in progress in our Lab.

While the filtration function of a DPF is amenable of many alternative solutions, the regeneration process presents difficulties that have not been resolved yet. For automotive applications of DPFs, soot combustion is the only acceptable solution for the regeneration of the filter. The collected soot is burned and gaseous products of the combustion, mainly CO and CO₂, escape to the outlet of the filter. The process of soot combustion is the most important part of filter operation. *When* regenerations begin and *how* they proceed are parameters that affect engine operation and are crucial for the filter integrity itself.

Specifically, research on DPF regeneration focuses on achieving—under all engine operating conditions—the lowest possible temperature that regeneration onsets, so that the filter operates with low levels of soot loading. Highly loaded filters induce high pressure drop and adversely affect the operation of the engine [14]. Furthermore, a highly loaded filter can lead to an uncontrolled regeneration, accompanied by excessive heat release and the risk that the filter is damaged (melted or cracked) [15].

Many approaches have been devised and tested to achieve low temperature regeneration, but none has been completely successful. Nevertheless, the most promising ones [16] employ the use of some catalyst and are usually coupled with some type of diesel catalytic converter and carefully tuned engine management control.

Before proceeding to examine the filtration and regeneration processes in more detail, a word about diesel exhaust particulate matter is in order. Diesel ex-

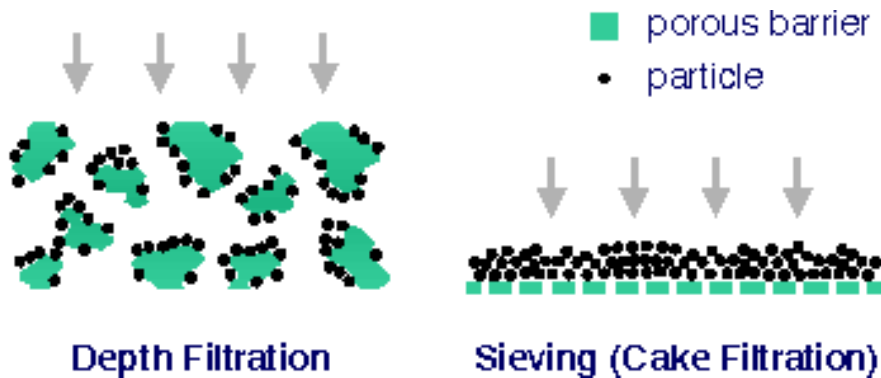


Figure 3.4: Deep-bed filtration vs. cake filtration

haust particles are approximately spherical, with diameters ranging from 10 to 1000 nm [17, 18]. The diameters follow a log-normal distribution and the mean of the distribution is near 100 nm [19].

Particles consist of a carbonaceous core, on which sulfates and partially oxygenated hydrocarbons are absorbed [20]. The hydrocarbon fraction is called is the volatile organic fraction (VOF), and originates from unburned fuel and lubricating oil. The VOF is adsorbed or condensed at the particles at temperatures below 200 °C and is desorbed above 400 °C [21]. The VOF is of special interest in case the fuel of the vehicle is doped with a catalyst and thus the particles also contain catalyst metal oxides. Then VOF can be may be oxidized at low temperatures (below 250 °C), starting the so-called erratic regenerations [22]. Particulate particles may also contain metal additive oxides such as Cerium and Ferrocine, which originate from fuel additives and promote the catalytic oxidation of carbon (Section 3.1.3).

Below, we review in some more detail the filtration and regeneration processes in the diesel particulate filter. This should facilitate the formulation of the wall-flow DPF and illustrates the difficulties that have to be circumvented in order to achieve DPF designs that are reliable and efficient for automotive applications.

3.1.2 Filtration and loading

The basic operation in particulate collection by any type of diesel filter is separation of the gas-borne particles from the gas stream by deposition on the collecting surface. This separation involves passage of the gas through a porous barrier which retains the particulates. Filters, depending on the type of this barrier, may be divided into (a) deep-bed filters, and (b) surface-type filters [23, 24]. In deep-bed filters, the mean pore size of filter media is bigger than the mean diameter of collected particles. The particles are deposited on the media through a combination of depth filtration mechanisms which are driven by various force fields, related to velocity and concentration gradients in the gas. In the surface-type filters, the pore diameter is less than the particle diameter. The particles are deposited on the media through sieving. These two types of filtration are shown in Figure 3.4.

Ceramic wall-flow monoliths work through a combination of depth and surface filtration. When the filter is completely clean, exhaust gas particles are deposited in the pores of the ceramic wall (depth filtration). When the depth filtration capacity of the ceramic wall is saturated, a particulate layer starts covering the filtration surface. Hence, surface filtration begins. Since the wall capacity is low, surface

filtration is predominant in wall-flow monoliths.

The highly-porous layer of collected diesel particulates is itself the principal filter medium in the surface-type filtration. This layer is commonly referred to as *filtration cake* and the process is called *cake filtration*. Particles larger than the cake's pores are stopped at the top of the cake through a sieving filtration mechanism. Smaller particles may be also filtered through sieving but are mainly trapped within the filter cake through deep-bed filtration. Particles that are not trapped within the soot layer are deposited at the end of it, on the filter wall, again by sieving. Thus, wall-flow DPFs always operate with high filtration efficiency, and only the finest particles are not trapped by the porous wall and by the deposit, and escape to the outlet channel.

In the case of fibrous and foam aerosol filters, only deep-bed filtration is observed, because the pores of these filters are larger than the diesel aerosol particles [25]. Particles are deposited on the filtration elements of the porous structure, i.e. either the fibers or the struts of the ceramic foam [10]. Similarly to the cake of the wall-flow DPF, the deposited particles act as elemental collectors themselves, retaining other particles from the aerosol flow.

Because accumulated particles act as elemental collectors, particle dendrites are formed and grow as the filtration process continues and more particles are deposited onto them. Thus, the soot deposit of both the wall-flow and deep-bed diesel particulate filters is essentially a mesh of particle dendrites [26, 27].

Deep-bed filtration mainly proceeds via the following three mechanisms of aerosol deposition [28]:

- Inertial impaction
- Interception
- Brownian diffusion

The three filtration mechanisms are typically explained for the case of a cylinder located in an aerosol flow. The cylinder is an elemental filter. In the case of fiber filters, each fiber of the mesh may be viewed as a cylinder. In foam filters, the ceramic struts are also more or less cylindrical. Finally, the dendritic structure of the soot deposit acts as a mesh of interconnected cylinders. Below we briefly review these three mechanisms; for a detailed analysis, consult [23, 24, 28].

Inertial impaction Inertial impaction mechanism is illustrated in Figure 3.5. A massive particle approaching a fiber will not exactly follow the air streamline, because of its inertia. It will follow a straighter path and end up on the cylinder. The more massive the particle, the greater will be the deviation the velocity of particle's approach. The phenomenon is characterized by the non-dimensional Stokes number:

$$St = \frac{C \rho_p d_p^2 u}{9 \mu d}$$

where ρ_p and d_p refer to the density and diameter of the particle, d is the diameter of the cylinder, μ and u are the viscosity and the velocity of the gas flow respectively. Finally, C is the *Cunningham correction factor*, accounts for slip flow effects and is a function of Knudsen number [23]:

$$C = 1 + Kn \sqrt{1.257 + 0.400 e^{-1.10/Kn}}$$

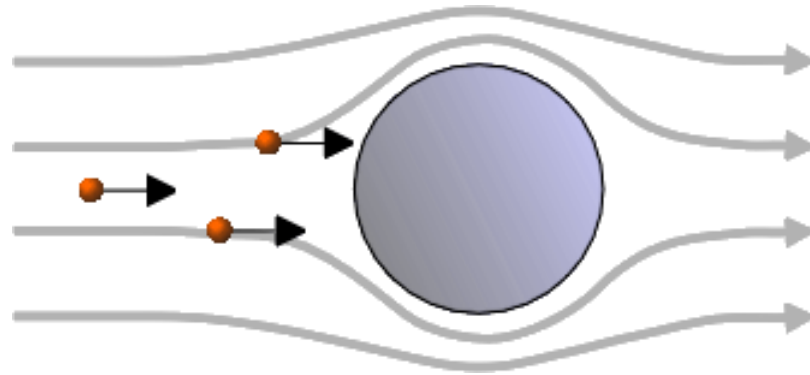


Figure 3.5: Inertial impaction

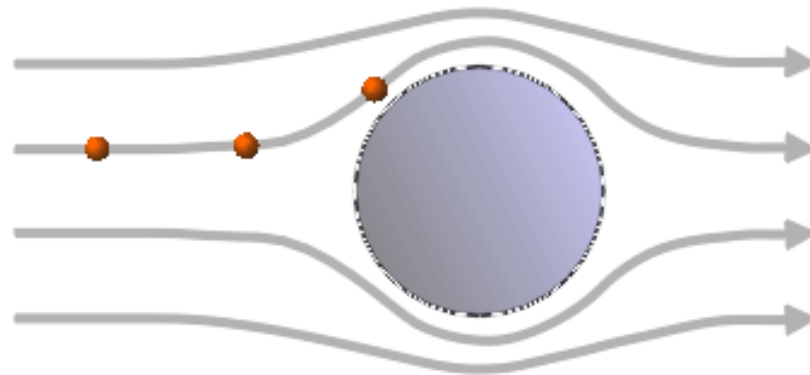


Figure 3.6: Interception

Interception Filtration by interception is dominant in aerosols with small particles flowing in greater velocities. A particle with very small mass—hence negligible inertia—in a high-velocity flow practically follows the streamlines of the field quite accurately. If the shorter distance between a streamline and the cylinder is a , then any particle with diameter $r > a$ traveling along this streamline will touch the cylinder and stick to it. This is schematically given in Figure 3.6. Interception is characterized by the *interception parameter* R , defined as the ratio between particle and cylinder diameter [23]:

$$R = \frac{d_p}{d}$$

Brownian diffusion Brownian motion of the smallest particles in an aerosol occurs because of the bombardment of the particles with gas molecules. This causes them to diverge from their streamlines following random paths and, if they are in the proximity of the cylinder, to contact it and be deposited to it. A concentration gradient establishes between the bulk of the flow and the flow near the cylinder and particles diffuse to the cylinder. With decreasing size of particles, Brownian motion increases and so does, in consequence, the efficiency of the deposition. For the quantitative description of the phenomenon, the Peclet number is employed [23]:

$$Pe = \frac{ud}{D}, \quad \text{where: } D = \frac{Ck_b T}{3\pi\mu d_p}$$

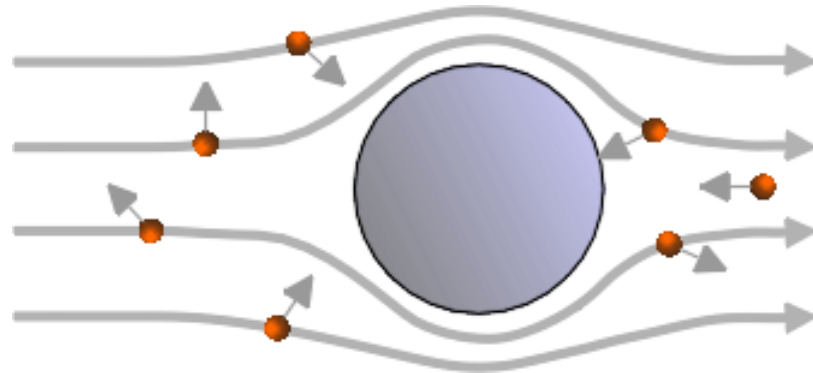


Figure 3.7: Brownian diffusion

D is the diffusivity of the particles and k_b the Boltzmann constant. Peclet number may be viewed as the ratio between transport due to convection and transport due to molecular diffusion.

3.1.3 Regeneration

All kinds of filters must be periodically regenerated, that is, the particulate matter that is accumulated in the filter must be periodically removed. The filter regeneration process depends on the particular application, especially on the filter type and the collected matter. In automotive applications, the soot deposit is removed from the filter by burning it. On-site soot oxidation is the only feasible way to regenerate automotive DPFs because the filter is mounted on the exhaust line, thus it may not be easily removed to be cleaned. Oxidation is caused by exhaust gas species such as O_2 or NO_2 and any catalyst possibly present in the DPF or the soot itself. The products of the oxidation are gases (primarily CO and CO_2) that escape to the outlet of the filter.

Even before clogging, highly loaded filters exhibit unfavorable operation characteristics [14]. The presence of the filter in the exhaust line induces some pressure drop which is felt by the engine as additional load. Induced pressure drop (and the corresponding engine load) increases rapidly as a function of the particulate matter collected in the filter. Therefore, the engine does not operate neither smoothly nor economically. Consequently, DPF induced pressure drop must be kept in the lowest levels possible.

A second reason that high filter loads are undesirable is that their filtration efficiency may deteriorate with loading. This is true only for the fiber and foam filters. After some point, the filter is unable to retain the particles. Clusters of accumulated matter are detached by the filter and escape to the outlet [9].

Finally, when regeneration of a highly loaded filter finally occurs, it may endanger the integrity of the filter itself. Since soot combustion is accompanied by significant exothermy, regeneration always results in filter heating. Heavily loaded filters are difficult to regenerate in a controlled fashion. Onset of regeneration will probably lead to excessive heat release in certain locations within the filter, which is usually followed by cracks due to thermal stresses [15] or, in extreme cases, local filter melting.

The regeneration process If no special regeneration technique is used, thermal regeneration begins in a DPF when two conditions are fulfilled: (a) the temperature of the soot is high enough (above 550 °C) to enable its oxidation by the exhaust gas oxygen and (b) the necessary oxygen is provided by the gas flow. Both depend on the operating point of the engine.

Since neither the temperature nor the exhaust gas flow is uniform within the filter, regeneration does not start simultaneously everywhere, but in certain points where the conditions are favorable. From these points, regeneration propagates in the filter, enhanced by the heat release due to regeneration itself. Propagation depends on the exhaust gas flow (which is continuously changing in real-world driving conditions), and on the distribution of temperatures and accumulated soot in the filter.

Bearing in mind that, in urban driving conditions, the engine usually operates in low loads, there is a high probability that no regeneration occurs until the filter is highly loaded. Since this should be avoided for the reasons mentioned above, several *forced regeneration techniques* have been devised, to regenerate the filter under all driving modes. The principles, advantages and disadvantages of the most promising forced regeneration techniques are discussed below.

Forced regeneration techniques A straightforward way to regenerate a DPF under low engine loads is to increase the temperature of the exhaust gas after it leaves the combustion chamber of the engine. This can be done with the use of electric resistances or a fuel burner [16]. Whatever the heating device, it does not operate continuously; rather, the pressure drop along the DPF is continuously monitored and the heating device operates if the DPF pressure drop exceeds some limit. Such systems are called *active* regeneration systems.

The main advantage of this approach is that the onset of regeneration is guaranteed regardless of the DPF's operating conditions. Nevertheless, the disadvantages are multiple. The installation of the heating device and the pressure drop sensors increase the initial as well as the running cost of the vehicle, because of increased fuel consumption. Finally, the installation of such a complicated system also raises the issue of its reliability and cost of service.

To circumvent the above problems, automotive manufacturers have also considered *passive* regeneration systems, which do not introduce any new subsystems in the exhaust line. Instead, passive subsystems are designed so that the conditions for regeneration onset in the DPF are favorable under all driving modes. Passive regeneration systems usually seek to lower the temperature at which soot begins to get oxidized. This implies the use of a catalyst; the term *catalytic* regeneration is then used and is to be contrasted with the *thermal* regeneration of the DPF when no catalyst is present.

There are currently two approaches to catalytic regeneration [16]. The first, the washcoated DPF, is inspired by the success of the catalytic converters. The idea is to apply a catalytically active washcoat on the interior surface of a DPF (the walls of the wall-flow DPF or the ceramic mesh of a foam of fiber filter). The deposited soot that is in contact with the precious metal catalyst is then oxidized in lower temperatures than without catalyst. The second approach uses a catalyst in liquid form that is added in the fuel before it is burned. The catalyst is a liquid solution of some metal oxide, usually Cerium (Ce) or Ferrocine (Fe). In this way, the catalyst enters the engine's combustion chamber with the fuel and the soot particles that are

formed contain the catalyst. As a result, the soot deposit in the filter contains the catalyst and it is oxidized in lower temperatures.

In principle, the washcoated DPF is much more attractive than any other regeneration method. This stems from its simplicity, low initial cost, no operating cost and no need for service. Its primary disadvantage, though, is the low catalyst–soot contact area, especially in the case of the wall-flow DPF, since only the soot deposited within the pores of the washcoat is in contact with the catalyst. Deep-bed filters such as foam filters are better in this regard, because they have much higher surface area and more soot is in contact with the catalyst [9]. Research is ongoing in improving washcoated DPF technology, and combine it with advanced catalyst technologies such as the NO_x-storage catalyst [29, 30].

A promising regeneration technology based on the washcoated filter is the CRT (Continuously Regenerating Trap), covered by patents by Johnson-Matthey [31], which is based on positioning a oxidation catalyst upstream the DPF that oxidizes NO to NO₂. Subsequently, NO₂ reacts with the particulate matter of the DPF.

The additive-assisted regeneration resulting in uniform distribution of the catalyst in the particulate deposit. This addresses the problem of soot–catalyst contact area in the wall-flow DPF but reintroduces the complexity and increased cost needed by the additive dosimetry device. Moreover, after every regeneration, catalyst ash remains in the filter and gradually increases the induced pressure drop and clogs the filter. This reduces the life span of the filter, which must be removed and cleaned after 30000–50000 Km of continuous operation.

A certain manufacturer ([2]) has already produced about 400,000 passenger cars equipped with a diesel particulate filter that uses a Cerium based fuel additive and a wall-flow DPF [1, 2, 32]. The system is coupled with the fuel post-injection technique, which enriches the exhaust gas with fuel injected in the cylinder after the combustion phase, in order to increase the VOF content of the soot. This is essentially an active regeneration system, since the additive dosimetry and fuel post-injection is controlled by a computerized engine management system, based on the monitoring of the DPF pressure drop as an indication of DPF soot loading. The system is highly innovative and is covered by a number of patents [33, 34, 35].

The effect of the VOF Owing to the very close contact with the catalyst metal oxides, the VOF content of the particles may be oxidized at temperatures below 250 °C. Thus, a slow regeneration procedure may start in specific points in the DPF where the local soot loading, composition, and temperatures are favorable. Under certain circumstances the heat release from the oxidized VOF leads to further carbon oxidation by the additive oxides at temperatures higher than 350 °C. The resulting additional exothermic reactions may locally increase the temperature to above 500 °C, thus allowing thermal oxidation of carbon by exhaust gas oxygen. This process is called erratic regeneration and was first systematically reported by Lepperhoff et al. [22, 36].

The presence of VOF may have a positive or negative impact on the DPF operation: On the one hand, it may assist the onset of a regeneration in low temperatures, but on the other hand it may promote an uncontrolled regeneration in a heavily loaded filter. The post-injection method is an attempt to benefit from the presence of the VOF to regenerate the filter in lower temperatures. Again, modeling is needed in this regard.

3.2 Overview of the DPF modeling problem

3.2.1 Loading–regeneration level

For the diesel particulate filter, the loading–regeneration level of the model corresponds to the kinetics and washcoat level of the monolithic catalytic converter model. The target of the modeling at this level is to quantitatively describe the fundamental phenomena involved in the operation of the DPF. These are:

- Loading
- Pressure drop
- Regeneration
- VOF adsorption–desorption

Filter loading modeling implies prediction of the filtration efficiency of the filter and the characteristics of soot deposit. In principle, the filtration efficiency of the filter should be predicted, so as to determine (a) the particle concentration finally emitted from the vehicle, and (b) the mass of the soot that is accumulated in the filter. Ideally, not only the amount of the accumulated soot has to be determined but also its morphology, because it significantly affects filtration efficiency itself, pressure drop and regeneration.

The pressure losses of the exhaust gas flow depends on the DPF’s geometry, the distribution of the deposit layer, the exhaust gas flow rate and temperature. It is noteworthy that the distribution of flow resistances within the DPF affects the flow at its inlet, since flow adjusts itself and is channeled through the low-resistance regions of the filter. Thus, the accurate computation of the induced pressure drop is important for the prediction of the exhaust gas flow and the further evolution of the accumulated soot within the filter. Furthermore, the pressure drop of the DPF is needed for the design of the exhaust line, because it affects the operation of the engine.

For an active regeneration system such as an additive assisted regeneration system, the pressure drop induced by the DPF is continuously monitored. Modeling can be used to connect it with the soot mass loading of the filter. Work towards the feasibility of this approach has been presented by Stratakis and Stamatelos [37].

For the chemical reactions that take place during the regeneration phase (i.e. carbon and hydrocarbons thermal and catalytic oxidation), the rate expressions determine the soot consumption and the accompanying heat release. Arrhenius-type rate expressions are typically employed in all models that have been presented in the literature, e.g. [38, 5, 39].

Finally, the importance of the VOF content of the soot lies in two facts:

- Pressure drop depends on the amount of VOF in the soot deposit [40], and
- VOF is oxidized at temperatures considerably lower than the respective temperatures of dry soot. Local, partial regenerations may therefore occur due to heat release from VOF oxidation [41].

Soot particles of the diesel exhaust contain VOF from the moment they are formed in the engine’s combustion chamber, but the VOF content of the soot deposit can

change depending on the operation point of the filter. Specifically, at low temperatures, heavy hydrocarbons in the gaseous phase can be adsorbed on the deposited soot, increasing its VOF portion; at increased temperatures, VOF desorbs or is oxidized (burned) from exhaust gas oxygen. Adsorption, desorption and oxidation of soot VOF are still obscure phenomena. Hence, their modeling is considerably difficult and the VOF content effect has been neglected in almost all DPF modeling efforts.

It must be noted that, in order to model a diesel particulate filter at this or any other level, the geometry of the filter must be known. This is straightforward only in the case of the wall-flow DPF. For fiber or foam filters, where the structure of the DPF is not well defined, the complexity of the geometry is accounted for via averaging quantities and statistical distributions. For example, the filter void fraction and the distribution of fiber diameters are employed for the characterization of the geometry of the fiber filter [10, 11].

3.2.2 Channel level

At the channel level, the objectives of modeling are to determine:

1. the distribution of the exhaust gas flow along the channel of a wall-flow filter or along the inner channel of any radial-flow deep-bed filter, and
2. the convective heat transfer between the exhaust gas and the solid phase (DPF ceramic and deposit of soot)

The flow and pressure distribution along the channel of the DPF depends on flow resistances along both the axial direction and the direction normal to the soot layer and ceramic wall, the latter being much higher than the former. Therefore, the accuracy of the flow field predictions at the channel level depends on the pressure drop submodel accuracy. In its turn, convective heat transfer between the exhaust gas flow and the solid phase depends on the flow distribution computations.

Thus, modeling at the channel level depends strongly on the lower level of pressure-drop and regeneration modeling, just as the catalytic converter's channel model depends on the washcoat and kinetics modeling. Again, the DPF's channel model is developed using a quasi-steady-state approach: the transient terms from the mass and energy balances for the gas flow are omitted. For more details, see the corresponding discussion for the catalytic converters model (Section 2.2.4).

3.2.3 Reactor level

Similarly to the monolithic catalytic converter, modeling at the reactor level deals only with the problem of heat transfer at the solid phase of the DPF. The input data of the reactor level model are the heat sources that were computed at the loading-regeneration level (due to VOF adsorption–desorption and soot combustion) and at the channel level (due to convective heat transfer between the exhaust gas and the DPF). Output is the temperature field of the DPF.

In fact, every aspect of DPF modeling at the reactor level is analogous to the monolithic catalytic converter modeling at the same level because, in both reactors, the only interaction between channels is through heat conduction. In principle, the same computational model implementation could be used for both reactors.

Thus, in a manner analogous to the monolithic catalytic converter models, the reactor model can be one-, two- or three-dimensional. One-dimensional DPF models

assume uniform flow and temperature distributions across the monolith's inlet and consider their variations only in the axial direction. Multi-dimensional models work on clusters of channels and accounted for flow/temperature variations between the channel clusters.

Contrary to the monolithic catalytic converter, though, DPF modeling suggests the use of a three-dimensional reactor model, because the DPF operation is strongly three-dimensional. This is particularly true for regeneration modeling, which requires three-dimensional computation of the temperature field and the soot deposit distribution. To back this argument, one should consider that regeneration is not a local phenomenon but forms a combustion front that *propagates* in the filter. Thus, one- or two-dimensional models are expected to be a considerable compromise in accuracy of DPF behaviour prediction.

Nevertheless, only one-dimensional reactor models for the DPF have been presented in the literature until now [38, 5, 4]. In this work, we formulate both a 1D and a 3D heat transfer model for the DPF, each with different scope and application range. The 3D model is implemented by interfacing our 1D channel model with commercial FEM software. The ABAQUS and ANSYS FEM software packages have been linked with the 1D DPF model, creating two instances of a 3D model [42, 43]. The 3D model has been applied for the prediction of the behaviour of a modular SiC DPF that inherently exhibits prominent three-dimensional heat transfer behaviour.

3.3 Loading and pressure drop model

In this section, we present in detail the models for the prediction of loading, pressure drop and regeneration for the wall-flow particulate filters. The theory lying under the loading and pressure drop model has been already presented in the literature for the filtration and pressure drop of aerosols flowing through porous media. Here, we apply it for the case of the wall-flow filter.

3.3.1 Loading

Calculation of loading in this category of filters presents no difficulties. Typical filtration efficiency of a wall-flow DPF is about 90–95% and it remains approximately constant, regardless of the exhaust gas flow rate. Thus, filtration efficiency of a wall-flow DPF is assumed to be constant and no particularly complicated model is needed. Instead, a fixed percentage of the particulate mass of the exhaust gas is assumed to be filtered and deposited in the channel walls.

The soot deposit forms a layer on the walls of the inlet channels of the wall-flow DPF. The model does not consider the details of the structure of the deposit layer. Of interest is only the axial distribution of the layer's porosity and thickness for each channel because both are important for the correct estimation of the induced pressure drop.

For some fixed amount of filtered mass, the thickness of the deposit layer that it is formed depends on its porosity. The porosity of the particulate layer is found to be dependent on the loading conditions, (exhaust gas flow rate, particulate composition etc.) [40]. In practice, though, we have no theoretical background to calculate the porosity as a function of the loading conditions. Therefore, it is assumed constant, its value is considered a tunable parameter of the model, and all phenomena that influence it are lumped into this value.

We may recall from Section 3.1.2 that the actual filtration process of the wall-flow DPF is much more complicated and the approach may seem oversimplified. In fact, we could formulate a more sophisticated model for filtration in the wall and the deposit of this filter type. In concept, such a model should be built on the grounds of the filtration mechanisms described in Section 3.1.2—but there are at least three reasons that such an effort is presently out of place.

First, since the filtration efficiency of the wall-flow DPF is already very high, building such a model would provide additional insight only regarding the porosity of the soot deposit. The problem here is that it is doubtful if one could ever have the additional data required for reliable calculations, namely characteristics of the particles and how these correlate to the filtration efficiency of the soot deposit. Such difficulties are evident in the case of the deep-bed particulate filter (foam or fibrous DPF) [10, 11], where the formulation of a filtration model cannot be bypassed.

Second, it is probably the case that a simplified pressure drop model—for which porosity data are significant—can give acceptable accuracy for our engineering model. For an engineering work, it is vital to keep things as simple as possible.

Third, there are presently much more urgent problems in DPF modeling, which are connected to the regeneration process in the filter. Of these problems, this work attempts to address the issues of VOF content and 3D reactor modeling but much work remains to be done. A detailed filtration model for the DPF is therefore of the lowest priority.

3.3.2 Pressure drop

In the wall-flow DPF, pressure drop is induced as the exhaust gas flows through the deposit and the wall of the filter. This is essentially a problem of fluid flow through a porous medium, where pressure drop should be correlated with the thickness of the medium and geometrical characteristics of the porous medium and the temperature and mass flow rate of the gas. In our problem, we have two resistances to the flow (the deposit layer and the filter wall), connected in series. The total pressure drop is the sum of these resistances, i.e.:

$$\Delta p = \Delta p_1 + \Delta p_2 \quad (3.1)$$

As a first approximation, the classical Darcy's law can be used in this regard. It was postulated in 1856 as a result of measurements of pressure drop of water flowing through packed beds of sands. In differential form, the Darcy's flow equation can be written as:

$$-\frac{dp}{dx} = \frac{\mu u}{K} \quad (3.2)$$

where dp is the differential change in pressure over a length dx , μ is the dynamic viscosity of the fluid, u is the fluid velocity and, finally, K is the permeability of the porous medium. The permeability is conceived to be a property of the solid porous medium and independent of the fluid; it depends on such properties of the porous medium as porosity, pore size distribution and surface area.

The Forchheimer relationship is an alternative to the Darcy's law; it extends the latter by adding a term for nearly-quadratic dependence upon fluid velocity:

$$-\frac{dp}{dx} = \frac{\mu u}{K} + \frac{\rho u^n}{B} \quad (3.3)$$

In the above equation, n is a number close to 2, ρ is the fluid density, and B is a second permeability-like property, that is again dependent only on the porous

material. The Forchheimer relationship is supposed to give better results when applied to the case of high mass flow rates (high fluid velocities).

The first (linear) term in the Forchheimer equation has been designated as the viscous term, while the second (approximately quadratic) term has been designated as the inertia term. It is suggested by theory [44] that the viscous term is connected to pressure losses due to viscous forces exerted in the fluid, while the inertia term is connected to repeated expansions, contractions and direction changes experienced by the fluid due to its complex motion through the pores and channels of the porous medium.

Further variations of the Darcy and Forchheimer relationships have been developed to account for *slip flow effects*. When the pore diameter of the medium d_{pore} is much greater than the mean free path of the fluid molecules λ , it is assumed that the flow velocity at the wall is zero. The Darcy's and Forchheimer relationships have been developed for exactly such flows. Nevertheless, the gas flow at the wall may be greater than zero in case the mean free path is comparable or greater than the pore diameter of the porous medium; this is the case of slip flow.

The Knudsen number $Kn = \lambda/d_{pore}$ is the dimensionless quantity that should be checked for the presence of slip flow. The mean free path of the gas molecules can be calculated by the formula:

$$\lambda = \frac{\mu}{p} \sqrt{\frac{\pi RT}{2M}}$$

Obviously, slip flow can be neglected for $Kn \gg 1$ while it becomes prominent for $Kn \approx 1$.

Slip flow conditions are usually met in rarified or slow velocity gas flows through fine-grained porous media. The observed effect of slip flow is that the pressure drop is reduced to values lower than those predicted by the Forchheimer equation. This gives permeability values that are lower than those obtained for non-slip-flow conditions, which is unacceptable because both K should be dependent on porous medium properties only.

In the original work of Bissett and Shadmann [3], the Forchheimer relationship has been used for the prediction of pressure drop through the DPF soot layer and wall, neglecting slip flow effects. Nevertheless, slip flow is relevant in the case of the DPF, since the Knudsen number for the flow through the soot layer may be calculated to be approximately equal to 1, assuming mean pore diameter of the soot layer equal to $0.1 \mu m$ [32].

In a recent publication, Versaevel et al. [45] have performed an experimental and computational study on the permeability of the soot layer of a DPF, where the effect of slip flow has been included. They provide experimental evidence that the porosity of the soot deposit is not constant but depends on flow conditions. Their work includes a small review of a number of relationships that have been proposed to correct the Forchheimer equation for the case of slip flow. Such relationships define the permeability as a function of either the mean free path of the gas molecules λ or the Knudsen number Kn . It appears that there is no consensus regarding the correction to account for slip flow effects.

For the case of the DPF soot layer, Versaevel et al. used the Darcy's law. Combining (3.1) and 3.2, the total pressure drop becomes:

$$\Delta p = \frac{\mu um}{A(\rho_1 K_1)} + \frac{\mu uw_s}{K_2} \quad (3.4)$$

where m is the soot layer mass, w_s is the wall thickness and A is the cross-sectional area of the flow. They found that it was sufficient for their experiments to use the above equation provided that the product $\rho_1 K_1$ was assumed proportional to λ :

$$\rho_1 K_1 = c \frac{\lambda}{\lambda_{ref}} \quad (3.5)$$

The proportionality factor c was determined to 0.55 [Da kg/m³].

Sorenson et al. [46] have found that $\rho_1 K_1$ is a decreasing function of the pressure drop Δp along the soot layer and attribute it to the compression of the soot layer when Δp increases. The approach of Versaevel et al. is consistent with these results but implies that this behaviour is connected with the slip flow effect. It is probable that both explanations are true.

The work of Versaevel et al. was the starting point for this work. It employed the DPF computational model that was the precursor of the model that we develop herein [5]. Since its accuracy was found acceptable, no changes to the pressure drop submodel have been attempted and the pressure drop prediction follows the above discussion, but the experimental findings of the work of Stratakis et al [40] regarding the values of the $\rho_1 K_1$ product were employed.

3.4 Regeneration model

In the following, we shall describe a model that accounts for thermal, catalytic and CRT regeneration mechanisms, assuming that the catalyst is uniformly distributed in the soot layer. This assumption corresponds to the case that engine fuel is doped with a catalytically active additive and thus the soot particles produced already contain the catalyst when they are deposited in the DPF walls.

A two-reactions mechanism for the VOF desorption and catalytic combustion has also been formulated but has not been validated experimentally. It is included here only to indicate how the regeneration model could accommodate this effect. For a complete treatment of the VOF effect, the pressure drop submodel should also be updated, since VOF combustion or desorption reduces the pressure drop of the filter.

The model described herein refines and extends the thermal and catalytic regeneration model that was developed by Koltsakis and Stamatelos [5]. In its turn, the latter model had been based on the original work of Bissett and Shadmann [3] for the thermal regeneration of the DPF. Compared to previous works, the main improvements of the present model are the following [47]:

- The geometry of the soot layer is viewed with more detail; the soot layer is assumed to consist of four trapezoids instead of four rectangles.
- The reaction scheme of the model is refined in respect to thermal and catalytic oxidation of carbon.
- The reaction scheme is also extended to incorporate oxidation of carbon by NO₂ and hydrocarbon content of the soot.
- The depletion of the additive particles because of oxidation and transformation to inactive ash is accounted for.

- Approximations involved in the model formulation and solution procedure of the catalytic regeneration model presented in [5] are removed.

In the following, we first deal with the geometrical description of the soot layer. Then, the regeneration model is formulated. This requires (a) the definition of a scheme of reactions that occur in the soot layer, (b) the definition of mass balance equations for the chemical species of the gaseous and solid phase, (c) the definition of a balance equation for the heat released/adsorbed by the chemical reactions, and (d) the analytical spatial integration of the balance equations. Our objective is to describe filter regeneration as an initial value problem, i.e. to formulate a system of differential equations which is integrated numerically through time.

3.4.1 Geometry of the channels and the soot layer

Because of the repeating geometry of the DPF, we may restrict its mathematical treatment to a fundamental channel volume of the trap. It is convenient to define it as shown in Figure 3.8. That is, this fundamental volume consists of one inlet channel and four quarters of the four adjacent outlet channel. The boundaries are assumed to be adiabatic and no flow occurs through them to the rest of the outlet channel. The rationale for this assumption is explained in Section 3.5 below.

To formulate the balance equations pertinent for regeneration modeling, we consider a small part of this fundamental volume, of length Δz . At this part of the channel, a layer of soot of mass m and thickness w has already accumulated. The wall's thickness is w_s and the length of the channel edge is ℓ . The channel's cross-section is given schematically in Figure 3.9. (Note that the substrate of the DPF also contains a small amount of soot but it is safely neglected because wall soot capacity is very low.) Exhaust gas flow is perpendicular to the soot layer and wall. Exhaust gas species are consumed or produced as gas flows through the soot layer. In what follows, we shall use the subscript j to discriminate between physical properties of the soot layer ($j = 1$) and the wall ($j = 2$).

It is evident from Figure 3.9 that the soot layer consists of four trapezoids. The soot mass and the deposit thickness are therefore related as:

$$m = 4\rho_1(l - w)w\Delta z, \quad \text{or:} \quad w = \frac{1}{2} \left(\ell - \sqrt{\ell^2 - \frac{m}{\rho_1\Delta z}} \right) \quad (3.6)$$

This relation is used by the model to compute the thickness of the deposit, which, in its turn, is needed for the calculation of the filter pressure drop and flow field distribution.

As a consequence of the trapezoid distribution of the soot layer, the area perpendicular to the flow $A(x)$ (i.e. the area that the flow 'faces' at each x) is also changing along x :

$$A(x) = \begin{cases} 4(2x + \ell)\Delta z & \text{if } -w \leq x \leq 0 \\ 4\ell\Delta z & \text{if } 0 \leq x \leq w_s \end{cases} \quad (3.7)$$

From the above, we may readily obtain by integration the volume of the soot layer V_1 and the volume of the wall V_2 where gas flows. The volume of the soot layer is the control volume where all reactions occur. It is:

$$V_1 = \int_{-w}^0 A(x)dx = 4\Delta z(\ell - w)w \quad (3.8)$$

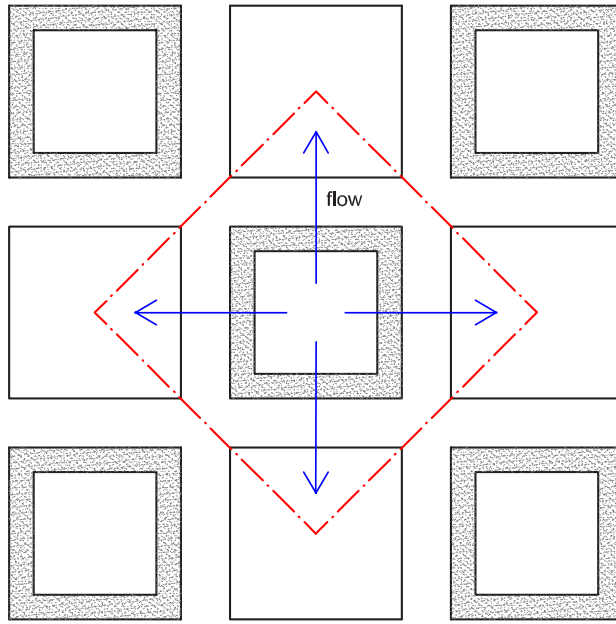


Figure 3.8: Cross-section of a wall-flow monolith channel with accumulated soot. The red boundary indicates the elementary volume considered by the model

while the volume of the wall where gas flows is:

$$V_2 = \int_0^{w_s} A(x)dx = 4\Delta z \ell w_s \quad (3.9)$$

Note that V_2 is *not* equal to $4\Delta z(\ell + 0.5w_s)w_s$, which is the total volume of the wall, because, within the wall, gas is not allowed to flow diagonally due to the presence of the neighbouring channels. (See also Figure 3.8.)

3.4.2 Reaction Scheme

When a fuel additive is used to assist regeneration, additive is present in the formation process of the particles in the combustion chamber of the engine. Therefore, the soot particles that are deposited in the trap contain bonded metal oxide par-

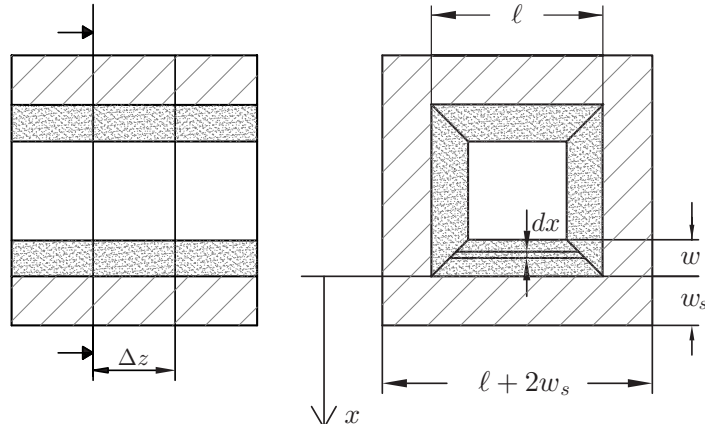


Figure 3.9: Cross-section of a wall-flow monolith channel with accumulated soot

Reaction	Rate expression
1 $C + O_2 \longrightarrow CO_2$	$r_1 = k_1 y_3$
2 $C + \frac{1}{2}O_2 \longrightarrow CO$	$r_2 = k_2 y_3$
3 $C + 2NO_2 \longrightarrow CO_2 + 2NO$	$r_3 = k_3 y_{10}$
4 $C + NO_2 \longrightarrow CO + 2NO$	$r_4 = k_4 y_{10}$
5 $C + 4CeO_2 \longrightarrow 2Ce_2O_3 + CO_2$	$r_5 = k_5 \psi_{16} \xi_{16}$
6 $C + 2CeO_2 \longrightarrow Ce_2O_3 + CO$	$r_6 = k_6 \psi_{16} \xi_{16}$
7 $Ce_2O_3 + \frac{1}{2}O_2 \longrightarrow 2CeO_2$	$r_7 = 0.5k_7 y_3(1 - \psi_{16})\xi_{16}$
8 $C_nH_m + (2n + m) CeO_2 \longrightarrow (n + \frac{1}{2}m) Ce_2O_3 + n CO + \frac{1}{2}m H_2O$	$r_8 = k_8 \psi_{16} \xi_{16} \psi_7 \xi_7$
9 $C_nH_m \xrightarrow{\text{evaporation}} C_nH_m(gas)$	$r_9 = k_9 \psi_7 \xi_7$
where: $k_n = A_n e^{-E_n/R_g T}, \quad n = 1 \dots 9$	

Table 3.1: Extended reaction scheme and rate expressions of the DPF model

ticles. These particles react with the carbon and VOF of the soot in much lower temperatures compared to those needed for oxygen.

Therefore, the regeneration model that we develop herein contains three categories of reactions, which account for:

- Thermal oxidation of soot by exhaust gas oxygen and nitrogen dioxide
- Effect of catalytic oxidation of soot by additive particles
- Effect of catalytic oxidation and physical desorption of adsorbed hydrocarbon

The reaction scheme of the model along with the corresponding rates are given in Table 3.1. It is noted that the reactions of Table 3.1 involve reactants both in the solid and the gaseous phase; their molar fractions are denoted as y_i and ψ_i respectively. The indeces of the molar fractions y_i and ψ_i correspond to the numbers of chemical species; the numbering key is given in Table 3.2. All reaction rates are assumed first order and are expressed per unit volume of soot deposit, i.e. $[\text{mol}/(\text{m}^3 \text{soot} \cdot \text{s})]$.

Chemical description of the thermal oxidation of soot corresponds to the original work of Bissett and Shadmann [3], which predicted carbon oxidation to CO_2 . The only addition here is a similar reaction for oxidation to CO . The oxidation of carbon from gaseous-phase NO_2 is completely analogous to that by O_2 and it is implemented in the same way. Finally, modeling of the effects of additive and VOF is more original and deserves more discussion, which follows in the next two sections.

Index	Chemical Species	Index	Chemical Species
1	N ₂	9	NO
2	CO	10	NO ₂
3	O ₂	11	(n/a)
4	CO ₂	12	(n/a)
5	H ₂ O	13	(n/a)
6	(n/a)	14	(n/a)
7	HC	15	(n/a)
8	(n/a)	16	CeO ₂

Table 3.2: Numbering of the chemical species of the reaction scheme. (n/a)=not available

Effect of additive There are two major hypotheses for the catalytic activity of fuel additives [48]: the electron-transport theory, and the oxygen-transport theory. According to the first theory, electrons are transported from the additive to the carbon of the soot and weaken the bonds of the carbon matrix; this makes reaction with oxygen easier. According to the second theory, the additive reacts with the gas oxygen first and stores oxygen atoms. Subsequently, the additive reacts with the carbon, which is oxidized by the oxygen stored at the additive. Thus, the additive acts as an intermediate whose presence enhances carbon oxidation.

The approach described here follows the second theory. It is assumed that the catalytic oxide is Ceria (Ce) but the same approach is applicable for any catalytic oxide with two oxidation states.

Specifically, when Ceria is in the low oxidation state, it forms a 3-valent Ce oxide (Ce₂O₃); when it is in a high oxidation state, it forms a 4-valent Ce oxide (CeO₂). It is assumed that all Ceria present in soot exists in one of these two states. The first step of the mechanism is oxidation of Ce₂O₃ by O₂ to produce CeO₂. The second step involves reaction of CeO₂ with soot carbon, which causes Ceria to return to its 3-valent state.

Note that, when a soot particle is burned, the additive particle it contained cannot form chemical bonds with other carbon particles again. Thus, Ce₂O₃ which results from reduction of CeO₂ is deposited in the trap as additive ash and may not participate in further carbon oxidation.

The reaction scheme for catalytic oxidation of carbon was first presented by Koltsakis and Stamatelos [5]. The same approach is employed here, yet there are two reactions for carbon oxidation to CO and to CO₂. Nevertheless, the reaction rates deviate from those used in [5]. Moreover, reduction of additive availability because of ash deposition is tested here for the first time.

For the oxidation and reduction of the catalytic metal oxide, the auxiliary quantities ψ_{16} and ξ_{16} are employed. The first is defined as the availability of high-oxidation-state metal oxides (CeO₂):

$$\psi_{16} = \frac{\text{mol CeO}_2}{\text{mol Ce}} = \frac{\text{mol CeO}_2}{2 \times \text{mol Ce}_2\text{O}_3 + \text{mol CeO}_2}$$

while the second is the total metal oxides content of the soot:

$$\xi_{16} = \frac{\text{mol Ce}}{\text{mol C}} = \frac{2 \times \text{mol Ce}_2\text{O}_3 + \text{mol CeO}_2}{\text{mol C}}$$

The quantity ψ_{16} may be viewed as a solid-state molar fraction of CeO₂, analogous to the molar fraction y_i of the gaseous phase species, while ξ_{16} may be viewed as the total Ceria capacity of soot. Thus, the rates of reactions 5 and 6 are taken proportional to $\psi_{16}\xi_{16}$, which is the solid-state concentration of CeO₂ (since $\psi_{16}\xi_{16}$ has dimensions of [mol/(m³soot·s)]. The rate of reaction 7 is proportional to $0.5(1 - \psi_{16})\xi_{16}$, the solid state concentration of Ce₂O₃.

It should be noted that, in concept, ψ_{16} and ξ_{16} are functions of x . For simplicity, no such spatial profiles will be considered, though. Thus, by ψ_{16} and ξ_{16} we shall denote their averages along the soot layer.

Effect of hydrocarbon content (VOF) Our target here is the extension of the reaction scheme so that it incorporates phenomena of hydrocarbon adsorption, desorption and catalytic oxidation. Modeling of such phenomena presents more difficulties compared to the catalytic carbon oxidation. A number of issues arise:

- The VOF content of the soot emitted by the engine is not constant. Contrary to the catalyst content of soot, which is set by the manufacturer of the system, the VOF content depends on and varies considerably with engine type (DI, IDI, turbocharged), injection pressure, exhaust gas recirculation (EGR) rate and engine operation point (speed and load; exhaust temperature).
- The percentage that remains adsorbed in the DPF depends on its temperature. Above 400 °C, most VOF is vaporized and only dry soot remains in the filter.
- Prolonged operation of a filter highly loaded with dry soot under low exhaust gas temperature conditions may lead to adsorption of heavy exhaust gas hydrocarbons in the deposited particulate.

The simplest case one can consider is to neglect the hydrocarbon adsorption in the particulate layer and take into account only desorption and catalytic oxidation. Neglecting adsorption is more or less inevitable since the adsorption process has not been experimentally investigated and understood yet.

On this basis, Kandylas and Stamatelos [39] first made an attempt to extend the catalytic regeneration model to include desorption and oxidation of the soot VOF. They have added reactions 8 and 9 of Table 3.1 to the reaction scheme, to take into account (a) reaction of adsorbed hydrocarbon with the catalytic oxide, and (b) evaporation and desorption of hydrocarbons at higher temperatures. No reaction for the direct oxidation of hydrocarbon by exhaust oxygen is included in the scheme. The rationale is that, at low exhaust temperatures, VOF oxidation by O₂ is negligible (it is limited by the kinetics of this reaction) and VOF only reacts with the catalyst; at high exhaust temperatures, adsorbed hydrocarbons are already evaporated before reaction with O₂ begins. Thus, reaction 8, effective only at low temperatures, is probably sufficient for the description of catalytic VOF oxidation.

Similarly with the catalytic oxidation of C, a new quantity ξ_7 is defined, which is the hydrocarbon capacity of soot. It is defined in an analogous manner with ξ_{16} , i.e.:

$$\xi_7 = \frac{\text{maximum mol HC}}{\text{mol C}}$$

Essentially, the hydrocarbon capacity of the soot corresponds to the total amount of hydrocarbon that is adsorbed in the soot layer just before regeneration starts. As a consequence of desorption and oxidation, hydrocarbon quantity in the soot layer

is gradually decreasing while regeneration proceeds. To include this effect in the model, we define the hydrocarbon availability as follows:

$$\psi_7 = \frac{\text{mol HC}}{\text{maximum mol HC}}$$

Hydrocarbon availability is exactly analogous to CeO₂ availability previously introduced for catalytic carbon oxidation.

Similarly to the corresponding quantities for the additive, it should be noted here that ψ_7 and ξ_7 are viewed as average quantities along the soot layer.

Just as reactions 5 and 6, the rate of reaction 8 is proportional to the concentration of CeO₂ in the soot deposit $\psi_{16}\xi_{16}$. In the work of Kandylas and Stamatelos, this was—apart from temperature—the only dependence of the rate; no other dependence was expected. Here, we also introduce a proportional dependence on hydrocarbon availability $\psi_7\xi_7$. The reason is the following:

Independence of the reaction rate on ψ_7 implies that, in the soot particles, the VOF is in much greater quantities compared to the catalyst, thus $\psi_7 \approx 1$ through a regeneration. This could be valid in soot deposits generated from IDI engines and in conditions that no VOF has desorbed. For modern DI engines though, the VOF content of generated soot is much lower compared to IDI engines. It thus seems much more appropriate to assume that the rate is directly proportional to ψ_7 . This also zeroes the rate of reaction 8 as hydrocarbon vanishes.

For the evaporation and desorption of the VOF, no available data exist. We can make the crude assumption that the percentage of evaporated VOF content follows the distillation curve of the diesel fuel from which it originates. The dependence on temperature of the diesel fuel's distillation curve may be approximated by an exponential, Arrhenius-type function. This assumption is supported:

- by the fact that desorption of adsorbed liquids in microporous solids is an activated process [49] and, therefore, an Arrhenius-type dependence on temperature could be expected, and
- by the shape of the distillation curves of several diesel fuels that are given in [39] and indicate an exponential dependence on temperature.

The rate of desorption of VOF is thus taken proportional to VOF content itself and to an exponential rate similar to that used in the other rate expressions of the model.

3.4.3 Balance equations

After the definition of the reaction scheme, the balance equations of the model have to be formulated. As already discussed in Section 3.4.1, all balances correspond to an small part of the fundamental channel volume, of length Δz . A mass balance for each chemical species as well as a heat balance are needed. Below, we first proceed with the balances for the gaseous phase species, which are defined in an elementary volume $A(x)dx$ of the soot layer. The mass balances for solid phase species follow, which are defined in respect to the total layer thickness. The same applies for the heat balance. This set of balances, together with a set of the respective boundary conditions, complete the definition of the model.

O₂ and NO₂ balances We begin forming the mass balance equation for oxygen for a volume element of soot $A(x)dx$, as discussed in Section 3.4.1 above. The

balance equations of the model should include oxygen consumption due to reaction with (a) carbon, (b) the 3-valent additive (Ce_2O_3) and (c) the hydrocarbon content of the soot layer. For $-w \leq x \leq 0$, the balance is:

$$\frac{\dot{m}_g}{M_g}y|_x = \frac{\dot{m}_g}{M_g}y|_{x+\Delta x} + (k_1 + \frac{1}{2}k_2)y_3A(x)\Delta x + \frac{1}{4}k_7y_3(1 - \psi_{16})\xi_{16}A(x)\Delta x$$

which yields the differential equation:

$$\frac{\dot{m}_g}{A(x)} \frac{dy_3}{dx} = -M_g\sigma_3y_3 \quad (3.10a)$$

where:

$$\sigma_3 = k_1 + \frac{1}{2}k_2 + \frac{1}{4}k_7(1 - \psi_{16})\xi_{16} \quad (3.10b)$$

For $-w \leq x \leq 0$, no reactions occur and the oxygen concentration is constant, equal to the concentration at the soot–wall interface, i.e. $y(x) = y(x = 0)$.

The only other gaseous phase reactant is NO_2 and its balance equation is formed analogously to the O_2 balance. According to the reactions 3 and 4, NO_2 reacts with C to give CO and CO_2 , thus we get the following differential equation:

$$\frac{\dot{m}_g}{A(x)} \frac{dy_{10}}{dx} = -M_g\sigma_{10}y_{10} \quad (3.11a)$$

where:

$$\sigma_{10} = 2k_3 + k_4 \quad (3.11b)$$

CO, CO_2 , NO and H_2O balances All four species, CO, CO_2 , NO and H_2O are gaseous phase products of the reactions that we consider. Their treatment of each one as regards the mass balances is the same. We demonstrate this by dealing with the CO balance and then we extend to the rest of the gaseous phase products.

$$\frac{\dot{m}_g}{M_g}y_2|_x = \frac{\dot{m}_g}{M_g}y_2|_{x+\Delta x} - [k_2y_3 + k_4y_4 + k_6y_6 + nk_8\psi_7\xi_7\psi_{16}\xi_{16}]A(x)\Delta x$$

which yields the differential equation:

$$\frac{\dot{m}_g}{A(x)} \frac{dy_2}{dx} = M_g\sigma_2$$

where:

$$\sigma_2 = k_2y_3 + k_4y_4 + k_6y_6 + nk_8\psi_7\xi_7\psi_{16}\xi_{16}$$

For CO_2 , NO and H_2O , the same differential equation is found, with the exception that the term σ varies. This depends on the reactions where each species is involved. Thus, we have in general:

$$\frac{\dot{m}_g}{A(x)} \frac{dy_i}{dx} = M_g\tilde{\sigma}_i, \quad \text{where: } i = 2, 4, 5, 9 \quad (3.12a)$$

where:

$$\begin{aligned} \tilde{\sigma}_2 &= k_2y_3 + k_4y_{10} + k_6\psi_{16}\xi_{16} + nk_8\psi_7\xi_7\psi_{16}\xi_{16} \\ \tilde{\sigma}_4 &= k_1y_3 + k_3y_{10} + k_5\psi_{16}\xi_{16} \\ \tilde{\sigma}_5 &= 0.5nk_8\psi_7\xi_7\psi_{16}\xi_{16} \\ \tilde{\sigma}_9 &= 2k_3y_{10} + k_4y_{10} \end{aligned} \quad (3.12b)$$

C balance The soot mass balance equation gives the rate that soot disappears from the deposit owing to combustion. This happens because of reactions with O₂, NO₂ and CeO₂. In order to find the rate of soot mass change, we integrate, along the soot layer, the rates of consumption of soot due to the respective reactions:

$$\frac{1}{M_C} \frac{dm}{dt} = - \int_{-w}^0 \left[(k_1 + k_2)y_3 + (k_3 + k_4)y_{10} + (k_5 + k_6)\psi_{16}\xi_{16} \right] A(x) dx \quad (3.13)$$

Ce and CeO₂ balances Two mass balance equations must be formulated for the catalytic additive, for Ce and CeO₂ respectively. First, we deal with the mass balance equation for Ce, which accounts for its depletion and the corresponding deposition of inactive Ceria ash, because of oxidation of CeO₂ molecules. Since ξ_{16} is averaged along the soot layer, the mass balance equation may not be formulated for a volume element $A(x)dx$ but, instead, should consider the whole soot layer at once.

$$\left(\int_{-w}^0 \frac{\rho_1 A(x) dx}{M_C} \right) \frac{d\xi_{16}}{dt} = \int_{-w}^0 - \left(4k_5 + 2k_6 + (2n + m)k_8\psi_7\xi_7 \right) \psi_{16}\xi_{16} A(x) dx \quad (3.14)$$

The mass balance for CeO₂ is similar to that for Ce, but contains an extra term for the production of CeO₂ because of Ce₂O₃ oxidation with O₂. Bearing in mind that the rate of CeO₂ consumption is $d(\xi_{16}\psi_{16})/dt$ [mol/(mol soot · s)], the balance equation for CeO₂ is:

$$\begin{aligned} & \left(\int_{-w}^0 \frac{\rho_1 A(x) dx}{M_C} \right) \frac{d\psi_{16}\xi_{16}}{dt} = \\ & \int_{-w}^0 \left[- \left(4k_5 + 2k_6 + (2n + m)k_8\psi_7\xi_7 \right) \psi_{16}\xi_{16} + k_7y_3(1 - \psi_{16})\xi_{16} \right] A(x) dx \end{aligned} \quad (3.15)$$

HC balance The HC mass balance describes the consumption of HC because of oxidation with CeO₂ and physical desorption. The amount of HC in the soot layer is $\psi_7\xi_7$, but it is assumed that the total HC capacity ξ_7 of the soot layer is constant throughout the regeneration. Then, the availability of HC ψ_7 changes according to the following differential equation:

$$\left(\int_{-w}^0 \frac{\rho_1 A(x) dx}{M_C} \right) \xi_7 \frac{d\psi_7}{dt} = \int_{-w}^0 - \left(k_8\psi_{16}\xi_{16} + k_9 \right) \psi_7\xi_7 A(x) dx \quad (3.16)$$

Similarly to the Ce and CeO₂ balances, the above mass balance is formulated directly for the whole soot layer, because ξ_7 and ψ_7 are average quantities and may not be defined for an elementary volume $A(x)dx$.

Note that, since there are only HC-consuming reactions in the present reaction scheme, and no adsorption effects are accounted for, the HC content of soot is monotonically decreasing. This should be more or less accurate for the regeneration phase of filter operation, although it is certainly not valid for the loading phase.

Heat balance Finally, the balance equation for heat is needed. It describes the heat exchange between the ceramic and gas because of the gas flow *through* the wall of the monolith. The total heat flow, expressed as [J/s], is obtained as the sum of the heat flows because of (a) reactions, (b) convection and (c) conduction along x .

$$\rho_j c_{p_j} A(x) \frac{\partial T}{\partial t} = -\dot{q}(x)A(x) + \frac{\partial}{\partial x} \left(A(x) \lambda_j \frac{\partial T}{\partial x} \right) - \dot{m}_g c_{p,g} \frac{\partial T_g}{\partial x} \quad (3.17)$$

where the heat flux $\dot{q}(x)$ [$\text{J}/(\text{m}^3 \text{soot} \cdot \text{s})$] is defined as the sum of the products of the reaction rates r_n (Table 3.1) and the reaction enthalpies ΔH_n :

$$\dot{q}(x) = \begin{cases} \sum_{n=1}^9 r_n \Delta H_n & \text{if } -w \leq x \leq 0 \\ 0 & \text{if } 0 \leq x \leq w_s \end{cases} \quad (3.18)$$

Obviously, no reactions occur as the gas flows through the ceramic wall, thus \dot{q} is zero in this region.

Boundary conditions Equations (3.10a)–(3.17) are a set of differential equations that define the regeneration model. To complete model's formulation, a set of boundary conditions is needed. This is defined as follows:

$$\text{At } x = -w : \quad y_i(x = -w) = y_i^{in}(t) \quad (3.19)$$

$$A(x = -w) \lambda_1 \frac{dT}{dx} = \dot{m}_g c_{p,g} [T - T_g^{in}] \quad (3.20)$$

$$\text{At } x = +w_s : \quad \frac{\partial T}{\partial x} = 0 \quad (3.21)$$

The second boundary condition at $x = -w$, equation (3.19) deserves some further comments. It implies that the gas and the solid temperatures are equal everywhere except at the inlet face of the deposit layer.* This boundary condition is due to Bissett and Shadmann [3]. Quoting them: "...a typical length scale over which the gas temperature adjusts to differences with the solid temperature is several orders of magnitude smaller than typical deposit layer thickness". Thus, it is safe to use boundary condition (3.19), in combination with the assumption that $T_g = T$ everywhere except at $x = -w$. This removes the need to compute a profile for gas temperature along x .

Furthermore, in the same work, Bissett and Shadmann mathematically prove that, if the temperature T is assumed uniform along the soot layer and deposit, the error of the solution of the system of balance equations obtained will be in the order of magnitude of a dimensionless parameter ϵ , defined as:

$$\epsilon = \frac{c_{p,g} \dot{m}_g w}{k_1 \bar{A}}, \quad (3.22)$$

where \bar{A} is the average of $A(x)$ along the soot layer, $\bar{A} = 4(l - w)w$. In that work, only reaction 1 was accounted for by the model, thus only k_1 appears in (3.22). The value of ϵ is of the order of 10^{-4} , which means that it is an excellent approximation to assume that the temperature T of the deposit is uniform along x . This also removes the need to compute a profile for solid temperature along x .

The above approximation is critical, because it implies that the reaction rates are constant along the soot layer. Therefore, the balance equations may be integrated *analytically* along x . This is demonstrated in the section that follows.

*Normally, instead of this boundary condition, we should use two separate boundary conditions at $x = -w$, (a) for the solid temperature: $\partial T / \partial x = 0$ and (b) for the gas temperature: $T_g(x = -w) = T_g^{in}$. Then, we should solve for the two coupled temperature profiles, $T(x)$ and $T_g(x)$.

3.4.4 Analytical spatial integration of balances

Our objective here is to integrate analytically the balance equations along the soot layer width (direction x). As discussed in the previous section, this is possible since the temperature of the soot is constant along the soot layer. The calculation should yield:

- the total consumption or production of each gaseous phase species Δy_i
- the total carbon mass consumption
- the total change in hydrocarbon and Ceria availability (ψ_7 and ψ_{16} respectively)
- the total heat release because of all chemical reactions

We proceed to the integration of the model's mass balances in the same order with Section 3.4.3.

O₂ and NO₂ balance integrations We first focus on the oxygen mass balance (3.10a). This is a linear differential equation that can be readily solved to give the following oxygen profile:

$$y_3 = \begin{cases} y_3^{in} \exp\left(-\frac{M_g \sigma_3}{\dot{m}_g} 4\Delta z (\ell + x - w)(x + w)\right) & \text{if } -w \leq x \leq 0 \\ y_3^{in} \exp\left(-\frac{M_g \sigma_3}{\dot{m}_g} 4\Delta z (\ell - w)w\right) & \text{if } 0 \leq x \leq w_s \end{cases} \quad (3.23)$$

and the total consumption of oxygen Δy in the soot layer can be then computed:

$$\Delta y_3 = y_{10}(-w) - y_{10}(0) = y_3^{in} \left[1 - \exp\left(-\frac{M_g \sigma_3}{\dot{m}_g} V_1\right) \right] \quad (3.24)$$

The NO₂ concentration profile is computed in an analogous manner from equation (3.11a). The total amount of NO₂ consumption in the soot layer is thus:

$$\Delta y_{10} = y_{10}(-w) - y_{10}(0) = y_{10}^{in} \left[1 - \exp\left(-\frac{M_g \sigma_{10}}{\dot{m}_g} V_1\right) \right] \quad (3.25)$$

It should be noted that the balance equation (3.10a) for O₂ may be transformed as follows:

$$-\frac{\dot{m}_g}{M_g \sigma_3} dy_3 = y_3(x) A(x) dx$$

which may be integrated from $x = -w$ to $x = 0$ to yield the following result:

$$\int_{-w}^0 y_3(x) A(x) dx = +\frac{\dot{m}_g}{M_g \sigma_3} \Delta y_3 \quad (3.26)$$

A completely analogous result may be obtained from the NO₂ balance equation (3.11a):

$$\int_{-w}^0 y_{10}(x) A(x) dx = +\frac{\dot{m}_g}{M_g \sigma_{10}} \Delta y_{10} \quad (3.27)$$

These integrals will be used in the spatial integration of the rest of the balances.

CO, CO₂, NO and H₂O balances integration It follows from the reaction scheme that CO, CO₂, NO and H₂O appear only as products, and therefore, the concentration y_i of each of these chemical species is not involved in any of the reaction rates. Therefore, the terms σ_i (see (3.12b)) do not contain the corresponding species concentration y_i . As a result, the balance equation for each product (3.12) may be directly integrated to give:

$$\int_{-w}^0 dy_i = \frac{M_g}{\dot{m}_g} \int_{-w}^0 \sigma_i A(x) dx, \quad \text{where: } i = 2, 4, 5, 9 \quad (3.28)$$

The integration results depends on the value of σ_i . Specifically, we have:

$$-\Delta y_2 = \frac{k_2}{\sigma_3} \Delta y_3 + \frac{k_4}{\sigma_{10}} \Delta y_{10} + \left(k_6 \psi_{16} \xi_{16} + n k_8 \psi_7 \xi_7 \psi_{16} \xi_{16} \right) \frac{M_g V_1}{\dot{m}_g} \quad (3.29)$$

$$-\Delta y_4 = \frac{k_1}{\sigma_3} \Delta y_3 + \frac{k_3}{\sigma_{10}} \Delta y_{10} + k_5 \psi_{16} \xi_{16} \frac{M_g V_1}{\dot{m}_g} \quad (3.30)$$

$$-\Delta y_5 = 0.5 m k_8 \psi_7 \xi_7 \psi_{16} \xi_{16} \frac{M_g V_1}{\dot{m}_g} \quad (3.31)$$

$$-\Delta y_9 = \frac{2k_3 + k_4}{\sigma_{10}} \Delta y_{10} = \Delta y_{10} \quad (3.32)$$

C balance integration The carbon balance refers to the soot layer as a whole and therefore it is already in integral form. Simplifying (3.13), the rate of soot mass consumption is:

$$\begin{aligned} \frac{dm}{dt} = & - M_C (k_1 + k_2) \int_{-w}^0 y_3(x) A(x) dx \\ & - M_C (k_3 + k_4) \int_{-w}^0 y_{10}(x) A(x) dx \\ & - M_C (k_5 + k_6) \psi_{16} \xi_{16} \int_{-w}^0 A(x) dx \end{aligned}$$

Substituting (3.26) and (3.27) to the above equation, we get the total rate of soot consumption, which is a sum of three terms. The first two account for the soot consumption because of oxidation by O₂ and NO₂, and the third gives the consumption because of oxidation with the additive:

$$\begin{aligned} \frac{dm}{dt} = & - \frac{M_C}{M_g} \frac{k_1 + k_2}{\sigma_3} \dot{m}_g \Delta y_3 \\ & - \frac{M_C}{M_g} \frac{k_3 + k_4}{\sigma_{10}} \dot{m}_g \Delta y_{10} \\ & - M_C (k_5 + k_6) \psi_{16} \xi_{16} V_1 \end{aligned} \quad (3.33)$$

Ce and CeO₂ balances integration Similarly to the carbon balance, the Ce balance (3.15) is already in integral form, since ξ_{16} is a quantity that is defined with respect to the total thickness of the soot layer. It may be readily simplified to give:

$$\frac{d\xi_{16}}{dt} = - \frac{M_C}{\rho_1} \left(4k_5 + 2k_6 + (2n + m) k_8 \psi_7 \xi_7 \right) \psi_{16} \xi_{16} \quad (3.34)$$

Obviously, the same applies for the CeO₂ balance. The corresponding mass balance becomes:

$$\begin{aligned}\frac{d(\psi_{16}\xi_{16})}{dt} = & -\frac{M_C}{\rho_1} \left(4k_5 + 2k_6 + (2n+m)k_8\psi_7\xi_7 \right) \psi_{16}\xi_{16} \\ & + \frac{M_C}{\rho_1} \left(k_7(1-\psi_{16})\xi_{16} \right) \frac{\int_{-w}^0 y_3(x)A(x)dx}{\int_{-w}^0 A(x)dx}\end{aligned}$$

and, substituting from equations (3.8) and (3.26), we get:

$$\begin{aligned}\frac{d(\psi_{16}\xi_{16})}{dt} = & -\frac{M_C}{\rho_1} \left(4k_5 + 2k_6 + (2n+m)k_8\psi_7\xi_7 \right) \psi_{16}\xi_{16} \\ & + \frac{k_7(1-\psi_{16})\xi_{16}}{\sigma_3} \frac{\dot{m}_g}{\rho_1 V_1} \frac{M_C}{M_g} \Delta y_3\end{aligned}\quad (3.35)$$

HC balance integration The hydrocarbon mass balance (3.16) may be also directly be employed to derive the rate of change of ψ_7 :

$$\frac{d\psi_7}{dt} = -\frac{M_C}{\rho_1} \left(k_8\psi_{16}\xi_{16} + k_9 \right) \psi_7 \quad (3.36)$$

Heat balance integration Finally, we have to integrate the heat transfer balance (3.17) along x to get the total heat exchange. Substituting the boundary condition (3.19) and that $T_g = T = const$, we integrate from $x = -w$ to $x = w_s$:

$$\begin{aligned}\rho_1 c_{p,1} \frac{\partial T}{\partial t} \int_{-w}^0 A(x)dx + \rho_2 c_{p,2} \frac{\partial T}{\partial t} \int_0^{w_s} A(x)dx = & (\Delta H_1 k_1 + \Delta H_2 k_2) \int_{-w}^{w_s} y_3(x)A(x)dx \\ & (\Delta H_3 k_3 + \Delta H_4 k_4) \int_{-w}^{w_s} y_{10}(x)A(x)dx \\ & (\Delta H_5 k_5 + \Delta H_6 k_6) \psi_{16}\xi_{16} \int_{-w}^{w_s} A(x)dx \\ & 0.5 \Delta H_7 k_7 (1 - \psi_{16}) \xi_{16} \int_{-w}^{w_s} y_3(x)A(x)dx \\ & (\Delta H_8 k_8 \psi_{16}\xi_{16} \psi_7\xi_7 + \Delta H_9 k_9 \psi_7\xi_7) \int_{-w}^{w_s} A(x)dx \\ & - \int_{-w}^{w_s} \frac{\partial}{\partial x} \left(\dot{m}_g c_{p,g} (T - T_g^{in}) \right) dx.\end{aligned}$$

which finally yields:

$$\begin{aligned}\frac{dQ}{dt} = & (\rho_1 c_{p,1} V_1 + \rho_2 c_{p,2} V_2) \frac{\partial T}{\partial t} = -\frac{(\Delta H_1 k_1 + \Delta H_2 k_2)}{\sigma_3} \frac{\dot{m}_g}{M_g} \Delta y_3 \\ & - \frac{(\Delta H_3 k_3 + \Delta H_4 k_4)}{\sigma_{10}} \frac{\dot{m}_g}{M_g} \Delta y_{10} \\ & - (\Delta H_5 k_5 + \Delta H_6 k_6) \psi_{16}\xi_{16} V_1 \\ & - \frac{0.5 \Delta H_7 k_7 (1 - \psi_{16}) \xi_{16}}{\sigma_3} \frac{\dot{m}_g}{M_g} \Delta y_3 \\ & - (\Delta H_8 k_8 \psi_{16}\xi_{16} \psi_7\xi_7 + \Delta H_9 k_9 \psi_7\xi_7) V_1 \\ & + \dot{m}_g c_{p,g} (T - T_g^{in}).\end{aligned}\quad (3.37)$$

In the above, Q is the heat which is exchanged between the gas and the soot and wall. This heat exchange is due to chemical reactions and convection as gas flows through the soot layer and the wall. This heat source term is used to compute the temperature change of soot, wall and gas. This is accomplished at the channel level of the model, where two more heat source terms are accounted for: heat conduction through the wall and soot, and heat convection due to gas flow that is *parallel* to the inlet and outlet of the channel.

Solution Equations (3.33)–(3.37) define a system of differential equations that are integrated numerically over time. The initial conditions of the problem are comprised by the profiles of mass flow rate, inlet gas temperature and gas concentrations over time. Solution over time is forwarded employing the explicit Euler method.

3.5 Channel model

The channel model presented herein follows the approach of Bissett [38] and Kolt-sakis et al. [50].

As already mentioned, the wall-flow filter consists of a series of channels, arranged in an orthogonal grid, that are alternatively plugged at one end. We shall refer to the channels that are open at the filter's inlet and plugged at the filter's outlet as *inlet* channels. Similarly, we shall refer to those channels that are plugged at the filter's inlet and open at the filter's outlet as *outlet* channels.

The exhaust gas flows into the inlet channels of the filter and, since they are plugged at the other end, is forced to flow through the channel wall to four adjacent outlet channels. Reversely, gas flows into each outlet channel from four adjacent inlet channels. This arrangement is shown in Figure 3.8.

Adjacent channels interact because of (a) heat conduction and (b) mixing of exhaust gas at the outlet channel. In fact, interactions between channels should be handled by modeling at the reactor level. Nevertheless, we examine this issue here because it is important so as to decide which is the volume element that calculations at channel level refer to. Of course, we assume here that a three-dimensional reactor model is used.*

It may be shown that the second type of interaction (mixing of exhaust gas at the outlet channels) has to be *neglected* if a realistic model is to be formulated. To make our argument clear, an example is helpful.

In principle, at a point z along the axis of the filter, gas flowing from each adjacent inlet channel has different temperature and mass flow rate. If we do *not* neglect mixing, the mass flow rate at a point $z + \Delta z$ is the sum of the mass flow rates at z , while their temperature should be computed as an average, weighted with the mass flow rates. What is important here, is that this temperature is needed for the computation of heat convection to/from the walls at $z + \Delta z$.

Thus, for the determination of the convective heat transfer along a channel, information from the adjacent channels is needed, if we do not neglect mixing. Since this is valid for all channels, we have to treat every channel individually. While we

*If we employ a one-dimensional reactor model, all channels are treated identically and no channel interactions are assumed.

could formulate such a detailed model, it is not sensible to do this in terms of computational power requirements.

It is our choice therefore to neglect the mixing of the exhaust gas at the outlet channel. It is convenient then to define one inlet channel and four quarters of the four adjacent outlet channels as the volume element for channel level computations.* The volume element has also been depicted in Figure 3.8. Neglecting mixing is equivalent to assuming that the boundaries of the element are adiabatic. No flow occurs through them to the rest of the outlet channel. From the standpoint of modeling, the whole filter is constructed by tiling this elementary volume.

The purpose of the channel model is to calculate the flow distribution of the exhaust gas at the inlet and outlet channel and the heat transfer between the gas and the wall due to convection. Our model consists of three balance equations, regarding

1. the conservation of the exhaust gas mass flow,
2. the conservation of the axial component of momentum of exhaust gas,
3. the conservation of the energy of the exhaust gas, and

Below, we examine each one of them in detail. We shall distinguish between exhaust gas properties in the inlet and outlet channel and the soot layer/wall employing the subscripts *in*, *out* and *w* respectively.

Conservation of mass of the exhaust gas The exhaust gas mass balances state that, at each axial point of the inlet channel, the change of the exhaust gas flow is equal to the flow leaving (entering) the input (output) channel via the porous wall.

$$\frac{\partial}{\partial z}(\rho_{in}v_{in}) = -(4/\ell)\rho_w v_w \quad (3.38)$$

$$\frac{\partial}{\partial z}(\rho_{out}v_{out}) = +(4/\ell)\rho_w v_w \quad (3.39)$$

Apparently, the exhaust gas velocity component that is perpendicular to the wall is not constant through the soot layer, because the latter is a trapezoid. Here, we use as reference point the inlet face of the wall ($x = 0$). Thus, we denote by v_w the velocity through the wall and, consequently, $4/\ell$ is the specific area of the channel wall.

Conservation of z-component of momentum of the exhaust gas The balance equation for the axial component of the momentum of the gas states that the axial pressure variation is due to convective transport of the z-component of momentum and the viscous drag forces exerted in the gas flow. The balance equation is the same for both channels.

$$\frac{\partial p}{\partial z} + \frac{\partial}{\partial z}\rho_i v_i^2 = \frac{-a\mu(T)v}{D^2}, \quad i = in, out \quad (3.40)$$

The viscous drag is caused because there is a gradient of the axial velocity of the gas, as axial velocity reduces to zero at the walls. According to Bissett and Shadmann [38], these drag forces should be near those observed for an impermeable wall,

*Henceforth, when we refer to the outlet channel, we shall mean the four outlet channel quarters of this volume element.

because only a small fraction of the gas penetrates the wall at each axial point. The correlation for laminar flow is appropriate in the channels of the wall-flow DPF.

It must be noted that, in the above equation, there is no term for convective transport of the z-component of momentum through the porous wall, because we assume that the exhaust gas flow through the wall is perpendicular to the wall's face.

Conservation of energy of the exhaust gas Energy is transferred between the axially-flowing exhaust gas through the gas–solid interface and because gas flow to and from the porous wall. The energy balance for the inlet channel is:

$$c_{p,g} \frac{\partial}{\partial z} (\rho_{in} v_{in} T_{in}) = -(4/\ell) \rho_w v_w T_{in} + h_{in} (4/\ell) (T_w - T_{in}) \quad (3.41)$$

The corresponding balance for the outlet channel differs in second term that concerns energy transport via the flow through the porous wall. Apart from the sign of the term, the temperature is different, because the gas leaving the porous wall has the temperature of the wall.

$$c_{p,g} \frac{\partial}{\partial z} (\rho_{out} v_{out} T_{out}) = -(4/\ell) \rho_w v_w T_w + h_{out} (4/\ell) (T_w - T_{out}) \quad (3.42)$$

Solution procedure The solution procedure first calculates the axial distribution of the mass flow rate. An original pressure distribution along the inlet and outlet channel is first assumed. Given the pressure drop along the soot layer and the wall, eq. (3.4) is used to compute the flow for each point z at the axial direction. Then, the axial velocities at each point may be computed using (3.38) and (3.39). The pressure drop distribution along the z axis may then be extracted by (3.40), which should match the originally assumed pressure drop distribution. This suggests the implementation of a trial-and-error solution procedure.

Having calculated the axial pressure and mass flow rate distribution, the gas temperature distribution is calculated for the inlet and outlet channels using equations (3.41) and (3.42).

The boundary conditions that are used for the above solution procedure are the following:

$$\begin{aligned} \text{At } z = 0 : \quad & u_{out}(z = 0) = 0 \\ & T_{in}(z = 0) = T_{inlet} \\ \text{At } z = L : \quad & u_{in}(z = L) = 0 \end{aligned}$$

The boundary conditions are imposed by the structure of the filter, since the inlet channel is plugged at the rear (outlet) of the filter ($z = L$) while the outlet channel is plugged at the front (inlet) of the filter ($z = 0$).

3.6 Reactor model

As argued in the previous section, we assume that the only interaction between different channels is via heat conduction. The two reactor level models that are described below are therefore heat transfer models for transient heat conduction in the wall-flow DPF.

The first is a simple, one-dimensional adiabatic model of heat conduction along a monolith's channel. This reactor model, together with the model modules described previously, comprise the CATWALL model, which is a commercial product of the Laboraroty of Thermodynamics and Thermal Engines, University of Thessaly [51]. Henceforth, the name CATWALL will be used for brevity for either the full 1D model for DPF regeneration, or any of its components.

The second is a full-featured three-dimensional model of the filter that was implemented by linking the 1D DPF model a finite element method (FEM) software suite. Two instances of this model have been created, since the 1D DPF model was linked to both ABAQUS and ANSYS commercial software suites. Both of the FEM suites substitute the 1D reactor model of CATWALL to provide fully three-dimensional temperature–stress field calculations.

The primary assumptions for the formulation of the model are similar to those employed for the three-way catalytic converter model. Specifically, we assume that:

- Heat losses from the front and the rear face of the monolith are neglected in all models that have appeared in the literature.
- Heat losses from the monolith's side face are neglected in the one-dimensional version of the model. Thus, the 1D CATWALL is adiabatic, which is acceptable in the simplified for 1D modeling, since the filter is always well insulated. This approximation is raised in the case of the three-dimensional model that results from the interfacing of CATWALL with a FEM software, since the FEM software allows the user to impose any boundary condition on the model without much difficulty.
- The flow rate and temperature profiles of the exhaust gas at the inlet of the filter are usually considered uniform unless they are measured.

Furthermore, the one-dimensional channel model of the DPF inevitably assumes that all channels operate under identical conditions at the filter inlet. On the contrary, the three-dimensional model allows for the effect of non-uniform distribution of exhaust gas temperature and mass flow rate at the inlet of the filter.

Usually, no such detailed data are available in routine measurements. Nevertheless, the velocity profile in front of the DPF is mainly affected by the DPF itself, depending on the distribution of the deposit inside the filter. Therefore, an extra module for the estimation of the flow field in front of the filter was developed in order to complement the 3D reactor model. Thus, in the 3D reactor model described herein, the assumption that channels operate under identical inlet conditions is raised in respect of the gas flow distribution, while it is retained for the gas temperature distribution.

3.6.1 1D reactor model

According to the above assumptions, an one-dimensional heat balance equation is formulated for the simple, 1D DPF model. It implements 1D heat conduction along the soot layer and the wall of the channel.

$$\rho_s c_{ps} \frac{\partial T_s}{\partial t} = \lambda_{s,z} \frac{\partial^2 T_s}{\partial z^2} + \dot{Q}_{total} \quad (3.43)$$

where the source term \dot{Q}_{total} is the sum of all heat sources sinks at each axial position z , i.e.:

$$\dot{Q}_{total} = +h_{in}(4/\ell)(T_g - T(z)) + h_{out}(4/\ell)(T_g - T) + \frac{dQ}{dt} \quad (3.44)$$

In the above equation, the source term dQ/dt represents the heat released by chemical reactions and heat convected from the gas flowing perpendicularly to the soot layer and wall. The source terms $h_i(4/\ell)(T_g - T)$ represents heat convected to the wall because of gas flow parallel to the soot and wall.

The 1D heat transfer balance is a parabolic partial differential equation that is solved numerically using a simple Euler discretization scheme [52]. The initial condition is

$$T(z, t = 0) = T_0 \quad (3.45)$$

while the boundary conditions are:

$$\left. \frac{dT}{dz} \right|_{z=0} = \left. \frac{dT}{dz} \right|_{z=L} = 0 \quad (3.46)$$

This indicates that no heat transfer occurs the surrounding air and the inlet/outlet of the filter.

3.6.2 3D reactor model

A non-uniform three-dimensional temperature field in the filter is the result of (a) heat losses to the ambient air, and (b) the non-symmetric structure of the filter, which is especially true for SiC block filters. Block filters are constructed by smaller filter blocks, made of SiC, which are arranged in a Cartesian grid and are glued together using a special cement layer (Figure 3.10 below). The cement layer has different physical properties than the SiC, especially lower thermal conductivity.

The three-dimensional model involves calculation of the interaction between the adjacent channels of the DPF filter. Since the only interaction between channels is assumed to be through heat transfer, the heat balance calculation in three dimensions should be solved by the model.

$$\rho_s c_{p,s} \frac{\partial T}{\partial t} = \nabla \cdot (\lambda \nabla T) + \dot{Q}_{total} \quad (3.47)$$

The source term \dot{Q}_{total} is, analogously to (3.44), the sum of all heat sources, but now it is a three-dimensional field, i.e.: $\dot{Q}_{total} = \dot{Q}_{total}(r, \vartheta, z)$ (cylindrical coordinates).

The solution is accomplished by either ANSYS or ABAQUS, which calculates the three-dimensional temperature field in the filter relying on the CATWALL model to provide the heat source terms involved in the heat transfer balance. This requires the interfacing of the FEM software with the 1D CATWALL core model. The interfacing is possible through the use of the user-subroutine feature of the above FEM software suites, that allows the user to write custom functions for properties or source terms of the elements. Such user subroutines are customarily written in FORTRAN, which is also the language of the CATWALL implementation. Since the interfacing of such a complex model as CATWALL with ANSYS is not trivial, the details of the implementation are subsequently presented separately.

The calculation of the non-uniform temperature field in the filter allows the model to account for the so-called partial regenerations, after which significant portions of the soot deposited remain unburned in the filter because of unfavourable conditions

for regeneration propagation (usually low temperature). Partial regenerations affect the distribution of the flow field at the inlet of the filter, since the flow is then channeled through the low flow resistance areas of the filter.

As already mentioned, a submodel has been developed in this work in order to take into account this effect. According to this submodel, the filter channels are viewed as a set of flow resistances in parallel. The objective of the model is to distribute the total mass flow rate at the inlet of the filter so that the pressure drop induced from each channel is the same. In fact, not every channel of the filter is treated separately, because of the excessive computational power required. Rather, the model separates sectors of channels that are treated identically. These sectors correspond to the meshing of the filter that is used from ANSYS for the temperature field calculation.

For the determination of the pressure drop from each channel sector, the procedure described in the DPF channel model is employed (Section 3.5). Because of the quadratic term of eq. (3.40) and the dependence of physical properties on the pressure and temperature of the gas at each point, the pressure drop Δp_i for each sector i of channels is a non-linear function of the mass flow rate \dot{m}_i at the inlet of the sector: $\Delta p = f(\dot{m}_i)$. As already mentioned, there is not a closed-form expression for the function f , and, given \dot{m}_i , the pressure drop Δp_i may only be calculated by a trial-and-error procedure, following the usual procedure for pipe networks [53].

Nevertheless, the function f is *nearly* linear, because the pressure losses are mainly induced by the gas flow through the soot layer and the wall. Therefore, the total pressure losses for each channel may be approximately computed by a relation of the form $\Delta p_i = R_i \dot{m}_i$, where R_i is the flow resistance of the sector.

This fact has been exploited in order to develop an iterative procedure to compute the flow distribution at the filter inlet. The procedure features the following steps:

Step 1 Provide an initial guess for the flow rate \dot{m}_i of each sector. Assuming that the cross-sectional (frontal) area of each sector is A_i , the total cross-sectional area is A and the total inlet mass flow rate is \dot{m} , we provide the initial guess that $\dot{m}_i = \dot{m}(A_i/A)$, which corresponds to uniform flow distribution.

Step 2 Calculate the induced pressure drop for each sector $\Delta p_i = f(\dot{m}_i)$.

Step 3 Calculate the approximate linear flow resistance R_i for each sector: $R_i = \Delta p_i / \dot{m}_i$.

Step 4 Calculate the approximate linear flow resistance of the whole filter: $\bar{R}^{-1} = \sum R_i^{-1}$

Step 5 Calculate an approximate value for the pressure drop of the whole filter: $\Delta p = \bar{R} \dot{m}$.

Step 6 Calculate new values for the flow rates of each sector: $\dot{m}'_i = \Delta p / R_i$.

Steps 2–6 are repeated until a set of flow rates for each sector is obtained so that the calculated induced pressure drop Δp_i is the same for every sector. The above iterative procedure converges quickly (usually after 3 to 10 iterations) to the desired set of mass flow rates.

3.6.3 3D heat transfer calculation by CATWALL-ANSYS interfacing

In order to solve the problem of the calculation of the three-dimensional temperature field of the filter by interface CATWALL with the general-purpose FEM software, the user programmable features of the FEM package are used. This involved the development of (a) a model of the diesel particulate filter in the ANSYS environment and (b) a set of interface subroutines that handle the task of data interchange between CATWALL and ANSYS or ABAQUS. The interface concept is the same for both ANSYS and ABAQUS. For the purpose of the presentation of the interface, we will assume the case of ANSYS–CATWALL interface, because it is more complete than the ABAQUS–CATWALL interface.

Finite element model of the DPF The solid model of the filter of the ANSYS FEM software is the description of the geometric shape of the DPF. The volumes comprising the solid model are then assigned material properties. The solid model is then used to generate the finite-element model that is actually used by the FEM solver.

The solid model of the DPF is given in Figure 3.10. Evidently, only a quarter of the cylindrical DPF is model, because of the symmetry of its structure. The solid model comprises of different volumes for the main part of the SiC filter blocks, the inlet and outlet regions of the blocks (where the plugs are), the adhesive of the filter blocks (cement), the insulation mat and the canning. Depending on the volume, different material properties are assigned. In this case, the material properties assigned were the thermal capacity, thermal conductivity and density.

Evidently, the solid model of the filter is simplified, in the sense that the detailed structure of the filter with its grid of channels and plugs is replaced by continuous volumes. The modeling of the filter structure as a continuum was done for simplicity and speed of the computation. This approach necessitates the use of bulk quantities for the density and the heat conductivity of the SiC filter blocks, which are computed using the void fraction of the filter structure, that is:

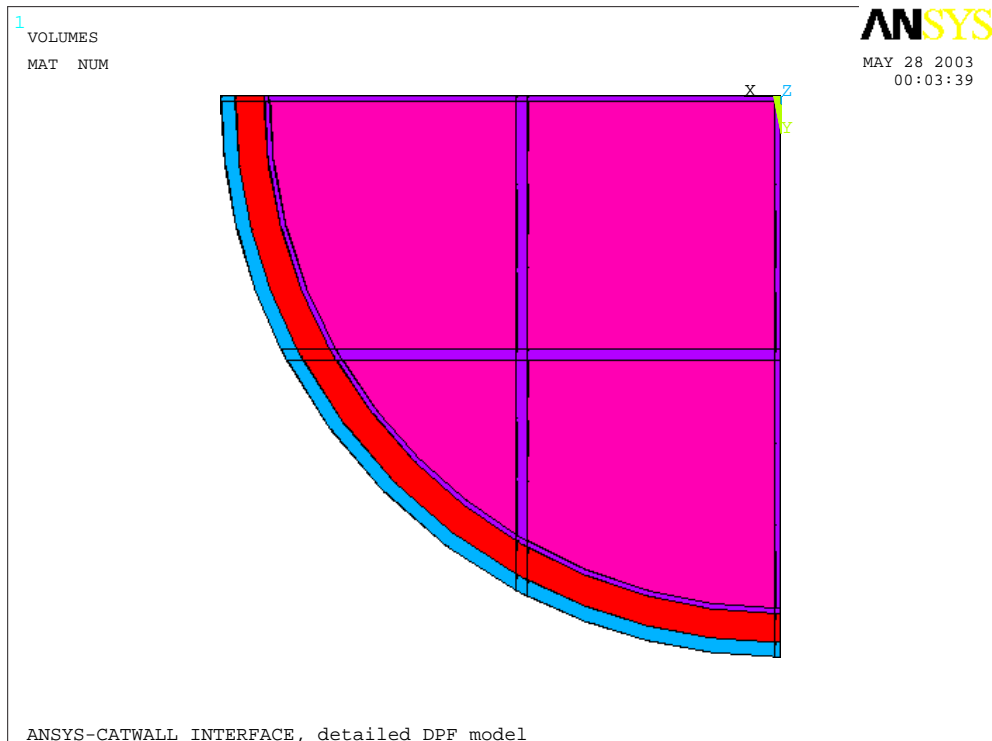
$$\rho_{bulk} = \varepsilon \rho \quad \lambda_{bulk} = \varepsilon \lambda \quad (3.48)$$

Because of the presence of the plugs, the void fraction ε_{plug} of the inlet and outlet regions of the filter blocks is different from the void fraction of their main part. Therefore, separate volumes are defined for the plug regions of the solid model, as already mentioned above. These volumes are assigned the bulk density and heat conductivity of the plug regions that were computed using ε_{plug} instead of ε . The (real and bulk) temperature dependent material properties of the SiC, adhesive, insulation mat and canning that were used in this work are given in Table 3.3.

ANSYS meshes the solid model to construct the finite element model of the DPF, which consists of elements and nodes. For ANSYS, the element type that was chosen for meshing was SOLID70, which is a thermal solid element. It has eight nodes with a single degree of freedom, temperature, at each node. The meshed finite element model of the DPF that has been used in this work is illustrated in Figure 3.11. In conjunction with grid generation, two fundamental points have to be noted.

First, there is no restriction—that is imposed from CATWALL—regarding the cross-sectional shape of the elements. Each row of elements along the axial direction that corresponds to SiC (magenta-coloured areas of Figure 3.11-a) is referred to as a

(a)



(b)

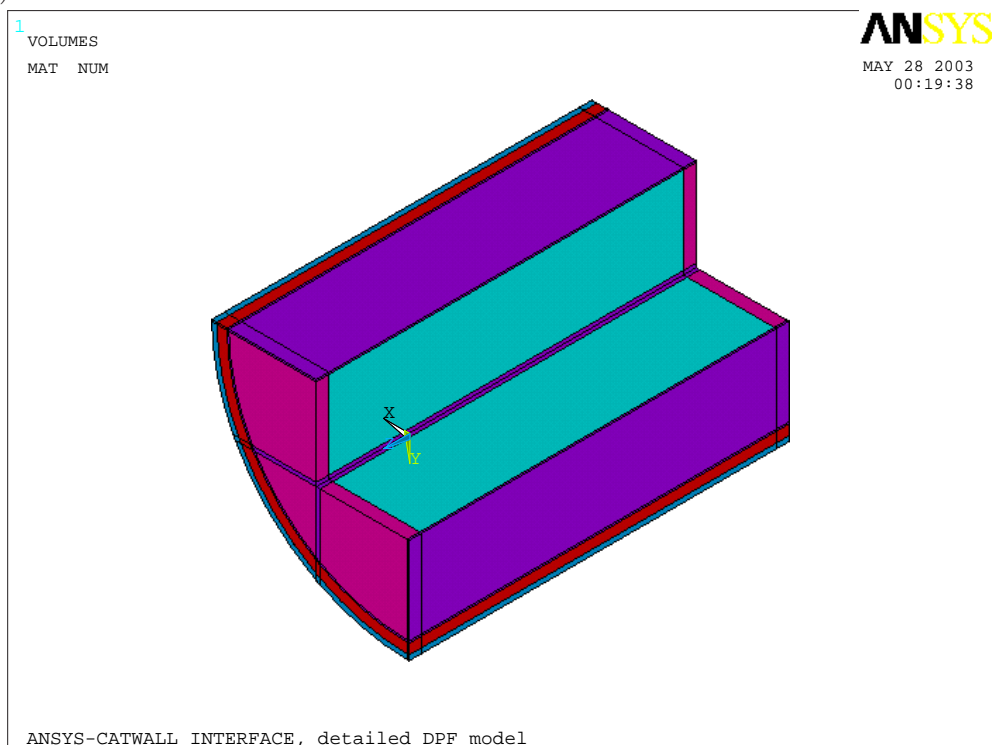


Figure 3.10: Solid model of the DPF. Different materials are designated by different colors. (a) Front view: blue=canning, red=insulation, purple=adhesive, magenta=SiC-plug region. (b) Side view, with the central filter block and adhesive removed. The different materials for the plug region (magenta) and the main region (cyan) of the SiC filter blocks are visible.

Temper- ature [°C]	SiC				adhesive		insulation		canning	
	real	bulk (main)	bulk (plug)	c_p	λ	c_p	λ	c_p	λ	c_p
25	57.1	21.4	39.3	686	0.187	740	0.04	1190	15.2	466.5
250	35.4	13.3	24.4	1005	0.222	1012	0.05	1190	19.4	538.2
500	24.6	9.2	16.9	1123	0.241	1141	0.08	1190	22.4	588.1
7500	19.8	7.4	13.6	1182	0.242	1188	0.12	1190	24.5	623.8
1000	15.0	5.6	10.3	1219	0.302	1200	0.17	1190	26.2	651.7
1250	13.0	4.9	8.9	1230	0.350	1205	0.23	1190	27.5	670.0
	ρ				ρ		ρ		ρ	
	1800	675	1238		137		300		7900	

Table 3.3: Thermophysical properties of SiC, adhesive, insulation mat and canning. All values in SI Units. Void fractions for the calculation of bulk values: $\varepsilon = 0.375$, $\varepsilon_{\text{plug}} = 0.688$

sector and represents a single channel for CATWALL.* The obvious implication is that CATWALL should be invoked as many times as the number of sectors, namely the number of elements at a cross-section of the filter. Thus, the finer the grid we have, the more times CATWALL will be invoked, with direct consequences to the computational cost of the model.

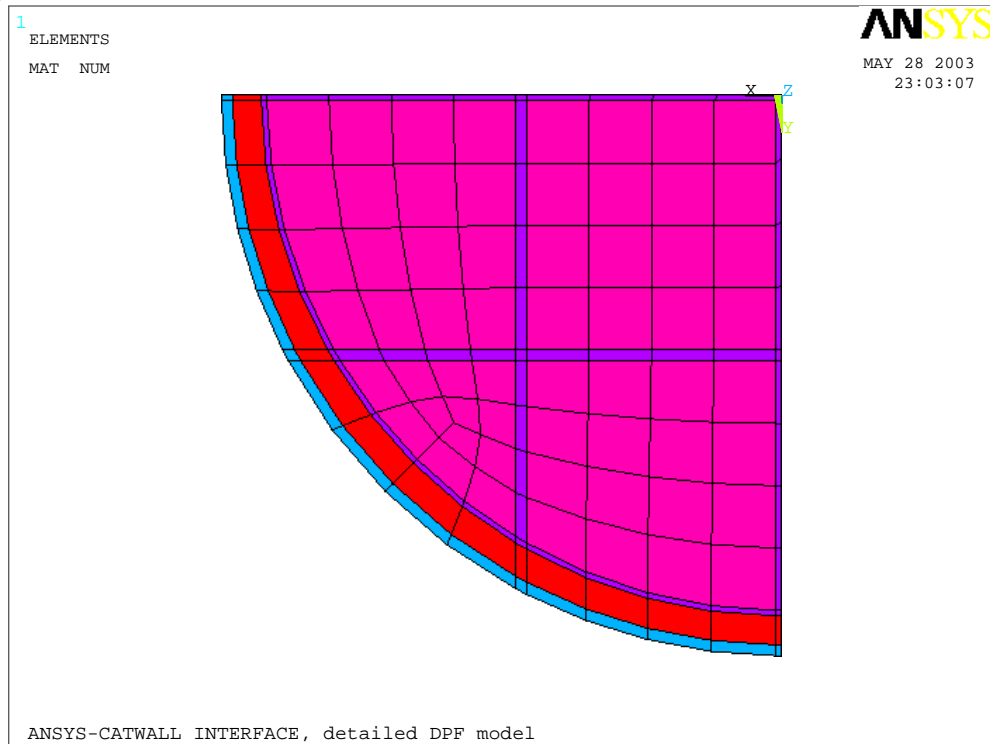
Second, the grid designed for the FEM analysis must be orthogonal along the axial direction, with fixed element length, which is an integer multiple or submultiple of the discretization length Δz of CATWALL. Essentially, the finite element model of the face is extruded along the axial direction in order to produce the total finite element model. The requirement for axial orthogonality is imposed by the structure of the filter itself, while the fixed element length is imposed by a limitation of CATWALL, which operates on a fixed axial discretization interval Δz . The above two requirements must be met, so that a mapping of the CATWALL and the ANSYS grids is possible, so that heat source and temperature information may be exchanged between the two grids. The latter point brings to the foreground the issue of interface implementation, which is discussed below.

Interface implementation Through the interface between CATWALL and ANSYS, the element number, temperature, heat source term and time are communicated. Essentially, the ANSYS gives the current time, element number and element temperature as input to the user subroutine, and expects to receive the element heat source term as user subroutine output. The task for the user subroutine is to convert its input so that it is sensible for CATWALL, subsequently call CATWALL for the calculations, and finally re-convert CATWALL output and feed it back to the ANSYS.

The concept of the interfacing between CATWALL and ANSYS is given schematically in Figure 3.12. It is evident that the implementation of two basic modules was

*The cross-sectional area for each element corresponds to a group of filter channels. All channels belonging to the same sector have thus identical temperature and heat source distributions and are thus treated as one channel by both FEM software and CATWALL.

(a)



(b)

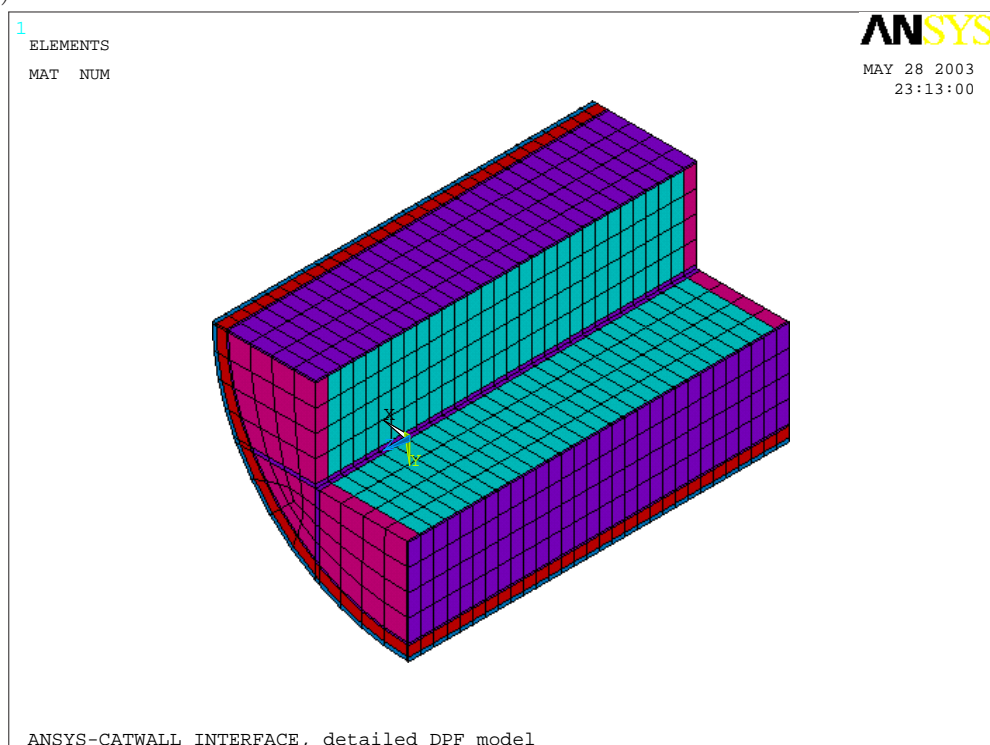


Figure 3.11: Finite element model of the DPF, produced after meshing the solid model. (a) Front view: blue=canning, red=insulation, purple=adhesive, magenta=SiC–plug region. (b) Side view, with the central filter block and adhesive removed.

required, because of the non-compatible operation and grid design of CATWALL and ANSYS. The restrictions of the grid design and the functionality of the two basic modules is discussed in brief below.

- *Grid mapping module.*

There are two co-existing (though incompatible) grids for the filter: The FEM grid consists of elements (and nodes for each element) while the CATWALL grid consists of sectors and nodes for each sector. Therefore, a mapping procedure must be implemented between the two grids to achieve exchange of information. Specifically, the procedure uses the internal numbering of elements of the FEM software. If the length for axial discretization is the same for both the FEM grid and the CATWALL grid, then each element number also corresponds to a single pair of CATWALL sector and node numbers. In this case, there is a one-to-one correspondence between the two grids, which also applies to the heat source and temperature data.

If the CATWALL grid is finer than the FEM grid (the usual case) then one element number corresponds to a set of CATWALL nodes. In this case, the sum of heat sources from CATWALL is given to ANSYS as the element heat source term, and temperature data passed to CATWALL is assumed equal for all nodes corresponding to the specific element. The situation is inverted if the CATWALL grid is coarser than the FEM grid. Then the heat source calculated for a single CATWALL node is divided to the corresponding ANSYS elements, and the CATWALL node temperature is computed as the average of the corresponding element temperatures. These considerations should make clear why the discretization length of the FEM grid along the axial direction must be an integer (sub)multiple of the CATWALL discretization length.

- *Field buffering module.* The FEM software may call the user subroutine more than once for each element. Each time that the user subroutine is called, the heat source term is requested and temperature is supplied back as a result for the next time step. Nevertheless, it is not efficient in terms of computational power to call CATWALL for the sector to which the element belongs each time the FEM software requires it. The reason is that the CATWALL operates on the whole sector and not on a per-node basis.

Therefore, a special module was implemented, which buffers the temperature and heat source fields. Whenever the FEM software takes a new time step, CATWALL is called as many times as the numbers of the sectors, and the resulting heat source field is stored in a buffer. When a heat source term is requested, it is extracted on the buffer and passed to the FEM software. The temperature value that returns from the FEM software is stored to the temperature field buffer. At the next time step of the FEM software, the temperature field is passed from the buffer to CATWALL and the next heat source field is computed.

Solution procedure The heat losses of the DPF to the surrounding air are taken into account by imposing surface convective boundary conditions on the external nodes of the DPF model. The value of the heat convection coefficient (film coefficient) from canning to ambient air, depends on the specific filter layout in exhaust system and vehicle speed, usually being in the range 20–100 W/(mK). The highest

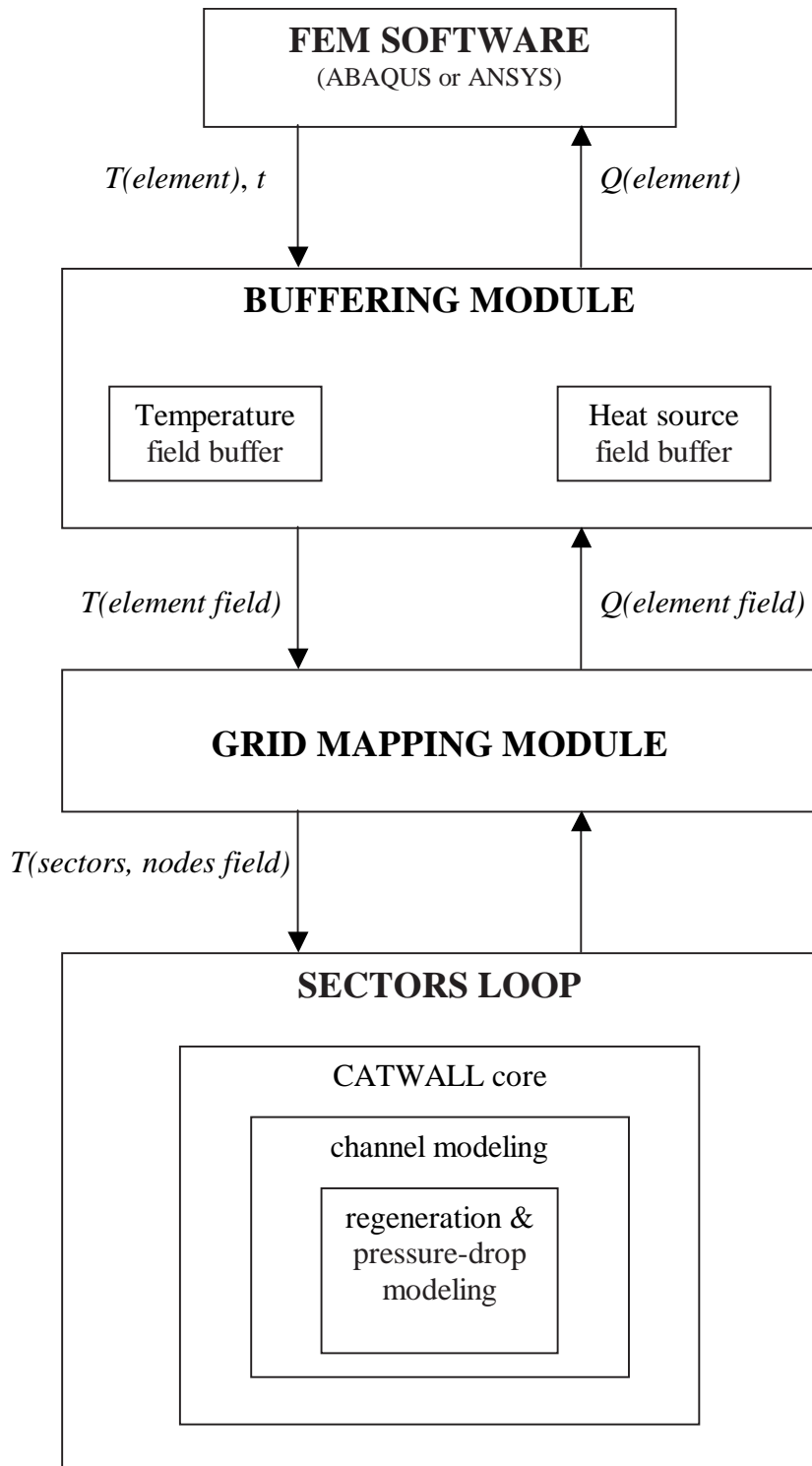


Figure 3.12: Structure of CATWALL–FEM software interfacing modules

values of the range typically include the effect of radiation exchange to the surroundings which becomes important when the can surface temperature exceeds 400 °C.

An indicative running time of 2 seconds per 1 second of real filter operation is observed for meshing used in this work, which features $144 \times 50 = 7200$ elements in total (144 elements on each cross-section) for the whole DPF filter, which includes the $5.66'' \times 6''$ SiC/adhesive filter structure, the insulation mat and the canning.

Finally, a significant advantage of interfacing CATWALL with FEM software to calculate the three-dimensional temperature field is the ability to carry out thermo-mechanical analysis. Calculation of thermal stresses in the DPF is a very important feature of the model, since crack formation due to thermal stresses is a common reason of filter failure. Details of the stress analysis procedure have been presented in [42]. Similar to the thermal analysis, the cell structure of the DPF is modeled by a “homogenized” isotropic linear elastic material with Young’s modulus $E = 19$ GPa, Poisson’s ratio $\nu = 0.15$, thermal expansion coefficient $\alpha = 4 \cdot 10^6$ °C⁻¹ and mass density $\rho = 0.72$ gr/cm³. The adhesive is modeled also by an isotropic linear elastic material with $E = 1.5$ GPa, $\nu = 0.2$, $\alpha = 2.7 \cdot 10^6$ °C⁻¹ and $\rho = 1.26$ gr/cm³.

A note on usability Although the operating principle of the ABAQUS–CATWALL and the ANSYS–CATWALL interfacing is the same, it should be noted that the resulting tools differ significantly as regards their usability. The ANSYS–CATWALL interfacing is much more advanced. Special scripts have been written in the ANSYS programming language, that directly feed the interfacing routines with information about the element meshing. As a result, CATWALL understands every change of the element mesh without user intervention. This should be contrasted to the ABAQUS–CATWALL interface, where the necessary mesh information should be written in a text file that had to be read by CATWALL before the beginning of the calculations. Furthermore, the user may use any type of elements on the face of the converter, triangular or rectangular, in any arrangement. This allows the creation of non-uniform meshes that focus on regions of significant temperature and stress gradients. On the contrary, the ABAQUS–CATWALL interface operates only with rectangular elements that have to be arranged in a cartesian grid, which is a significant disadvantage for efficient use.

Of course, the above are valid at the present status of development, and could be easily reversed; They refer to the status of the interface routines and auxiliary scripts, and they do not imply anything about the capabilities of ANSYS or ABAQUS themselves. Nevertheless, they should not be considered as mere implementation details. In our view, the above differences serve as a good example between an academic tool and a real-world engineering tool. The ABAQUS–CATWALL interface was developed first, mainly in order to prove the feasibility of the interfacing concept. Although the potential for further development existed with ABAQUS, the motive to evolve the 3D model into a more complete engineering tool was provided by an industrial partner, which funded the re-implementation of the interface with ANSYS. The extended capabilities of the interface provided flexibility and easy, efficient use compared to the previous implementation. These were essential requirements from the industry’s side, in order to integrate the ANSYS–CATWALL tool in their research and development activities.

3.7 Conclusions

Summarizing the model development, symmetrically to the 3WCC model, the kinetics, washcoat, channel and reactor level models presented in this chapter form CATWALL, a model for the operation of wall-flow diesel particulate filters. CATWALL has evolved into a commercial product of the Laboratory of Thermodynamics and Thermal Engines (LTTE), University of Thessaly [54] and is currently in use by several industrial partners as an engineering tool for the optimization of exhaust aftertreatment systems.

The 1D version of the model may be employed as a stand-alone command-line program, or may be used through a graphical Matlab/Simulink front-end. Similarly to CATRAN, the Matlab/Simulink front-end for CATWALL was developed in co-operation with an industrial partner to facilitate communication with models of the other components of the engine-piping-aftertreatment devices system and allow for computer-aided engineering.

The tuning of CATWALL kinetic parameters is currently based on dedicated TGA experiments for the determination of the activation energies, and limited manual tuning for the estimation of the frequency factors of the model. Model tuning is significantly easier for CATWALL, nevertheless the methodologies employed for the catalytic converter model are also applicable here with no further modifications. Linking of the genetic algorithm code with the CATWALL code is planned for the future.

CATWALL has also been linked with commercial finite-element software, in order to account for the three-dimensional temperature field and the inlet flow maldistributions, phenomena which are much more prominent in the diesel filter's operation compared to the catalytic converter. A significant potential of this approach is the determination of the thermal stress fields in the diesel filter, which is expected to be valuable for the detailed optimization of the filter's structure.

Finally, further support both the 1D and the 3D versions of the model are provided by a set of tools for the pre- and post-processing and, most importantly, for the quality assurance of the measured (input) data, which is currently under development by other workers in LTTE [55]. These tools are implemented as Visual Basic for Applications (VBA) code under the Microsoft Excel development environment and are expected to increase the quality of the whole modeling methodology, and to suggest directions for further improvements of the model.

3.8 Summary

- Modeling of the loading, pressure drop and regeneration characteristics of the wall-flow diesel particulate filter has been approached from an engineering viewpoint. Similarly to the catalytic converter model, the DPF model design pursues simplicity and accounts for the most significant phenomena that occur during the operation of the DPF in a simplified manner.
- The overall modeling problem has been split into four parts: Loading and pressure drop modeling, regeneration modeling, channel modeling and reactor modeling.
- The prediction of the regeneration behaviour of the DPF is the cornerstone

of the problem. A significantly improved regeneration model has been presented, that (a) eliminates rough approximations regarding the geometry of the soot layer, and (b) features an extended reaction scheme, which includes a catalytic regeneration mechanism, the CRT mechanism, and the effect of VOF desorption.

- Analytical solutions have been obtained for the concentration profiles of gaseous phase species through the soot layer and the wall. The solution procedure is built on the principles of the pioneering work of Bissett and Shadmann. This eliminates the need for integration of mass and energy balances in the spatial direction normal to the wall.
- The 1D core of the model has been interfaced with the ABAQUS and ANSYS FEM software models. These two variants are equivalent in the sense that the respective FEM software functions as a reactor level model and calculates the 3D temperature field distribution in the filter because of heat conductances between the channels. The two variants differ in their usability though, the ANSYS being more advanced in this regard and enabling more versatility and much quicker changes of the FEM meshing.
- The resulting 3D model has the additional capability to compute the stresses that are exerted on the DPF because of the temperature field, which is very important since the main problem of the DPFs is the formation of cracks due to excessive stresses.

List of symbols

Roman Letters

a	Viscous drag term, eq. (3.40) [–]
A	1. Frequency factor of reaction rate expression, [mol/(m ³ s)]
	2. Area, [m ²]
c_p	Specific heat capacity, [J/(kgK)]
d_h	Hydraulic diameter, [m]
ΔH	Molar heat of reaction, [J/mol]
E	Activation energy of reaction rate expression, [J]
h	Convection coefficient, [W/(m ² s)]
k	Arrhenius-type rate factor, [mol/m ³ s]
K	Permeability, [m ²]
ℓ	Length of inner channel edge, [m]
M	Molecular mass, [kg/mol]
\dot{m}_g	Mass flow rate, [kg/s]
m	1. Soot mass, [kg]
	2. Number of carbon atoms in hydrocarbon molecule, [–]
n	Number of hydrogen atoms in hydrocarbon molecule, [–]
p	Pressure, [Pa]
\dot{Q}	Heat source term, [J/s]
r	Reaction rate, [mol/m ³ s]
R	Flow resistance, [Pa(kg/s ⁻¹)]
R_g	Universal gas constant, [8.314 J/(mol·K)]
t	Time, [s]
T	Temperature, [K]
u_z	Axial exhaust gas velocity, [m/s]
V	Volume, [m ³]
w	Thickness of soot layer, [m]
w_s	Thickness of filter wall, [m]
x	Transverse direction (perpendicular to channel's side), [m]
y	Molar fraction at the gaseous phase, [–]
z	Axial direction, [m]

Greek Letters

ϵ	Dimensionless quantity, defined in (3.22)
ε	Volume fraction, [–]
λ	1. Thermal conductivity, [W/(m·K)]
	2. Gas mean free path, [m]
μ	Viscosity, []
ξ	Total Ce/hydrocarbon capacity of soot, [–]
ρ	Density [kg/m ³]
ψ	Molar fraction of CeO ₂ or hydrocarbon, [–]

Subscripts/superscripts

i	species index, [–]
-----	--------------------

<i>in</i>	inlet channel/inlet of the soot deposit
<i>inlet</i>	inlet of the filter
<i>j</i>	index for (a) soot deposit ($j = 1$) or (b) ceramic wall ($j = 2$)
<i>n</i>	reaction index
<i>g</i>	gas
<i>out</i>	outlet channel/outlet of the soot deposit
<i>w</i>	wall

Abbreviations

CRT Continuously Regenerating Trap

DPF Diesel particulate filter

VOF Volatile organic fraction

References

- [1] Johannes Winterhagen. Der neue peugeot 607. *ATZ Automobiltechnische Zeitschrift*, 102(5):300–308, 2000.
- [2] PSA Peugeot Citroën Exceeds 2002 Sales Target. Press Release – 07/01/2003.
- [3] E. J. Bissett and F. Shadmann. Thermal regeneration of diesel-particulate filters. *American Institute of Chemical Engineers Journal*, 31(5):753–758, 1985.
- [4] G. C. Koltsakis and A. M. Stamatelos. Modeling thermal regeneration of diesel particulate traps. *American Institute of Chemical Engineers Journal*, 12:1662–1672, 1996.
- [5] G. C. Koltsakis and A. M. Stamatelos. Modeling catalytic regeneration of diesel particulate traps. *Industrial & Engineering Chemistry Research*, 35:2–13, 1996.
- [6] Martin J. Murtagh and David Hickman. Diesel particulate filter overview: Material, geometry and application. *SAE paper 2003-01-1350*, 2003.
- [7] Douglas M. Beall, David L. Hickman, and Gregory A. Merkel. Cordierite Body. *U.S. Patent 6,541,407 B2*, 2003.
- [8] Shuichi Ichikawa, Yasushi Uchida, Aiko Otsuka, Takashi Harada, Toshiyuki Hamanaka, Ken Nagashima, and Makoto Nagata. Material Development of High Porous SiC for Catalyzed Diesel Particulate Filter. *SAE paper 2003-01-0380*, 2003.
- [9] Debora Fino, Paolo Fino, Guido Saracco, and Vito Specchia. Innovative means for the catalytic regeneration of particulate traps for diesel exhaust cleaning. *Chemical Engineering Science*, 58:951–958, 2003.
- [10] G. N. Pontikakis, G. C. Koltsakis, and A. M. Stamatelos. A mathematical model for the dynamic particulate filtration in diesel foam filters. *Journal of Particulate Science and Technology*, 17(3):179–200, 1999.
- [11] G. N. Pontikakis, G. C. Koltsakis, and A. M. Stamatelos. Dynamic filtration modeling in foam filters for diesel exhaust. *Chemical Engineering Communications*, 188:21–46, 2001.
- [12] J. Gieshoff, A. Schäfer-Sindlinger, U. Hackbarth, O. Teysset, C. Colignon, C. Rigaudeau, O. Salvat, H. Krieg, and B. W. Wenclawialk. Regeneration of catalytic diesel particulate filters. *SAE paper 2001-01-0907*, 2001.
- [13] R. Domesle, E. Koberstein, H.-D. Pletka, and H. Voelker. Process and catalyst for the reduction of the ignition temperature of diesel soot filtered out of the exhaust gas of diesel engines. *US patent 4,515,758*, 1983.
- [14] A. M. Stamatelos. A review of the effect of particulate traps on the efficiency of vehicle diesel engines. *Energy Conversion & Management*, 38(1):83–99, 1997.
- [15] Kazushige Ohno, Koji Shimato, Noriyuki Taoka, Hong Santae, Takeshi Ni-nomiya, Teruo Komori, and Olivier Salvat. Quasi-continuous particle trap regeneration by cerium additives. *SAE paper 2000-01-0185*, 2000.

- [16] Hans-Otto Hermann, Oliver Lang, Ingo Mikulic, and Volker Scholz. Partikelfiltersysteme für Diesel-Pkw. *Motortechnische Zeitschrift*, 9(652–660), 2001.
- [17] D. E. Hall, C. L. Goodfellow, P. Heinze, D. J. Rickeard, G. Nancekievill, G. Martini, J. Hevesi, L. Rantanen, M. P. Merino, T. D. B. Morgan, and P. J. Zemroch. A study of the size, number and mass distribution of the automotive particulate emissions from european light duty vehicles. *SAE paper 982600*, 1998.
- [18] M. Wyser, A. Mayer, U. Matter, D. Kieser, J. Czerwinski, Mr. Schiedegger, and Mr. Weidhofer. VERT: diesel nano-particulate emissions: properties and reduction strategies. *SAE paper 980539*, 1998.
- [19] M. W. Vincent, P. Richards, and S. L. Cook. Particulates reduction in diesel engines through the combination of a particulate filter and fuel additive. *SAE paper 982654*, 1998.
- [20] J.H. Johnson, S.T. Bagley, L.D. Gradz, and D.G. Leddy. A review of diesel particulate control technology and emissions effects. *SAE paper 940233*, 1994.
- [21] G. A. Stratakis and A. M. Stamatelos. Thermogravimetric analysis of soot emitted by a modern diesel engine run on catalyst-doped fuel. *Combustion and Flame*, 132:157–169, 2003.
- [22] J.C. Summers, S. Van Houtte, and D. Psaras. Simultaneous control of particulate and NOx emissions from diesel engines. *Applied Catalysis B: Environmental*, 10:139–156, 1996.
- [23] C. N. Davis. *Air Filtration*. Academic Press, Orlando, FL, 1973.
- [24] N. A. Fuchs. *The Mechanics of Aerosols*. Pergamon Press, 1964.
- [25] Oh S.H., MacDonald J.S., Vaneman G. L., and Hegedus L.L. Mathematical modeling of fibrous filters for diesel particulates – theory and experiment. *SAE paper 810113*, 1981.
- [26] R. C. Brown. *Air Filtration*. Pergamon Press, 1994.
- [27] A. C Payatakes and L. Grado. Dendritic deposition of aerosols by convective brownian diffusion for small, intermediate and high particle knudsen numbers. *American Institute of Chemical Engineers Journal*, 26(3):443–454, 1980.
- [28] C. N. Davis, editor. *Aerosol Science*. Academic Press, 1966.
- [29] Shinaya Hirota et al. Exhaust gas purification system. *U.S. Patent 6546721B2*, 2002.
- [30] Shizuo Sasaki. Device for purifying the exhaust gas of an internal combustion engine. *U.S. Patent 6490857B2*, 2003.
- [31] B. J. Cooper, H. J. Jung, and J. E. Thoss. Treatment of diesel exhaust gas. *U.S. Patent 4,902,487*, 1990.
- [32] O. Salvat, P. Marez, and G. Belot. Passenger car serial application of a particulate filter system on a common rail direct injection diesel engine. *SAE paper 01-0473-2000*, 2000.

- [33] Olivier Salvat, Jacques Portaller, and Patrice Le Tallec. Regeneration system for a diesel engine exhaust gas particulate filter. *U.S. Patent 6,412,276B1*, 2002.
- [34] Olivier Salvat and Patric Le Tallec. System for assisting the regeneration of a particle filter integrated into an exhaust line of a motor vehicle diesel engine. *U.S. Patent 6,397,584B2*, 2002.
- [35] Patrice Le Tallec and Olivier Salvat. System for assisting the regeneration of a particle filter integrated into an exhaust line of a motor vehicle diesel engine. *U.S. Patent 6,484,496*, 2002.
- [36] Lepperhoff G., Lueders H., Barthe P., and Lemaire J. Quasi-continuous particle trap regeneration by cerium additives. *SAE paper 950369*, 1995.
- [37] G. A. Stratakis and A. M. Stamatelos. Flow distribution effects in the loading and catalytic regeneration of diesel particulate filters. *Proc Instn Mech Engrs, Part D: J. Automobile Engineering*, 2003. (*Submitted*).
- [38] E. J. Bissett. Mathematical model of the thermal regeneration of a wall-flow monolith diesel particulate filter. *Chemical Engineering Science*, 39:1233–1244, 1984.
- [39] I. P. Kandylas and A. M. Stamatelos. Modeling catalytic regeneration of diesel particulate filters taking into account adsorbed hydrocarbon oxidation. *Industrial & Engineering Chemistry Research*, 38:1866–1876, 1999.
- [40] G. A. Stratakis, D. L. Psarianos, and A. M. Stamatelos. Experimental investigation of the pressure drop in porous ceramic diesel particulate filters. *Proc Instn Mech Engrs, Part D: J. Automobile Engineering*, 216:773–784, 2002.
- [41] G. A. Stratakis, G. S. Konstantas, and A. M. Stamatelos. Experimental investigation of the role of soot volatile organic fraction in the regeneration of diesel filters. *Proc Instn Mech Engrs, Part D: J. Automobile Engineering*, 217:307–317, 2003.
- [42] G. N. Pontikakis, A. M. Stamatelos, K. Bakasis, and N. Aravas. 3-D catalytic regeneration and stress modeling of diesel particulate filters using ABAQUS FEM software. *SAE paper 2001-01-1017*, 2002.
- [43] G. N. Pontikakis and A. M. Stamatelos. 3-D catalytic regeneration modeling of diesel particulate filters. *Proc Instn Mech Engrs, Part D: J. Automobile Engineering*, 2003. (*Submitted*).
- [44] W. W. Pulkrabek and E. I. Ibele. The effect of temperature on the permeability of a porous material. *Int. J. Heat Mass Transfer*, 30(6):1003–1109, 1987.
- [45] P. Versaevel, H. Colas, C. Rigaudeau, C. Noirot, G. C. Koltsakis, and A. M. Stamatelos. Some empirical observations on diesel particulate filter modeling and comparison between simulations and experiments. *SAE paper 01-477-2000*, 2000.
- [46] S. C. Sorenson, J. W. Hoj, and P. Stobbe. Flow characteristics of SiC diesel particulate filter materials. *SAE paper 940236*, 1994.

- [47] G. A. Stratakis, G. N. Pontikakis, and A. M. Stamatelos. Experimental validation of a fuel additive assisted regeneration model in sic diesel filters. *American Institute of Chemical Engineers Journal*, 2003. (*Submitted*).
- [48] D. W. McKee. The catalyzed gasification reactions of carbon. *Chem. Phys. Carbon*, 16:189–199, 1981.
- [49] J. Kaerger and D. M. Ruthven. *Diffusion in Zeolites and Other Microporous Solids*. John Wiley & Sons, 1992.
- [50] G. C. Koltsakis and A. M. Stamatelos. Modes of catalytic regeneration in diesel particulate filters. *Industrial & Engineering Chemistry Research*, 36:4155–4165, 1997.
- [51] Laboratory of Thermodynamics and Thermal Engines. *CATWALL Diesel Particulate Filter Modeling Software, Version V4R3*. University of Thessaly, Volos, May 2003.
- [52] Joel H. Ferziger. *Numerical Methods for Engineering Applications*. John Wiley & Sons.
- [53] W. F. Stoecker. *Design of Thermal Systems*. McGraw-Hill, 3rd edition, 1989.
- [54] Laboratory of Thermodynamics and Thermal Engines. *CATRAN Catalytic Converter Modeling Software, Version V4R3*. University of Thessaly, Volos, April 2003.
- [55] G. Konstantas and A. M. Stamatelos. Quality assurance of exhaust emissions test data. *Proc. Instn Mech Engrs, Part D*, 2003. (*Submitted*).

Chapter 4

Parameter estimation

Here, we deal with the tuning of the model that was developed in Chapter 2. Successful tuning of the catalytic converter model is a crucial factor for its usability in a CAE exhaust line design procedure. Until now, the tuning of the models presented in the literature was manual. The need for an automated tuning procedure had been recognised but the few attempts towards this direction were confined in simplified cases. Here, we develop a computer-aided tuning procedure, transforming the tuning problem into an optimization problem and applying optimization techniques. The tuning procedure that we develop should be able to tune the model using standard experiments, preferably driving cycle tests. The tuning procedure is validated in a subsequent chapter.

4.1 Previous tuning practice

Although the successful modeling of catalytic converters has been achieved only with the aid of tunable parameter models, not much work has been carried out in the direction of computer-aided tuning. In most cases, parameter tuning is still done in an empirical manner. For the inhibition terms of the reaction rates, the kinetics provided in the historical work of Voltz et al. [1] were used in the majority of the modeling attempts. The order of magnitude of the apparent activation energies is approximately known for most reactions and could be used as a starting point. Then, one would manually try to adjust the pre-exponential factor and, to a lesser extent, the activation energy of each reaction in order to adequately fit the computed curves to the experimental ones.

Montreuil et al. [2] were the first to present a systematic attempt for the tuning of the parameters of their steady state three-way catalytic converter model. They compiled an experimental database of steady state efficiencies for two catalyst formulations and fitted the parameters of their model according to the database. This was done by defining a merit function of the tunable parameters as the square differences between experimental and computed values, and minimizing it with the aid of the conjugate gradients method. The chemical reactions submodel contained 95 parameters. By grouping the tunable parameters according to each kinetic subsystem, they progressively tuned all model parameters in a semi-empirical way. The results of the procedure were applied subsequently to predict the efficiency of a catalytic converter in a driving cycle test, with limited success [3].

Dubien and Schweich [4] also published a methodology to determine the fre-

quency factor and the activation energy of simple rate expressions from light-off experiments. They used theoretical calculations to provide an initial approximation of the tunable parameters and then optimized the parameters similarly with Montreuil et al., i.e. defining a merit function and using the downhill simplex method to minimize it. Their approach was successful but of limited practical value, because it was only applicable to non-competing reactions. It was therefore restricted to the study of simple mixtures of reactants and could not be used to fit parameters of a realistic reaction scheme.

In this work, we formulate a procedure to tune the catalytic converter model in the case of the diesel oxidation catalyst and the three-way catalytic converter, using routine experiments. The merit function approach is also used here and, in order to minimize it, the methods of conjugate gradients and genetic algorithms are employed. We investigated the characteristics of the parameter space, first, using a conjugate gradients approach. This approach resulted in acceptable optimization in the case of the diesel oxidation catalyst but did not work efficiently for the more difficult case of the 3WCC. Therefore, we switched to a genetic algorithms optimization routine, which seems to provide more robust optimization, at the cost of increased computational time.

4.2 Formulation of the optimization problem

In order to tune the parameters of the model, one or more different experiments or tests available are employed. Moreover, for each experiment or test, there are usually multiple responses, e.g. measurements of various species concentrations at the catalyst outlet, temperature at several points of the monolithic converter etc. Measured responses are usually available as a function of time for each experiment.

Modeling provides an estimation for each one of the measured responses. The computation for each response depends on the values of the tunable parameter of the model. The *tuning* of the model requires that the tunable parameters be fitted in order to minimize the error between available measurements and the respective computations.

Thus, the problem of model tuning is a parameter-fitting problem, and it may be tackled as an optimization problem. This involves the development of two components:

- *A performance measure*, which qualitatively assesses the goodness-of-fit of the model for each possible set of parameter values, i.e. it assesses the error between measured and computed responses.
- *An optimization procedure*, which finds a set of tunable parameters giving an optimum value for the performance measure, i.e. yields in modeling results that are as close to the measured results as possible.

Some discussion about the above two components of the optimization methodology is given below.

4.2.1 Performance measure

All efforts in the field of tuning practice so far have used the above approach. Nevertheless, the formulation of a pertinent performance measure was not given much

focus compared to the optimization procedure. The performance measure, though, links the optimization procedure with the model and its definition is important for the success of the optimization methodology. Furthermore, there are reasons that are related to modeling assessment (and unrelated to the parameter estimation/optimization problem) that call for a careful performance measure definition.

Specifically, despite the richness and diversity of the modeling efforts that may be found in the bibliography, it is somewhat surprising that the assessment of the success of the models has always been qualitative—more specifically, by inspection. That is, the usual practice is to plot together the measurements and results of one or more simulations, inspect the resulting graph and comment about the quality of simulation results. Although such a visualization procedure is absolutely necessary to gain insight about the behaviour of a model and make a rough evaluation of its success, the introduction of a *quantitative criterion* (or a set of criteria) may aid in several directions where qualitative inspection seems inadequate. There are two reasons for this:

- *Inspection is dependent on the scale that results are viewed and may therefore be misleading.* Today's catalytic converters are very efficient and reach light-off very fast compared to previous generations systems. As a result, outlet emissions range within several orders of magnitude, depending on the mode of converter operation. Thus, comparison between calculation and measurement may be difficult to assess purely by inspection. Quantitative criteria could be helpful to better assess modeling accuracy, unbiased from system configuration.
- *There is considerable difficulty to compare the performance of different models.* In order to compare different models directly, the models should be tested in the same set of measurements and the results should be plotted together for direct comparison. If this is not possible (as is the case for modeling results presented in the bibliography from different researchers) a generally accepted, quantitative criterion, could give an idea for the comparative performance of different modeling approaches.

Consequently, the formulation of the performance measure is useful *per se*, for the quantitative assessment of modeling results. The ultimate goal of the performance measure formulation is to express in a quantitative manner what is perceived by human intuition as the quality of the fit of the catalytic converter model to experimental results.

4.2.2 Optimization method

A properly formulated performance measure may be combined with an optimization method, to provide a methodology for the catalytic converter model parameters tuning. Any optimization method chosen for this task should take into account the following points:

1. We have no analytical expression of the performance measure, because it involves the output of the catalytic converter model
2. The performance measure is a non-linear function of the tunable parameters.
3. The parameter space is n -dimensional, where n is the number of the parameters being tuned.

4. The parameter space is continuous, since the tunable parameters are continuous real variables.
5. The search on the parameter space must be constrained, the constraints depending on each tunable parameter.
6. The parameter space may be unimodal or multimodal; this depends on both the protocol of the experiments used for model tuning and the parameters being tuned.
7. For each function evaluation, a run of the model must be invoked. Since this is very demanding in terms of computational power, the method of choice should perform as few function evaluations as possible.

As Goldberg [5] summarizes, there are three main categories of optimization and search techniques: (a) conventional calculus methods, (b) enumerative methods and (c) randomized methods.

The calculus based methods are local methods (because they proceed exploiting information only from the neighbourhood of the current point), presume that the parameter space is continuous and usually require derivatives values or their numerical approximations (to detect the gradient of the neighbourhood and decide how to proceed).* Typically, they are efficient but fail to find a global minimum in a multimodal parameter space. A typical example is the conjugate gradients method, that was the first method we tested (Section 4.4 below).

Enumerative methods simply evaluate all the possible points of the search space in order to find an extremum. Enumerative methods are simple but inefficient and are completely useless for problems with large search spaces, especially spaces of many dimensions.

Randomized methods, on the other hand, employ random choice of evaluation points, in contrast with the deterministic choice of calculus based methods. This does not necessarily mean, however, that these methods are completely random; otherwise, they would be equivalent to enumerative techniques.

Two popular families of randomized methods for the optimization of multimodal functions is *Simulated Annealing* and *Genetic Algorithms*. Both procedures are not completely random; they choose search directions following certain rules. However, the term *randomized* implies that these rules are not deterministic but employ random choice of search points.

* * *

In this work, we first attempt to define a performance measure that is suitable for use in driving cycle tests, typical for the experimental assessment of catalytic converter behaviour. The requirements and rationale for its formulation are given in Section 4.3.

Then, the development of the optimization procedure is discussed. A conjugate gradients method was originally tested (Section 4.4). The success was limited apparently because the parameter space of the problem is multimodal. Its failure motivated the development of a genetic algorithm, detailed in Section 4.5, that circumvented the difficulties of the previous attempts and resulted in a workable methodology for catalytic converter parameter tuning.

*Not all calculus methods require the use of derivatives; the most efficient do, however.

4.3 Performance measure formulation

4.3.1 Requirements for the performance measure

In order to formulate a performance measure for the assessment of catalytic converter simulation results, we first have to decide which are its desired features. Of course, this is an issue of critical judgement of the problem at hand. We have compiled a list of features that is neither definite nor exhaustive but, instead, is open to corrections, additions and improvements.

1. In real world measurements, several physical quantities are monitored, usually including concentrations of several gaseous-phase species, gas temperatures at various positions in the converter, gas mass flow rate etc. The performance measure should incorporate as much information is available from these measurements as possible.
2. The performance measure should range between two finite extreme values. Extremes should correspond to zero and maximum deviation between calculation and experiment.
3. The extrema of the performance measure should be the same for all physical quantities that may be used and all different measurements where the performance measure may be applied. That is, the performance measure should somehow be normalized so that its extrema do not depend on the either the measured quantities or the experimental protocol.
4. The performance measure should focus on regions of the measurement where conversion efficiency is *not near* its minimum or maximum possible value (0% and 100% respectively).
5. The performance measure should prove (*a posteriori*) to be proper for use in conjunction with an optimization procedure.

Requirement 1 implicitly acknowledges the fact that a measurement contains errors. In order to estimate kinetic parameters as accurately as possible, maximum information from an experiment should be used, so that measurement errors are mutually cancelled.

Requirements 2 and 3 have been set to ensure that the performance measure obtained from one experiment can be directly compared with the performance measure from another experiment.

Requirements 4 and 5 are relevant because we intend to use a performance measure within an iterative optimization procedure to estimate kinetic parameters of a lumped parameters model.

To support requirement 4 we have to note that, theoretically, the kinetic parameters that have to be estimated may range from zero to infinity. In practice, kinetic parameters are allowed to range from a minimum value (which implies zero catalytic activity) to a maximum value (which implies extremely high catalytic activity). In its turn, conversion efficiency may range from 0% to 100%. A model may predict regions of the measurement with conversion efficiency near 0% even if the kinetics are wrongly set to extremely low values. On the other hand, a model may predict regions of the measurement with conversion efficiency near 100% even if the kinetics are wrongly set to extremely high values. Consequently, the correct values of the

kinetic parameters can be only found if the performance measure focuses on regions where conversion efficiency is moderate.

Finally, requirement 5 is a consequence of the fact that the choice of the performance measure defines the optimization space, where the optimization algorithm should search for optimum kinetic values. A transformation of the performance measure also transforms the optimization space and certain transformations could be non-advantageous for optimization purposes. Since there is no way to predict the behaviour of the optimization algorithm in beforehand, the applicability of the performance measure of our choice has to be tested in real optimization cases.

4.3.2 Measurements exploitation

We begin the formulation of the performance measure with the examination of the measured information that are available for use in a typical catalytic converter test.

Since we are particularly interested in real-world operating conditions of the converter, we focus on engine-bench and driving cycle tests. When such tests are performed, several physical quantities are monitored. Usually, measured quantities of interest for our case are (a) inlet/outlet concentrations of gaseous-phase species and (b) gas temperatures at inlet, outlet and probably other positions within the converter.

Given a scenario of inlet conditions as a function of time and a set of geometrical, physical and chemical activity characteristics of the catalytic converter, the primary objective of a catalytic converter model is to predict the conversion efficiency of a catalytic converter regarding legislated pollutants.

Consequently, any performance measure that may be formulated should at least contain the measured information regarding the legislated gaseous pollutants. Herein, we are particularly concerned with three-way catalytic converter tests, thus the measured concentrations of CO, HC and NO_x are exploited.

Information about the concentrations of the catalytic converter at inlet and outlet may be incorporated in the model either considering the species concentration y directly, or considering the conversion efficiency \mathcal{E} of the converter for that species. We shall use the conversion efficiency, according to the requirement list which was set in paragraph 4.3.1; the rationale for this choice will be examined in paragraph 4.3.4 that follows.

We did not manage to devise a way to incorporate temperature information in a satisfactory way in our performance measure.

4.3.3 Error positiveness

To account for the goodness of computation results compared with a measurement that spans over a certain time period, we have to define an error quantity e for each time instance. This gives the deviation between computation and measurement for a certain quantity and is usually summed/integrated over time to calculate an overall error value.

Whichever the error definition may be, error should be positive or zero, for two reasons. First, an negative error definition is not of much interest, unless we want to know the direction of the error, i.e. if computation is higher or lower than the measurement. Second, the summation of errors over time that we intend to perform will cause positive and negative errors to mutually cancel, producing nonsensical results.

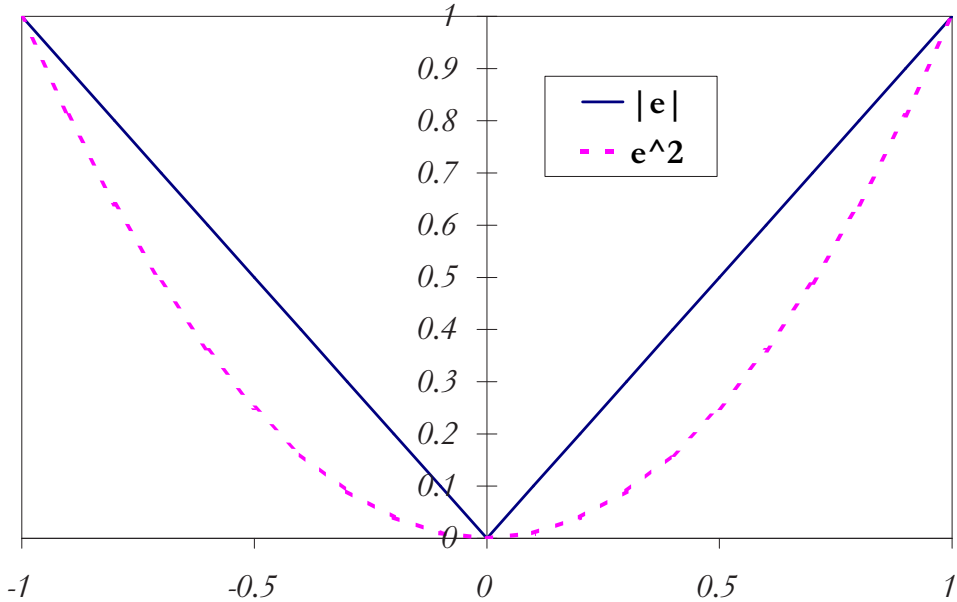


Figure 4.1: Comparison between absolute vs. squared error

There are two common ways to make an arbitrary variable $e \in \mathbb{R}$ positive: either by taking its absolute value $|e|$ or its squared value e^2 . The only difference between the two approaches, is that e^2 emphasizes big error values compared to $|e|$. That is, e^2 punishes high-error regions (regions where modeling is weaker) much more severely than low-error regions (where modeling is more accurate). Instead, $|e|$ punishes high- and low-error regions in a uniform way. This is graphically shown in Figure 4.1, where both $|e|$ and e^2 are plotted against e .

In case we intend to use the resulting performance measure only to get an idea for modeling results or to compare different models, our choice is not very significant. It only depends on the emphasis we choose to give in high-error regions compared to low-error regions. It should be noted, though, that, in principle, the exaggeration of high-error regions could depreciate a good simulation containing a small part of highly erroneous results.

However, we expect that the choice is significant in case we intend to use the performance measure in conjunction with an optimization procedure, which tries to find tunable parameter estimates resulting in minimum error between computation and measurement. The reasons are presented in the following.

Given a vector of tunable parameters $\boldsymbol{\theta} = [\theta_1, \theta_2, \dots, \theta_n]^T$, the n -dimensional optimization space is formed by the performance measure $F(\boldsymbol{\theta})$, if the latter takes all possible values of $\boldsymbol{\theta}$. Any optimization procedure benefits from an optimization space that has a steep slope towards the extreme value that we seek for, i.e. when $\partial F / \partial \boldsymbol{\theta}$ has a high absolute value. The performance measure F is an increasing function of the error between computation and measurement. Thus, in order to decide if it is more beneficial to base the performance measure on the absolute or squared error, we have to compare the absolute values of $\partial |e| / \partial \boldsymbol{\theta}$ and $\partial e^2 / \partial \boldsymbol{\theta}$.

This is readily done by writing the above derivatives as:

$$\left| \frac{\partial |e|}{\partial \boldsymbol{\theta}} \right| = \left| \frac{\partial |e|}{\partial e} \right| \cdot \left| \frac{\partial e}{\partial \boldsymbol{\theta}} \right|, \quad \left| \frac{\partial e^2}{\partial \boldsymbol{\theta}} \right| = \left| \frac{\partial e^2}{\partial e} \right| \cdot \left| \frac{\partial e}{\partial \boldsymbol{\theta}} \right| \quad (4.1)$$

Thus, we only have to compare the absolute values values of $\partial|e|/\partial e$ and $\partial e^2/\partial e$, which are:

$$\left| \frac{\partial|e|}{\partial e} \right| = +1, \quad \left| \frac{\partial e^2}{\partial e} \right| = 2e \quad (4.2)$$

Evidently, this means that the gradient of e^2 is lower than the gradient of $|e|$ when $|e| \leq 0.5$ and vice verca.

$$\left| \frac{\partial e^2}{\partial e} \right| \leq \left| \frac{\partial|e|}{\partial e} \right| \quad \text{for } 0 \leq |e| \leq 0.5 \quad (4.3)$$

$$\left| \frac{\partial e^2}{\partial e} \right| \geq \left| \frac{\partial|e|}{\partial e} \right| \quad \text{for } 0.5 \leq |e| \quad (4.4)$$

Thus, we may conclude that

$$\left| \frac{\partial e^2}{\partial \theta} \right| \leq \left| \frac{\partial|e|}{\partial \theta} \right| \quad \text{for } |e| \leq 0.5 \quad (4.5)$$

For all other values of $|e|$, the inverse holds. This implies that an absolute-error based performance measure $F(|e|)$ is more beneficial than a squared-error based one $F(e^2)$, only for $|e| \leq 0.5$ and vice verca.

For reasons that will be explained in detail in the following section, we intend to define error e in terms of the conversion efficiency \mathcal{E} , in a way that $|e|$ ranges between 0 and 1. In that case, a $F(e^2)$ approach is more beneficial in the beginning of the optimization procedure, where error values are expected to be high. As optimization proceeds, error values will gradually decrease below 0.5 and a $F(|e|)$ approach becomes more advantageous.

It should particularly be noticed that, if $|e| \rightarrow 0$, then $\partial F(e^2)/\partial \theta \rightarrow 0$. This means that an optimization algorithm based on a $F(e^2)$ performance measure will have asymptotically increasing difficulties searching for the exact position of an extreme point. On the contrary, $F(|e|)$ will not face such a difficulty. The disadvantage is that it will be more inefficient in the initial stages of the optimization.

In short, it seems that the approach one adopts is roughly equivalent to weighing between optimization accuracy and speed. This work is oriented towards accuracy rather than speed and thus will define a performance measure that is based upon the *absolute* error between computation and measurement.

4.3.4 Error definition

The absolute error $|e|$ between a measured quantity \hat{P} and its corresponding computed value P is usually defined in two ways: Either as

$$|e| = |\hat{P} - P| \quad (4.6)$$

or as

$$|e| = \left| \frac{\hat{P} - P}{\hat{P}} \right| \quad (4.7)$$

As discussed in the previous section, the two candidates quantities for P are (a) concentration y and (b) conversion efficiency \mathcal{E} . Both \hat{y} and $\hat{\mathcal{E}}$ may become zero in regions of any measurement. If this is the case, error defined according to eq. (4.7)

becomes infinite. This is not a desirable feature, according to requirement 2 set in paragraph 4.3.1. Therefore, eq. (4.7) does not provide an acceptable way to define error between measurement and computation and should be discarded. Instead, the error definition in eq. (4.6) does not present such an non-advantageous feature and therefore becomes our choice.

Proceeding one step further, we have to decide which of the two candidate quantities, y or \mathcal{E} , will be used with the chosen error definition. Both of the properties have values within a finite range: $0 \leq y \leq y_{in}$ and $0 \leq \mathcal{E} \leq 1$. Thus they comply with requirement 2 of the previous section. Nevertheless, if we use y with eq. (4.6), we get:

$$0 \leq |e| = |\hat{y} - y| \leq y_{in} \quad (4.8)$$

where y_{in} is the concentration at the converter's inlet. Thus, the error's maximum value is dependent on the test and, in the context of the same test, on the measured quantity. This does not satisfy requirement 3 regarding the need for a normalized error definition.

On the other hand, using conversion efficiency \mathcal{E} , we get a normalized absolute error:

$$0 \leq |e| = |\hat{\mathcal{E}} - \mathcal{E}| \leq 1 \quad (4.9)$$

which exactly satisfies requirement 3. This makes \mathcal{E} our choice to use with the error definition of eq. (4.6). This also explains why, in the previous section, we only considered the region $|e| < 1$ for the error values.

It should be noted that the above analysis remains valid even if the squared error is used instead of the absolute error. Thus, the same conclusions would have been reached, even if, in paragraph 4.3.3, we had opted for a squared-error based performance measure.

4.3.5 Performance measure definition for single-response tests

Below, we attempt to formulate the performance measure for a catalytic converter test where only one physical quantity is monitored, that is, only one response is available. In the next paragraph, we extend the performance measure to the case where multiple responses are available for a test.

For a measurement that spans over some time period, error between computation and measurement is a function of time and the tunable parameter vector: $e = e(t; \boldsymbol{\theta})$. We name *performance function* f a function of the error e which is subsequently summed over some time period T to give the performance measure F . In mathematical notation, and omitting the parameter vector $\boldsymbol{\theta}$ for notation simplicity, the performance function is defined as:

$$f(t) = f(e(t)) \quad (4.10)$$

where time t takes discrete values, $t_k = k\Delta t$, with $k \in \mathbb{N}$ and Δt being the discretization interval. The performance measure is subsequently formed by the sum of the performance function over time:

$$F = F\left(\sum_{k=0}^N f(t_k)\right), \quad N = T/\Delta t \quad (4.11)$$

Using this terminology, the *least-squares* performance measure, which is the most commonly used performance measure, is readily formed by (a) defining the performance function as equal to the squared error and (b) defining the performance

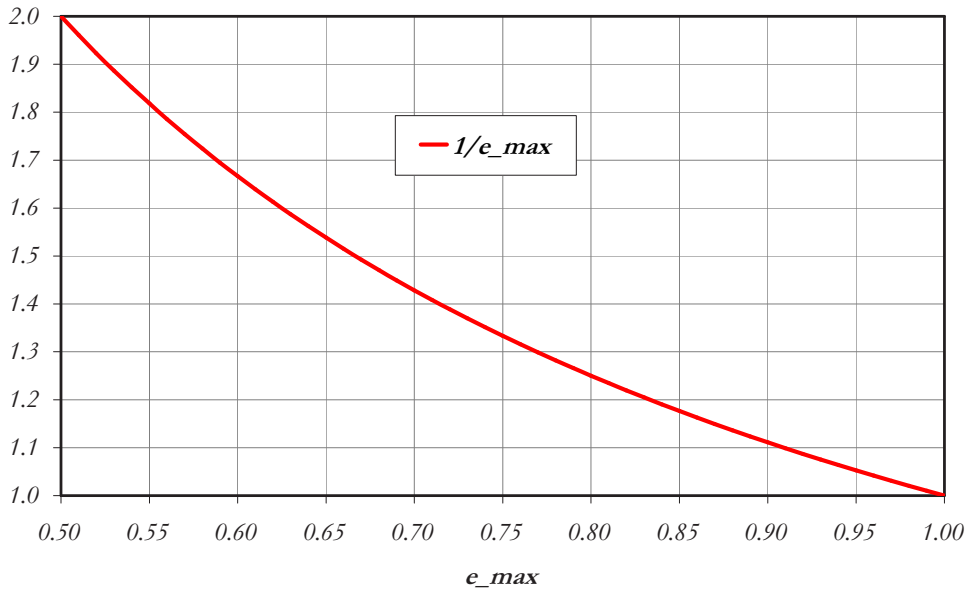


Figure 4.2: Graph of f_2/f_1 ratio

measure as the sum of the performance function over the time period of the measurement:

$$f(t_k) = e^2(t_k), \quad F = \sum_{k=0}^N f(t_k) \quad (4.12)$$

Then, the optimization procedure searches for a parameter vector that minimizes the performance measure.

In this work, we will deviate from the least squares approach for two reasons:

- We have previously (paragraph 4.3.3) concluded that, in the context of parameter estimation of a catalytic converter model, we may perform more accurate optimization using the absolute instead of the squared error.
- According to the least-squares approach, the maximum value of the performance measure depends on $N = T/\Delta t$. Thus, the least-squares performance measure does not comply with requirement 3 of paragraph 4.3.1 that suggests that the performance measure extrema be the same for all possible measurements.

To formulate a more appropriate performance measure, we note that, if we divide the sum of the performance functions with N , we get the average of the performance functions μ_f . Using the absolute error, we may arrive to the following formulation of f and F :

$$f_1(t_k) = |e(t_k)|, \quad F_1 \equiv \mu_{f_1} = \frac{\sum_0^N f_1(t_k)}{N} \quad (4.13)$$

The performance measure now ranges in the same range with the performance function f for all possible measurements:

$$0 \leq f_1 = |e| \leq 1, \quad 0 \leq \mu_{f_1} = \mu_{|e|} \leq 1 \quad (4.14)$$

The only disadvantage of the above formulation is that the performance measure uniformly focuses on all modes of the catalytic converter operation, while, according to requirement 4, it is preferable to focus in regions with moderate conversion efficiency. To incorporate such a feature into the above performance measure, we may define the maximum error between computation and measurement as:

$$e_{max}(t_k) = \max\{\hat{\mathcal{E}}_{t_k}, 1 - \hat{\mathcal{E}}_{t_k}\} \quad (4.15)$$

and then modify f as shown below. We do not need to change the definition of F .

$$f_2(t_k) = \frac{|e(t_k)|}{e_{max}(t_k)}, \quad F_2 \equiv \mu_{f_2} = \frac{\sum_0^N f_2(t_k)}{N} \quad (4.16)$$

When measured conversion efficiency tends to its minimum or maximum value, i.e. when $\hat{\mathcal{E}} \rightarrow 0$ or $\hat{\mathcal{E}} \rightarrow 1$, then $e_{max} \rightarrow 1$ and $f_2 \rightarrow f_1$. When measured conversion efficiency is moderate, i.e. when $\hat{\mathcal{E}} \rightarrow 0.5$, then $e_{max} \rightarrow 0.5$ and thus $f_2 \rightarrow 2f_1$. Consequently, $f_2/f_1 = 1/e_{max}$ increases hyperbolically from 1 to 2, as e_{max} decreases from 1 to 0.5 (Figure 4.2). Thus, for the same error value, f_2 increases for moderate catalytic activity, which is desired according to requirement 4.

Essentially, f_1 indicates error while f_2 indicates error normalized to the maximum possible error. This makes f_2 more sensible to get insight about model accuracy when several measurements are available. Regardless of the measurement, f_2 may take all values in the range $[0, 1]$. If $f_2 = 0$, computation is exact; if $f_2 = 1$, computation is as far from measurement as possible. On the contrary, $f_1 \in [0, e_{max}]$, which means that its maximum value depends on $\hat{\mathcal{E}}$. Thus, f_1 is indirectly dependent on the measurement, which is not preferred (requirement 3).

4.3.6 Performance measure definition for multi-response measurements

Catalytic converter tests usually involve measurements of multiple species concentrations (multiple responses). According to paragraph 4.3.2, in a typical three-way catalytic converter test, we have to exploit the measured responses of CO, HC and NO_x concentrations at converter inlet and outlet.

In this case, the performance measure defined by eq. (4.16) is applied to each response, and we subsequently get a total performance measure F as the average of the individual performance measure. For the case that CO, HC and NO_x concentration responses are available, the performance measure becomes:

$$F = \frac{F_{CO} + F_{HC} + F_{NO_x}}{3}, \quad (4.17)$$

where

$$F_i \equiv \mu_{f_i} = \frac{1}{N} \sum_0^N \frac{|e(t_k)|}{e_{max}(t_k)}, \quad i = \text{CO, HC, NO}_x. \quad (4.18)$$

4.4 Optimization with Conjugate Gradients

The conjugate gradient (CG) minimization algorithm is a conventional calculus based method. It was initially a method for minimizing quadratic functions, that was later extended to include arbitrary functions. It proceeds from point to point

in the parameter space, using information from the neighbourhood of each point, gradually converging to the minimum.

The CG method works well only when the parameter space is unimodal (it has exactly one minimum). Given a starting point, the method will move ‘downhill’ until it reaches to a minimum but has no way to tell if it is a local or a global minimum. Hence the point of convergence depends on the starting point given to the algorithm and consequently the method will most probably be trapped in a local minimum.

Thus, CG is not the method of choice for multimodal functions. It is not the most efficient way to minimize unimodal functions either; quasi-Newton methods are supposed to perform faster [6]. Nevertheless, we chose to start with this method for three reasons. First, in the beginning of this work, we had no way to guess if the parameter space was unimodal or multimodal. In other words we could not a priori know if a calculus based method would be sufficient or a global search method would be needed, so we took the simple step first. Second, this method was simple to implement and acceptably efficient. Finally, there was evidence in the literature [2] that it could give useful results, albeit in simple cases.

The CG method belongs to the category of Direction Set methods. In order to minimize a function $F(\boldsymbol{\theta})$ (which, in the context of the conjugate gradients method is usually referred to as the *merit function*), all Direction Set methods start at a point $\boldsymbol{\theta}$ in the n -dimensional space and proceed by (a) choosing a vector direction \mathbf{h} , (b) minimizing along this direction and (c) choosing a new direction and repeating the procedure. The line minimization along the vector direction \mathbf{h} is performed with an appropriate one-dimensional minimization routine.

Direction Sets methods differ from each other only in the way they choose the next direction \mathbf{h}_{i+1} to minimize, after a line minimization along \mathbf{h}_i is completed. The category of Direction Set methods includes the steepest descent method and the quasi-Newton methods. For a detailed treatment of all Direction Set methods methods (and calculus-based optimization in general) consult the textbook of Luenberger [6]; for a computer-oriented approach, consult the “Numerical Recipes” of Press et al. [7].

In detail, the conjugate gradients method performs successive line minimizations along the directions \mathbf{h}_i , which are set to be:

$$\mathbf{h}_{i+1} = \mathbf{g}_{i+1} + \gamma_i \mathbf{h}_i, \quad (4.19)$$

where

$$\mathbf{g}_i = -\nabla f(\boldsymbol{\theta}) \quad (4.20)$$

$$\gamma_i = \frac{\mathbf{g}_{i+1} \cdot \mathbf{g}_{i+1}}{\mathbf{g}_i \cdot \mathbf{g}_i} \quad (4.21)$$

$$\mathbf{h}_0 = \mathbf{g}_0 \quad (4.22)$$

It can be proved [7] that the vectors \mathbf{h}_i (along which we perform the minimizations) satisfy the conjugacy condition:

$$\mathbf{h}_i \cdot \mathbf{H} \cdot \mathbf{h}_j, \quad j < i \quad (4.23)$$

where \mathbf{H} is the Hessian matrix of the function f at point P :

$$[\mathbf{H}]_{ij} = \left. \frac{\partial^2 F}{\partial \theta_i \partial \theta_j} \right|_P. \quad (4.24)$$

Minimizing along a direction \mathbf{h}_i which is conjugate to the previous direction \mathbf{h}_i means that the gradient along the direction \mathbf{h}_{i+1} is perpendicular to the direction \mathbf{h}_i . Thus, minimization along \mathbf{h}_{i+1} will not spoil the previous minimization along \mathbf{h}_i . If the merit function F is an exact quadratic form, n line minimizations (where n is number of components of vector $\boldsymbol{\theta}$) along the conjugate directions \mathbf{h}_i will lead to the minimum. Practically, our merit function is not an exact quadratic form, therefore the repetition of the n line minimizations is needed in order to converge to the minimum.

In this work, we used the FORTRAN-77 implementation of the conjugate gradients algorithm that is given in the book of Press et al. [7]. The derivatives of the merit function were computed numerically, since analytical expressions of the derivatives of the merit function are not obtainable. The algorithm is slightly modified according to Luenberger [6] to include algorithm restarts.

4.4.1 Constraints

The tunable parameters of the model are not usually free to vary without limits. More or less complicated constraints are set in order to restrict their values to regions that make sense scientifically. In this work, very simple constraints were required: each parameter θ had to be restricted between a minimum and a maximum value (θ_{min} and θ_{max} respectively).

To handle the constraints, we follow Bates and Watts [8] and enforce a logistic transformation on the parameter θ , of the form:

$$\theta = \frac{\theta_{max} - \theta_{min}}{1 + e^{-\varphi}}$$

or equivalently

$$\varphi = \ln \left(\frac{\theta - \theta_{min}}{\theta_{max} - \theta} \right). \quad (4.25)$$

It may be noticed that $\varphi \in (-\infty, +\infty)$ while $\theta \in [\theta_{min}, \theta_{max}]$. Hence, we may now express the problem of parameter vector θ estimation as the following problem of *unconstrained* function minimization:

$$\text{minimize } F(\varphi), \quad F : \mathbb{R}^n \rightarrow \mathbb{R}^1$$

where the elements of the transformed parameters vector φ are defined by the transformation (4.25), given the constraint vectors θ_{min} and θ_{max} . As a merit function F , we used the performance measure defined previously in (4.17).

It must be stressed that, using (4.25), we optimize in respect to the reparametrized parameters vector φ , which may take any real value. Thus we have transformed a constrained minimization problem into an *unconstrained* minimization problem. The conjugate gradients method is an unconstrained minimization technique. Therefore, it may only be applied to the transformed problem (4.4.1) and cannot be used directly to minimize in respect to θ .

The CG method initially was tested tuning the diesel oxidation catalyst model. The DOC model was chosen as a first step because it involves less tunable parameters and is in general simpler than its 3WCC counterpart. Indeed, the results were encouraging [9]. When we proceeded to the 3WCC kinetics tuning, however, the method failed, because the parameter space was multimodal and the CG algorithm was trapped in local minima.

In order to tune the 3WCC model efficiently, it was necessary to ‘guide’ the CG algorithm by manually fixing some parameters according to our experience and personal judgement of the problem at hand. Only then was the outcome successful [10] and some important conclusions could be drawn:

1. The semi-automatic procedure resulted in far more accurate tuning than the completely manual one.
2. It became clear that the potential of the tunable parameters model was bigger than we had expected.
3. It seemed that even increased accuracy could be attained with the aid of a global-search procedure that also offer reduced manual interference.

The above points motivated the implementation of a global search method for the optimization procedure, specifically a Genetic Algorithm. The main concepts of the Genetic Algorithm are summarized in the next section.

4.5 Optimization with Genetic Algorithms

In general, Genetic Algorithms (GAs) and Simulated Annealing (SA) are the two most widespread approaches to global optimization. They are, in fact, two families of methods. There are many variants of algorithms that belong to these two families, as well as the so-called hybrid methods. The latter combine these methods with calculus based methods [11] for high-accuracy optimization.

Both Simulated Annealing and Genetic Algorithms borrow their paradigm from the nature. Simulated Annealing, as its name implies, immitates the way metals anneal, which is equivalent of finding a state with minimum energy. The paradigm of the Genetic Algorithms, on the other hand, is the evolution of species through the continuous rearrangement of the genetic material. Nature seems to explore the vast space of possibilities of gene combinations to build new organisms that are optimally fit to their environment.

For the global search procedure required for the tuning of the catalytic converter model, we opted for genetic algorithms. Our choice was primarily based to the fact that GAs are probably more powerful than simulated annealing. There is some analogy between the way SA and GAs work. The simulated annealing method may be viewed as a genetic algorithm with “naïve evolution” (evolution with mutation but reproduction without mating), i.e. it is analogous to weakened GA. The subject is discussed in some detail by Falkenauer [12]; the GA seems to be of a “higher level of sophistication”, which is intuitively comprehensible since the optimization of metalic crystal structures is probably less complicated than the optimization of living organisms.

4.5.1 General

This exploration process in nature has one target, namely the adaptation of the individuals and the species to their environment. The evaluation is straightforward: Well adapted and fit individuals live longer; less fit individuals die; highly capable and quick adopting species dominate; otherwise, they become extinct.

Thus, the process of evolution may be viewed as an optimization process, where the nature explores the extremely complicated parameter space that is defined by the type and arrangement of the genes, in order to find species that are well adopted to the environment and capable to survive. This continuous genetic rearrangement provides also the flexibility for new variations of individuals or new species to evolve if the environment changes, so that life continues to exist.

It is noted that Genetic Algorithms are not strictly optimization methods. In fact they were developed in the framework of Artificial Intelligence, self-adapting systems and machine learning [5, 13]. These matters are off-topic and thus not discussed here. We mention them, though, to give an idea about the flexibility and power of the genetic algorithms and to stress a consequence of this flexibility: there are no black-box GAs that can be used as optimization methods [14].

Indeed, genetic algorithms is a versatile family of methods based on some very powerful ideas. To apply a GA successfully, however, one has to make some important decisions about some aspects of the GA; if the decisions are unfortunate, the GA may work inefficiently or fail to work at all. We may say that the GA user adapts the GA to the problem at hand. Once this adoption has been accomplished successfully, the GA will show its power.

The following section, provides the description of the main ideas under any GA implementation as well as a brief account of the details of the algorithm developed in this work. We do not attempt any kind of investigation on the theoretical background of the GAs; we only attempt to adopt a GA for our optimization problem and test basic ideas to improve its robustness and performance. The long-term objective is to build a tool that is oriented to the engineer who needs a tuning procedure, is no GA expert and, in fact, knows nothing about optimization at all.

4.5.2 The Genetic Algorithm operation concept

A genetic algorithm is a kind of artificial evolution. What evolves is a population of solutions to a problem; each solution is an individual in the population. Individuals are born, mate, reproduce, are mutated and die as in natural systems. Furthermore, advantage is given to the more fit individual to live longer and produce more children. A very clear description of the method that these operations are accomplished is given by Falkenauer [12, pp. 29–30]:

GAs are applied to a problem as follows:

1. The search space of all possible solutions of the problem is mapped onto a set of finite strings over a finite (usually very small) alphabet. That is, an *encoding* is chosen, such that each point in the search space is represented by a string called *chromosome*. The GA will work with these representations of solutions, rather than with the solutions themselves.
2. An initial population of solutions is selected. This first generation is usually selected at random. Unlike standard optimization techniques, a GA performs a parallel search over a set of points in the search space, thus lessening the probability of being stuck in a local optimum.
3. A *fitness* is computed for each of the individuals in the population, reflecting the way each individual is, in comparison to the others,

nearer to the optimum. This value expresses the observed quality of the solution each individual represents.

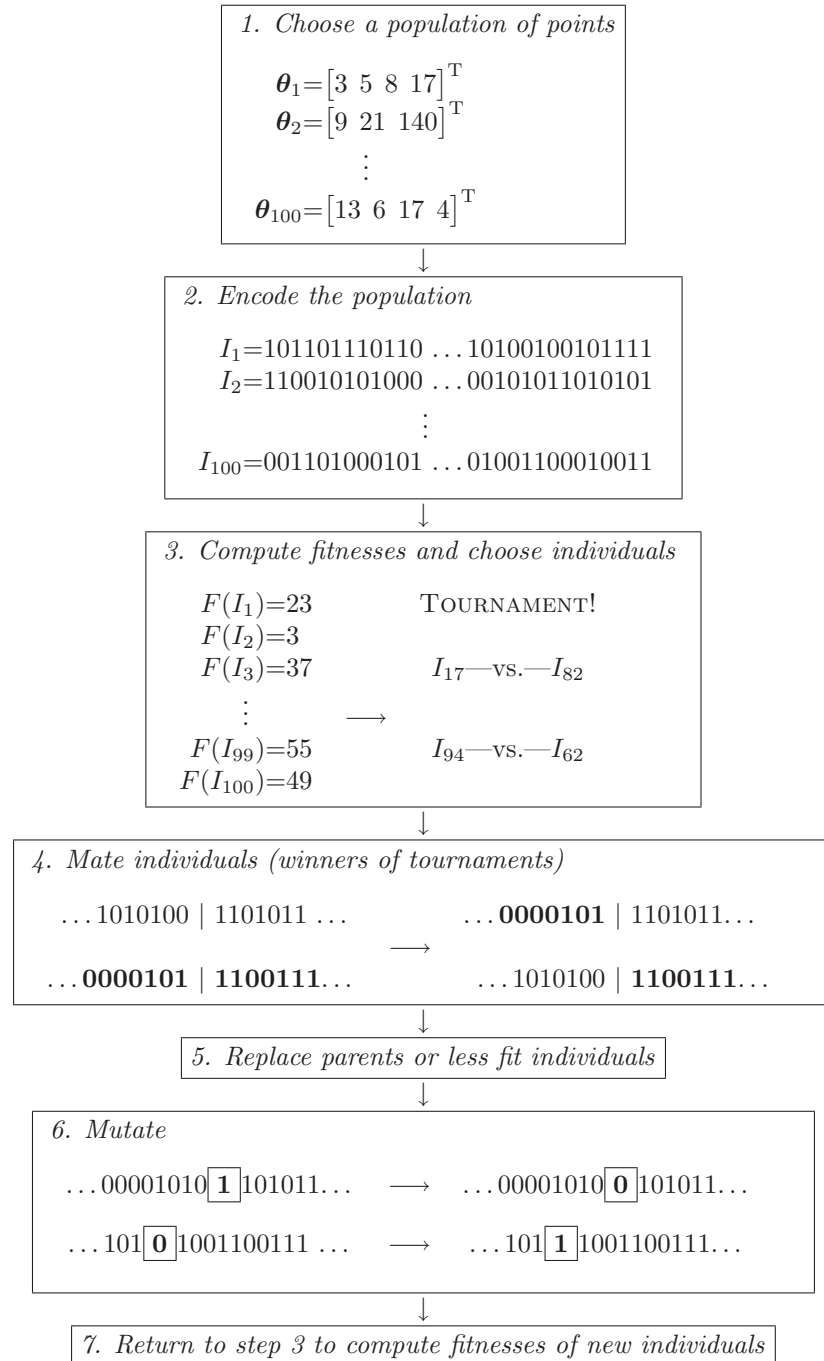
4. The more fit individuals are selected according to a *noisy selection*, i.e. individuals are selected randomly, but with probability increasing with fitness. The GAs are thus essentially a *stochastic* (randomized) optimization technique.
5. The selected individuals form the *parent set*—they are *crossed over* (by pairs) to produce their *progeny*. A crossover consists in joining together non-corresponding bits of each parent in order to constitute two new individuals.
6. Another noisy selection is performed, this time biased towards the less fit individuals. These are replaced by the progeny obtained in the previous step. Unlike standard optimization techniques, the GAs proceed by replacing the weak part of a population with new individuals, rather than replacing the current best solution with a new candidate.
7. A small part of the resulting population is mutated, i.e. small random changes are made in a few randomly selected individuals. In some GA applications, a small randomly chosen portion of the population is also subject to another genetic operator, the *inversion*—genes, while retaining their meaning, change their position on the chromosome.
8. At this point a new population has been constituted, and the optimization process starting at point (3) can be repeated. GAs are thus *iterative algorithms*.

The above description is illustrated schematically in Figure 4.5.2. The outcome of a GA is *not* a series of generations of random solutions. Instead, generations of solutions gradually improve and better children are produced; the procedure, albeit randomized, is consistently directed towards better solutions, until the optimum solution is reached. This process is based on two fundamental concepts of GA operation: Selection and recombination.

Specifically, the GA evolves a population of solutions by recombining parts of the solutions (called *building blocks*) that are present in the population, in order to build new, improved solutions. The idea of recombination of genetic material is fundamental in every GA and implies that each one of the individuals may contain useful features, i.e. building blocks of the optimum solution. A genetic algorithm's power depends very much on the ability to effectively recombine the building blocks that are contained in the population to build new, improved solutions.

To provoke evolution, the GA assumes that the building blocks of an improved solution are most likely to be found among the best individuals of the population. Therefore, *selective pressure* is imposed on the population. All individuals mate and reproduce but more fit individuals are given advantage over less fit individuals: they reproduce with higher probability and their features are given more chances to propagate in the population and be combined with features from other individuals.

From this viewpoint, population diversity is important. Highly fit individuals are promoted but less fit individuals are not useless and are also given some probability to survive, albeit small. If we impose very strong selective pressure, that is, if

**Figure 4.3:** GA operation concept

we give too much advantage to the very fit individuals from the beginning of the evolution, we run the risk that a few, initially more fit individuals, reproduce and mate in excessive rates compared to the rest of the population. Then, the GA population loses its diversity quickly and converges to a population that is dominated by the offsprings of these few individuals. This phenomenon is called *premature convergence*.*

Even when selective pressure is carefully adjusted, the GA will not work properly if it cannot recombine parts of the individual solutions effectively so that improved solutions are generated. This implies that the recombination process should be able to recombine building blocks not in an arbitrary way, but in a way that is meaningful to the problem that is being solved. For this reason, there is a strong connection between the encoding of the GA and its recombination operator [12, 15].

Of course, the algorithm described above and illustrated in Figure 4.5.2 is just a prototype, which corresponds to the ‘classic’ GA concept. This prototype is adopted to the target problem usually by modifying the choice of encoding, selection scheme, deletion scheme, and recombination operator and mutation operators. Our choices in conjunction with the catalytic converter model tuning are presented in the rest of this chapter.

Finally, we note that this GA concept has several limitations and more drastic changes to it have been proposed by Goldberg [15]. The resulting genetic algorithms bear little resemblance with the classic GA above; the concept remains the same, though: they are always population-based algorithms that recombine the building blocks of solutions with a bias towards the superior ones.

4.5.3 Encoding

The GAs work with a population of points and not a single point. Usually, points are encoded. In that case, GAs operate on the encoded points which are the representations of the points of the actual search space—GAs know nothing about the actual search space.

The encoding describes a mapping from the space of the possible solutions of the problem (the *phenotypic level*) to the space of chromosomes that represent the solutions (the *genotypic level*). The GA only sees the fitness values of the genotypes and operates on the genotypes themselves, hence the importance of the encoding.

The choice of the encoding is a very important part of the genetic algorithm, because the performance and robustness of the algorithm is dependent on whether the encoding is well suited for the problem at hand or not, i.e. if it is appropriate for the optimization function and its parameters space. If the encoding fails to represent the actual search space in a way that is advantageous for the operation of the GA, the GA may work inefficiently or fail completely. Thus the multitude of works on the encoding that have appeared in the literature e.g. [16, 17, 18, 19, 20, 5, 12]

The considerations that are taken into account for the choice of the encoding are: whether the function variables (and, consequently, the parameter space) are continuous or discrete; whether the variables are real or integer numbers or they are not numbers at all; and whether the mapping will be one-to-one, one-to-many or many-to-one [12].

* On the other hand, low selective pressure may result in a very inefficient search. If less fit individuals reproduce in great numbers, the evolution procedure is hindered and there is no guarantee that better generations of individuals will appear. In the limit, suppressing selective pressure completely results in a random search.

For the problem of model tuning, we have to optimize a function that is continuous on its real, continuous variables. In such problems, the usual approach is to use a one-to-one encoding. Both the binary and real encoding have been tested in the process of this work.

A real-encoded genetic algorithm operates on a vector of real parameters φ . This vector may be the same with the vector of tunable parameters θ . Each vector φ is a chromosome, i.e. an individual in the population. In that case, the genotypic and phenotypic level of the genetic algorithm are identical.

In the problem of catalytic converter kinetics estimation, the parameter vector θ is constructed of the pre-exponential factors and the activation energies E of the reaction rates. The pre-exponential factors A may range over several orders of magnitude and therefore a logarithmic transformation was imposed, so that the transformed parameters \tilde{A} were used to construct the chromosomes φ . Each \tilde{A} is defined as follows:

$$A = 10^{\tilde{A}} \Leftrightarrow \tilde{A} = \log A \quad (4.26)$$

Thus, each individual of the population

$$\theta = [A_1, E_1, A_2, E_2 \dots A_N, E_N]^T$$

is encoded in the following vector:

$$\varphi = [\log A_1, E_1, \log A_2, E_2 \dots \log A_N, E_N]^T$$

The multiparameter concatenated binary encoding takes one more encoding step, and converts the real values of the parameters to their binary counterparts. Assuming a parameter of the model φ , that belongs to an specified interval: $\varphi = [\varphi_{min}, \varphi_{max}]$, we linearly map the interval $[\varphi_{min}, \varphi_{max}]$ to the integer interval $[0, 2^\ell]$ and we subsequently transform to binary code. ℓ is the binary code string length. Higher values of ℓ mean a higher resolution over the interval $[\varphi_{min}, \varphi_{max}]$. The resolution is

$$\delta = \frac{\varphi_{max} - \varphi_{min}}{2^\ell - 1} \quad (4.27)$$

To construct a code for the multiparameter case, we encode every single parameter $\varphi_1, \varphi_2, \dots, \varphi_n$ and we simply concatenate the codes produced. An example of the procedure for $\ell = 4$ is given in Table 4.1.

Since the coupling of encoding with the recombination operator is very important, both the binary and the real encoding were tested with a variety of recombination operators. The binary encoding was tested with one-point, two-point and uniform crossover, while the real encoding was tested with BLX and SBX crossover. It has been found that the combination of real encoding with the SBX crossover outperformed all other methods in terms of robustness and efficiency. For more details regarding the recombination operators, see Section 4.5.5 below.

4.5.4 Fitness and Selection

The fitness of each individual in a GA population corresponds to the merit function of a conventional, calculus-based optimization method. It reflects if an individual is near or far from the optimum. Since individuals are promoted in the evolution procedure if they are highly fit, genetic algorithms are essentially maximization techniques in respect to the fitness of the individuals.

Phenotypic level		Genotypic level		
Real	Integer	Binary integer		
φ_{min}	→ 0	→	0000	
$\varphi_{min} + \delta$	→ 1	→	0001	
$\varphi_{min} + 2\delta$	→ 2	→	0010	
...	
$\varphi_{min} + (2^\ell - 1)\delta = \varphi_{max}$	→ 15	→	1111	
Point vector $\boldsymbol{\varphi} = [\varphi_1, \varphi_2, \dots, \varphi_n]^T$:		12	5	...
Multiparameter concatenated code:		[1100	0101	...
		1001]		

Table 4.1: Encoding of a single parameter and code concatenation to construct multiparameter code

To convert our minimization problem to a maximization one, we define fitness F' of an individual in the population as:

$$F'(\boldsymbol{\varphi}) = 1 - F(\boldsymbol{\varphi}) \quad (4.28)$$

where F is the performance measure that has been defined in (4.17).

The fitness of each individual is involved in the selection procedure of the GA. Random individuals are selected for mating, the procedure being biased to more fit individuals. Via selection we force populations to evolve, and care should be taken on how to accomplish this, to avoid premature convergence of the population.

Owing to the importance of selection, several techniques to accomplish selection have appeared in the literature—a review is given by Bäck. One of the first and most widespread techniques is *roulette wheel selection* [5]. This selection procedure gives to each individual a selection probability of:

$$p_i = \frac{F_i}{\sum_{i=1}^{N_{pop}} F_i} \quad (4.29)$$

That is, the selection probability of an individual is proportional to its fitness.

This selection scheme may lead the GA to premature convergence, if one individual gets a high probability in the early steps of the evolution. This stems from the fact that the absolute values of fitnesses are used in the selection scheme. What is needed is a selection scheme that does not use fitness directly but uses them to perform comparisons between individuals. Such is linear normalization, a modification of the roulette wheel selection scheme that is advocated by Davis [20].

The drawback of linear normalization is that it is somewhat awkward. A much more elegant technique, *tournament selection*, is available [21, 22, 12]. In the tournament selection, couples of individuals are extracted at random from the populations and their fitnesses are compared. The individual with the higher fitness value is the winner and is selected to mate. This technique does not lead to premature convergence and it is also more appealing than others as it seems to be more ‘natural’. It simulates mutual ‘competition’ of individuals during random ‘encounters’. Tournament selection is used throughout this work.

4.5.5 Genetic operators

Genetic algorithms obtain each population from the previous one by application of various genetic operators. The basic operators of the genetic algorithm implemented here are *crossover* and *mutation*. Crossover is the recombination operator; it recombines two or more individuals (parents) to build new ones (children) from their parts. Mutation operates on a single individual. Its purpose is to introduce genetic material by randomly changing the chromosome of an individual.

Binary encoding operators The actual implementation of each operator depends on the encoding. For a binary coded GA, three crossover variations are usually used: *single-point crossover*, *two-point crossover* and *uniform crossover* [23]. For the mutation operator, random and creep mutation is employed. One-point and uniform crossover and random mutation are schematically presented in Figure 4.4

The crossover operators that have been tested in this work use two parent chromosomes. In the case of single-point crossover, one of the $\ell - 1$ chromosome crossing points is chosen at random and both parents are sliced at this point. Then, the chromosomes exchange the slices from the same (both left or right) side to yield to different children chromosomes.

In the two-point variant, the parent chromosomes are sliced at *two* crossing points. The offsprings are formed by exchanging the slices that lie between the crossing points. Alternatively, one may imagine multi-point crossover variants but they are rarely used.

In uniform crossover, each offspring is constructed by transferring each bit from one parent with fixed probability; otherwise the bit from the second parent is transferred. The bits from the two parents that are not used for the first offspring, form the second one. On the other hand, they may be highly disruptive to the parts of a chromosome that are beneficial. The choice involves experimenting. In this work, the one-point crossover operator gave the best results for binary encoding.

Mutation, which, similarly to what happens in nature, randomly changes the value of one or more genes of the chromosome. Each gene of the chromosome has a possibility p_m to be subject to mutation. In our case, where we use binary encoding, mutation changes the value of a random gene from 0 to 1 and vice versa.

A second mutation operator that is also used in this work is *creep* mutation. Creep mutation operates on the *decoded value* of the chromosome instead of a gene. In other words, it operates on the phenotype instead of the genotype. It changes the value of one of the variables φ_i of the phenotype by a small fraction. The operation upon the phenotypes makes creep mutation an exception that has no correspondence in living systems.

The role of the crossover is the *exploration* of the search space, randomized but consistently directed to better solutions. It is most important in the beginning of the GA run. When the GA has converged to the region where the optimum lies (the *exploitation* phase), mutation becomes more important. Creep mutation is particularly useful in this regard. It is local in scope, thus resembling the conventional calculus methods and it is only useful in the last stages of a GA run.

Real encoding operators Many crossover operators for real-encoded genetic algorithms have been presented in the literature, of which a review and comparative analysis is given by Herrera [17]. Two crossover operators have been tested in this work, the BLX- a crossover (Blend Crossover) [24] and the SBX (Simulated Binary

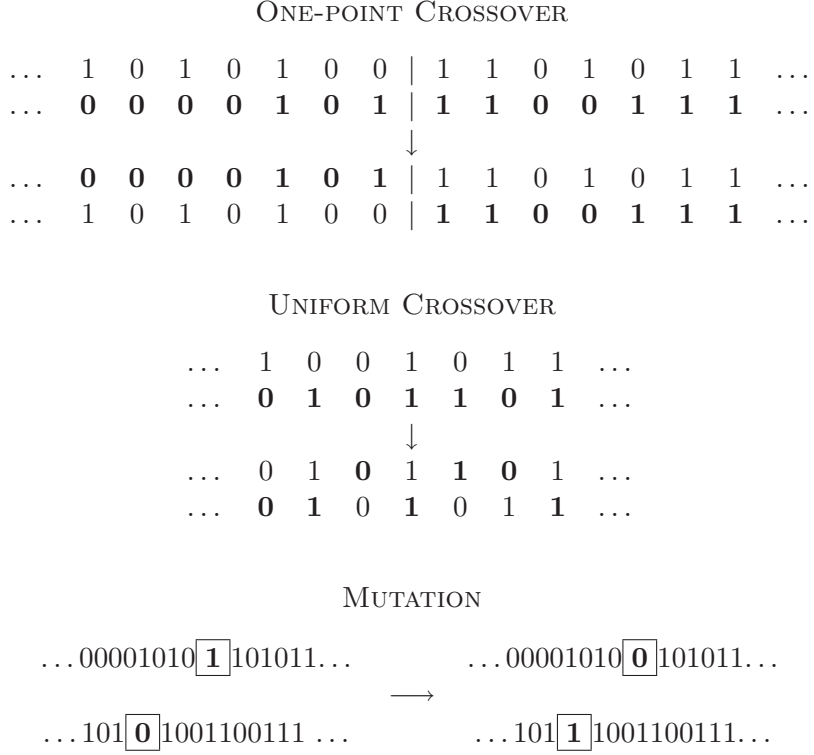


Figure 4.4: Binary mutation and crossover operators

Crossover) [25, 26]. To illustrate how this operators work, we assume that two chromosomes are selected for reproduction:

$$\begin{aligned}\boldsymbol{\theta}^{(1)} &= [\theta_1^{(1)}, \theta_2^{(1)}, \dots, \theta_N^{(1)}] \\ \boldsymbol{\theta}^{(2)} &= [\theta_1^{(2)}, \theta_2^{(2)}, \dots, \theta_N^{(2)}]\end{aligned}$$

and two offspring are generated:

$$\begin{aligned}\boldsymbol{\theta}^{(1')} &= [\theta_1^{(1')}, \theta_2^{(1')}, \dots, \theta_N^{(1')}] \\ \boldsymbol{\theta}^{(2')} &= [\theta_1^{(2')}, \theta_2^{(2')}, \dots, \theta_N^{(2')}]\\ \end{aligned}$$

The BLX- a crossover generates two offsprings where each component $\theta_i^{(1')}$ and $\theta_i^{(2')}$ is a randomly chosen number on the interval:

$$[\theta_L - a(\theta_H - \theta_L), \theta_H + a(\theta_H - \theta_L)] \quad (4.30)$$

where

$$\theta_H = \max(\theta_i^{(1)}, \theta_i^{(2)}) \quad (4.31)$$

$$\theta_L = \min(\theta_i^{(1)}, \theta_i^{(2)}) \quad (4.32)$$

The SBX crossover operator generates two offsprings $\boldsymbol{\theta}^{(1')}, \boldsymbol{\theta}^{(2')}$ of which the components are defined as follows:

$$\theta_i^{(1')} = 0.5 \left[(1 + \beta_q) \theta_i^{(1)} + (1 - \beta_q) \theta_i^{(2)} \right] \quad (4.33)$$

$$\theta_i^{(2')} = 0.5 \left[(1 - \beta_q) \theta_i^{(1)} + (1 + \beta_q) \theta_i^{(2)} \right] \quad (4.34)$$

The term β_q is the spread factor that is calculated by the following relationship:

$$\beta_q = \begin{cases} (2u)^{\frac{1}{\eta+1}} & \text{if } u \leq 0.5, \\ \left(\frac{1}{2(1-u)}\right)^{\frac{1}{\eta+1}} & \text{otherwise.} \end{cases} \quad (4.35)$$

The distribution index η is a parameter of the algorithm, and has the value of 2 in this work. A large value of η gives a higher probability for creating near-parent solutions and a small value of η allows distant solutions to be selected as children solutions. Finally, u is a random number between 0 and 1.

On an average, the SBX operator creates solutions similar to what a binary crossover operator would create if variables were coded in sufficiently large strings. As mentioned in Section 4.5.3, several preliminary runs of the genetic algorithm indicated that a real encoding with the SBX crossover yielded the most powerful genetic algorithm, compared to both its BLX- a variant and its binary coded counterparts.

The mutation operator that was used with the real-coded genetic algorithm was random mutation. Random mutation on an individual $\boldsymbol{\theta}^{(1)} = [\theta_1^{(1)}, \theta_2^{(1)}, \dots, \theta_N^{(1)}]$ changes a random chromosome $\theta_i^{(1)}$ to a value $\theta_i^{(1')}$ that is chosen randomly from the interval $[\theta_{\max}, \theta_{\min}]$.

4.5.6 Deletion

In step 6 of the GA method given in Section 4.5.2, we quote that each individual that has been obtained by a reproduction instance replaces a less fit individual, chosen for deletion via a noisy selection procedure. This is category of Genetic Algorithms is usually called *steady-state* GAs and is contrasted to the *generational* GAs.

The generational GAs keep two distinct populations, the parents population and the children population. In each reproduction instance, two individuals of the parents population produce one or two children that are placed in the children population. Thus, the size of the children population gradually increases. When it becomes equal to that of the parents population, the parents population is deleted, the children population becomes the parents population and a new generation begins, hence the name “generational” GA.

The choice between steady-state and generational genetic algorithms is related to the fundamental issue of selective pressure vs. population diversity. Goldberg and Deb [27] have shown that the steady state GA imposes much higher selective pressure than the generational genetic algorithm. Davis [20], on the other hand, advocates that this is acceptable and in fact more efficient in real world problems. This is nevertheless an empirical observation, dependent on the problem at hand.

There are some more differences between steady-state and generational algorithms [23] but, apart from Goldberg’s analysis about selective pressure, arguments backing the one or the other approach are qualitative. We have tested both a generational and a steady-state* variant of our GA, and our experience confirmed Goldberg’s analysis. The steady-state GA fairly quickly converged to a sub-optimum solution. The generational variant better found its way to the minimum and was therefore adopted.

*Specifically, a steady-state *without duplicates* GA variant, following Davis [20].

4.6 Conclusions

In the above, we have presented the design decisions for a genetic algorithm for the estimation of the tunable parameters of our engineering catalytic converter model. The algorithm was adapted so as to perform successfully using a previously defined performance measure (Section 4.3) and engine or driving-cycle tests. The GA evolved after the conjugate gradients method was rendered inadequate because of the multimodality of the problem's search space.

The genetic algorithm is based in the operating concept of a 'classic' GA. It departs from the prototype Genetic Algorithm that is usually the starting point of GA-oriented optimization methods development. It is a generational GA that uses real encoding, tournament selection, simulated binary crossover and random mutation. The choices have been made after screening many other common alternatives for GA encoding, selection and operators respectively.

In general, the genetic algorithm provides a flexible paradigm for multi-dimensional optimization in multimodal search spaces that has been in active development for many years. Apart from the theoretical advances on the subject, genetic algorithms have matured enough so as to be applied in many different scientific disciplines. An early collection of such applications has been presented by Davis [20]; examples of mechanical and chemical engineering applications have also appeared, e.g. [28, 29, 30, 31]. The development of the genetic algorithm described in the present chapter does not aspire to contribute to the field of optimization methods more than just being yet another successful application of the GA paradigm.

Nevertheless, it fills a significant gap in the framework of catalytic converter modeling, in that, together with the developed performance measure, it provides a robust and efficient method for the estimation of tunable parameters of apparent kinetic models without relying on human intuition. The introduction of this genetic algorithm is thus a significant step towards an integrated methodology for the catalytic converter modeling.

Specifically, the parameter estimation is accurate and reliable. This fact has removed any uncertainty regarding successful model tuning that was previously inhibiting the introduction and testing of new model formulations. The advances in catalytic converter modeling that have been presented in Chapter 5 were possible only after the parameter estimation methodology gave acceptable results, because it enabled the reliable and unambiguous assessment of different modeling approaches. Moreover, it paves the way for the reliable use of the model as a tool in the automotive industry, because it removes the dependency of the model's applicability on the experience of the engineer-user.

The evidence for the combined performance of the genetic algorithm and the catalytic converter advanced model is provided in the next chapter in the form of selected case studies.

4.7 Summary

- A computer-aided tuning procedure has been developed that transforms the problem of catalytic converter model tuning into an optimization problem and applies standard optimization techniques to tackle it.
- The tuning procedure that we developed is able to tune the model using inlet

and outlet concentration measurements from routine driving cycle tests.

- Attacking to the problem of model tuning as an optimization problem involved the development of two components: A *performance measure*, which qualitatively assesses the goodness-of-fit of the model for each possible set of parameter values, and an *optimization procedure*, which finds a set of tunable parameters that gives an optimum value for the performance measure.
- The performance measure is based on the comparison of the measured and computed efficiency of a catalytic converter for the three major pollutants, CO, HC_s and NO_x. The performance measure has a number of properties that are advantageous for its use with an optimization routine as well as a stand-alone standard measure for the performance of a model.
- The first optimization algorithm that was implemented was based on the conjugate-gradients method. Preliminary results suggested that the targeted optimization space is multimodal and a global search procedure is appropriate. Nevertheless, this approach revealed that the potential of the tunable parameters models is higher than initially expected, provided they are appropriately tuned.
- Subsequently, a genetic algorithm was developed and several combinations of encodings, crossover and mutation operators were tested. The best results were obtained with a real encoded generational GA with simulated binary crossover and random mutation which therefore adopted.
- The optimization methodology that combines the genetic algorithm and the performance measure developed herein presents a significant advance in the framework of catalytic converter modeling. It guarantees the reliable tuning of the model without depending on user experience and intuition, and thus it is an invaluable tool for both model development (through reliable testing of further enhancements), and for the model application (by ensuring its efficient use by the exhaust systems designer).

List of symbols

Roman letters

A	Pre-exponential factor (tunable parameter), [-]
e	Error between measurement and computation, [-]
E	Activation Energy (tunable parameter), [-]
\mathcal{E}	Conversion efficiency, [-]
f	Performance function, [-]
F	Performance measure, [-]
ℓ	Binary code string length, [-]
n	Number of optimized parameters, [-]
N	Number of points for performance measure evaluation (4.11), [-]
N_{pop}	Number of individuals in the population, eq. (4.29), [-]
p	Selection probability, [-]
P	computed response
\hat{P}	measured response from experiment
t	Time, [s]
T	Time period for performance measure evaluation, [s]
y	Concentration, [-]

Greek Letters

δ	Binary code resolution
β_q	Spread factor, (4.33), [-]
η	Distribution index (4.33), [-]
θ	Tunable parameter
μ	Average
φ	Transformed (encoded) tunable parameter

Subscripts

exp	experiment
i	response
r	experimental run
res	response

Abbreviations

CG	Conjugate Gradients
GA	Genetic Algorithm
SA	Simulated Annealing

References

- [1] S. E. Voltz, C. R. Morgan, D. Liederman, and S. M. Jacob. Kinetic study of carbon monoxide and propylene oxidation on platinum catalysts. *Industrial Engineering Chemistry — Product Research and Development*, 12:294, 1973.
- [2] C. N. Montreuil, S. C. Williams, and A. A. Adamczyk. Modeling current generation catalytic converters: Laboratory experiments and kinetic parameter optimization — steady state kinetics. *SAE paper 920096*, 1992.
- [3] T. Shamim, H. Shen, S. Sengupta, S. Son, and A. A. Adamczyk. A comprehensive model to predict three-way catalytic converter performance. *Transactions of the ASME, Journal of Engineering for Gas Turbines and Power*, 124(421–428), 2002.
- [4] C. Dubien and D. Schweich. Three way catalytic converter modeling. numerical determination of kinetic data. In *CAPOC IV, Fourth International Congress on Catalysis and Automotive Pollution Control*, Brussels, 1997.
- [5] David E. Goldberg. *Genetic Algorithms in Search, Optimization and Machine Learning*. Addison-Wesley Publishing Company, 1989.
- [6] David G. Luenberger. *Linear and Nonlinear Programming*. Addison-Wesley Publishing Company, second edition, 1989.
- [7] Press W. H., B. P. Flannery, S. A. Teukolsky, and W. T. Vetterling. *Numerical Recipes in FORTRAN-77. The Art of Scientific Computing*. Cambridge University Press, England, 1988. Also freely available online at <http://www.nr.com>.
- [8] Bates and Watts. *Nonlinear Regression Analysis and its Applications*. John Wiley & Sons, 1988.
- [9] G. N. Pontikakis, C. Papadimitriou, and A. M. Stamatelos. Kinetic parameter estimation by standard optimization methods in catalytic converter modeling. *Chemical Engineering Communications*, 2003. *In Press*.
- [10] G. N. Pontikakis and A. M. Stamatelos. Mathematical modelling of catalytic exhaust systems for EURO-3 and EURO-4 emissions standards. *Proc Instn Mech Engrs, Part D: J. Automobile Engineering*, 215:1005–1015, 2001.
- [11] Tae-Yun Park and Gilbert F. Froment. A Hybrid Genetic Algorithm for the estimation of Parameters in Detailed Kinetics Models. *Computers Chem. Engng*, 22(Supplement):S103–S110, 1998.
- [12] Emanuel Falkenauer. *Genetic Algorithms and Grouping Problems*. John Wiley and Sons, 1998.
- [13] Hugo de Garis. Genetic Programming: GenNets, Artificial Nervous Systems, Artificial Embryos. PhD thesis, Brussels University (ULB), 1992.
- [14] Emanuel Falkenauer. Applying genetic algorithms to real-world problems. In Lawrence David Davis, Kenneth De Jong, Michael D. Vose, and L. Darrell Whitley, editors, *Evolutionary Algorithms*, pages 65–88. Springer, New York, 1999.

- [15] David E. Goldberg. *The Design of Innovation – Lessons from and for Competent Genetic Algorithms*. Genetic Algorithms and Evolutionary Computation. Kluwer Academic Publishers, 2003.
- [16] Alden H. Wright. Genetic algorithms for real parameter optimization. In Gregory J. Rawlins, editor, *Foundations of genetic algorithms*, pages 205–218. Morgan Kaufmann, San Mateo, CA, 1991.
- [17] Francisco Herrera, Manuel Lozano, and Jose L. Verdegay. Tackling real-coded genetic algorithms: Operators and tools for behavioural analysis. *Artificial Intelligence Review*, 12(4):265–319, 1998.
- [18] Annie S. Wu and Kenneth A. De Jong. An examination of building block dynamics in different representations. In Peter J. Angeline, Zbyszek Michalewicz, Marc Schoenauer, Xin Yao, and Ali Zalzala, editors, *Proceedings of the Congress on Evolutionary Computation*, volume 1, pages 715–721, Mayflower Hotel, Washington D.C., USA, 6-9 1999. IEEE Press.
- [19] Franz Rothlauf, David Goldberg, and Armin Heinzl. Bad codings and the utility of well-designed genetic algorithms. Illigal Report No. 200007, 2000. Illigal Genetic Algorithms Laboratory, University of Illinois at Urbana-Champaign.
- [20] Lawrence Davis. *Handbook of Genetic Algorithms*. Van Nostrand Reinhold, 1991.
- [21] J. E. Baker. Adaptive selection methods for genetic algorithms. In J. J. Grefenstette, editor, *Proceedings of the First International Conference on Genetic Algorithms and Their Applications*, pages 101–111, Hillsdale, New Jersey, 1985. Lawrence Erlbaum Associates.
- [22] Darrell Whitley. The GENITOR algorithm and selection pressure: Why rank-based allocation of reproductive trials is best. In J. D. Schaffer, editor, *Proceedings of the Third International Conference on Genetic Algorithms*, San Mateo, CA, 1989. Morgan Kaufman.
- [23] G. Syswerda. A study of reproduction in generational and steady-state genetic algorithms. In G. Rawlins, editor, *Foundations of Genetic Algorithms*, pages 94–101. Morgan Kaufmann, 1991.
- [24] L. J. Eshelman and J. D. Schafer. Real-coded genetic algorithms and interval schemata. In L. D. Whitley, editor, *Foundations of Genetic Algorithms 2*, pages 92–99, San Mateo, 1993. Morgan Kaufmann.
- [25] Kalyanmoy Deb and Ram Bhushan Agrawal. Simulated binary crossover for continuous search space. *Complex Systems*, 9:115–148, 1995.
- [26] K. Deb and H. Beyer. Self-adaptive genetic algorithms with simulated binary crossover. Technical report No. CI-61/99, University of Dortmund, Department of Computer Science/LS11, 1999.
- [27] David E. Goldberg and K. Deb. A comparative analysis of selection schemes used in genetic algorithms. In G. Rawlins, editor, *Foundations of Genetic Algorithms*, pages 69–93. Morgan Kaufmann, 1991.

- [28] B. R. Jones, W. A. Crossley, and A. S. Lyrintzis. Aerodynamic and Aeroacoustic Optimization of Rotorcraft Airfoils via a Parallel Genetic Algorithm. *Journal of Aircraft*, 37(6):1088–1096, 2000.
- [29] R. Moros, H. Kalies, H. G. Rex, and Schaffarczyk St. A genetic algorithm for generating initial parameter estimations for kinetic models of catalytic processes. *Computers chem Engng*, 20(10):1257–1270, 1996.
- [30] D. Wolf and R. Moros. Estimating rate constants of heterogeneous catalytic reactions without supposition of rate determining surface steps — an application of a genetic algorithm. *Chemical Engineering Science*, 52(7):1189–1199, 1997.
- [31] L. Balland, L. Estel, J.-M. Cosmao, and N. Mouhab. A genetic algorithm with decimal coding for the estimation of kinetic and energetic parameters. *Chemometrics and Intelligent Laboratory Systems*, 50:121–135, 2000.

Chapter 5

Catalytic Converter Case studies

In this chapter, the model is validated and its predictive ability is demonstrated in three typical case studies, that feature different exhaust line layouts operated under both U.S. and European driving cycle conditions.

Different washcoat types are tested. The first case study employs a set of measurements of Pd/Rh catalyst, the kinetics of which were tuned with the conjugate gradients optimization method. The results of this case study revealed the potential of optimization methods for the computer aided tuning of the model and the limitations of the conjugate-gradients approach.

The two subsequent case studies, the “Variable Precious Metal Loading” case study and the “Variable cell density/wall thickness” case study were tuned employing the genetic algorithm. The former addresses the effect of precious metal loading variation in the efficiency of the catalytic converter, whereas the latter addresses the effect cell density variation. The model’s predictive ability is very good, demonstrating significant steps towards the prediction of the Precious Metal Loading effect. Moreover, the model’s predictive power suggests further potential regarding emerging technologies in the field of exhaust aftertreatment, such as NO_x storage catalysts.

5.1 The ULEV case study

The ULEV case study measurements were performed by dmc². The case study was designed in order to (a) tune and validate the catalytic converter model and (b) develop an exhaust line configuration that would enable a target vehicle to conform with the ULEV emission limits.

Two exhaust line configurations were tested in this case study, referred here as System B and System C. Both System B and System C consisted of a close-coupled catalyst (pre-catalyst) and an underfloor catalyst. The close-coupled catalyst had only one brick, while the underfloor catalyst had two bricks. All bricks had the same conventional substrate of 400 cpsi, with dimensions: 2.68×5.68×3.15. The details of the substrate are summarized in Table 5.1. The washcoat formulation of each brick varied for each brick; the corresponding data are summarized in Table 5.2. The final exhaust line would be a modified version of one of the two candidate systems, B and C.

The U.S. FTP measurement protocol was used for all measurements. Because of acquisition limitations, the measurements at the outlet of each brick could not be

Small diameter	2.68 inch
Big diameter	5.68 inch
Length	3.15 inch
Cell density	400 cpsi
Substrate thickness	6.5 mil

Table 5.1: Geometrical characteristics for each brick of the catalytic converters in Systems B and C

	Brick [–]	Washcoat loading [g/ℓ]	Precious metal loading [g/ft ³]	Pt:Pd:Rh ratio
System B	CC	6.5	110	Pd-only
	UF1 & 2	6.5	60	0:9:1
System C	CC	6.5	200	Pd-only
	UF1 & 2	6.5	60	0:9:1

CC=Close coupled brick, UF=Underfloor brick

Table 5.2: Washcoat formulation for each brick of the catalytic converters in Systems B and C

taken simultaneously. Instead, they were taken in three separate runs. Data were acquired from the inlet of the first (close-coupled) catalyst and the outlet of one brick. In each run, the outlet from a different brick was measured. Nevertheless, these limitations are not significant here, because only the close-coupled converter results will be employed. This is explained in Section 5.1.1.

The measurement setup included three vehicles, conforming to the TLEV, LEV and ULEV legislation respectively. The first set of measurements was performed with on a vehicle already in production that was conforming to the TLEV emission limits. Both System B and System C were tested with the TLEV-vehicle. The purpose of the TLEV-vehicle measurements was to tune the model parameters for each washcoat configuration.

The second set of measurements was conducted with a LEV-conforming vehicle. (That is, the raw emissions of the LEV-vehicle were different from those of the TLEV-vehicle.) The goal was to validate that the model, which had been already tuned at this point, was capable to predict the behaviour of both Systems B and C satisfactorily. Therefore, only the raw emissions of the LEV-vehicle measurements were initially given. Simulations were performed and the predictions were subsequently compared with the experimental data.

Indeed, it was shown that the model calculated the responses of both System B and System C for the LEV-vehicle with acceptable accuracy. The results of the LEV measurements and simulations also indicated that the System C performed better than System B with the LEV-vehicle, although both of them exhibited similar performance with the TLEV-vehicle. Therefore, it was decided that System C would be used as the base configuration for the ULEV-vehicle and System B would be completely dropped.

A refinement of the tuning was then performed for System C, using the measurements from both the TLEV- and the LEV-vehicle. Once again, the predictions

of the model for the ULEV-vehicle successfully compared with the corresponding measurements.

Since this is a rather extended case study, we are not going to present all measurements here. We are interested in the two first steps of the case study, that is, 3WCC model tuning using the TLEV-vehicle measurements, and subsequent validation employing the LEV-vehicle measurements.

The ULEV case study was one of the initial attempt to use a computer-aided procedure for model tuning. The catalytic converter model was tuned here with the conjugate gradients method. Both the pre-exponential factors and the activation energies of the rate expressions were tuned. The results were originally of limited success, in the sense that the conjugate gradients algorithm had to be guided manually to yield acceptable results. This was achieved using improved starting points for the CG method [1].

Specifically, the model was initially tuned using the CG method, the resulting kinetics were manually improved and then were fed back to the CG method to obtain better solutions. This cyclical, semi-automatic procedure was of limited general usefulness, because it relied on our previous experience. Nevertheless, a number of conclusions were drawn from this procedure, that were very important to decide the subsequent steps of this work:

1. The semi-automatic tuning procedure resulted in far more accurate tuning than the completely manual one.
2. This implied that the potential of the tunable parameters models was bigger than we had expected.
3. The combination of tunable parameters of the model and driving cycle experimental protocol resulted in a multimodal search space. This was also the reason that the conjugate gradients method could not attain a good solution without external aid.
4. Therefore, it became evident that increased accuracy could be attained with the aid of a global-search procedure that could also offer reduced manual interference.
5. The kinetic model originally contained a set of steam-reforming reactions [2]. It was found that the sensitivity of the model to these kinetic parameters was very low. This indicated that steam reforming could be omitted from the reaction scheme.
6. The above fact also indicated that an improved tuning procedure could not only help us tune the model more accurately, but it could also help us identify directions for improvement of the model itself.

The GA algorithm that was subsequently developed circumvented the optimization problems of the CG algorithm and proved capable of finding near-optimum solutions in the multimodal search space. Nevertheless, we present here the results of the ULEV case study, because of its importance in the process of evolution of the computer-aided tuning methodology, and because it shows the validity of the catalytic converter model also in the FTP cycle (all subsequent results are based on measurements of the European driving cycle test).

5.1.1 TLEV-vehicle results

We did not use the whole FTP cycle for model tuning, because the computational time needed for the optimization would be excessive. Instead, we were confined to the first 250 s that contain the light-off of the catalyst. We assumed that the model can perform equally well to the rest of the cycle if it is accurately tuned in this small part of it. The simulation results for the whole cycle that were obtained subsequently showed that this assumption is valid.

The results of the tuning for the TLEV-vehicle are presented in the form of computed vs. measured instantaneous concentrations of CO, HC and NO_x at the outlet of the close-coupled converter for the first 250 s of the FTP cycle (cold start phase). Figures 5.1 to 5.6 present the results for System B and System C tuning.

The reason that we present the predictions of the model for the close coupled converter is the following: The close-coupled converter is incorporated in the systems under study because, owing to its proximity to the engine, is subject to higher temperature from the beginning of the operation of the engine and quickly lights-off. The model's success or failure to predict the light-off behaviour of the close coupled converter demonstrates its usability as a CAE tool.

It must be stressed that, before the development of the computer-aided tuning methodology, the model could be tuned with similar success only for the CO and HC conversion. Manual tuning had never been successful for the NO_x conversion, regardless of the experience and effort of the user. The results of the TLEV-vehicle measurements revealed that this was not a shortcoming of the rate expression for the CO-NO reduction—as was initially suspected—but a failure of locating the optimum set of model parameters in a very complicated search space.

The TLEV-vehicle results revealed the power of a computer-aided tuning methodology and indicated a hidden potential of the model. Obviously, to back up these arguments, the model predictions had to be tested using different measurements—these of the LEV-vehicle.

5.1.2 LEV-vehicle results

The TLEV-vehicle results confirmed the validity of the tuning methodology but, in principle, provided no information about the quality of the model itself. No matter how successful the tuning of the model may be, the model has to be validated against different operating conditions without further tuning of any parameter values.

The LEV-vehicle measurements were employed for this purpose. Systems B and C were mounted on the car and the response of the system during the FTP cycle was measured. The inlet conditions for each brick were feeded to the model, which calculated the outlet concentrations of CO, HC and NO during the cycle. Then, these concentrations were compared with the measured ones.

The results of the calculations of the model for the first 250 s of the FTP cycle are presented in Figures 5.7 to 5.12. Evidently, the model presents very satisfactory accuracy, especially in the HC and NO_x results, where the light-off and the subsequent breakthroughs are matched very well. The CO kinetics on the other hand, seem to be overestimated, especially in System C. As a result, the model predicts 100% converter efficiency after 70 s, while the measurement presents emission peaks.

The reason for the failure of CO can be easily explained, if the original TLEV measurements are examined that were employed for model tuning. Clearly, the efficiency of the System C converter, shown in Figure 5.2 is approximately 100%. This behaviour may be predicted by the model using any big value for the CO

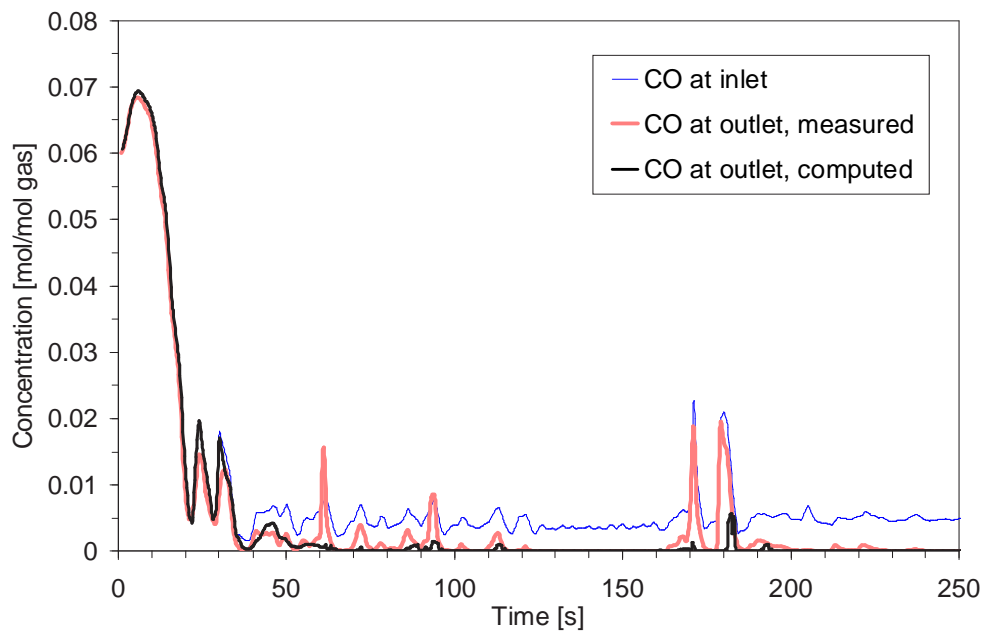


Figure 5.1: TLEV-vehicle with System B: Computed vs. measured CO concentrations, 0–250 s

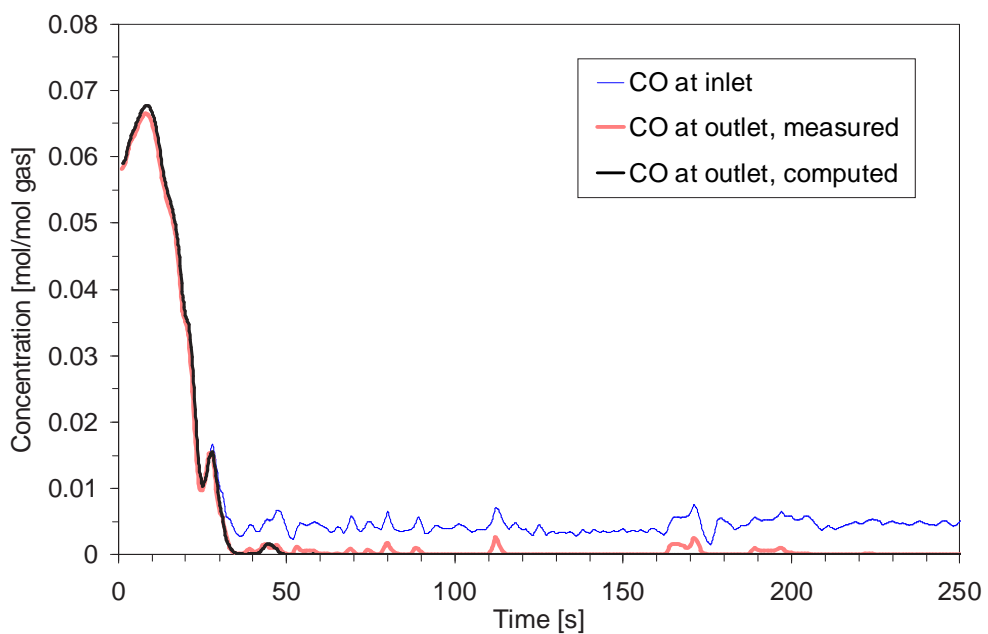


Figure 5.2: TLEV-vehicle with System C: Computed vs. measured CO concentrations, 0–250 s

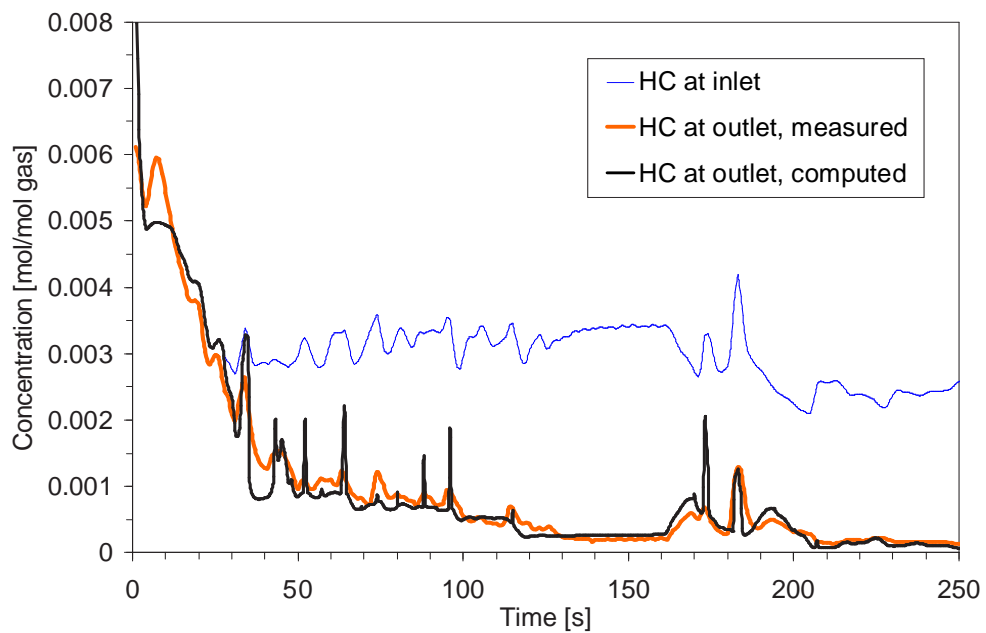


Figure 5.3: TLEV-vehicle with System B: Computed vs. measured HC concentrations, 0–250 s

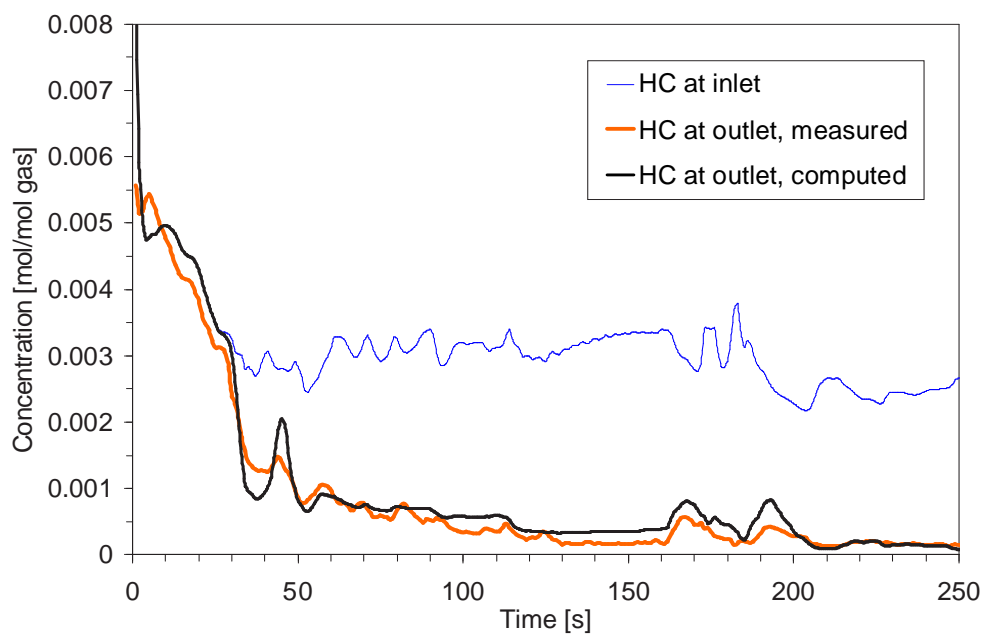


Figure 5.4: TLEV-vehicle with System C: Computed vs. measured HC concentrations, 0–250 s

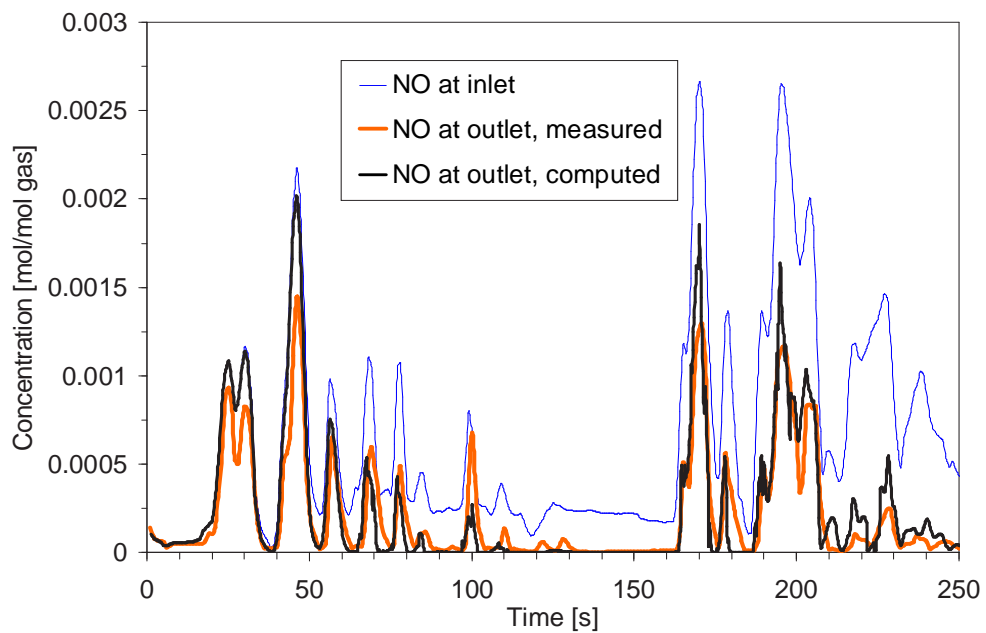


Figure 5.5: TLEV-vehicle with System B: Computed vs. measured NO concentrations, 0–250 s

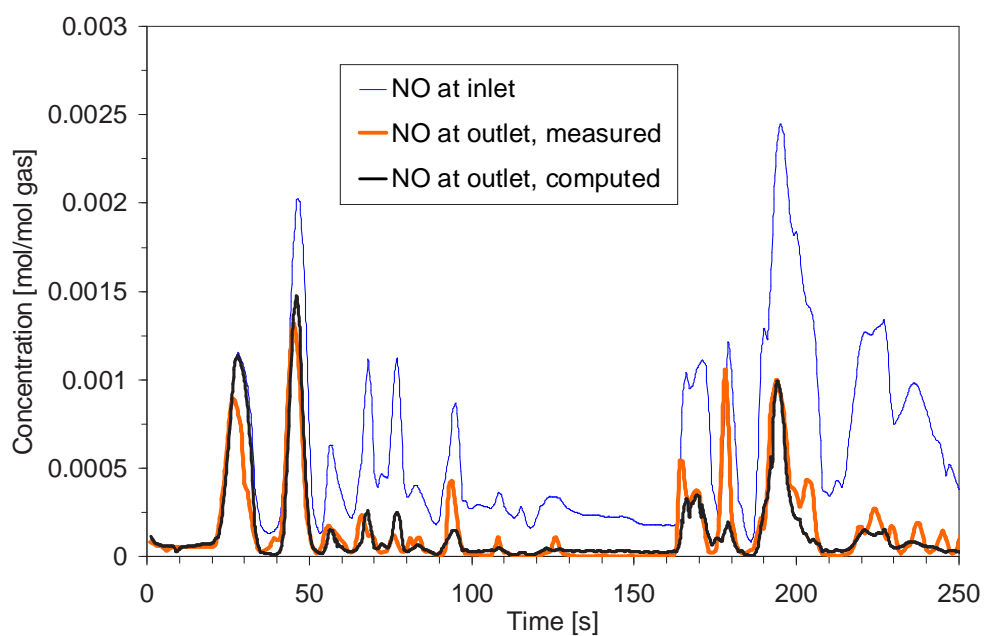


Figure 5.6: TLEV-vehicle with System C: Computed vs. measured NO concentrations, 0–250 s

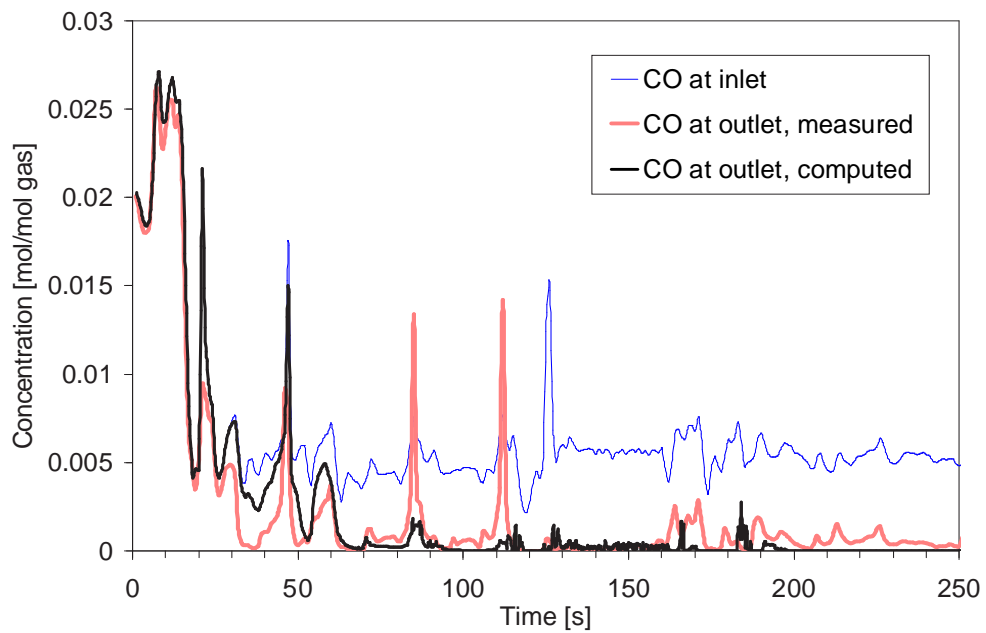


Figure 5.7: LEV-vehicle with System B: Computed vs. measured CO concentrations, 0–250 s

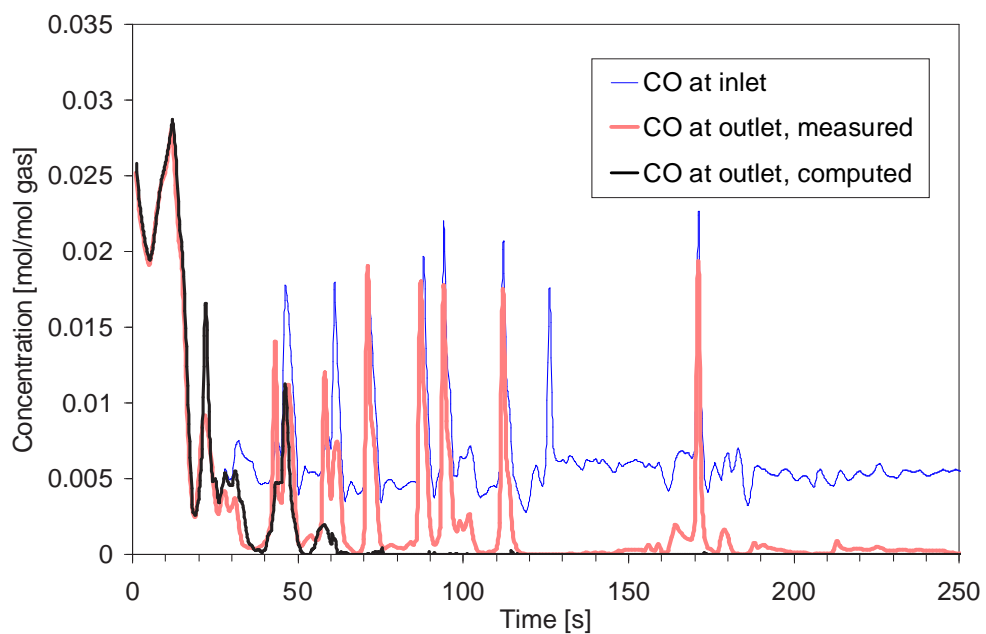


Figure 5.8: LEV-vehicle with System C: Computed vs. measured CO concentrations, 0–250 s

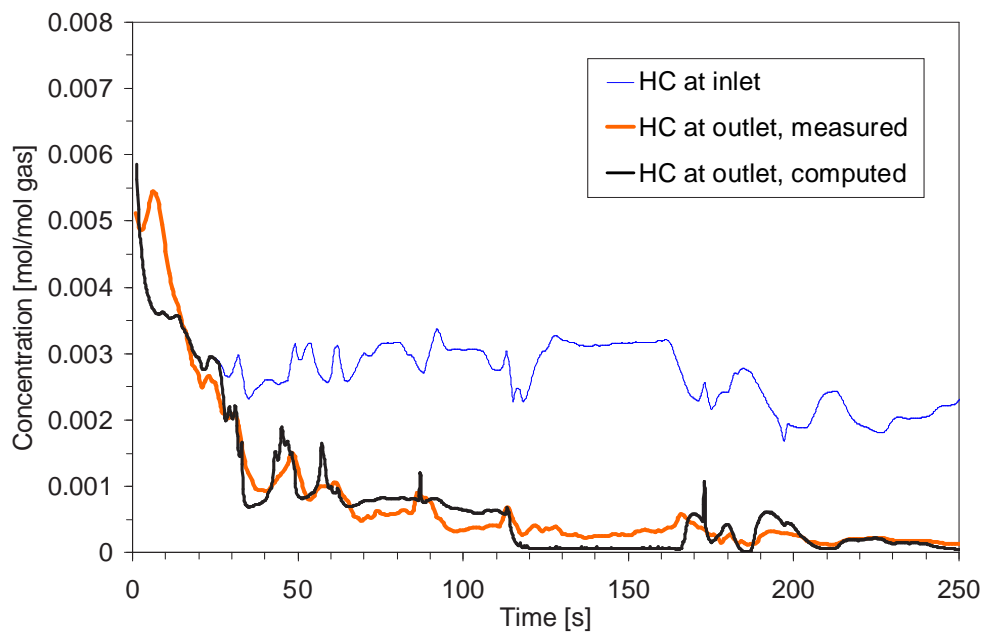


Figure 5.9: LEV-vehicle with System B: Computed vs. measured HC concentrations, 0–250 s

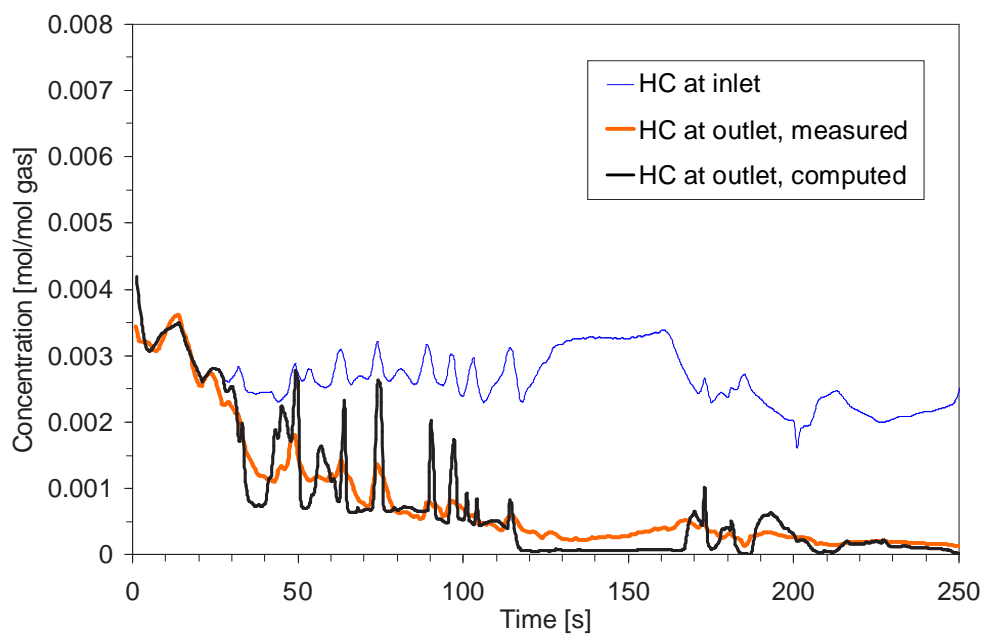


Figure 5.10: LEV-vehicle with System C: Computed vs. measured HC concentrations, 0–250 s

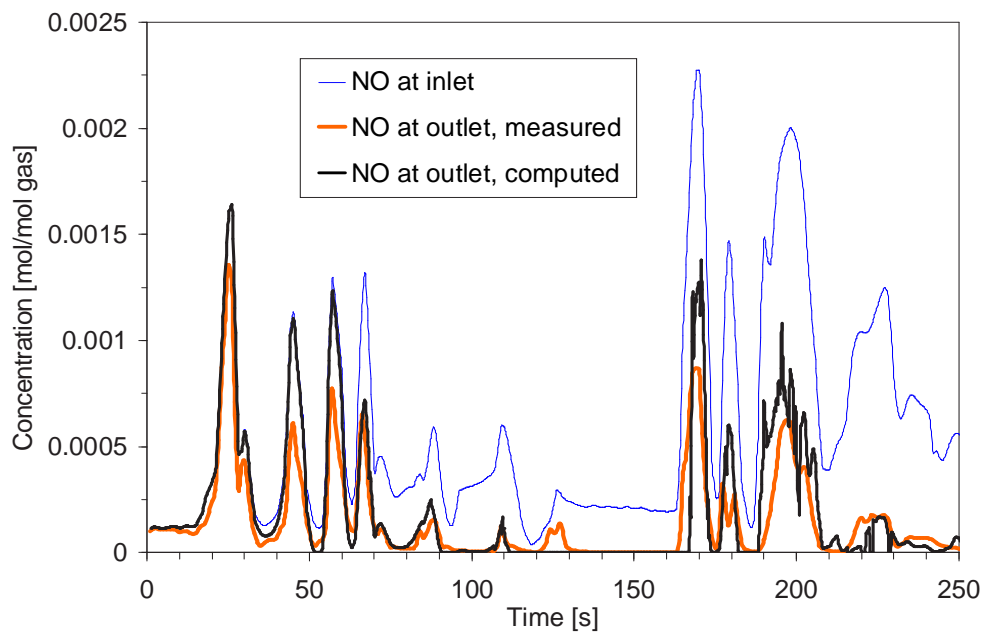


Figure 5.11: LEV-vehicle with System B: Computed vs. measured NO concentrations, 0–250 s

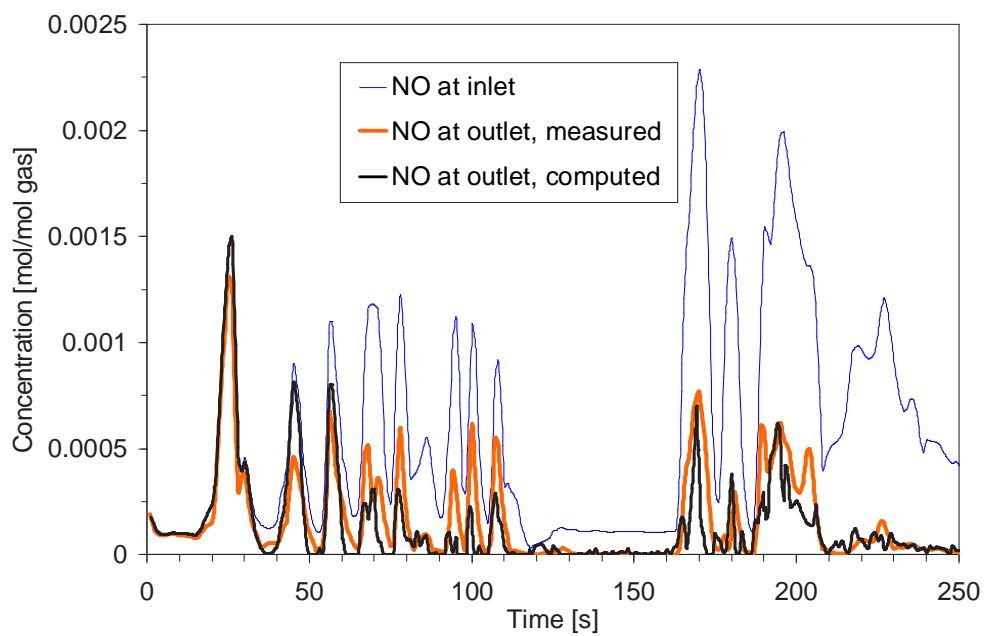


Figure 5.12: LEV-vehicle with System C: Computed vs. measured NO concentrations, 0–250 s

Small diameter	0.1226 m
Big diameter	0.1226 m
Length	0.2032 m
Cell density	400 cpsi
Substrate thickness	1.6510^{-4} m
Washcoat thickness	4.9510^{-5} m

Table 5.3: Geometrical characteristics for each brick of the catalytic converters of the PML case study

kinetics. From the viewpoint of optimization, the search space in this region is a plateau and contains no information that may be exploited by the optimization procedure. Thus, the kinetics value chosen by the model is essentially random value that falls in this plateau, and this is clearly revealed by the model validation with the LEV measurements.

Examining Figure 5.2 more carefully, one may notice that there are infact some small deviations of the outlet CO concentration from zero. This implies that a more sensitive search method could exploit them to find the correct kinetics value for CO. Apparently, this indicates the limitations of the semi-automatic, conjugate-gradients based optimization procedure that was used in this set of measurements.

An important conclusion that can be drawn for this discussion is that, as catalytic converter efficiency progressively improves, the information available to an optimization procedure for model tuning becomes more sparse. This is a consequence of the fact that such information is only contained during light-off and emission breakthroughs. The ULEV case study is dated back in 1998. For modern, more efficient catalytic converter modeling, a more accurate tuning procedure had to be developed. This has been achieved with the development of a genetic algorithm based tuning procedure which is subsequently applied in two case studies—the “Variable Precious Metal Loading” case study and the “Variable cell density/wall thickness” case study.

5.2 Variable Precious Metal Loading case study

5.2.1 Measurements set

The PML case study is a set of five european (MVEG) driving cycle test measurements of three-way catalytic converters. Five tests were conducted with a 2.4ℓ catalyst (cycles 599, 605, 609 and 624) and one was conducted with a 0.6ℓ catalyst (cycle 600). The catalytic converters were mounted underfloor on the exhaust line of a passenger car with a 2ℓ gasoline engine. The geometrical and loading characteristics of the catalytic converters bricks are given in Tables 5.3 and 5.4 respectively.

Four cycle measurements explore the effect of variation of the Precious Metal (PM) Loading of the washcoat (hence the name of the case study). That is, cycles 599, 605, 609 and 624 have their PM loading vary from 10 to $100\text{ g}/\text{ft}^3$. The fifth cycle (cycle 600) has the same PM loading with cycle 599 (2 bricks), but its length is a quarter of the length of the other converters (1/2 bricks).

Cycle	Bricks	Washcoat		
		loading [g/ℓ]	PML [g ft ³]	PML Ratio (Pt:Pd:Rh)
599	2	200	50	7:0:1
600	1/2	200	50	7:0:1
605	2	200	10	7:0:1
609	2	200	100	7:0:1
599	2	200	30	7:0:1

Table 5.4: Washcoat formulation for each brick of the catalytic converters of the PML case study

5.2.2 Model tuning for the 50 g/ft³ catalyst

The first step was to tune the model for a specific catalyst configuration in a typical driving cycle test and estimate the kinetic parameters of the model. Successful tuning in this phase implies that (a) the model incorporates the appropriate degrees of freedom in order to match the measurement, and (b) the tuning methodology is able to tackle the parameter estimation optimisation problem successfully. For this task, we employ the 599 cycle.

Instantaneous CO, HC and NO_x emissions at converter inlet and exit were measured over the 1180 s duration of the MVEG cycle. The measured catalyst's performance on this car is presented in Figure 5.13 for the 599 cycle. Obviously, the specific converter attains a significant overall efficiency: The emissions at catalyst's exit are diminished after the cold start phase. However, the emissions standards themselves are quite low: Thus, the model should not only accurately predict catalyst light-off, but it should also be capable of matching the catalyst's breakthrough during accelerations, decelerations and especially in the Extra-Urban, high speed part of the cycle.

In order to match this catalyst's behaviour, the model was tuned using the genetic algorithm-based optimization methodology. The tuning process resulted in the kinetics parameters of Table 5.5. The computed results are summarized in the form of cumulative CO, HC and NO_x emissions at catalyst's exit, compared to the corresponding measured curves in Figure 5.14. In addition, computed and measured temperatures at converter's exit are compared in Figure 5.15. Apparently, the model is capable of matching the catalyst's behaviour with a remarkable accuracy, allowing the performance of design optimisation studies.

Since one of our objectives of this work is to quantify the attainable accuracy, we proceed to a more detailed comparison of model predictions and measurements in the form of instantaneous CO, HC and NO_x emissions.

Figure 5.16 presents the computed and measured instantaneous CO emissions at converter inlet and exit during the first 390 s of the NEDC cycle: Apparently, the model successfully matches light-off behaviour of the catalyst, as well as subsequent breakthrough during acceleration. The role of oxygen storage and release reactions in matching the CO breakthrough behaviour is better assessed by including in the graph, the computed degree of filling of the total washcoat's oxygen storage capacity. Evidently, emission breakthroughs occur when the oxygen that is stored in the Ceria component of the washcoat does not suffice for the conversion of all pollutants.

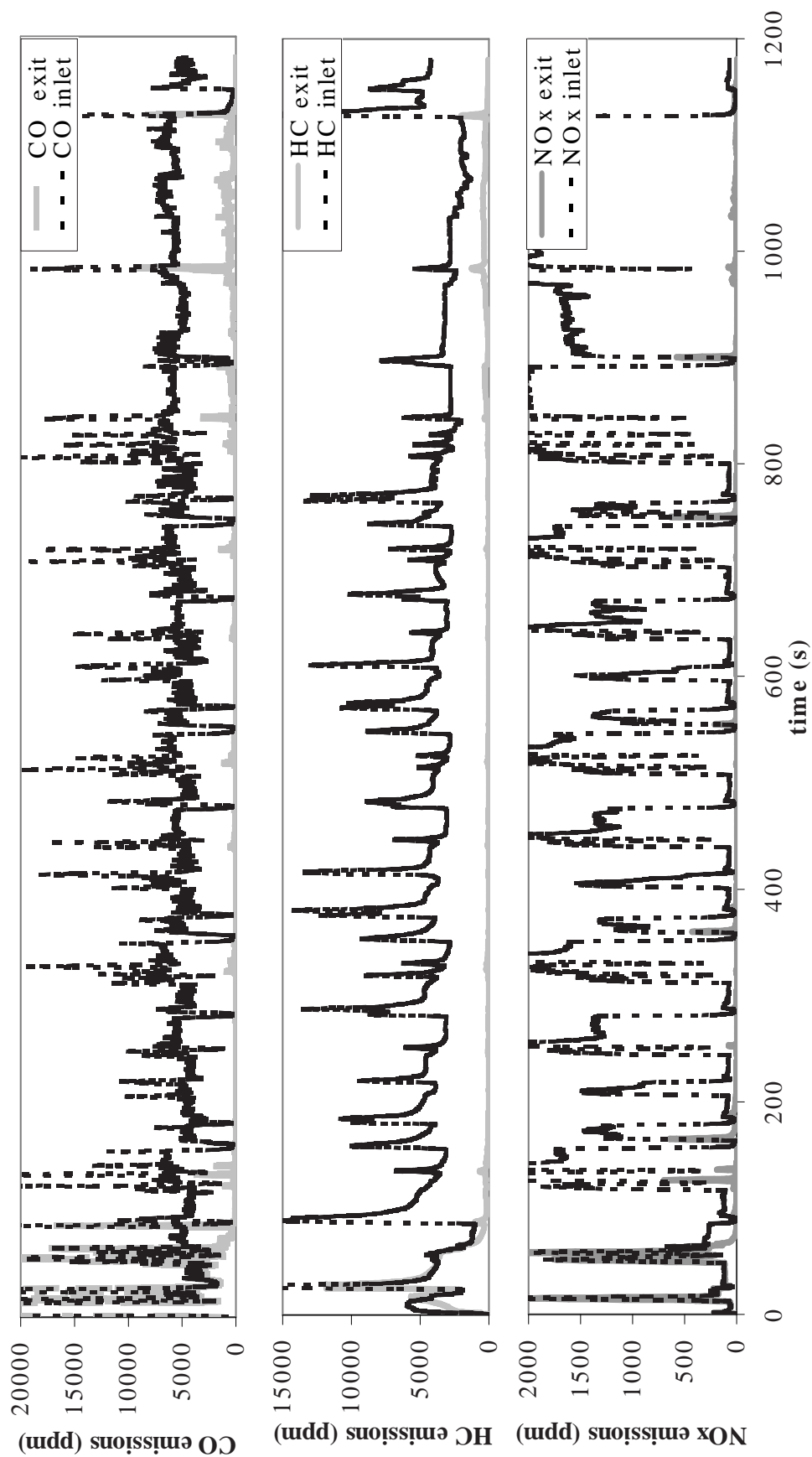


Figure 5.13: Measured instantaneous CO, HC and NO_x emissions at converter inlet and exit, over the 1180 s duration of the cycle

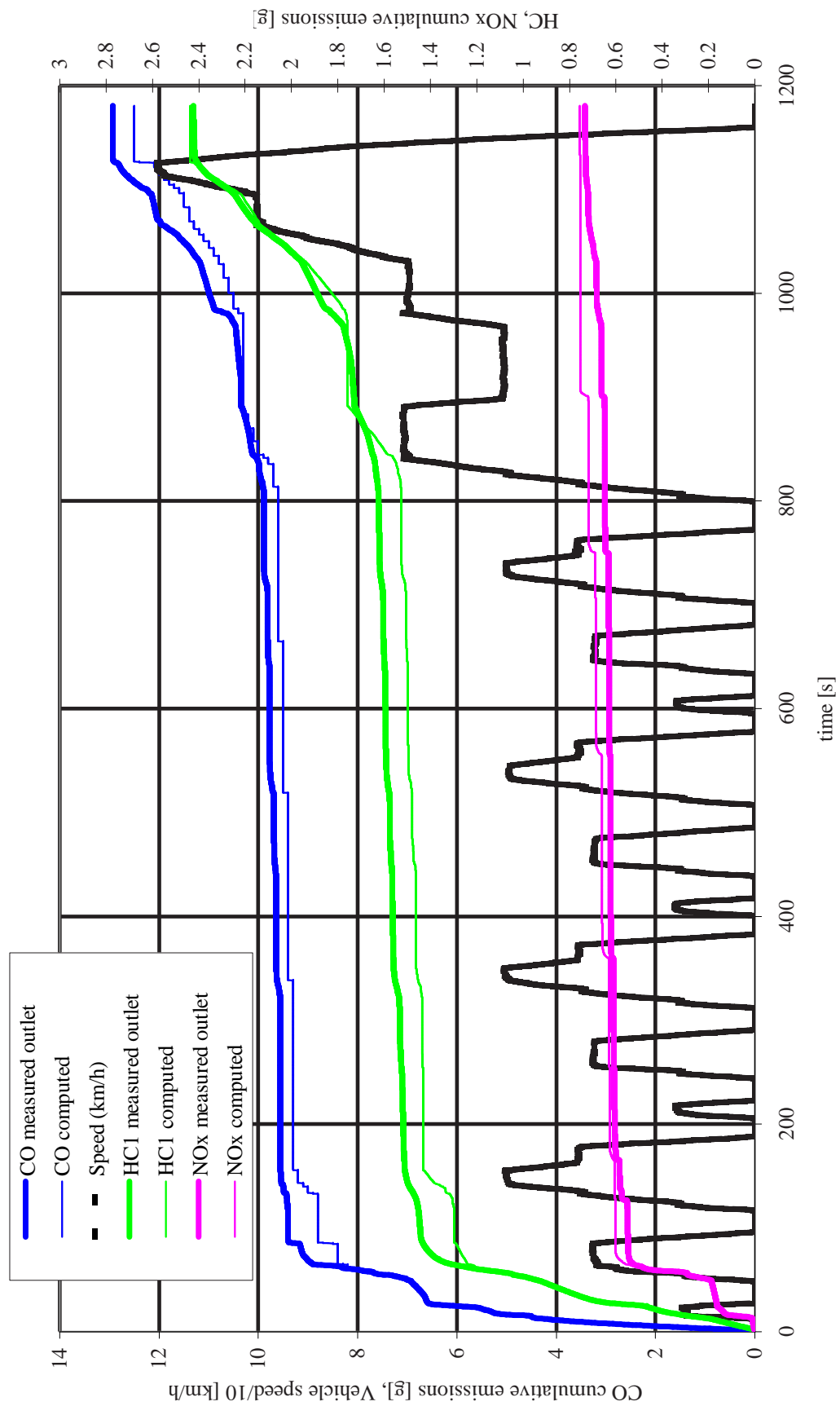


Figure 5.14: Cumulative CO, HC and NO_x emissions at converter inlet and exit, over the 1180 s duration of the 599 cycle

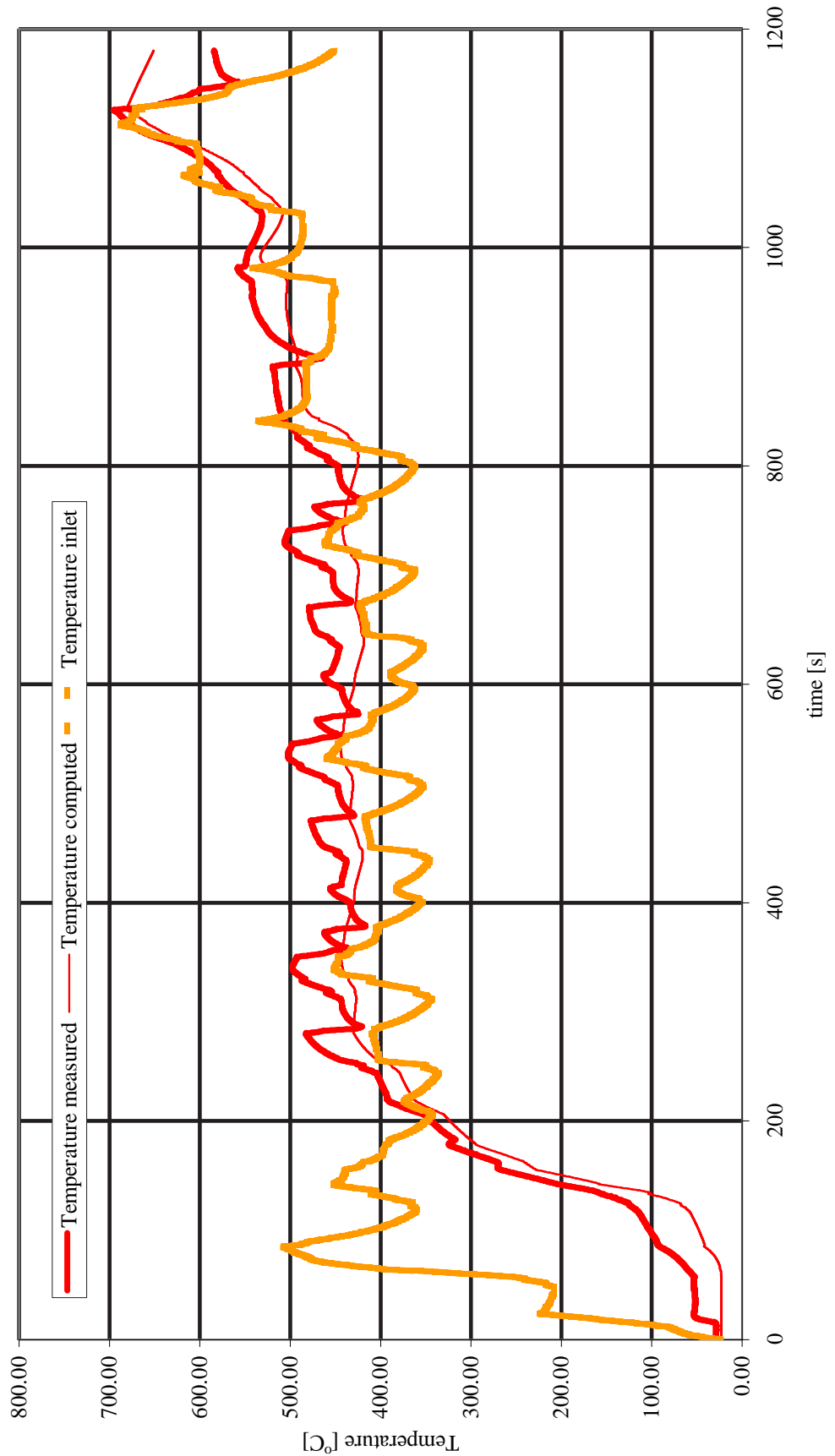


Figure 5.15: Cumulative CO, HC and NO_x emissions at converter inlet and exit, over the 1180 s duration of the 599 cycle

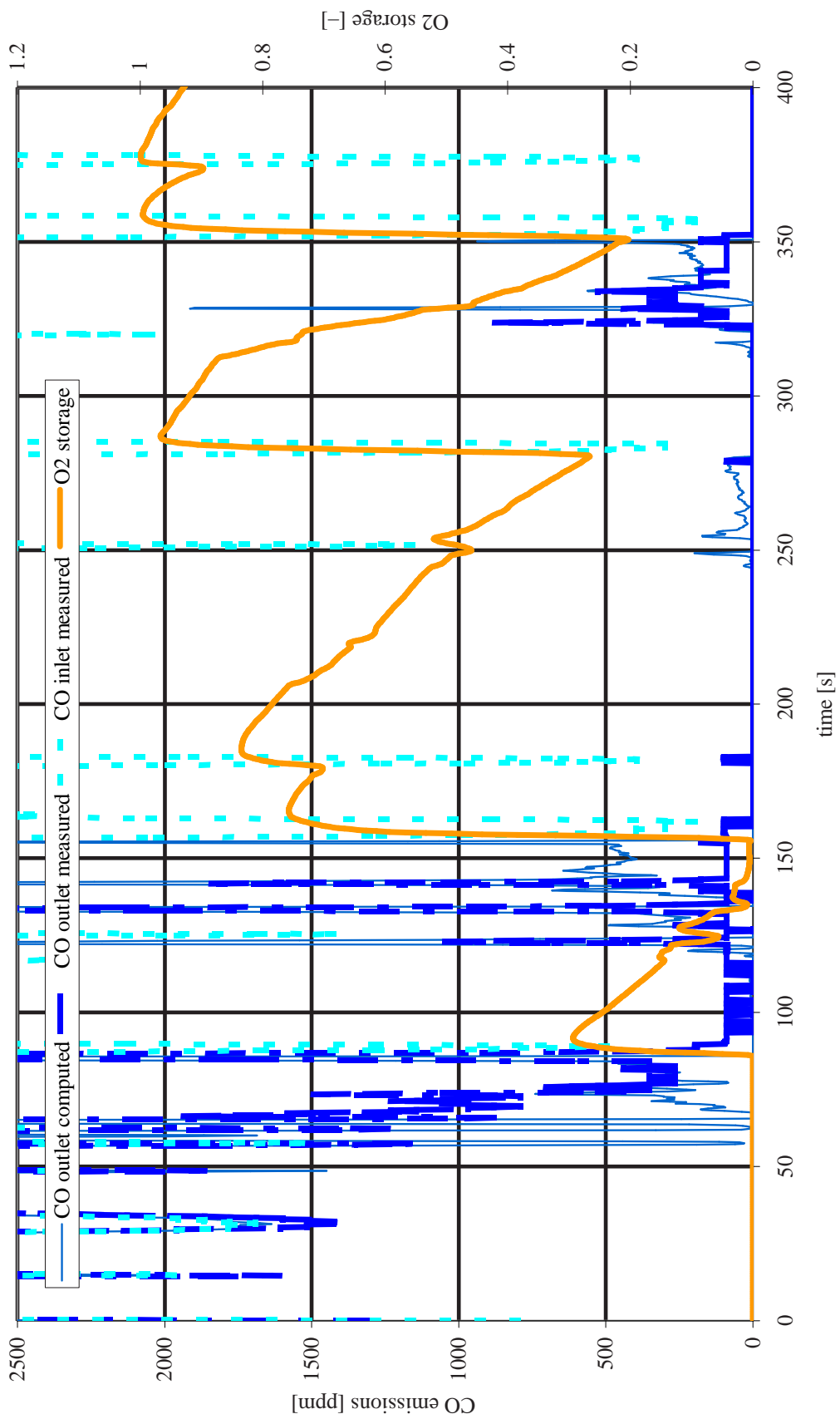


Figure 5.16: Instantaneous CO emissions at converter inlet and exit, over the first 400 s of the 599 cycle

1	$2\text{CO} + \text{O}_2 \longrightarrow 2\text{CO}_2$	$A_1 = 4.89 \cdot 10^{20}$	$E_1 = 90000$
2	$2\text{H}_2 + \text{O}_2 \longrightarrow 2\text{H}_2\text{O}$	$A_1 = 2.00 \cdot 10^{19}$	$E_1 = 90000$
3	$\text{CH}_{1.8}(\text{fast}) + 1.4\text{O}_2 \longrightarrow \text{CO}_2 + 0.9\text{H}_2\text{O}$	$A_1 = 3.61 \cdot 10^{20}$	$E_1 = 95000$
4	$\text{CH}_{1.8}(\text{slow}) + 1.4\text{O}_2 \longrightarrow \text{CO}_2 + 0.9\text{H}_2\text{O}$	$A_1 = 1.83 \cdot 10^{17}$	$E_1 = 120000$
5	$2\text{CO} + 2\text{NO} \longrightarrow 2\text{CO}_2 + \text{N}_2$	$A_1 = 1.54 \cdot 10^{11}$	$E_1 = 90000$
6	$2\text{Ce}_2\text{O}_3 + \text{O}_2 \longrightarrow 4\text{CeO}_2$	$A_1 = 2.94 \cdot 10^9$	$E_1 = 90000$
7	$2\text{Ce}_2\text{O}_3 + 2\text{NO} \longrightarrow 4\text{CeO}_2 + \text{N}_2$	$A_1 = 4.68 \cdot 10^{10}$	$E_1 = 90000$
8	$\text{CO} + 2\text{CeO}_2 \longrightarrow \text{Ce}_2\text{O}_3 + \text{CO}_2$	$A_1 = 7.85 \cdot 10^9$	$E_1 = 85000$
9	$\text{CH}_{1.8}(\text{fast}) + 3.8\text{CeO}_2 \longrightarrow 1.9\text{Ce}_2\text{O}_3 + \text{CO}_2 + 0.9\text{H}_2\text{O}$	$A_1 = 1.35 \cdot 10^{10}$	$E_1 = 85000$
10	$\text{CH}_{1.8}(\text{fast}) + 3.8\text{CeO}_2 \longrightarrow 1.9\text{Ce}_2\text{O}_3 + \text{CO}_2 + 0.9\text{H}_2\text{O}$	$A_1 = 2.43 \cdot 10^{13}$	$E_1 = 85000$

Table 5.5: Tuned kinetic parameters for the 50 g/ft³ catalyst

The same comparison for CO emissions for the cycle part from 400 s to 800 s is given in Figure 5.17. In this part of the cycle, the efficiency of the converter is 100% except from four small breakthroughs, which are of the order of 200 ppm, with maximum peaks of the order of 1000 ppm. The breakthroughs occur when the oxygen stored in the washcoat is gradually depleted. The prediction of the model is remarkably good, especially when the order of magnitude of the breakthroughs is considered. This successful prediction indicates that the oxygen storage reactions that are implemented in the model are capable of modeling the phenomenon with high accuracy.

Figure 5.18 presents the computed and measured instantaneous CO emissions at converter inlet and exit during the last 400 seconds of cycle. Again, the model is demonstrated to be capable of matching the characteristic behaviour of the catalyst in the Extra-Urban part of the cycle. All the 3WCC operation events (CO breakthroughs) are not only qualitatively, but also quantitatively approached by the model prediction. Again, the presentation in the same graph, of the variation of oxygen storage capacity filling percentage significantly improved understanding of the instantaneous catalyst's performance. The emission breakthroughs in this phase of the cycle are exaggerated compared to the previous figures, because of the higher exhaust gas flow rates.

The same quality of results is attained for the other two measured pollutants, hydrocarbons and NO_x. For brevity, we present the comparison between instantaneous measured and computed emissions for HC and NO_x for the whole extent of the MVEG cycle. NO_x emissions are presented in Figure 5.20 and the corresponding results for HC are presented in Figure 5.19.

The figures reveal that the model successfully matches light-off behaviour of the catalyst, as well as subsequent HC and NO_x breakthrough behaviour during accelerations. The connection between emission breakthroughs and oxygen storage phenomena in the washcoat is apparent here as well.

The prediction of HC emissions is of the very good quality. The model predicts the events (HC breakthroughs) of the urban and extra-urban part of the cycle, not only qualitatively, but also quantitatively, in a certain extent. In any case, though, modeling of HC conversion is hindered by the uncertainty of the content of the hydrocarbon mixture of the exhaust gas. It should be kept in mind that this complicated mixture is modeled as a mixture of two HC components, a fast and a slow oxidizing one, with ratio 85% to 15% respectively. The quality of results is

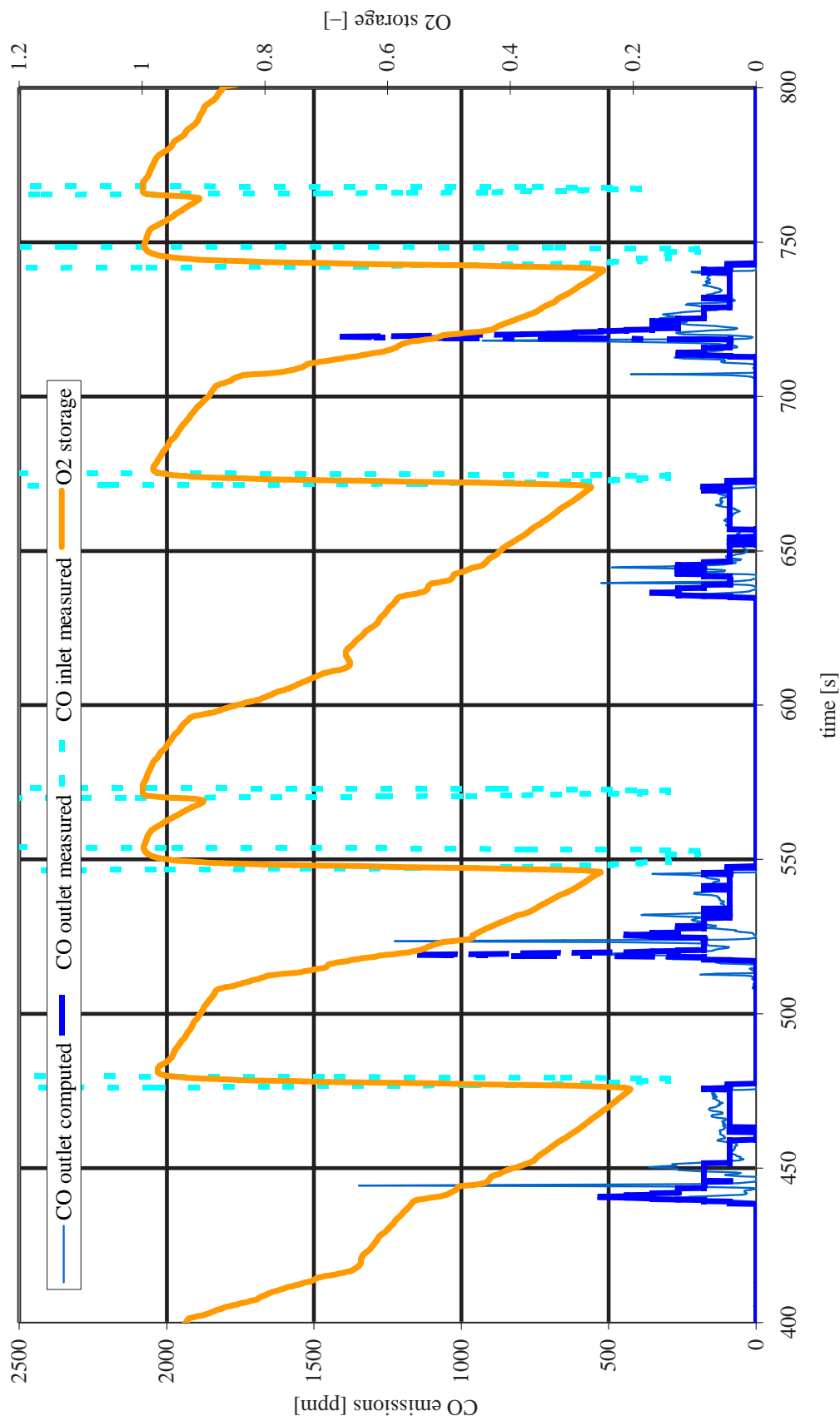


Figure 5.17: Instantaneous CO emissions at converter inlet and exit, between 400 s and 800 s of the 599 cycle

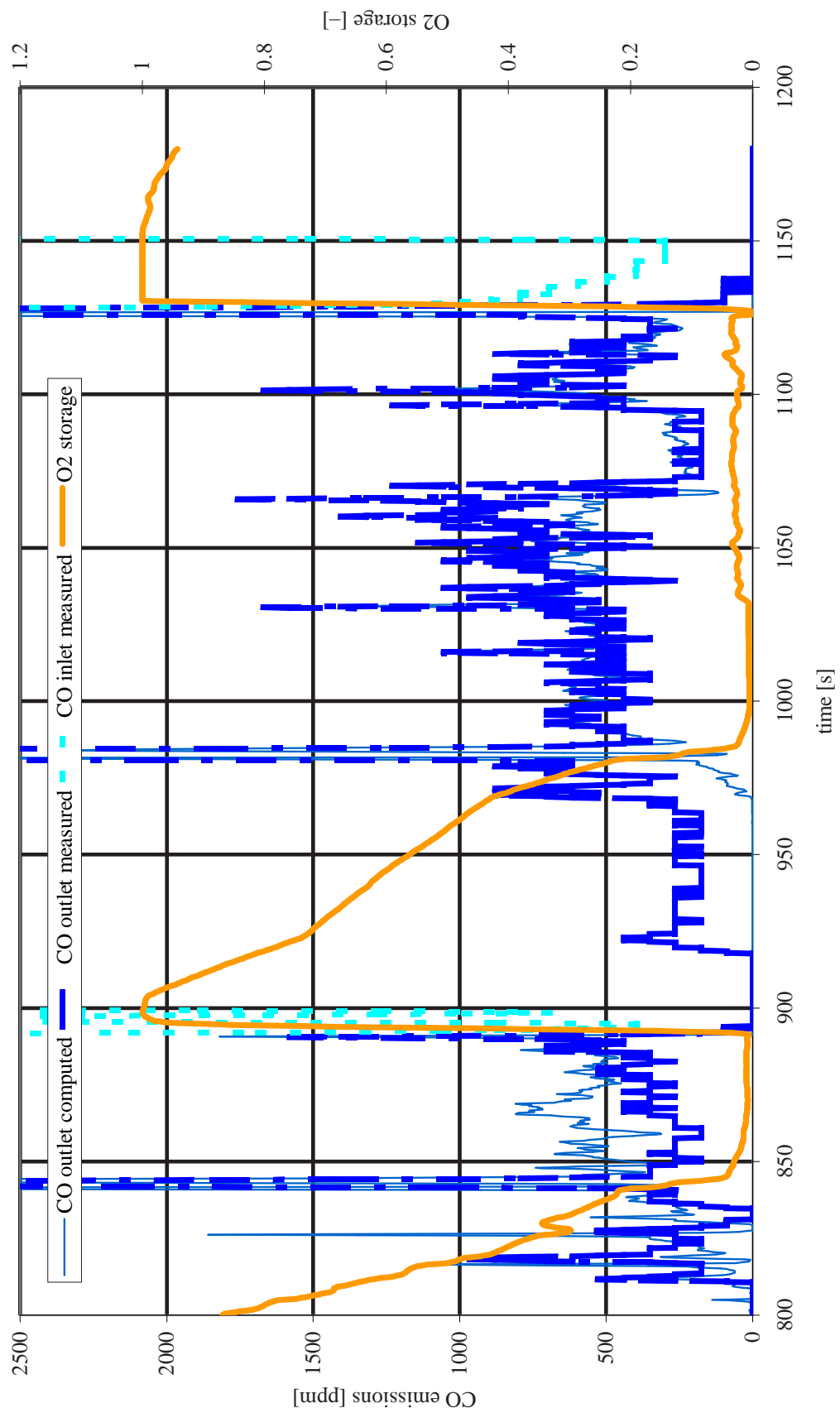


Figure 5.18: Instantaneous CO emissions at converter inlet and exit, over the last 400 s of the 599 cycle (extra-urban part)

Catalyst	CeO ₂ (wt%)	State	Oxygen Storage Capacity ($\mu\text{mol O/g}$)		
			350°C	500°C	700°C
Pd/C2	100	fresh	270	360	370
		aged	20	30	80
Pd/CZ3	70	fresh	870	990	1030
		aged	630	810	1070

Table 5.6: Steady-state oxygen storage capacities of fresh and aged model Pd automotive catalysts made with Ceria and Ceria-Zirconia

surprisingly good in respect to the roughness of the assumption.

Another weak point of the model can be spotted in the prediction of instantaneous HC emissions in the range from 85 to 120s. In this range, the inlet temperature of the exhaust gas lies around 400°C, however, the catalyst remains cold (exit temperature about 100°C). The oxygen storage capacity below 200°C is negligible. The model, though, assumes a constant value for oxygen storage capacity and erroneously predicts some conversion of hydrocarbon with stored oxygen in this range. The storage capacity depends on temperature as seen in Table 5.6, adopted from [3]

The implementation of temperature-dependent oxygen storage capacity in the corresponding submodel is a demanding task, which could be the subject of future research. Nevertheless, even with fixed oxygen storage capacity, the ability of the model to predict the oxygen storage and release behaviour is remarkable. The average storage capacity of 600 mol/m³ washcoat that was used in this case results in about 0.1mol storage capacity for the 2.4-litre full monolith (0.155 litre washcoat). This is in good agreement with typical values of modern catalysts, like those of Table 5.6, with an average value of 800 $\mu\text{mol O/g}$ Ceria–Zirconia (if the monolith has 248g washcoat and it is assumed about that 50% of the washcoat is Ceria–Zirconia).

The fit of the model for the NO_x curve is less successful than for the CO and HC curves. This is mainly attributed to the Voltz inhibition term for the CO and HC oxidation reactions. On the contrary, no appropriate inhibition term has been extracted for the reactions that involve NO_x. The model prediction for the NO_x is better in the urban-phase of the driving cycle compared to the extra-urban one. Nevertheless, the results are satisfactory, especially if it is taken into account that the NO_x emissions are very low and normally do not exceed 50 ppm.

To fit the model to the 599 cycle, only a subset of the kinetic parameters is tuned. The activation energies are more or less known from previous experience. They could be varied a little, but this is not necessary since the rate depends on both the pre-exponential factors and the activation energies (A and E) and any small difference can be compensated by respective modification of A . The oxygen storage capacity is also not tuned, since its approximate magnitude is estimated based on the washcoat composition (Ce, Zr), and is also checked by characteristic runs of the code. Finally, the H₂ oxidation kinetics is assumed to be approximately equal to that of CO oxidation. Thus, we are left with nine pre-exponential factors to be tuned: 4 reactions of gaseous phase species on the Pt surface, and another 5 reactions on the Ceria–Zirconia components of the washcoat.

The evolution of the genetic algorithm population of solutions is indicative of the problem difficulty and explains the limited success of manual tuning or tuning that uses gradient-based methods. To illustrate the evolution process, a graph of the evolution of maximum and average fitness of the population is presented in

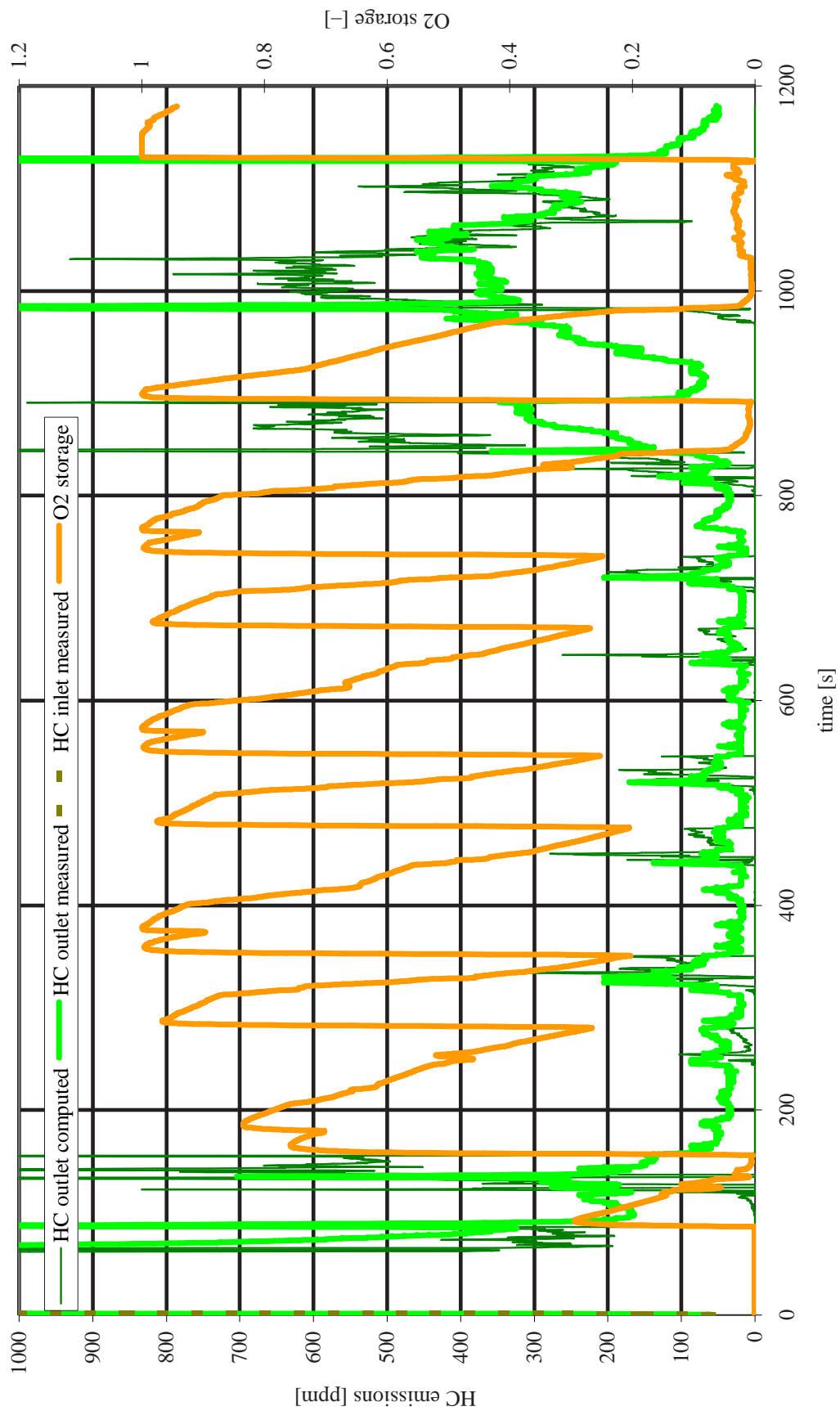


Figure 5.19: Instantaneous HC emissions at converter inlet and exit, over the 1180 s duration of the 599 cycle

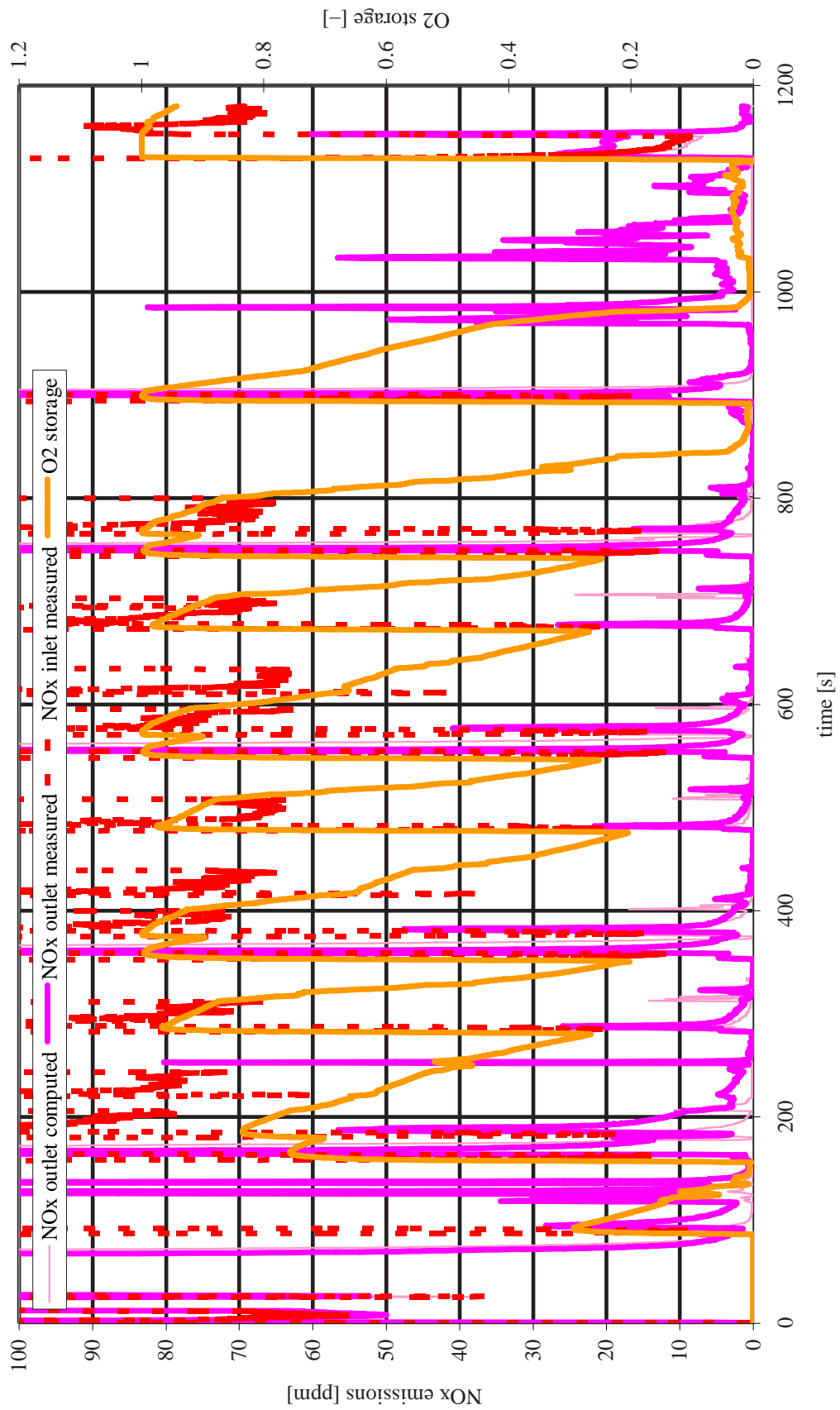


Figure 5.20: Instantaneous NO_x emissions at converter inlet and exit, over the 1180 s duration of the 599 cycle

Figure 5.21. The genetic algorithm quickly improves the maximum performance measure solution at the beginning of the run. Then, evolution is slower and after some point, it completely stalls. This indicates that the genetic algorithm population has converged to a specific attraction basin of the optimization space and not much improvement may be achieved. At this point, the algorithm is stopped. The specific computation required about 72 hours on a 2.4 GHz Pentium 4 computer.

It may be noted that the absolute value of the performance measure does not vary much during the GA run. This is a property of the performance measure formulation but also indicates the multi-modality of the problem, since it appears that many combinations of kinetic parameters lead to the same overall performance of the model.

The spread of individuals in the 20th, the 45th and the last (135th) generation is given in Figures 5.22, 5.23 and 5.24 respectively. The individuals are sorted in descending order according to their performance measure.

Figure 5.22 visualizes the spread of the kinetic parameters in the population of the genetic algorithm near the beginning of the procedure. The kinetic parameters are allowed to vary in certain intervals that are induced based on previous experience and are consistent with their physical role in the respective reactions. The different kinetic parameters pertaining to reactions that occur on the three distinct catalytic components of the washcoat (in our example, Pt, Rh and Ce) fall in three distinct intervals.

Figure 5.23 gives the spread of individual solutions in the 45th generation of the population. Apparently, the population has started converging for the pre-exponential factors of some reactions. This indicates that the kinetics of these reactions influence the quality of the model fit (and thus the performance measure value) much more significantly than the rest of the reactions.

Figure 5.24 presents the last population of the GA run. It is evident that the parameters for the oxidation of “slow” hydrocarbons with oxygen on Pt or with stored oxygen do not converge, whereas the rest of the parameters show clear signs of convergence. This could be attributed to the fact that the “slow” hydrocarbons are only 15% of the total hydrocarbon content and thus influence the total hydrocarbon efficiency of the catalyst much less compared to the “fast” hydrocarbons. The same absence of convergence is noticed for the kinetics of CO–NO reaction, whereas the complementary reaction of Ceria–NO shows clear signs of convergence. This fact hints to a lack of sensitivity of the model regarding the above three reactions. One should not deduce at this early investigation point, that these reactions are less important than the rest to the model’s accuracy and predictive ability. Experience shows that further reduction of the number of reactions leads to an observable deterioration of the model fitting ability.

For comparison purposes, the best set of kinetic parameters values derived at the three characteristic generations of the GA evolution are presented in Figure 5.25.

5.2.3 Model tuning for the 100 g/ft³ catalyst

The ability of the model to be fitted to a driving cycle test will be further examined using the 609 cycle of the PML case study. This measurement has been performed using a catalytic converter with the same dimensions and washcoat loading with the 599 cycle, but with double precious metal loading (see Table 5.4 on page 136).

Because of the change in the PM loading of the catalytic converter, the model

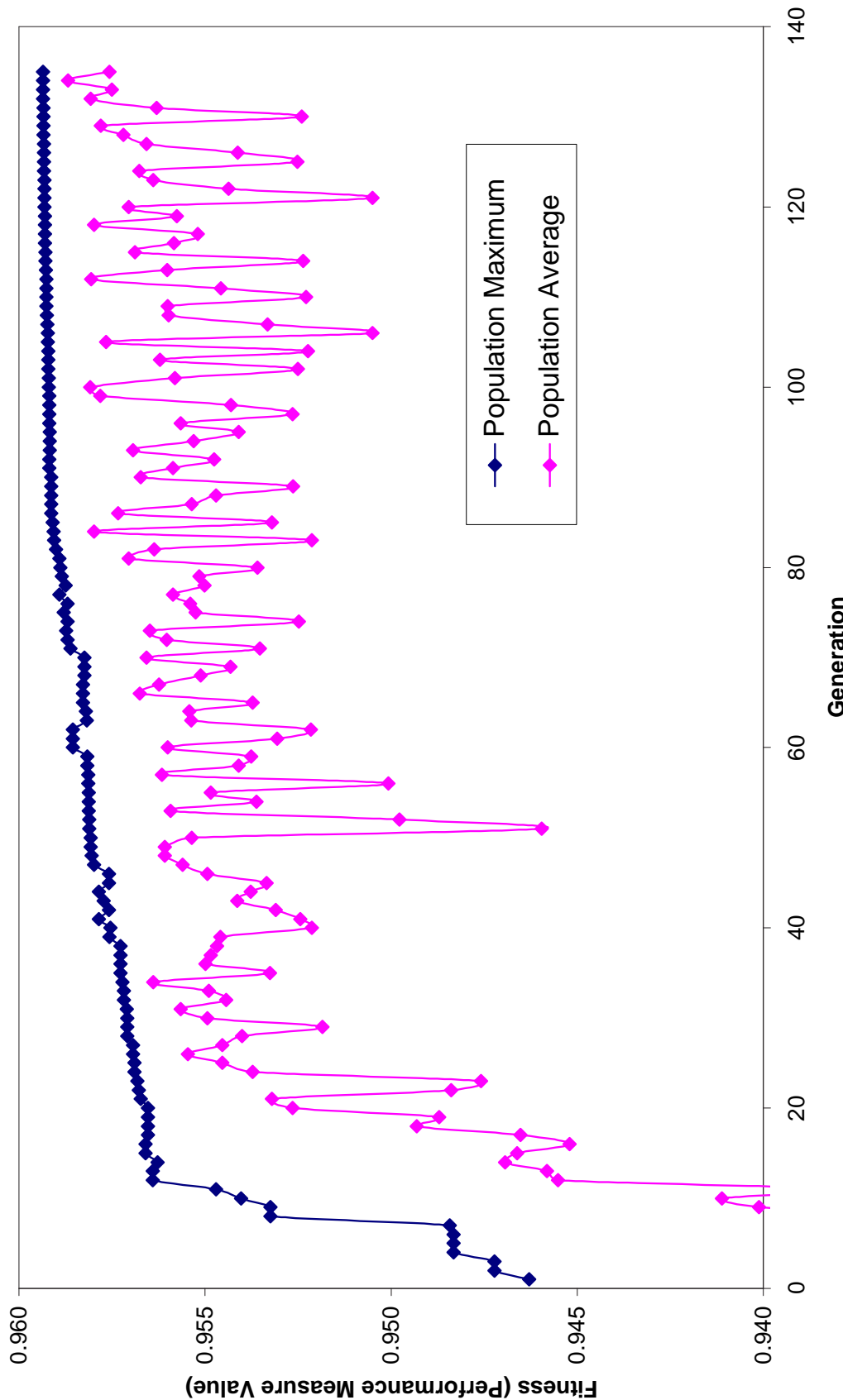


Figure 5.21: Evolution of the genetic algorithm: Maximum and average population fitness during the first 135 generations

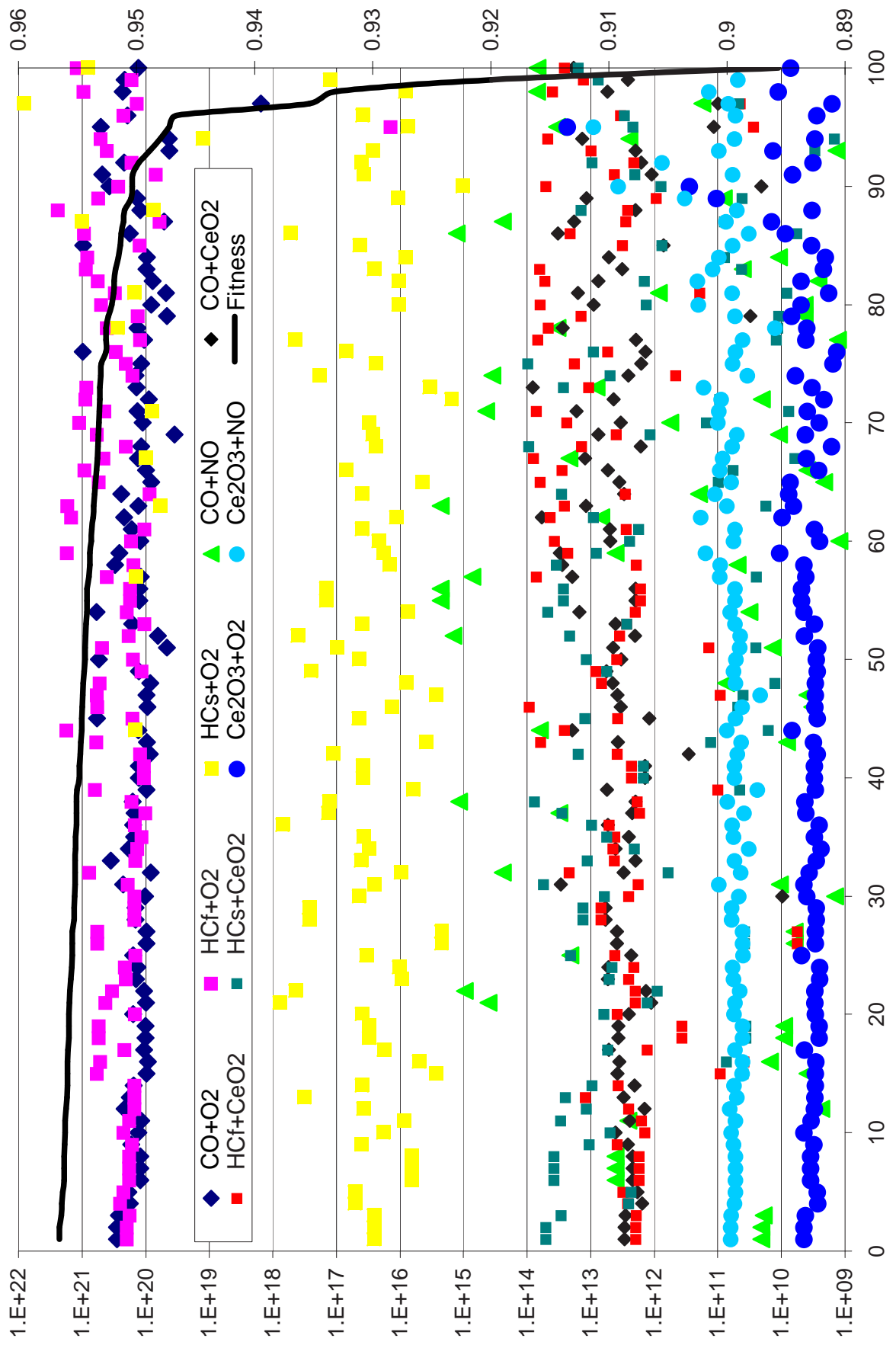


Figure 5.22: Spread of genetic algorithm population at the 20th generation

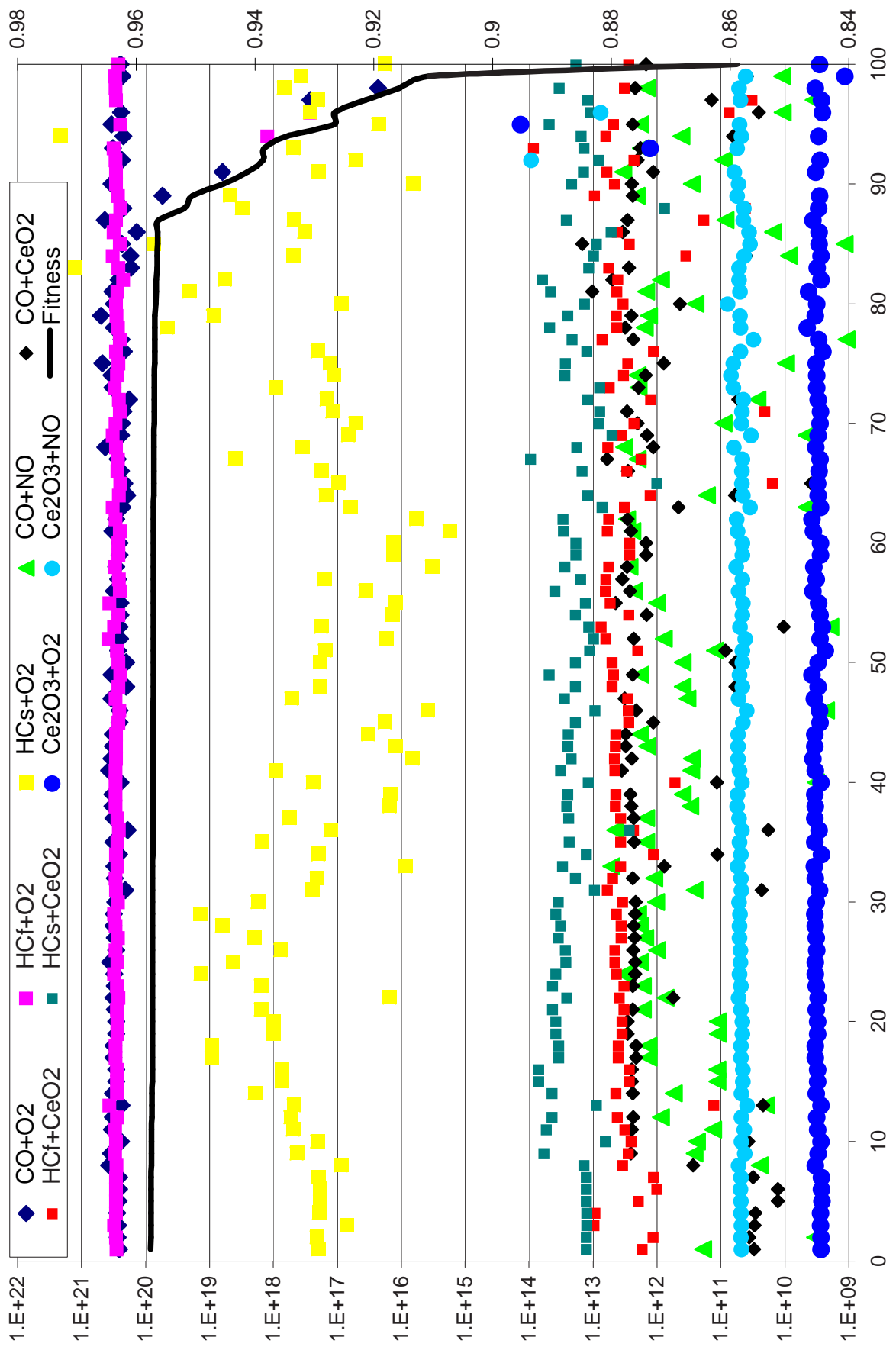


Figure 5.23: Spread of genetic algorithm population at the 45th generation

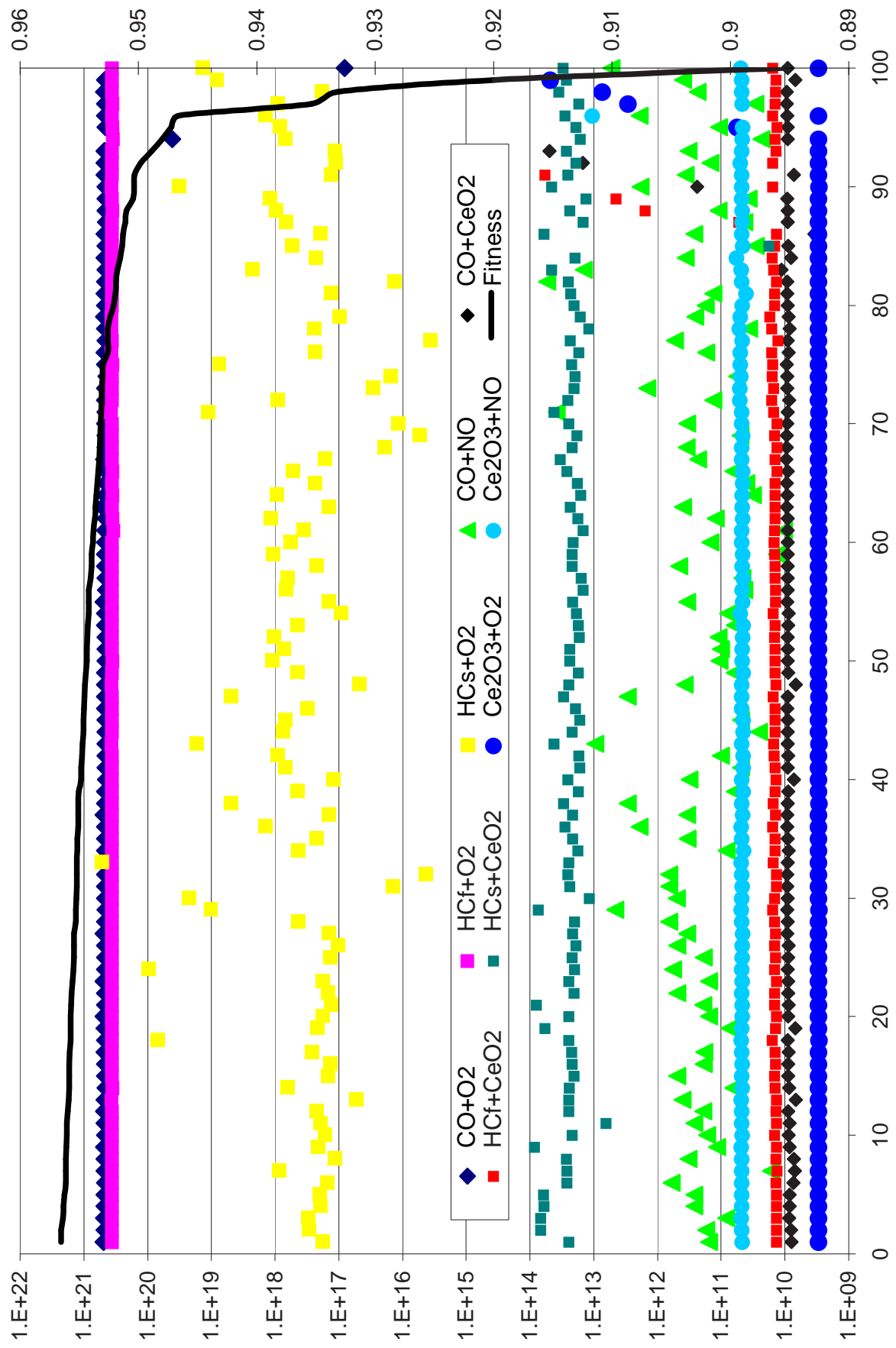


Figure 5.24: Spread of genetic algorithm population at the 135th generation

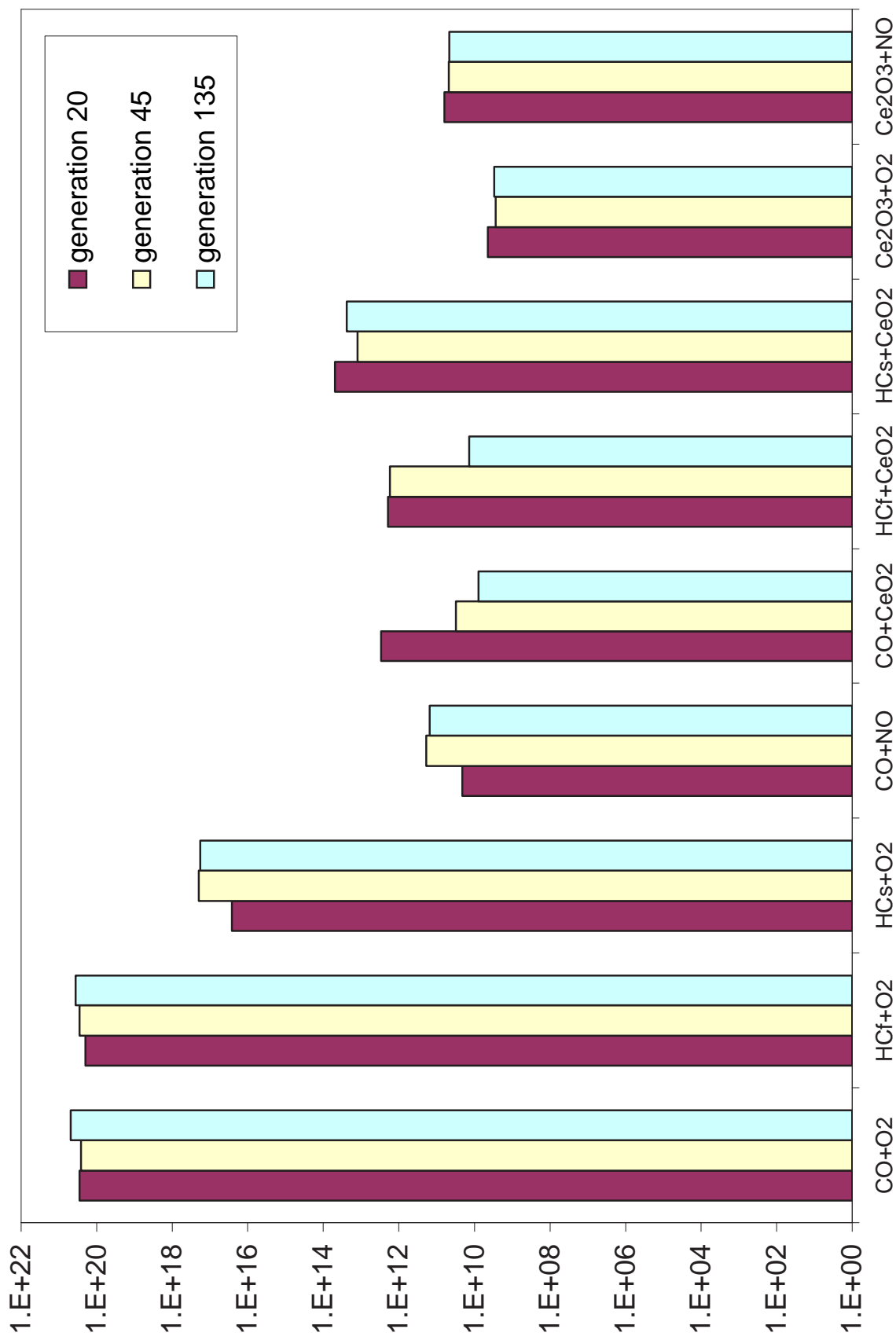


Figure 5.25: Comparison of best kinetics set at the 20th, 45th and 135th generation of the genetic algorithm run

1	$2\text{CO} + \text{O}_2 \longrightarrow 2\text{CO}_2$	$A_1 = 1.24 \cdot 10^{19}$	$E_1 = 90000$
2	$2\text{H}_2 + \text{O}_2 \longrightarrow 2\text{H}_2\text{O}$	$A_1 = 2.00 \cdot 10^{19}$	$E_1 = 90000$
3	$\text{CH}_{1.8}(\text{fast}) + 1.4\text{O}_2 \longrightarrow \text{CO}_2 + 0.9\text{H}_2\text{O}$	$A_1 = 1.95 \cdot 10^{19}$	$E_1 = 95000$
4	$\text{CH}_{1.8}(\text{slow}) + 1.4\text{O}_2 \longrightarrow \text{CO}_2 + 0.9\text{H}_2\text{O}$	$A_1 = 1.83 \cdot 10^{17}$	$E_1 = 120000$
5	$2\text{CO} + 2\text{NO} \longrightarrow 2\text{CO}_2 + \text{N}_2$	$A_1 = 4.97 \cdot 10^{22}$	$E_1 = 90000$
6	$2\text{Ce}_2\text{O}_3 + \text{O}_2 \longrightarrow 4\text{CeO}_2$	$A_1 = 5.40 \cdot 10^8$	$E_1 = 90000$
7	$2\text{Ce}_2\text{O}_3 + 2\text{NO} \longrightarrow 4\text{CeO}_2 + \text{N}_2$	$A_1 = 7.97 \cdot 10^9$	$E_1 = 90000$
8	$\text{CO} + 2\text{CeO}_2 \longrightarrow \text{Ce}_2\text{O}_3 + \text{CO}_2$	$A_1 = 1.55 \cdot 10^{10}$	$E_1 = 85000$
9	$\text{CH}_{1.8}(\text{fast}) + 3.8\text{CeO}_2 \longrightarrow 1.9\text{Ce}_2\text{O}_3 + \text{CO}_2 + 0.9\text{H}_2\text{O}$	$A_1 = 5.80 \cdot 10^{10}$	$E_1 = 85000$
10	$\text{CH}_{1.8}(\text{fast}) + 3.8\text{CeO}_2 \longrightarrow 1.9\text{Ce}_2\text{O}_3 + \text{CO}_2 + 0.9\text{H}_2\text{O}$	$A_1 = 2.74 \cdot 10^9$	$E_1 = 85000$

Table 5.7: Tuned kinetic parameters for the 100 g/ft³ catalyst

must be tuned again. The genetic algorithm was also used here for model tuning, and the resulting kinetics are given in Table 5.7

The results of the tuning are summarized in Figure 5.26, where the computed and measured cumulative emissions of this driving cycle test are compared. The results reveal that the fit of the model is acceptable but inferior compared to the respective cumulative results of the 599 cycle. In order to assess the fit of the model in more detail, we also present, in Figures 5.27–5.29, the comparison of instantaneous computed and measured emissions for CO, HC and NO_x respectively.

The results of the model for the CO emissions seem to be generally in agreement with the measurement. The catalyst light-off and the emission breakthrough during the urban part of the driving cycle test are fitted satisfactorily. Nevertheless, the model underestimates the efficiency of the catalyst at about 145 s. On the other hand, it is unable to be fitted to the extra-urban part of the cycle, where the increase of emissions is only qualitatively matched.

Modeling of the HC emissions is of similar quality with the CO results. Figure 5.28 reveals that the measured HCs at the converter's outlet gradually decline towards zero during the first 400 s of the cycle, whereas the corresponding computed curve is abrupt, predicting approximately zero HC at the outlet after about 160 s of the beginning of the test. This behaviour was also present in the 599 cycle. The gradual decline of measured HC emissions is attributed to the light-off of progressively heavier hydrocarbon molecules of the exhaust gas. The model does not incorporate such a degree of freedom and the fast/slow HC species approximation that is included in the model seems insufficient.

Nevertheless, no more HC species categories are introduced in the model, because this does not yield a significant improvement of the model's results, while it complicates the reaction scheme and therefore increases the degrees of freedom of the model. Furthermore, it becomes even more difficult to make an assumption for the proportion of each species in the exhaust gas. We therefore accept this inconsistency as inevitable because of measurement limitations.

It is notable that the measured peak observed at about 330 s, although it falls in the same area, is matched by the model with significant accuracy. This peak seems to be connected to the depletion of the stored oxygen from the washcoat. Moreover, the subsequent HC emission peaks during the urban part of the driving cycle, also occurring because of lack of stored oxygen, are both qualitatively and quantitatively predicted. This enhances our confidence to the oxygen storage submodel that has

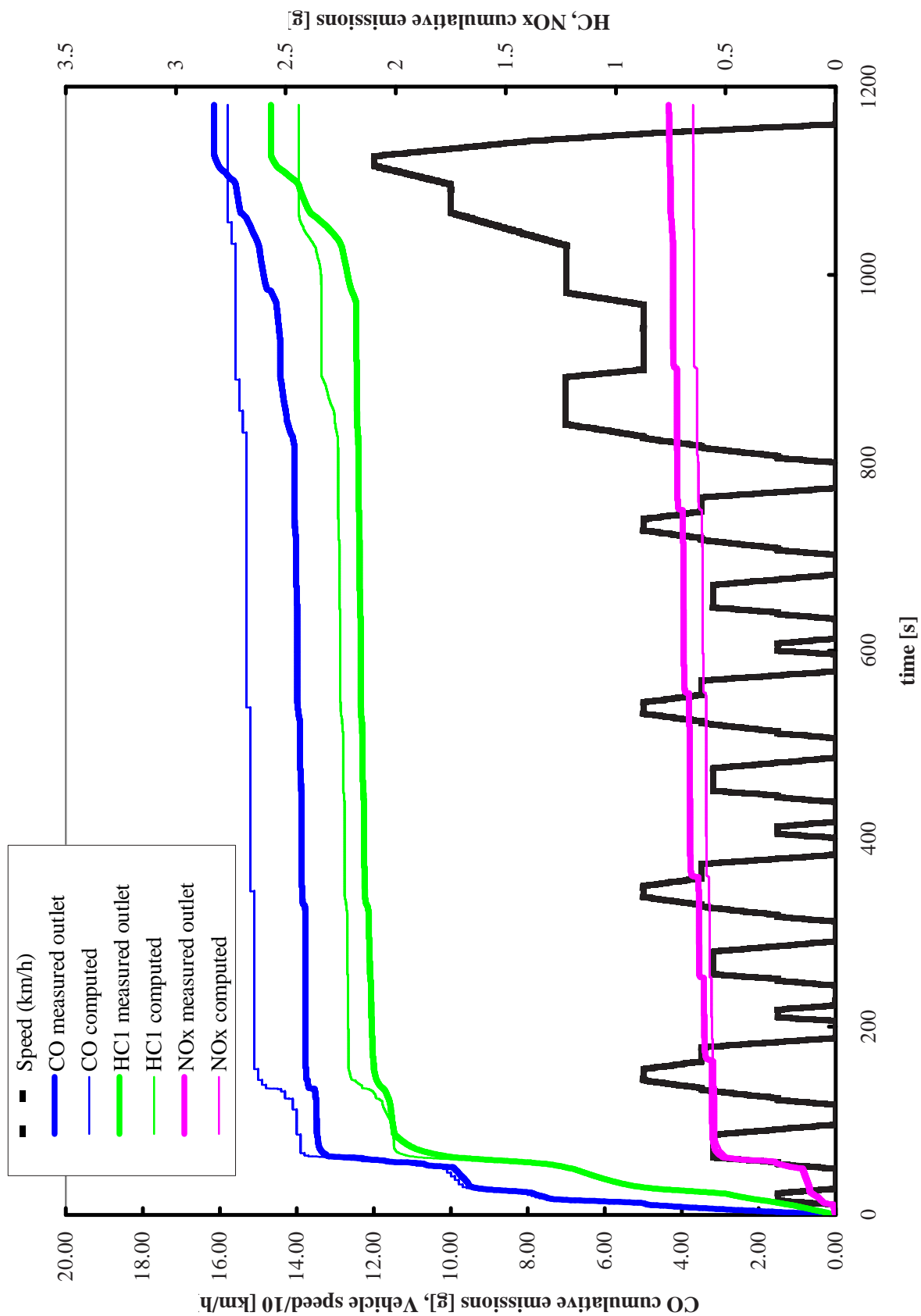


Figure 5.26: Cumulative CO, HC and NO_x emissions at converter inlet and exit, over the 1180 s duration of the 609 cycle

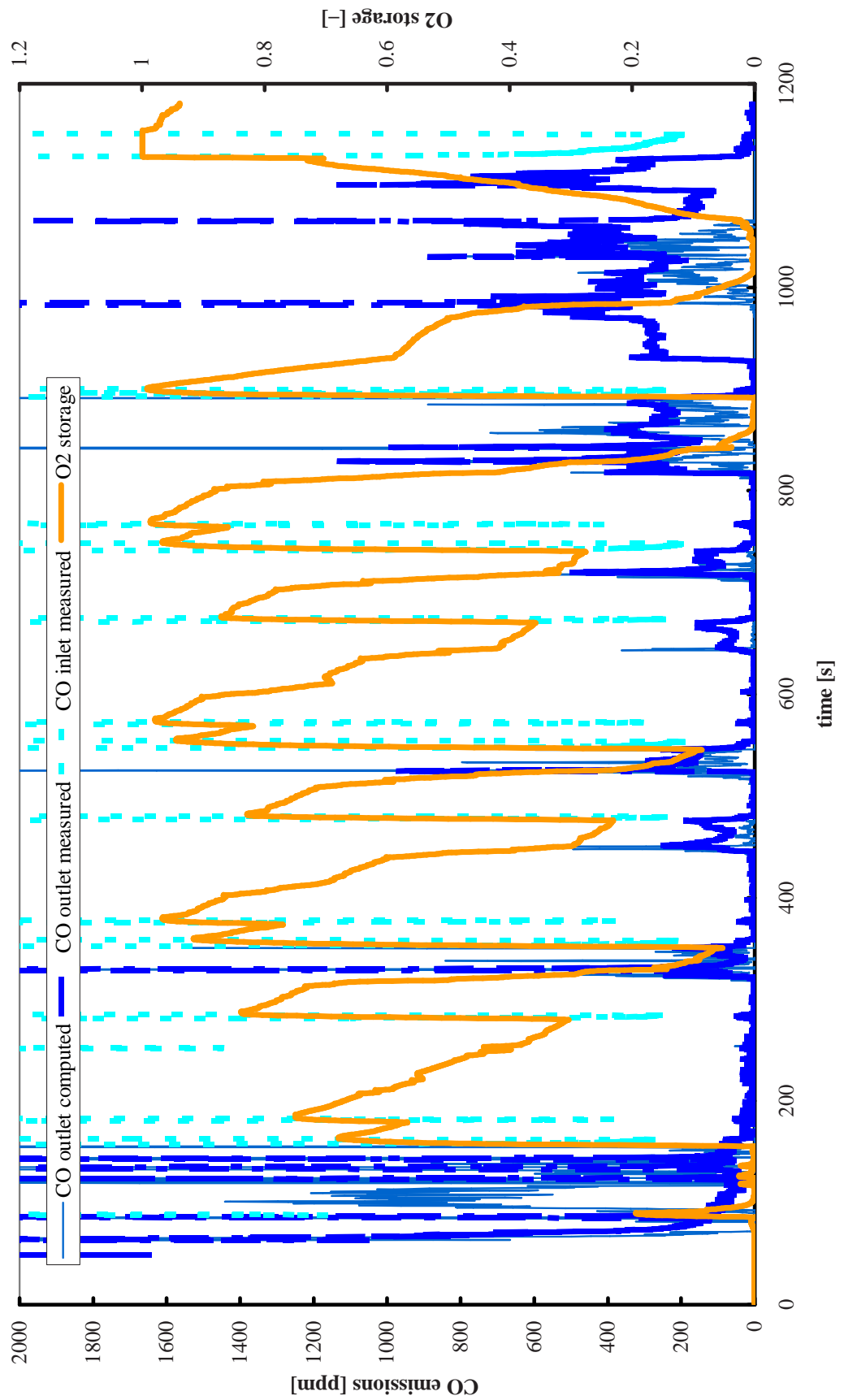


Figure 5.27: Instantaneous CO emissions at converter inlet and exit, over the 1180 s duration of the 609 cycle

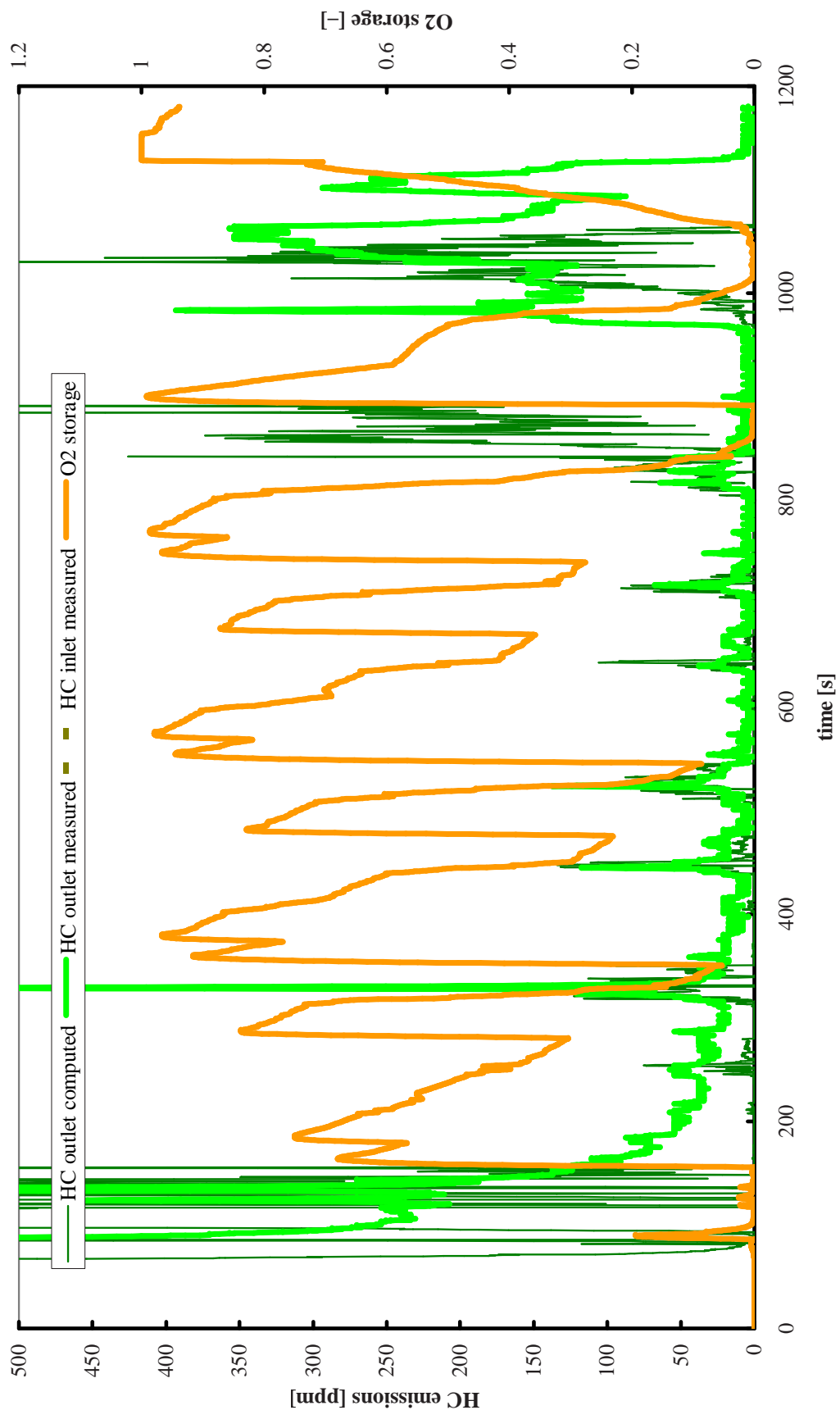


Figure 5.28: Instantaneous HC emissions at converter inlet and exit, over the 1180 s duration of the 609 cycle

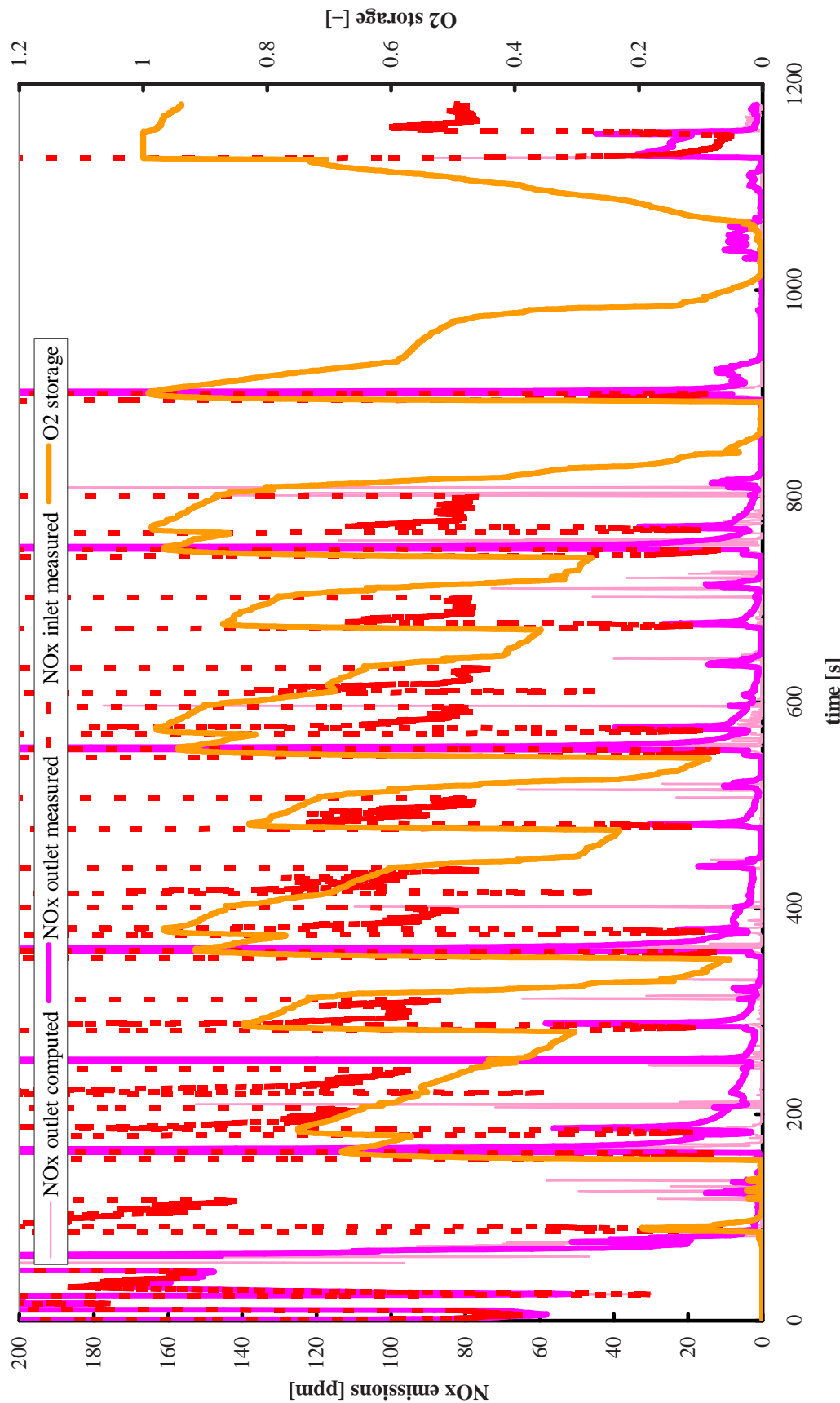


Figure 5.29: Instantaneous NO_x emissions at converter inlet and exit, over the 1180 s duration of the 609 cycle

been developed in this work.

Proceeding to the NO_x results, we note that the model is able to match the behaviour of the catalytic converter qualitatively—and, in some extent, also quantitatively—during the whole extent of the driving cycle. Similarly to the results of cycle 599, this is very satisfactory especially in view of the very low absolute values of NO_x emissions.

Summarizing the above, we could conclude that the catalytic converter model, when coupled with the genetic algorithm tuning methodology, may be fitted to the measurements with very good accuracy. The validity of the model may only be assessed, though, when it is used to predict the results of another converter configuration using the kinetic parameters that were obtained during the model tuning phase. The results of model validation are presented in the following section.

5.2.4 Model validation for the reduced size 50 g/ft³ catalyst

The above results indicate that the model formulation has the capability to match typical measurements of a three-way catalytic converter, and that the tuning methodology may be used successfully to fit the model to the measured data.

Additional evidence is provided below about the model's ability to predict the operating behaviour of a different catalytic converter configuration. This is achieved by using the model to predict an alternative configuration of a three-way catalytic converter with no further kinetic parameter adjustments.

Therefore, as a next step in the assessment of the model's accuracy and predictive ability, the model is employed in the prediction of the performance of an alternative underfloor converter of the same washcoat type, which is 1/4 the size of the original one. Since the same catalyst formulation and precious metal loading is employed, modelling of this case is performed using the same kinetics parameters of Table 5.5 which were estimated for the original converter. Only the external dimensions of the converter are changed to the ones of the reduced size converter and no further tuning of the kinetic parameters is performed. The results of the model are then compared to the measured results for this converter.

The results are compared to the measured performance in Figure 5.30, in the form of cumulative CO, HC and NOx emissions. Apparently, the model is capable of predicting the significant change in all three pollutants emissions that is caused by the reduction of the converter's volume, without changes in its kinetic parameters.

A better insight on the model's performance, also in association with oxygen storage and release behaviour, can be made, by a comparison of computed and measured instantaneous emissions of the pollutants. The comparisons are presented for the full length of the 600 cycle in Figures 5.31–5.33. These detailed results allow us to draw similar conclusions with the 599 cycle regarding the behaviour of the model. Specifically, it is evident that the prediction quality for the CO again outperforms that for HC and NO_x, and it matches the measurement with very good accuracy. The instantaneous HC emissions are also matched very well, and the model is able to predict all the breakthroughs that appear in the urban phase of the driving cycle. Of exceptional quality is the prediction of the last 800 s of the driving cycle (extra-urban phase). Finally, the NO_x prediction is also of good quality, far better than any other model results obtained so far. Despite the divergence from the measurement in the last phase of the extra-urban part of the cycle, the prediction quality is good enough to be useful in a catalytic converter evaluation and optimization procedure.

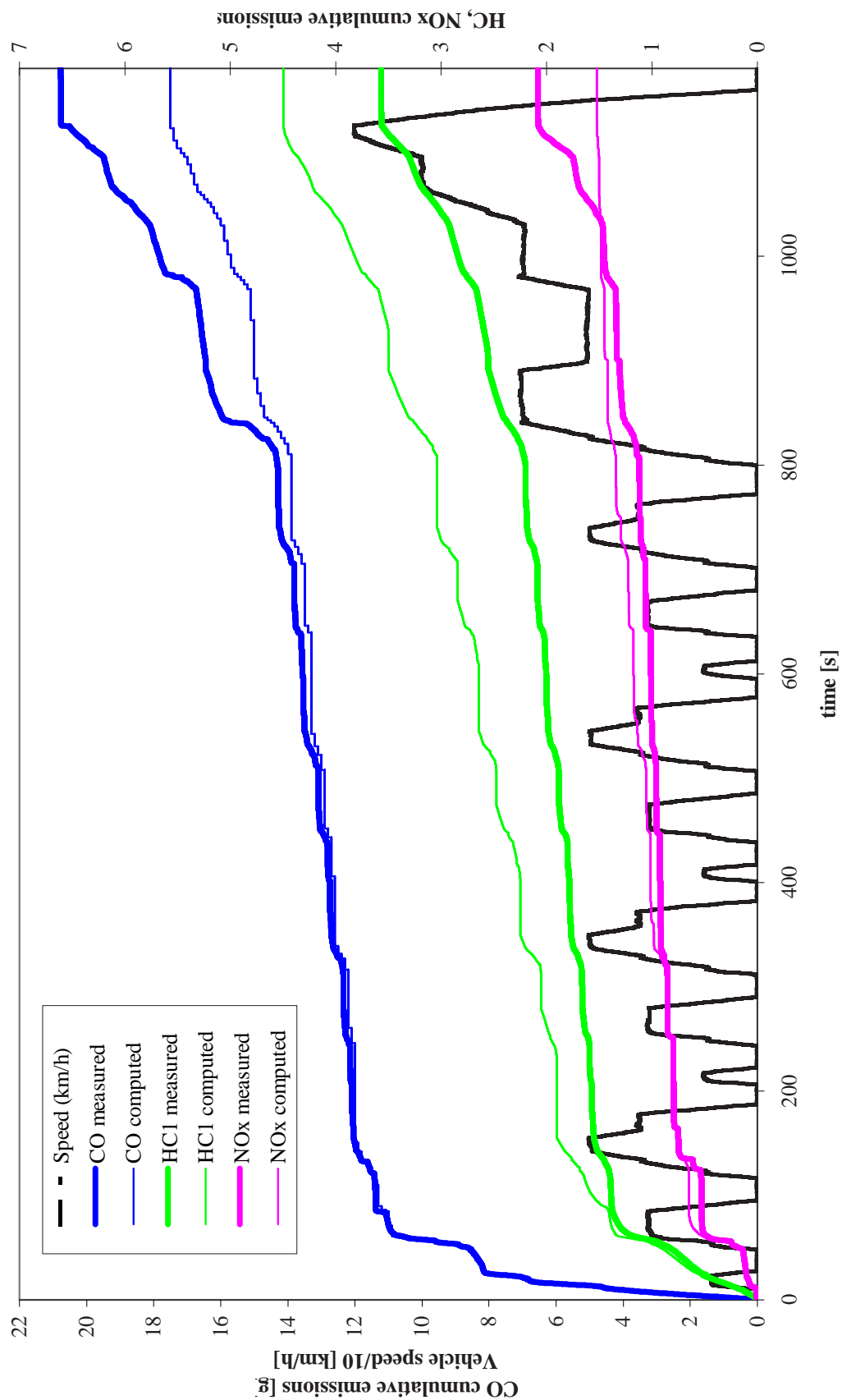


Figure 5.30: Cumulative CO, HC and NO_x emissions at converter inlet and exit, over the 1180 s duration of the 600 cycle

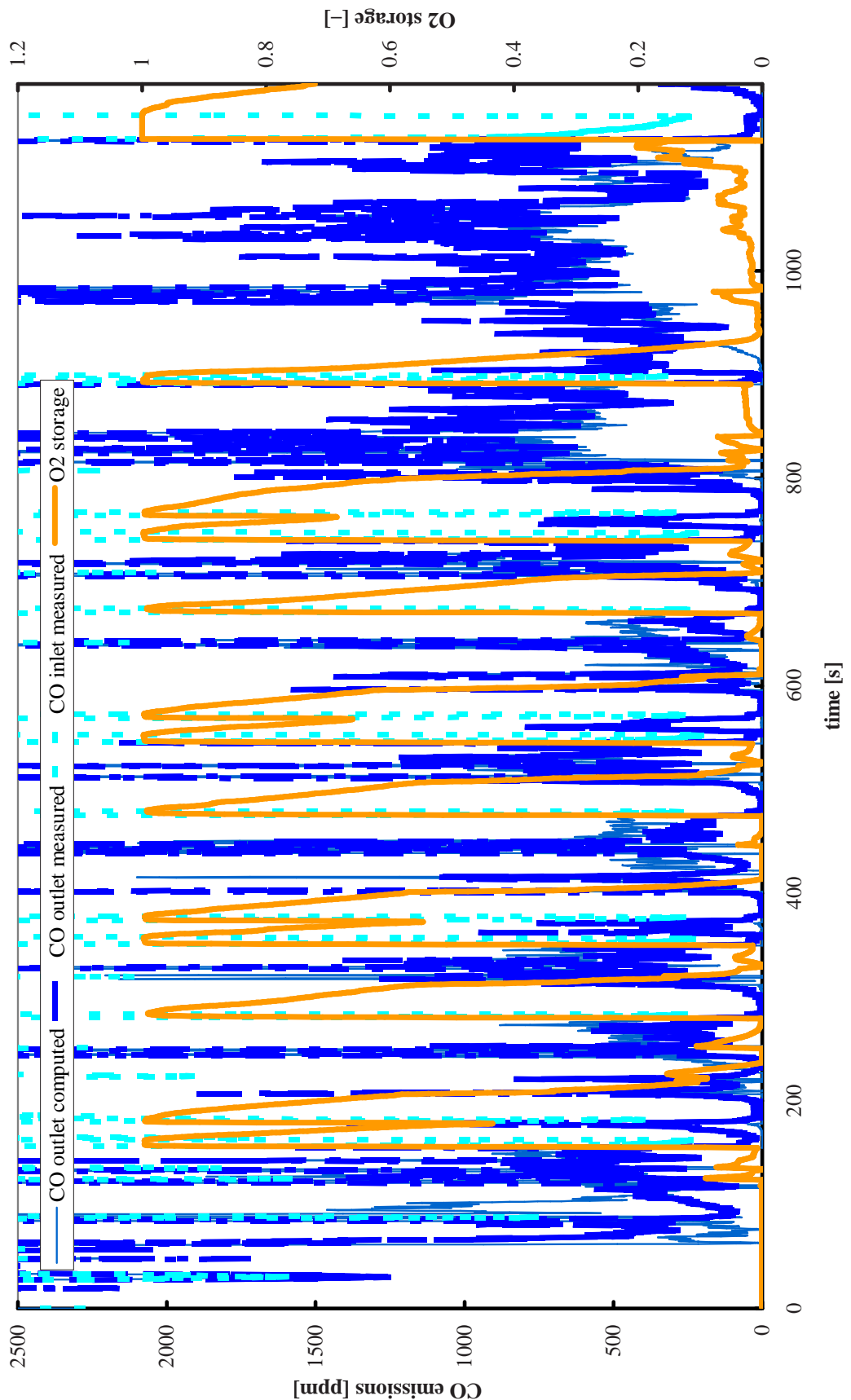


Figure 5.31: Instantaneous HC emissions at converter inlet and exit, over the 1180 s duration of the 600 cycle

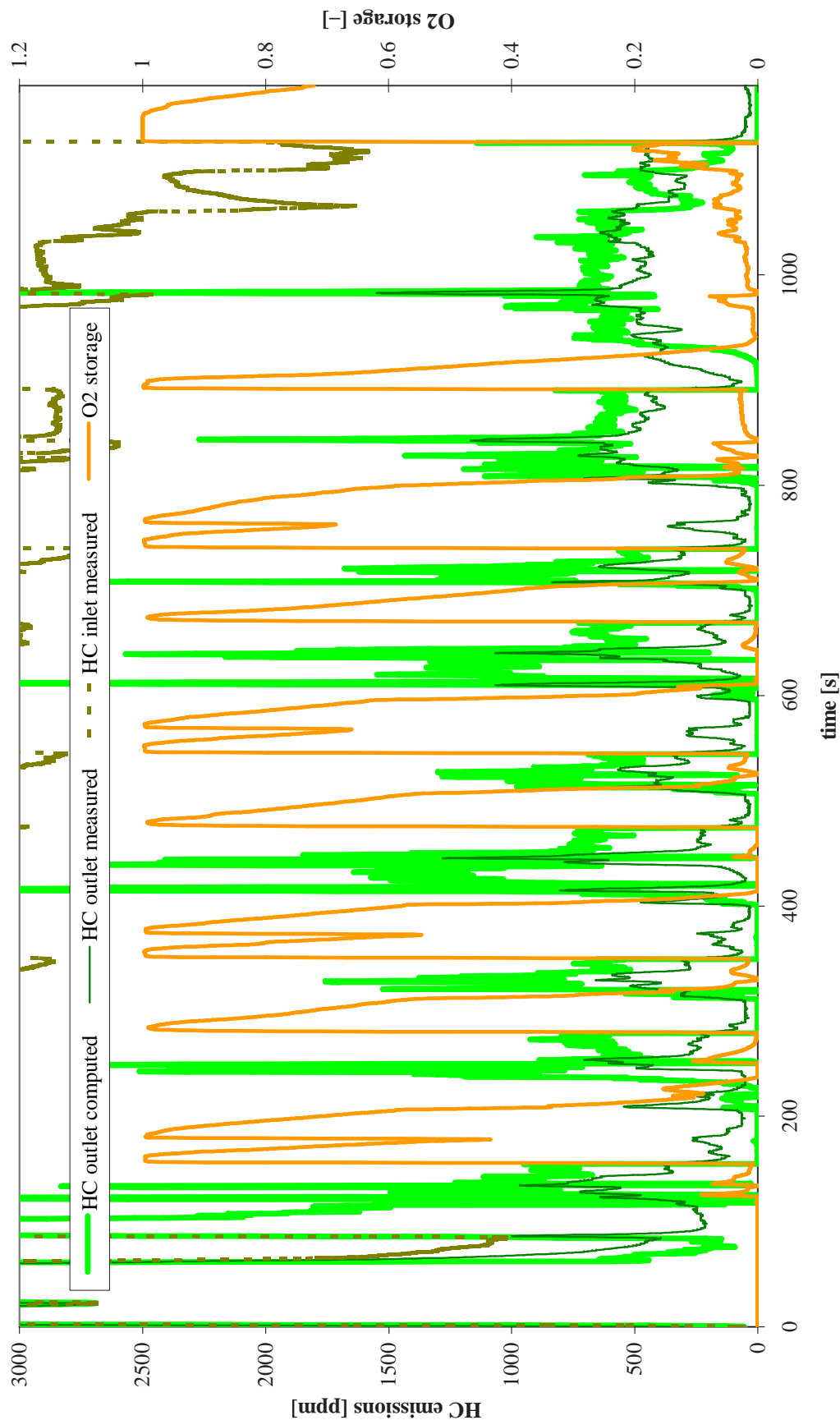


Figure 5.32: Instantaneous HC emissions at converter inlet and exit, over the 1180 s duration of the 600 cycle

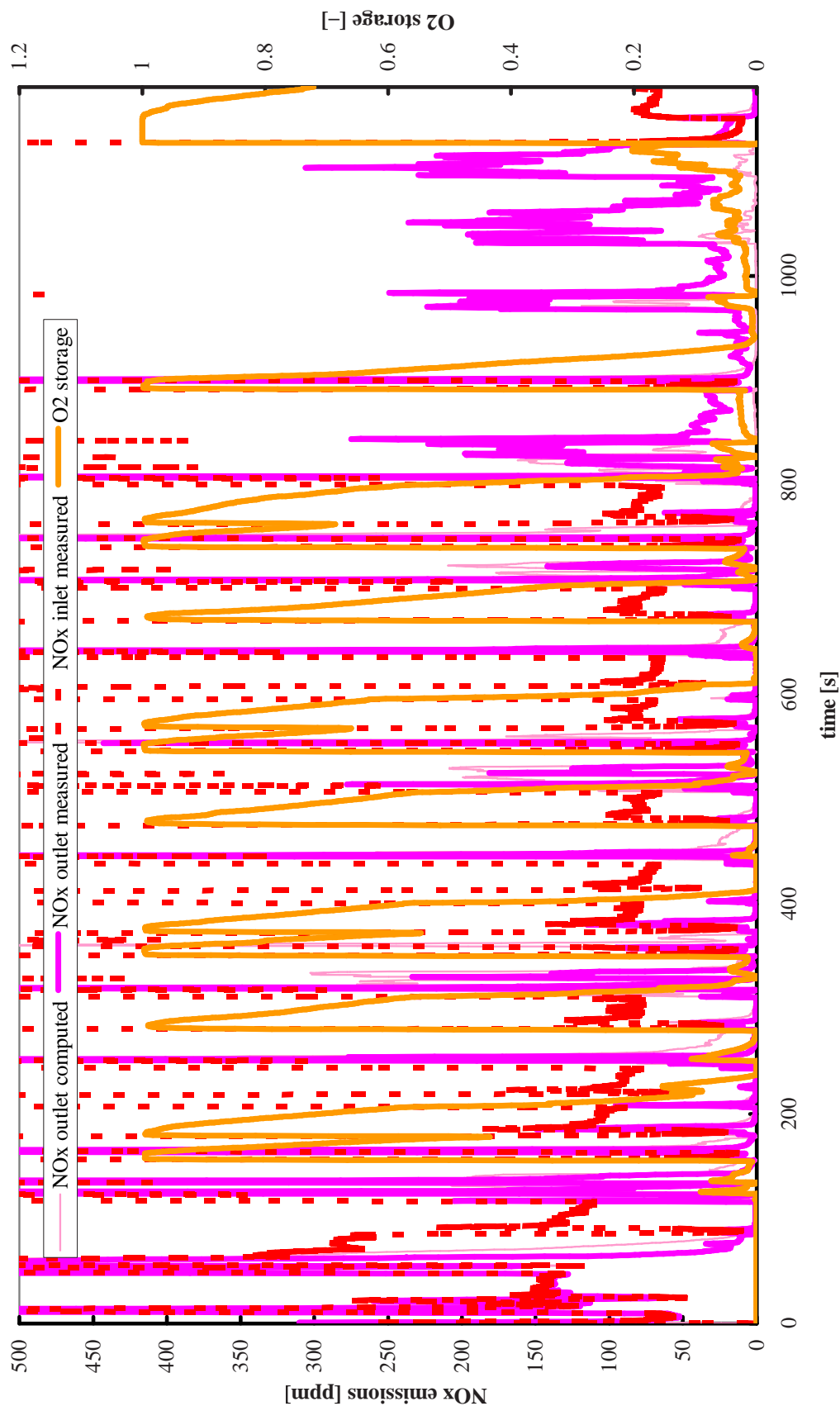


Figure 5.33: Instantaneous HC emissions at converter inlet and exit, over the 1180 s duration of the 600 cycle

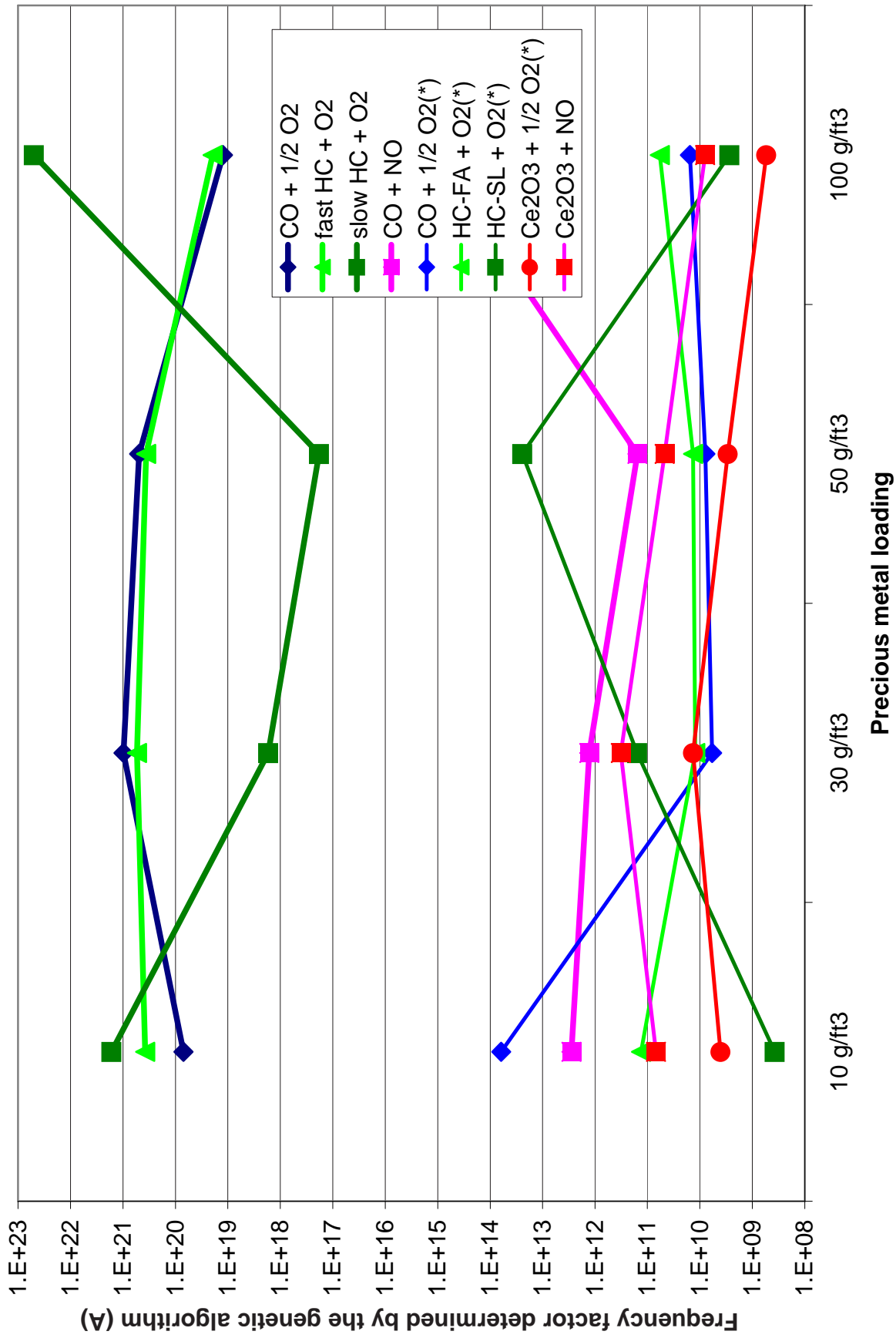


Figure 5.34: Comparison of the frequency factors (A) for different precious metal loading levels, determined by the genetic algorithm

These results provide evidence for the capabilities of the model, especially as regards the oxygen storage phenomena modeling, since it appears that oxygen storage plays a very important role in the operating behaviour of the catalytic converter. The results also indicate that the original tuning of the model is performed accurately and the kinetic values are realistic, so that they may be applied to accurately predict the effect of size reduction of the converter.

5.2.5 First steps towards the prediction of PML effect

The successful tuning of the model kinetics by means of the genetic algorithm methodology sets the scene towards the assessment of the effect of precious metal loading on the apparent kinetics of the catalyst.

As a first step in this direction, the genetic algorithm was employed to tune the kinetic model to match the behaviour of two additional catalyst formulations, with 30 and 10 g/ft³ precious metal loading respectively. The frequency factors determined in this way are plotted versus the precious metal loading in Figure 5.34.

The frequency factor of the oxidation reactions on Pt appear at the upper half of Figure 5.34, whereas the reactions on Rh and Ceria appear at the bottom half. The curves that correspond to the slow HC reaction on both Pt and Ceria have an odd behaviour and will be excluded from further study. These two reactions seem to be complementary (mirror-like). This has been already discussed in the context of genetic algorithm evolution.

Continuing the discussion of the observed trends, we see that the 30 and 50 g/ft³ catalysts demonstrate the highest activity regarding the oxidation of CO and hydrocarbons. As regards the CO–NO reaction, the 100 g/ft³ catalyst demonstrates the highest activity. However, this is not the case for the complementary reaction of Ceria with NO_x.

On the other hand, the behaviour of the CO and HC oxidation reactions on Ceria is opposite to the corresponding reactions on Pt. This hints to a possible trade-off between Ceria and Pt in order to obtain comparable performance for different washcoat formulations [4].

The improved 3WCC model described in this thesis along with the genetic algorithm parameter estimation methodology presents a valuable tool in the hands of the catalyst design engineer. Of course, this is only the first step in the direction of the prediction of the PML effect on the catalyst performance.

5.3 Variable cell density/wall thickness case study

5.3.1 Measurements set

For this case study, four sets of available test data were employed (I, K, L and M), ranging from 400 to 1200 cpsi cell density (Table 5.35). This sets consisted of test results for a close-coupled converter of about 1-liter volume, 100 g/ft³ Pd/Rh catalyst, installed on each bank of a V6 2.4 liter engined car (Mercedes-Benz E-Klasse, W210E24-640) according to the NEDC test procedure. The results comprised a 2Hz recording of exhaust gas mass flow rate, exhaust temperature at converter inlet, exhaust pollutants concentration (dry CO, NO_x emissions, wet total HC emissions) at catalytic converter inlet and exit, CO₂ and O₂ emissions.

It must be noted that a HC adsorption behaviour is observed by the comparison

	d [inch]	D [inch]	L [inch]	Vcomp [ft]	V [ft]	cpsi	Wall Thickness [mm]	W/C thickness [mm]	catalyst	PM loading [g/ft ³]	WC type	WC [g]	Substrate weight [g]
I	4.16	4.16	4.53	0.001	1.0097	400	0.166	0.228	0:14:01	100	TZ MLKX 5	248.5	442.6
K	4.16	4.16	4.53	0.001	1.0097	600	0.091	0.179	0:14:01	100	TZ MLKX 5	253.2	304.9
L	4.16	4.16	4.53	0.001	1.0097	900	0.063	0.144	0:14:01	100	TZ MLKX 5	253.5	261.3
M	4.16	4.16	4.53	0.001	1.0097	1200	0.063	0.122	0:14:01	100	TZ MLKX 5	246.1	299.6

Figure 5.35: Data for catalytic converters used in the IKLM case

of outlet measured vs. computed HC. This adsorption capability is advantageous for the operation of the catalytic converter. Mathematical modeling already plays a role in the design optimization of adsorbing systems for diesel catalysts [5]. For the 3WCC though, no HC adsorption–desorption submodel has been implemented; therefore the model fails to follow these trends.

Compared to the PML case, the specific data set is of lower quality. This was indicated by quality assurance procedures that are currently being developed [6]. Furthermore, we lack an UEGO signal for this test, which deprives us from a standard cross-checking capability, in contrast to the previous cases.

5.3.2 Icat – model tuning

For the tuning of the first 3WCC, in all stages of the tuning procedure, parameter estimation was performed using the data for the full NEDC cycle.

The cumulative emissions over the NEDC cycle are given in 5.38. The instantaneous CO, HC and NOx concentrations are also presented in Figures 5.39–5.42 respectively.

Obviously, the agreement between measurement and computation is not as good as the previous case. This is attributed to the bad quality of data mentioned above. However, it is interesting to note the very good prediction of NOx and CO instantaneous emissions at the catalyst exit and the qualitative prediction of the major events (e.g. breakthroughs).

5.3.3 Prediction of the effect of variable cell density/wall thickness

Once the model is tuned to represent the measured behavior of the 400 cpsi catalyst, it has been successfully employed for the prediction of the 600, 900 and 1200 cpsi catalyst performance [7, 8]. It is interesting to note a good overall agreement between predictions and measurements, although certain details of the cycles are not matched well.

The behaviour of the catalytic converter in the first 120s of the NEDC cycle is predicted very well for the 600, 900, and 1200 cpsi substrates, once the 400 cpsi behaviour is matched by the kinetic tuning procedure. This is illustrated in Figures 5.36 and 5.37, where the total HC predictions are compared to the measurements for two different vehicles (The kinetic parameters have been tuned for the first vehicle only). The figures are adapted from [8].

5.4 Conclusions – Future perspectives of 3WCC modeling

A significant step has been done in the frame of this work, towards making the model able to predict the effect of varying Precious Metal Loading and Oxygen Storage Components Loading in the washcoat. This was supposed to lie beyond the range of applicability of this class of models. It was believed by certain researchers that the detailed kinetic models would be capable of predicting such effects in the future. However, such capability has not yet been demonstrated by detailed kinetics models. On the contrary, now, even the future capability of elementary kinetics models to address such problems is now at stake.

As regards the prediction of the related effect of changing substrate cell density and wall thickness, the significant steps made towards PML effect prediction now

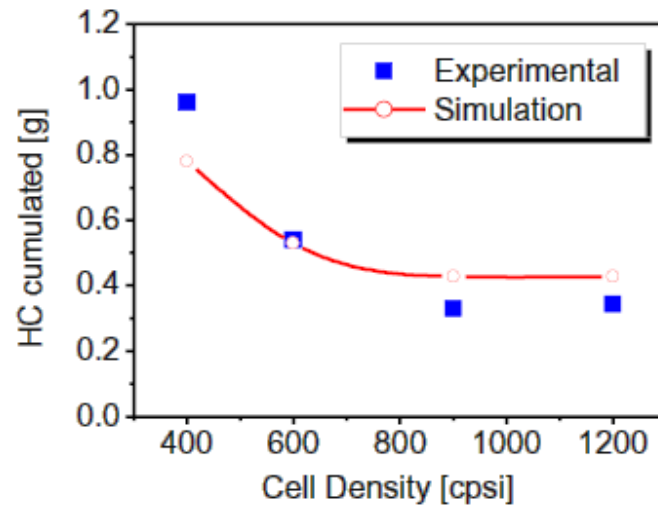


Figure 5.36: Prediction of HC emissions as a function of cell density, vehicle A.

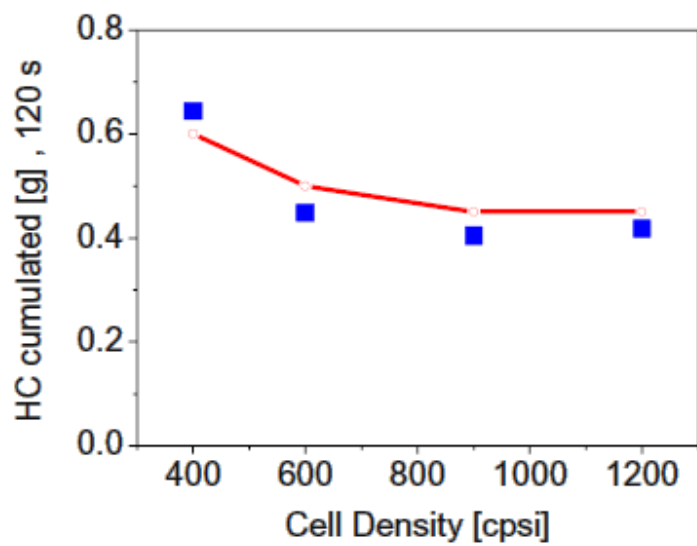


Figure 5.37: Prediction of HC emissions as a function of cell density, vehicle B. Model tuned for Vehicle A.

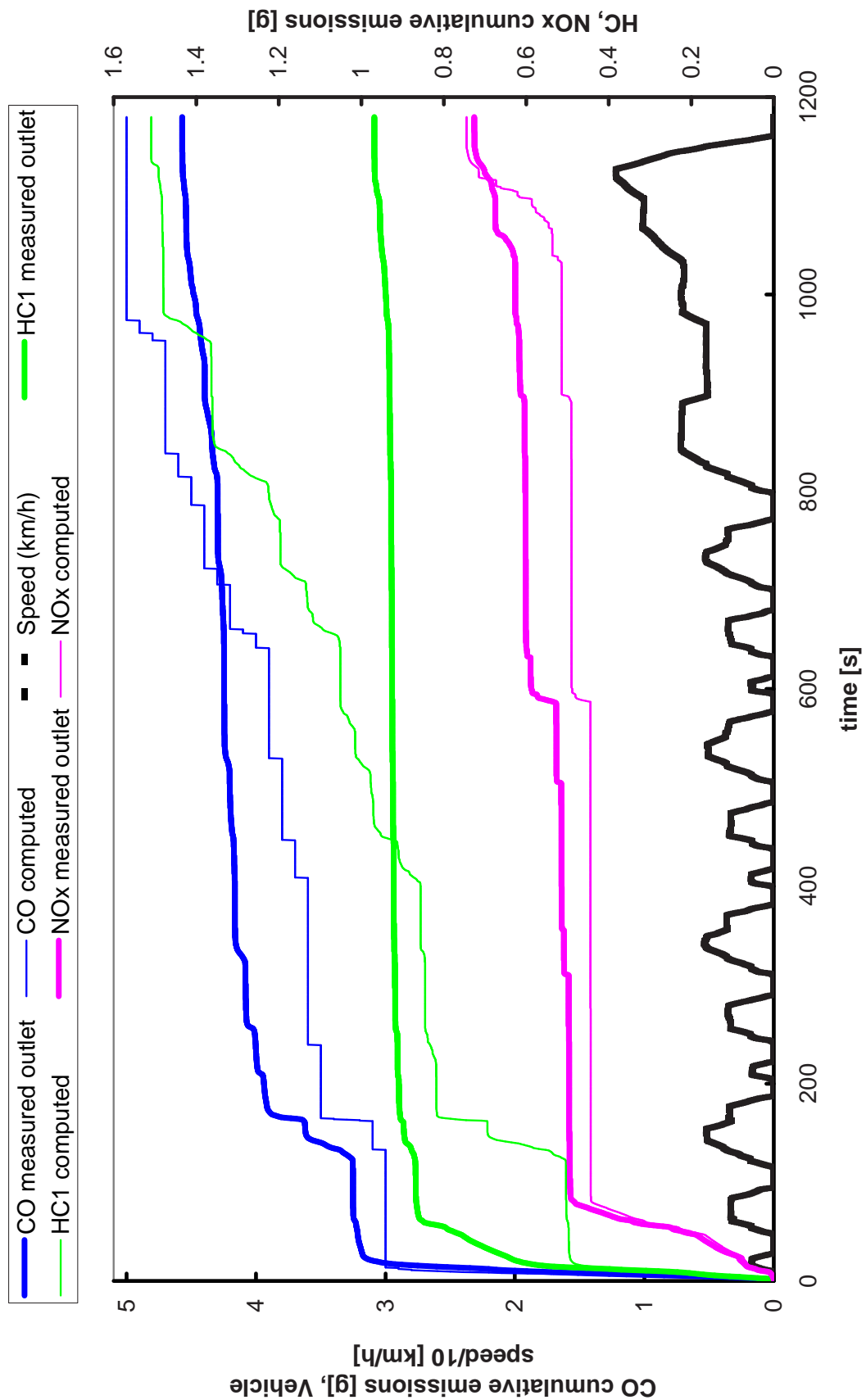


Figure 5.38: Comparison of computed vs. measured cumulative CO, HC and NOx emissions over the first part of the FTP cycle

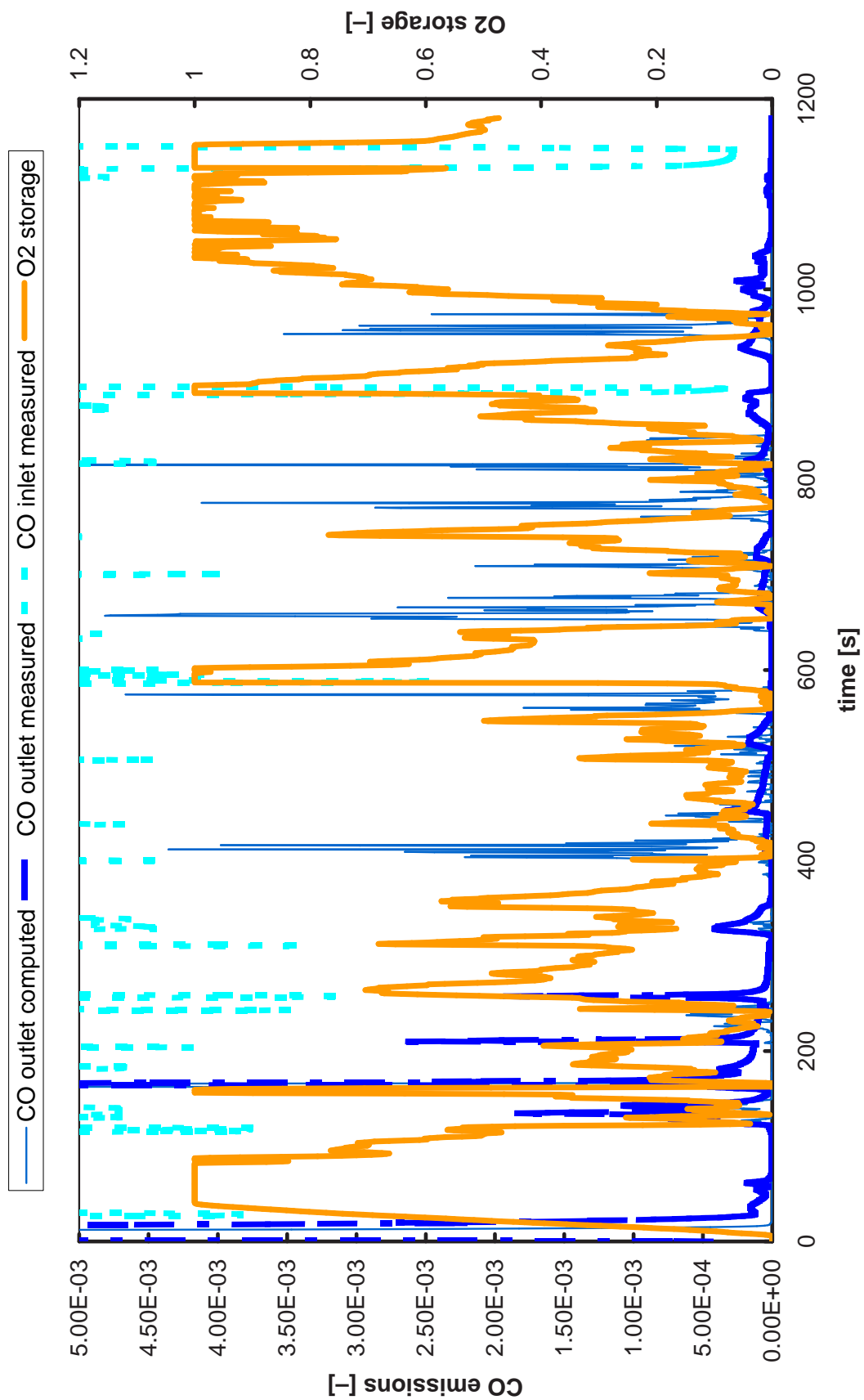


Figure 5.39: Comparison of computed vs. measured instantaneous CO emissions over the NEDC cycle

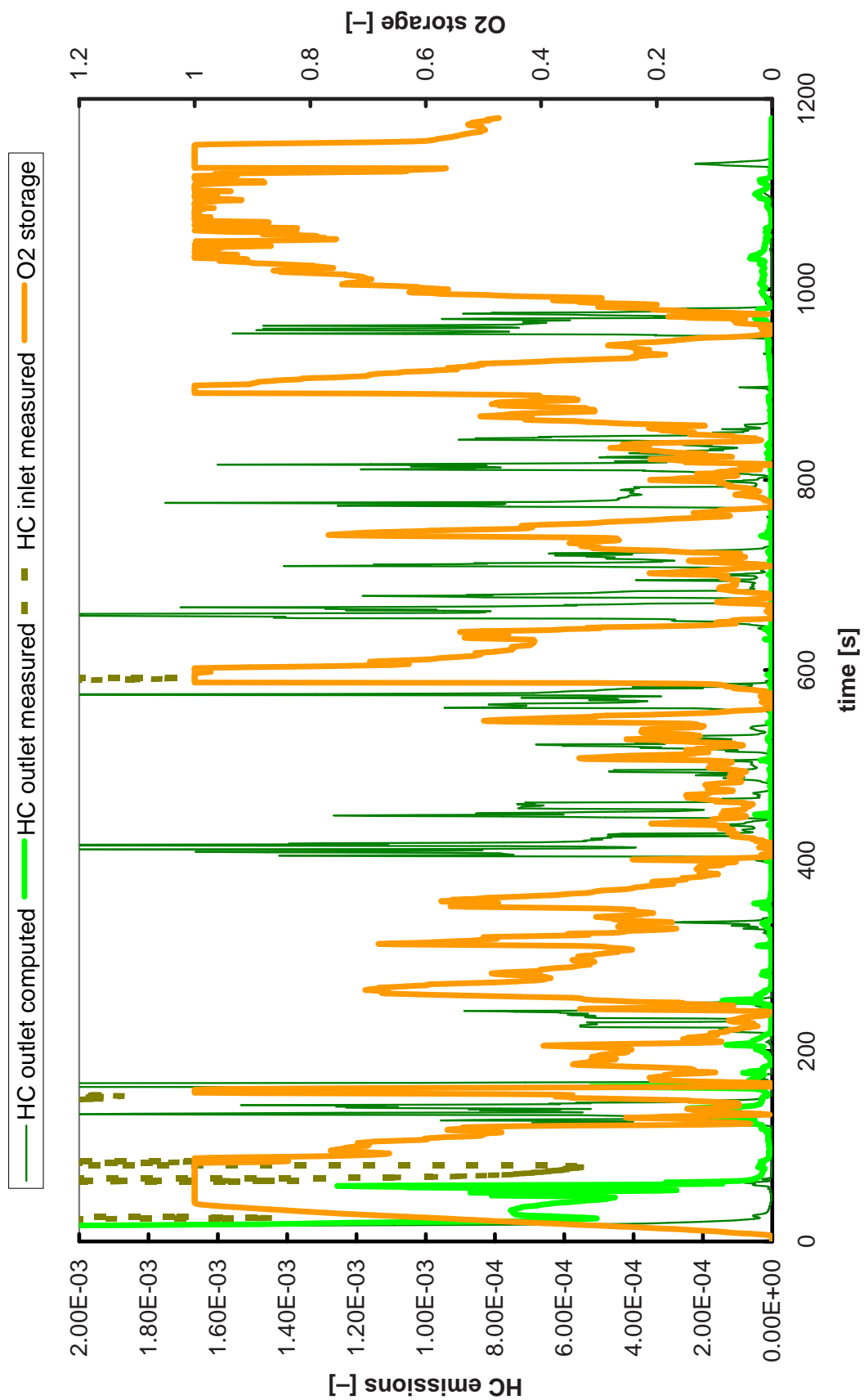


Figure 5.40: Comparison of computed vs. measured instantaneous HC emissions over the NEDC cycle

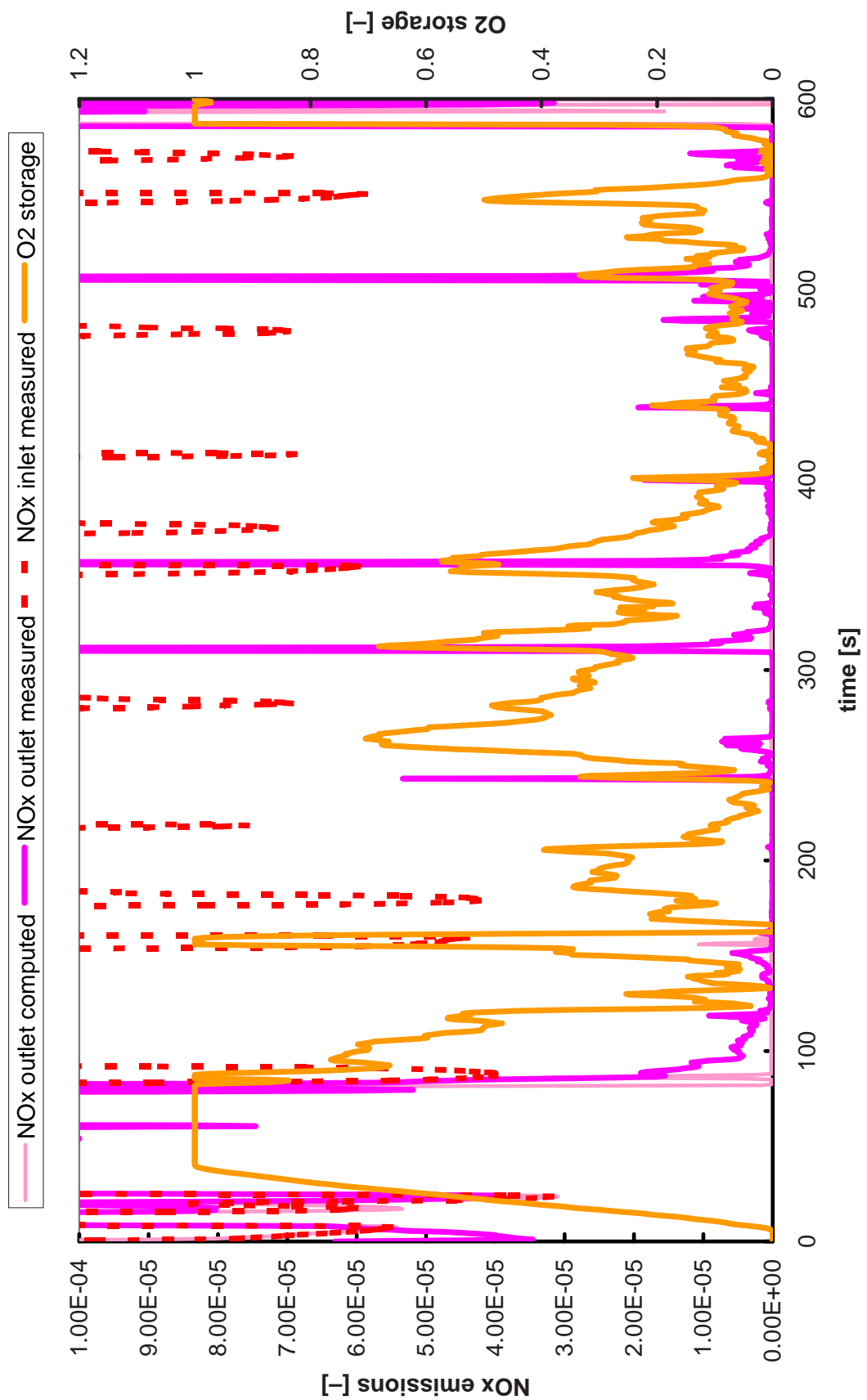


Figure 5.41: Comparison of computed vs. measured instantaneous NO_x emissions over the first 600s of the NEDC cycle

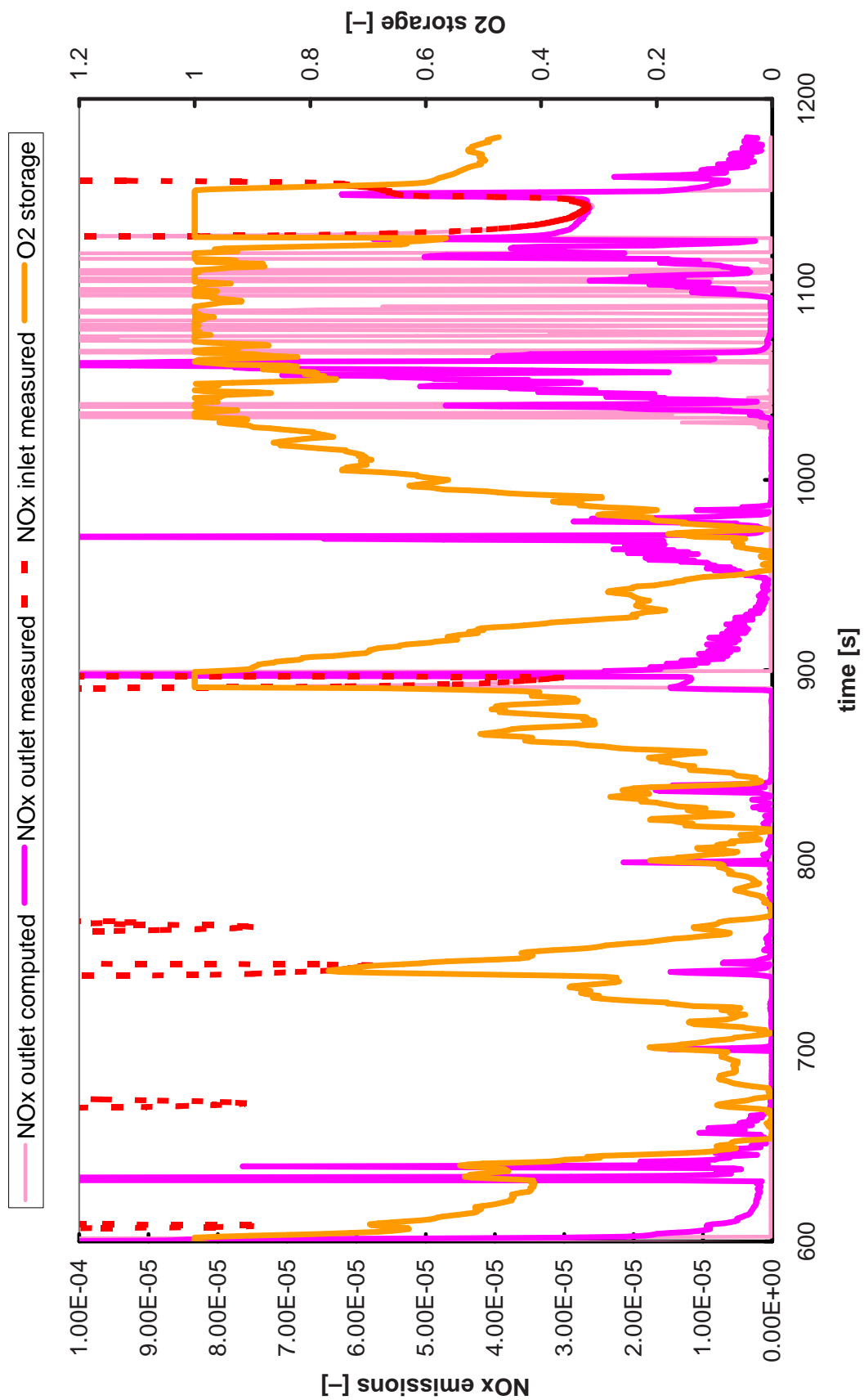


Figure 5.42: Comparison of computed vs. measured instantaneous NO_x emissions over the last 600s of the NEDC cycle

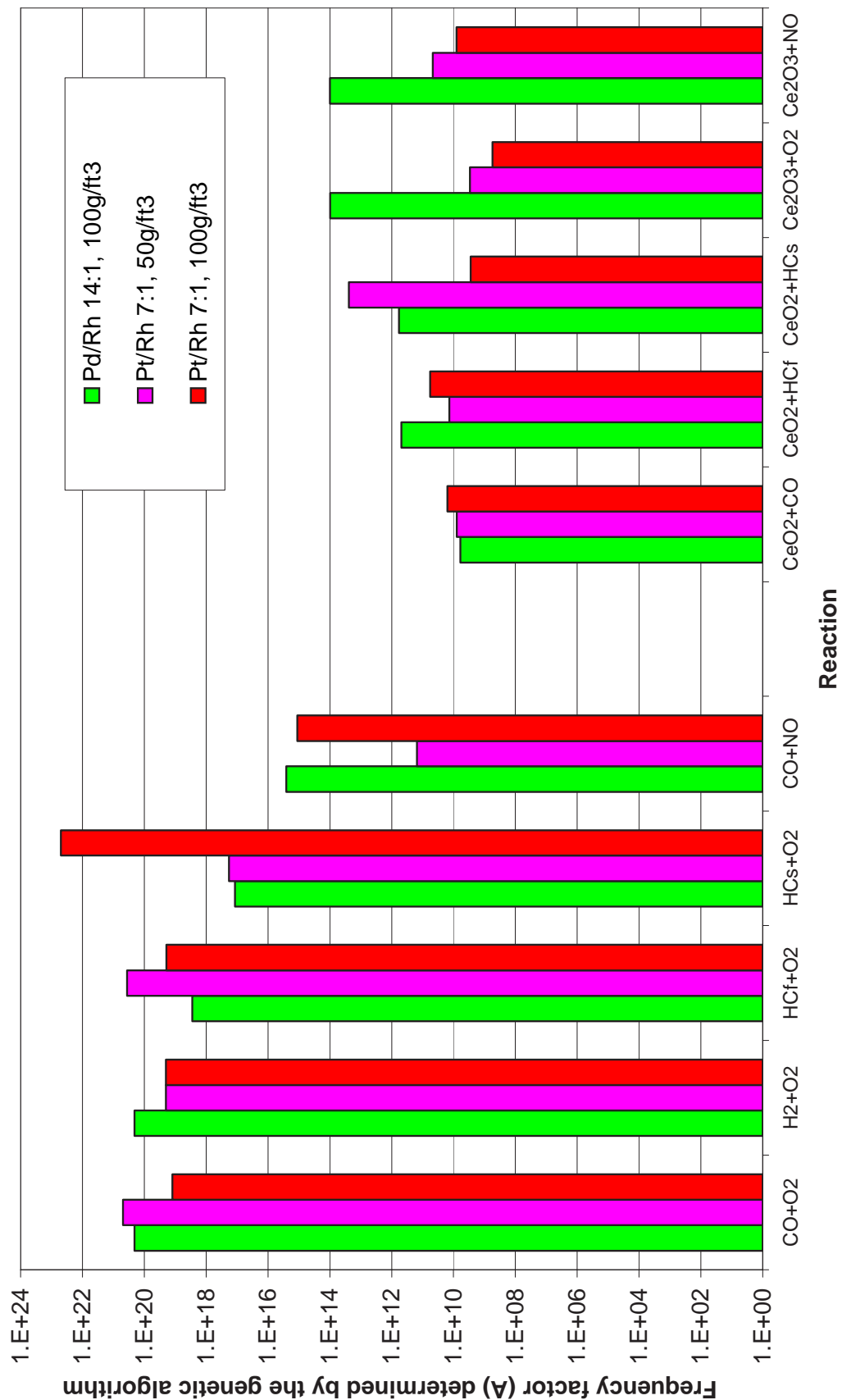


Figure 5.43: Comparison of the frequency factors (A) for three different catalyst formulations, as determined by the genetic algorithm

significantly improve our predictive ability, which has been demonstrated also in the past [9].

Now, maybe the most important improvements coming out of this work, are related to the applications of Computer Aided Engineering in further developments in emerging technologies, like the NO_x storage catalysts currently employed in gasoline direct injection (lean burn) engines and also to diesel engines of the next generation. The modeling of NO_x storage catalysts is already carried out by a tool based on our 3WCC model, with an inclusive reaction scheme that takes into account of the complex chemistry of NO_x storage and release in Barium-containing components of the washcoat of these catalysts. The added complexity of these catalysts makes their kinetic modeling much more complex than that of the 3WCC. Thus, in this case, elementary kinetic models are not yet attempted to be applied in modeling the real catalyst. On the contrary, our modeling approach, assisted by the powerful kinetic parameter estimation tool based on the genetic algorithm approach, makes feasible the development of compact yet effective reaction schemes for the NO_x storage catalysts. This research is under way by other researchers in our Lab, with very promising results.

Last but not least, the effective exploitation of the predictive capability of the tuned catalytic converter and diesel filter modeling in the design optimization of exhaust systems, will require the application of standard optimization methods, with the most attractive candidate being the genetic algorithm methodologies. Thus, multi-parametric optimization will be able to be effectively applied in the future (size, substrate cell density, Precious Metal and Washcoat loading, etc). This process needs to be customized as has been done in the past with standard engine design processes [10]. This is another promising area of research in our Lab.

5.5 Summary

- The CATRAN catalytic converter engineering model, formulated in Chapter 5, was applied here in a number of measurements from three different case studies.
- The conjugate gradients method was initially employed to tune the model. This method failed to tune the model appropriately, unless it was guided in the search space using improved starting points for the method. This resulted in a semi-automatic tuning procedure that finally provided good tuning results for the ULEV case study.
- The model's validity was subsequently tested in the same case study, by employing it to predict the performance of the catalytic converters when combined with a different engine. The model predicted the performance of the converters with good accuracy.
- The genetic algorithm based tuning procedure, that was developed in order to circumvent the limitations of the previous semi-automatic procedure, was employed in order to tune the model in the PML case study. The genetic algorithm managed to tune the model with very high accuracy, which exceeded that obtained with manual tuning or the conjugate gradients based method.
- The model was validated in the PML case study by allowing it to predict the performance of a catalytic converter with a quarter of the length of the

reference catalytic converter. The model's prediction again was very close to the measured results.

- The PML case study revealed that the successful predictions of the model could be attributed to the accurate prediction of the catalytic converter's oxygen storage behaviour. This supported the current reaction scheme formulation and especially the validity of the oxygen storage submodel.
- The overall performance of the model indicates that, when coupled with the genetic algorithm tuning procedure, it may be employed as a powerful tool for the optimization of monolithic catalytic converters under real-world operating conditions, using routine driving cycle measurements. the potential of the model seems to extend beyond what was originally expected for this class of models.

References

- [1] G. N. Pontikakis and A. M. Stamatelos. Mathematical modelling of catalytic exhaust systems for EURO-3 and EURO-4 emissions standards. *Proc Instn Mech Engrs, Part D: J. Automobile Engineering*, 215:1005–1015, 2001.
- [2] G. C. Koltsakis, P. A. Konstantinidis, and A. M. Stamatelos. Development and application range of mathematical models for automotive 3-way catalytic converters. *Applied Catalysis B (Environmental)*, 12(2–3):161–191, 1997.
- [3] M. Shelef, G. W. Graham, and R. W. McGabe. In A. Trovarelli, editor, *Catalysis by Ceria and related materials*, page 343. Imperial College Press, 2002.
- [4] H. S. Gandhi, G. W. Graham, and R. W. McCabe. Automotive exhaust catalysis. *Journal of Catalysis*, 216:433–442, 2003.
- [5] G. Pontikakis, G. Koltsakis, A. Stamatelos, R. Noirot, Y. Agliany, H. Colas, and P. Versaevel. Experimental and modeling study on zeolite catalysts for diesel engines. In *CAPOC V, Fifth International Congress on Catalysis and Automotive Pollution Control*, Brussels, 2000.
- [6] G. Konstantas and A. M. Stamatelos. Quality assurance of exhaust emissions test data. *Proc. Instn Mech Engrs, Part D*, 2003. (*Submitted*).
- [7] R. Domesle, D. Lindner, W. Mueller, L. Mussmann, M. Votsmeier, E. S. Lox, T. Kreuzer, M. Makino, and C. D. Vogt. Application of advanced three-way catalyst technologies on high cell density ultra thinwall ceramic substrates for future emission legislations. *SAE paper 2001-01-0924*, 2001.
- [8] M. Votsmeier, T. Bog, D. Lindner, J. Gieshoff, E. S. Lox, and T. Kreuzer. A System(atic) Approach towards Low Precious Metal Three-Way Catalyst Application. *SAE paper 2002-01-0345*, 2002.
- [9] J. Schmidt, A. Waltner, G. Loose, A. Hirschmann, A. Wirth, W. Mueller, J. van den Tillaart, L. Mussmann, D. Lindner, J. Gieshoff, K. Umehara, M. Makino, K. P. Biehn, and A. Kunz. The impact of high cell density ceramic substrates and washcoat properties on the catalytic activity of three way catalysts. *SAE paper 1999-01-0272*, 1999.
- [10] H. Blaxill, J. Downing, J. Seabrook, and M. Fry. A parametric approach to Spark-Ignition Engine Inlet-Port Design. *SAE paper 1999-01-0555*, 1999.

Chapter 6

Diesel Particulate Filter Case Studies

This chapter contains the application of the DPF models previously developed in two real-world case studies. The first consists of a matrix of experiments, where significant operating parameters of the filter were varied in order to study their effect on filter behaviour. The one-dimensional DPF model was applied in this case study. Comparing the results to the measurements indicated a good accuracy level of the DPF model, as regards both the prediction of temperatures and pressure drop of the filter.

The 1D model's results were inferior for very high and especially very low mass flow rates. This was attributed to three-dimensional flow field and temperature distributions in the filter, that cannot be accounted for by the 1D model. The second case study therefore attempts an application of the 3D version of the DPF regeneration model to a low mass flow rate case study, to examine its potential in more detailed analysis of filter operation, especially as regards regeneration propagation, flow field non-uniformities and thermal stress modeling.

Although the DPF model has not matured as much as its catalytic converter counterpart, the results presented herein indicate good agreement with the experimental findings and significant potential as a tool for the detailed analysis and optimization of DPF-based exhaust systems.

6.1 1D DPF model validation

Below, we demonstrate how the improved 1D filter regeneration model that was formulated in Chapter 3 is validated against full-scale experimental data. The software is subjected to a systematic validation procedure, against full-scale tests of the regeneration behaviour of a diesel filter fitted to a modern diesel engine run on catalyst-doped fuel. The main objectives of the validation procedure concern the assessment of the model's ability to predict the effects of exhaust mass flow rate, initial soot loading mass, volatile organic fraction of the soot and additive concentration in fuel.

6.1.1 Experimental

The validation was based on the results of engine bench regeneration experiments performed on one of the UTh/LTTE engine benches. The DW10-ATED engine from PSA was used.

The filter employed in these experiments was a SiC 14/200 IBIDEN filter (di-

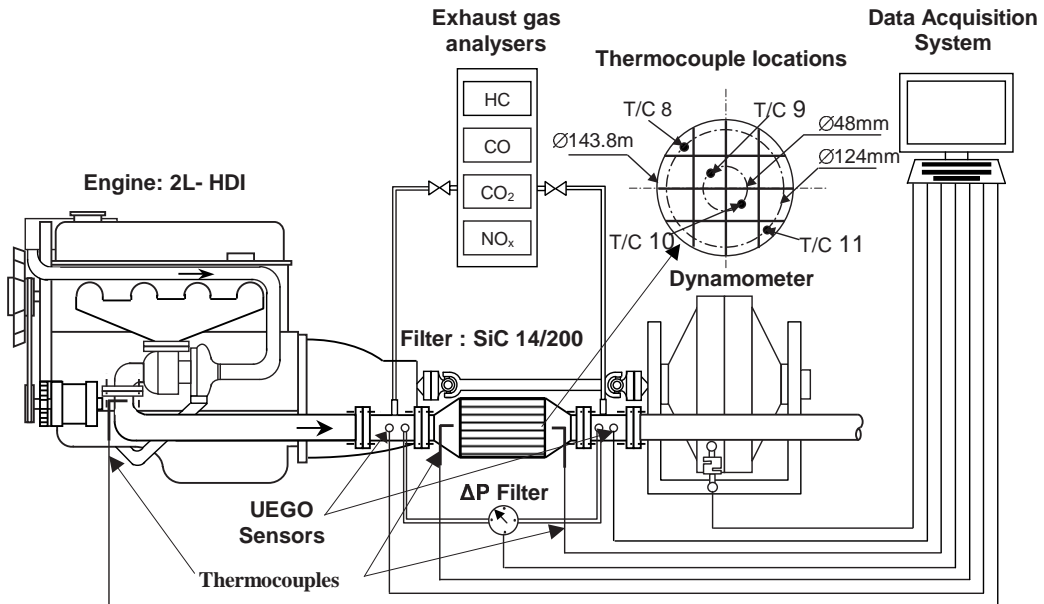


Figure 6.1: Experimental layout. Engine and digitally controlled dynamometer installation is shown along with exhaust gas analysers, main filter measurement lines, and data acquisition system

ameter × length: 5.66" × 6") fitted in the exhaust pipe of the DW10-ATED engine about 600 mm after the turbo. The temperatures were measured simultaneously, at the inlet and the exit of the filter, and inside the filter, along a filter diameter 15 mm deep from filter exit. The exhaust emissions of CO, CO₂, NO_x and HC were measured simultaneously before the filter. The O₂ concentration was calculated by the A/F ratio obtained from the UEGO sensor installed before the filter inlet. The experimental layout of the filter loading-regeneration experiments is presented in Figure 6.1.

The model's capacity to address the effect of the following design and operation parameters was validated:

- Fuel additive concentration
- Initial filter soot loading
- Conditions of soot accumulation
- Exhaust gas mass flow rate

Below, we present in brief the tests that were used for the validation regarding each one of the above effects.

Fuel additive concentration The effect of fuel additive concentration on the regeneration was checked by experiments with 0, 25 and 50 ppm Cerium fuel additive concentration in the fuel. The non-catalytic regeneration was performed at the increased engine speed-load point of 3800 rpm–60 Nm in order to meet the high exhaust temperatures levels that are necessary for the initiation of regular soot oxidation. The catalytic regenerations were performed at the characteristic medium

operation point of 2250 rpm–60 Nm, employing the increased engine speed point of 3800 rpm–60 Nm point as a reference for the thermal regeneration.

The filter had been previously loaded at the medium point of 3000 rpm, 40 Nm until a soot mass loading of the order of $6 \text{ g}/\ell$ filter was obtained.

The shift to a set of experiments with different fuel additive concentration was performed after filter cleaning and engine running for about 6 h to prevent possible memory effects to the fuel and soot composition.

Initial filter soot loading Indirect assessment of the effect of the soot deposit filtration characteristics was based on the variation of initial soot loading (3, 6 and $9 \text{ g}/\ell$ filter) obtained with adjustment of filter loading process duration assuming constant particulate emissions and no effects of the increased backpressure to the engine exhaust mass flow rate. The filter loading was performed with the engine running on 3000 rpm, 40 Nm with 25 ppm Cerium doped fuel.

Conditions of soot accumulation Two characteristic engine operation points were selected for the assessment of differences in VOF content of soot: 3000 rpm–40 Nm (10% VOF), versus 1800 rpm–90 Nm (2% VOF). These points are characterized by equivalent total particulate matter emissions and cover a range of filter wall temperatures from 300 °C to 400 °C that is responsible for the VOF variation[1]. Secondary effects due to the dynamic phenomena of adsorption-desorption may also affect soot oxidation kinetics.

Mass flow rate The effect of exhaust gas flow rate was examined by specially selecting the operating points of the engine so that approximately equivalent filter inlet temperature levels were achieved, in the range of 500 to 550 °C. Four engine points were chosen, with engine speed of 1500, 2250, 3000 and 4000 rpm, and engine load of 80, 60, 60 and 30 Nm respectively.

These points result to a variation in exhaust gas mass flow rate in the range from 28 to 100 g/s and represent the real conditions met under Urban and Extra-Urban driving conditions.

★ ★ ★

Each regeneration process was initiated after loading at the respective engine operating point using a combined step variation in engine load and engine intake airflow obtained with adjustment of turbocharger and EGR valves. The engine was left to run for 10 minutes on steady state conditions before the regeneration strategy was applied, duration considered long enough for thermal and chemical equilibrium to be reached.

The experimental protocol is summarized in Figure 6.1. The regeneration experiments were performed in combination with TGA experiments of soot samples taken directly from the filter loaded at the above operation points in order to improve our understanding of the kinetics of soot oxidation by Ceria and exhaust gas [2]. Previous experimental work by Stratakis and Stamatelos [3] in the direction of determination of pressure drop parameters as function of collected soot mass was employed to support pressure drop parameter selection.

	Experimental Parameters			
	Ce Concentration	Soot mass loading	Loading engine operation point	Regeneration engine operation point
Catalyst concentration	0ppm	6g/L	3000rpm x 40Nm	3800rpm x 60Nm
	*25ppm			2250rpm x 60Nm
	50ppm			
Soot mass loading	25ppm	3g/L	3000rpm x 40Nm	2250rpm x 60Nm
		*6g/L		
		9g/L		
Filter accumulation condition	25ppm	6g/L	*3000rpm x 40Nm (VOF:10%)	2250rpm x 60Nm
			1800rpm x 90Nm (VOF:2%)	
Filter regeneration condition	25ppm	6g/L	3000rpm x 40Nm	1500rpm x 80Nm (28g/s)
				*2250rpm x 60Nm (52g/s)
				3000rpm x 60Nm (70g/s)
				4000rpm x 30Nm (92g/s)

* Reference experiment

Table 6.1: Experimental protocol

6.1.2 Validation Results

Before carrying out the main validation process, it is necessary to determine reference values for pressure drop and kinetic parameters. Starting from the pressure drop parameters, the determination of the product of soot permeability times soot density, (denoted as $(\rho k)_p$ in this chapter) was based on experiments with single channel filters described in detail in [3]. A range between $3.5 \cdot 10^{-12}$ and $1.15 \cdot 10^{-11} \text{ kg/m}$ is reported for the $(\rho k)_p$ product over the medium range of engine speed and load. However these values are necessary to be reduced in order to match the pressure drop behaviour of the validation experiments. As is shown in Table 6.2, a constant, typical value of $(\rho k)_p = 2.25 \cdot 10^{-13}$ was successful in most simulations. The discrepancy between the experimental and calculated values could be partly attributed to soot and flow maldistribution effects [4] that cannot be taken into account by the 1D model. Concerning the wall permeability, a constant value of the order of $2 \cdot 10^{-13}$ was found capable to match the pressure drop curves of the whole range of validation experiments. This value is in accordance with those reported by other researchers [5]. Finally, the lack of measured data for collected soot density (values reported in the literature between 60 and 120 kg/m^3) made necessary the assumption of a typical value of 80 kg/m^3 .

A summary of the validation runs and the respective kinetic parameter values inserted in the model is presented in Table 6.2. The baseline for the determination of the activation energies E for thermal and catalytic regeneration reactions have been the extensive TGA analysis experiments of soot samples taken directly from the filter [2]. The following values for activation energy were determined from the above-mentioned experimental work:

- $E = 190 \text{ kJ/mole}$ for the complete thermal soot oxidation to CO_2 .
- $E = 150 \text{ kJ/mole}$ for the incomplete thermal soot oxidation to CO .
- $E = 120 \text{ kJ/mole}$ for the complete catalytic soot oxidation to CO_2 .
- $E = 80 \text{ kJ/mole}$ for the incomplete catalytic soot oxidation to CO .

The values of activation energies for catalytic oxidation correspond to dry soot oxidation for samples where the VOF content varied in the range between 2.5 and 8%.

Keeping constant the above values of activation energies, a certain amount of tuning of the frequency factors was allowed. The tuning of the frequency factor values assumes that the catalytic regeneration prevails in the temperature range from 400°C to 550°C , while thermal regeneration is more active at higher temperatures.

This situation is schematically presented in Figure 6.2 by means of comparison between the calculated thermal and catalytic reaction rates as functions of temperature. The catalytic soot oxidation to CO prevails at temperatures lower than 500°C , evidence of a mild catalytic oxidation. Soot oxidation to CO_2 , which indicates higher catalytic activity, becomes dominant after this point and until about 630°C . This assumption is in accordance with the experimental work of [2] that indicates an ignition temperature for the catalytic soot oxidation of the order of 500°C .

Furthermore, the parameter tuning assumes that thermal regeneration prevails above 630°C . In lower temperatures, thermal oxidation of soot to CO is present, but is still not as active as catalytic regeneration reactions.

Name of studied parameter	Value of studied parameter	Kinetic parameters									
		Thermal soot oxidation					Catalytic soot oxidation				
		A_1 (mole/m ³ s)	E_1 (J/mole)	A_2 (mole/m ³ s)	E_2 (J/mole)	A_3 (mole/m ³ s)	E_3 (J/mole)	A_4 (mole/m ³ s)	E_4 (J/mole)	A_5 (mole/m ³ s)	E_5 (J/mole)
Catalyst concentration	0ppm	20.5	0.02	2.8E-13	2.2E-13	1E13	1.9E5	5.5E10	1.5E5	-	-
	25ppm	14.2	0.14	2E-13	2.2E-13	80	1E13	1.9E5	5.5E10	3.5E11	1.2E5
Soot mass loading	50ppm	13.15	0.15	2.0E-13	2.0E-13					6E8	0.8E5
	3g/L	8	0.01	2.5E-13					4.5E11	3E8	
Filter accumulation condition	6g/L	14.2	0.02	2E-13	2.2E-13	80	1E13	1.9E5	5.5E10	3.5E11	1.2E5
	9g/L	20.5	0.19	2.0E-13	2.0E-13				2.5E11	6E8	0.8E5
Filter regeneration condition	3000rpm x 40Nm (VOF:10%)	14.2	0.14	2E-13	2.2E-13	80	1E13	1.9E5	5.5E10	4.5E11	1.2E5
	1800rpm x 90Nm (VOF:2%)	13.8	0.08	2.6E-13					2.5E11	9E8	
	1500rpm x 80Nm (mfr:28g/s)	14.2	0.07	2.2E-13					1E11	2E8	
	2250rpm x 60Nm (mfr:52g/s)	14.2	0.14	2.2E-13					3.5E11	6E8	
	3000rpm x 60Nm (mfr:70g/s)	16	0.17	2E-13	2.2E-13	80	1E13	1.9E5	5.5E10	3.5E11	1.2E5
	4000rpm x 30Nm (mfr:92g/s)	13.3	0.19	2.2E-13					6.5E12	3.5E11	0.8E5

Table 6.2: Catalytic converter data of the PML case study

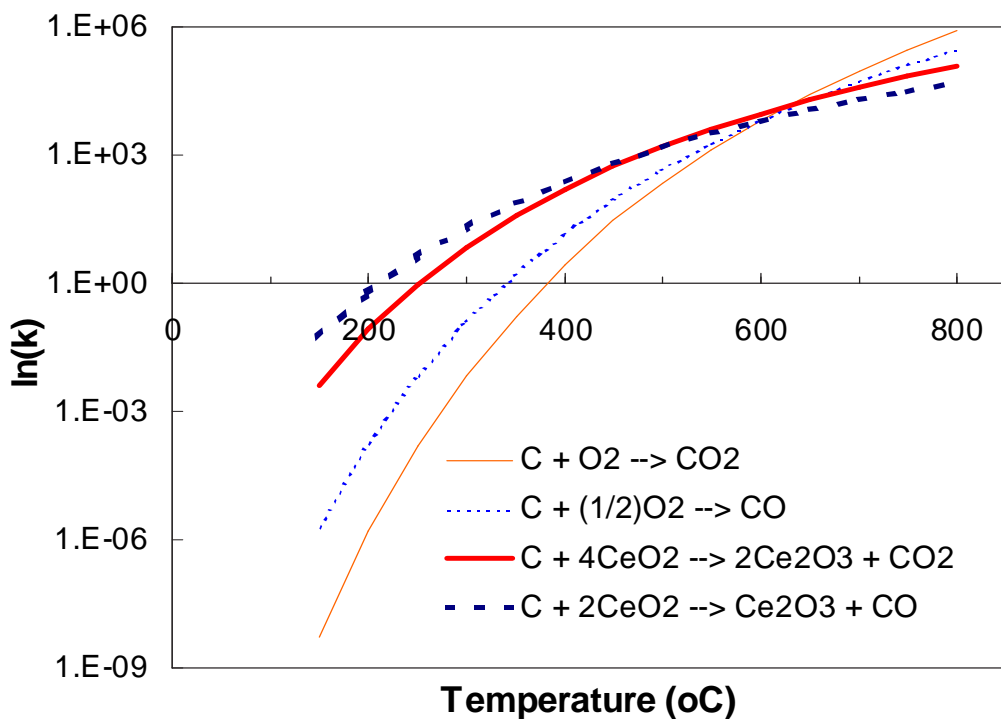


Figure 6.2: Comparison of thermal and catalytic regeneration reaction rates

As a general rule of thumb, the catalytic regeneration kinetics (frequency factors) were tuned to represent the experimentally determined, low temperature (catalytic) regeneration behaviour of the filter. Then, the ability of the tuned model to predict the effects of exhaust mass flow rate, initial soot loading mass, volatile organic fraction of the soot and additive concentration in fuel was checked.

In principle, the values of frequency factors should keep close to certain reference values for each reaction of the scheme. However, one must bear in mind that the catalytic reactor in the case of a fuel additive assisted diesel filter, is made up of the soot layer, which contains the catalyst dispersed in it, in a close contact with the soot. This reactor is destroyed during regeneration and re-built during filter loading. The reactor's characteristics may change according to the prevailing exhaust gas conditions during loading.

The exact determination of the catalytic oxidation frequency factor values was sensitive to the ratio of CO/CO₂ in the outlet exhaust gas during regeneration, indicating dependence from the filter loading and regeneration conditions. This observation is confirmed by Aoki et al [6] and is more enhanced in the case of catalytic regeneration. The assessment of the experimental results has shown that the following parameters affect to the CO/CO₂ ratio:

- Soot loading: increase of soot loading mass over 6 g/ℓ filter causes a significant increase to the produced CO during regeneration. The model can match this behaviour by a respective modification of the frequency factors of the respective reactions.
- Soot VOF content: increase of VOF content results in a shift towards higher CO than CO₂ production during regeneration.

- Exhaust gas mass flow rate: as the exhaust gas mass flow rate increases, the ratio of CO to CO₂ produced during regeneration also increases.

Based on the above reasoning, certain deviations from the reference kinetics of the catalytic reactions are observed in Table 6.2 and summarized below:

- It was found that the increase of the initial soot loading shifts the catalytic reaction kinetics to produce more CO and less CO₂.
- A severe decrease in the volatile organic fraction of the collected particulate, leads to a respective reduction of catalytic soot oxidation kinetics, which can be matched by a respective reduction of frequency factors of the catalytic oxidation reactions.

As expected, the tuned 1D model does not successfully predict filter operation at low flowrates. This is due to the importance of complex 3D effects, related to exhaust flow maldistribution and soot loading maldistribution across the filter face.

On the other hand, by comparison of model predictions with measurements, it was observed that the catalytic activity is reduced at very high flowrates (very low residence times). This effect needs to be further investigated.

As regards the pressure drop behaviour, a certain variation of soot permeability was allowed respectively, as function of the following factors:

- Effect of soot loading: thicker soot layer leads to lower permeability-density factor.
- Effect of Ceria concentration in fuel: higher Ceria concentration leads to lower soot permeability – density factor.
- Effect of VOF: higher VOF in soot leads to lower soot permeability- density factor.

Table 6.2 presents the wall permeability, soot density and soot permeability times density values inserted in the 1D model to simulate the pressure drop behaviour of the validation experiments.

The measured filter exit temperatures at the central line (measurements taken by thermocouple T/C 9) are compared with the predicted ones for each regeneration case, in Figures 6.3–6.11. The observed correlation is satisfactory. However a certain degree of inaccuracy in predicting the initial heating phase of the regeneration is observed. It is believed that this is a 3D phenomenon related to the change of average mass flowrate, due to the reduction in flow resistance in the central channels where regeneration starts first [4].

6.1.3 Discussion

The 1D DPF regeneration model is able to predict the effect of a significant number of design and operation parameters on the filter performance in a satisfactory way. In the following, certain important remarks from model validation are discussed in more detail. These remarks generally indicate directions for future, more refined experimental study.

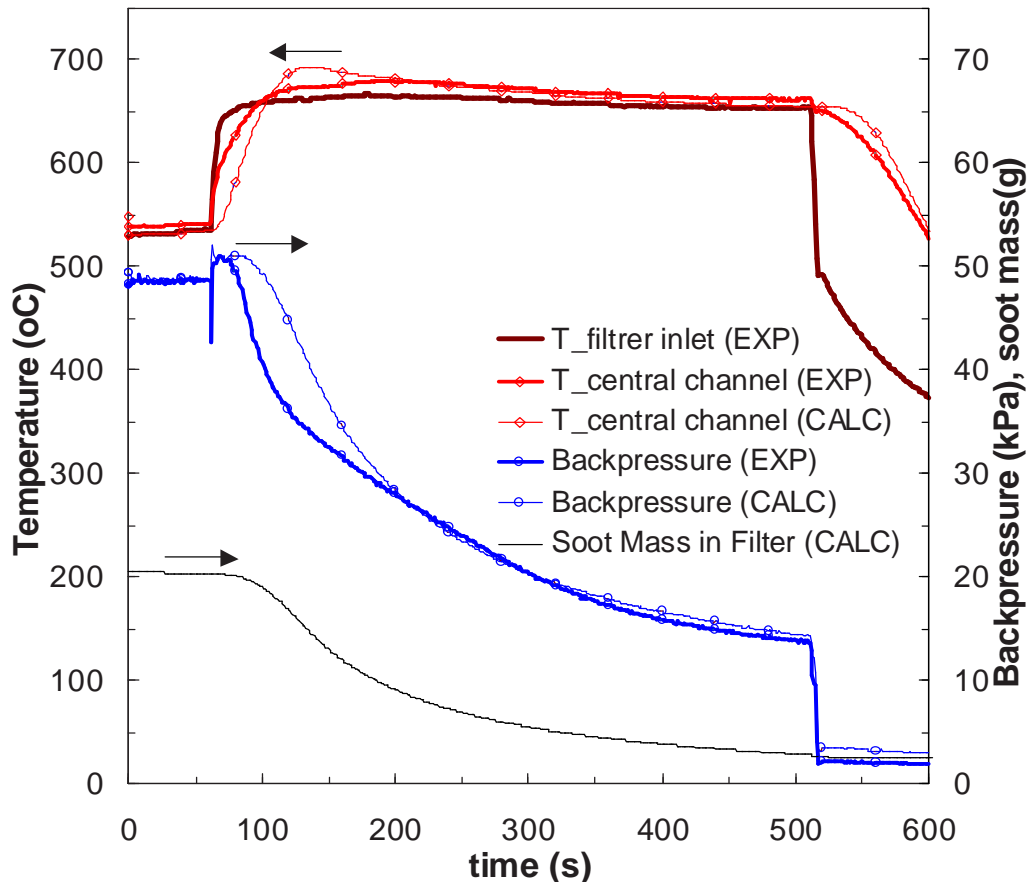


Figure 6.3: Simulation of regular soot (no Ceria added) filter regeneration. Measured and predicted trap temperatures near the exit of a central channel of a medium loaded filter (6g/l) with the engine running on 3000rpm, 40Nm without fuel additive-doped fuel. Also measurement and prediction of filter backpressure together with soot mass prediction are presented. Computation is made with $(\rho k)_p=2.8E-13$ kg/m, activation energy values: $E_1=1.9E5$, $E_2=1.5E5$ J/mole and frequency factor values: $A_1=1E13$, $A_2=5.5E10$ mole/m³.s. The values for E and A are used as reference point for catalytic regeneration

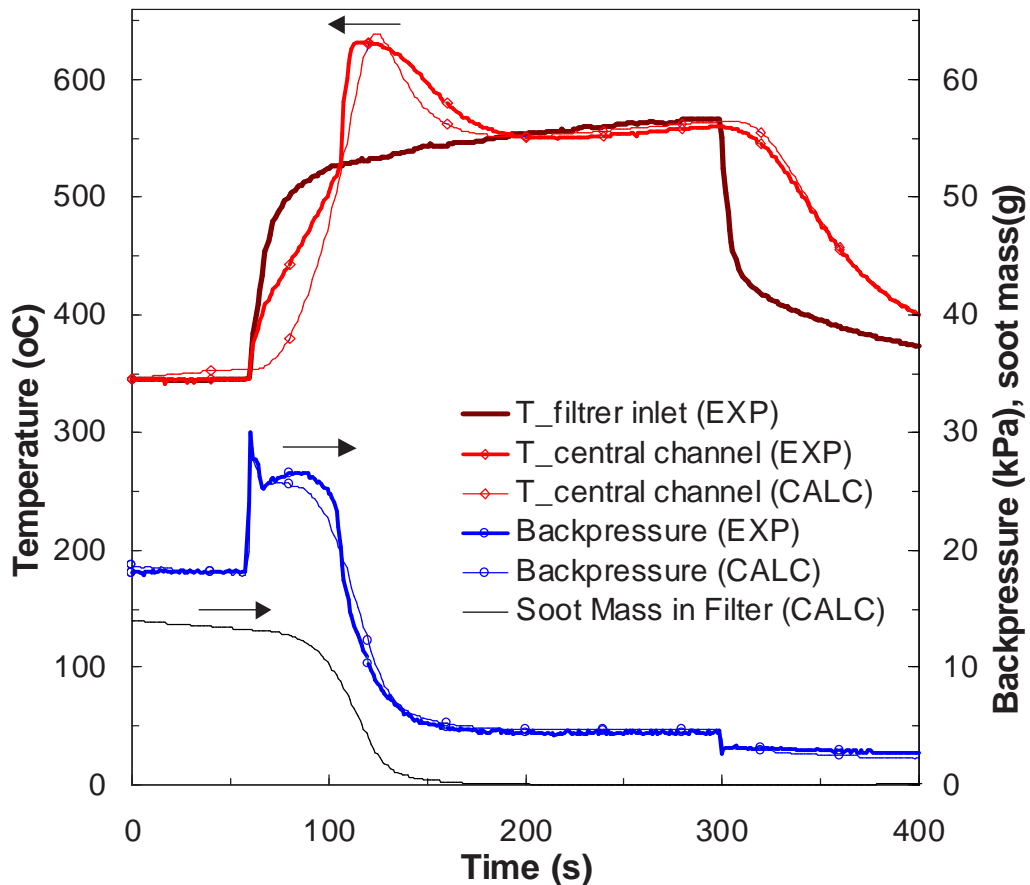


Figure 6.4: Simulation of regeneration of a filter loaded with soot emitted by the engine operating with 25ppm Cerium doped fuel.. Measured and predicted trap temperatures near the exit of a central channel of a medium loaded filter (6g/l) with the engine running on 3000rpm, 40Nm. Also measurement and prediction of filter backpressure together with soot mass prediction are presented. Computation is made with $(\rho k)_p=2.2E-13$ kg/m, activation energy values: E1=1.9E5, E2=1.5E5, E3=1.2E5, E4=0.8E5, E5=0.8E5 J/mole and frequency factor values: A1=1E13, A2=5.5E10, A3=3.5E11, A4=6E8, A5=8E8 mole/m³s. The values for E and A are used as reference point for catalytic regeneration

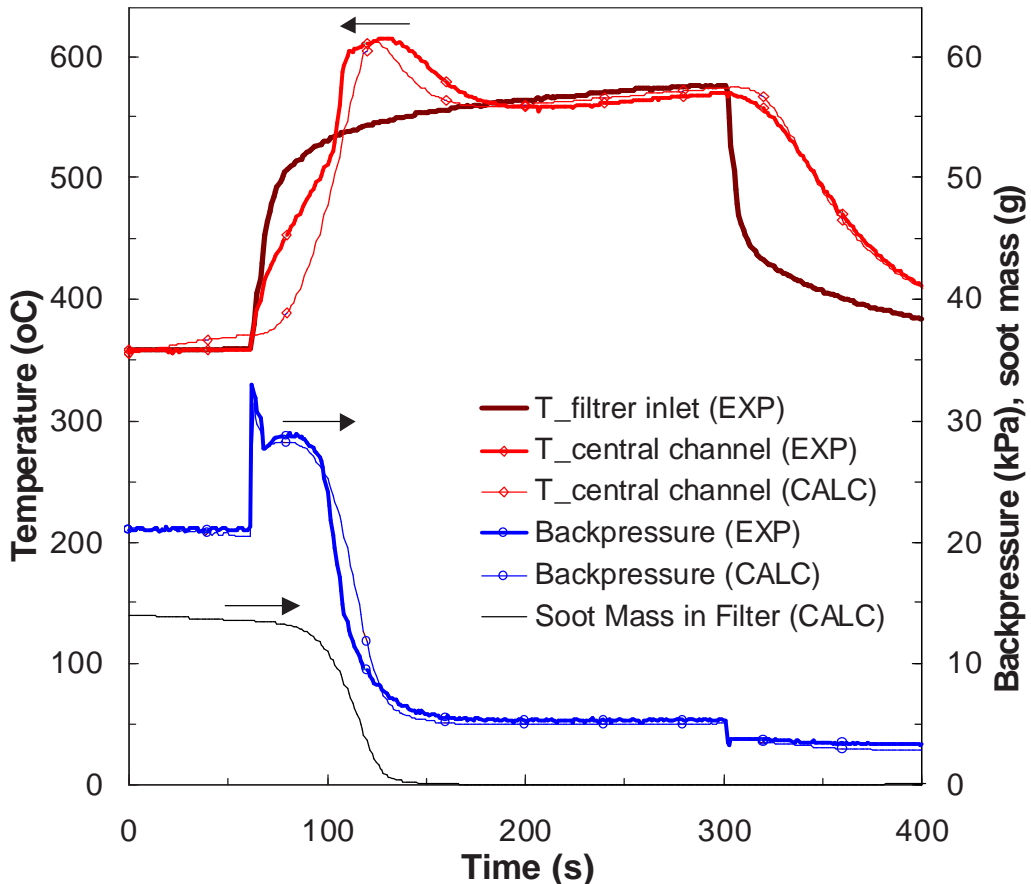


Figure 6.5: Simulation of regeneration of a filter loaded with soot emitted by the engine operating with 50ppm Cerium doped fuel.. Measured and predicted trap temperatures near the exit of a central channel of a medium loaded filter (6g/l) with the engine running on 3000rpm, 40Nm. Also measurement and prediction of filter backpressure together with soot mass prediction are presented. Computation is made with $(\rho k)_p=2.0E-13$ kg/m, activation energy values: E1=1.9E5, E2=1.5E5, E3=1.2E5, E4=0.8E5, E5=0.8E5 J/mole and frequency factor values: A1=1E13, A2=5.5E10, A3=3.5E11, A4=6E8, A5=8E8 mole/m3,s

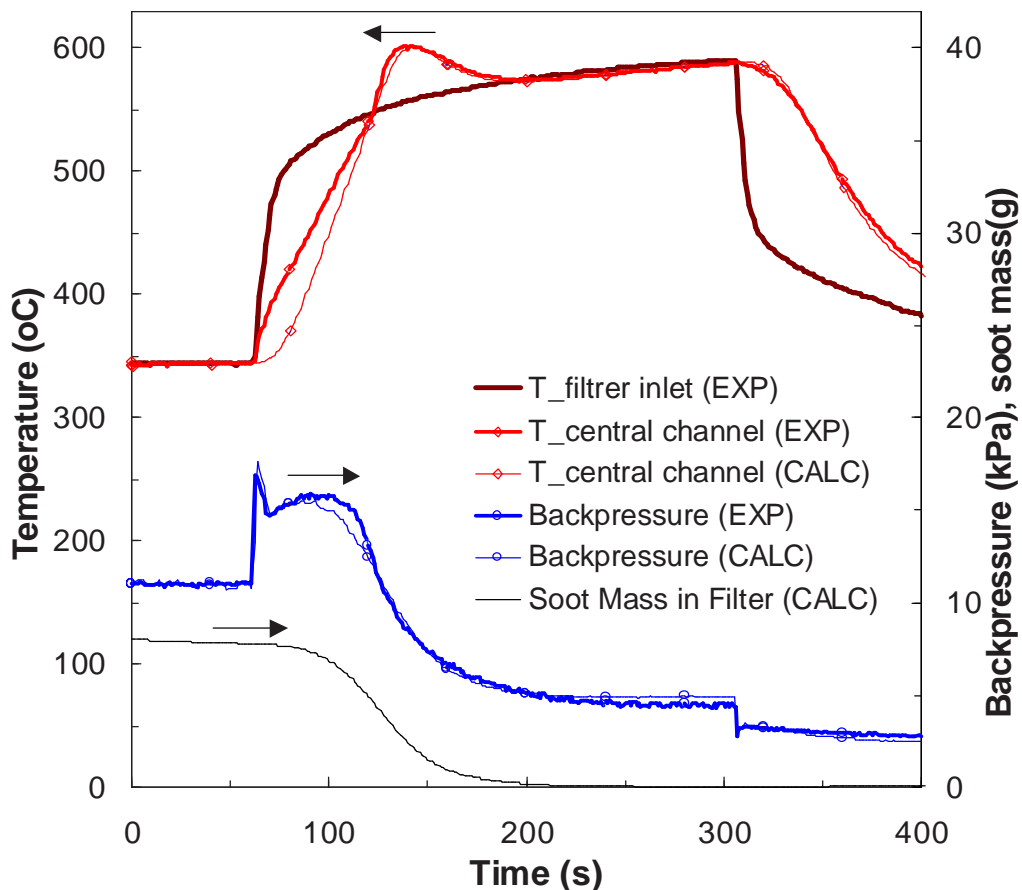


Figure 6.6: Simulation of a low soot mass loading (3g/l) filter regeneration. Measured and predicted trap temperatures near the exit of a central channel for a filter loaded with the engine running on 3000rpm, 40Nm with 25ppm Ce-doped fuel. Also measurement and prediction of filter backpressure together with soot mass prediction are presented. Computation is made with $(\rho k)_p=2.5E-13$ kg/m, activation energy values: E1=1.9E5, E2=1.5E5, E3=1.2E5, E4=0.8E5, E5=0.8E5 J/mole and frequency factor values: A1=1E13, A2=5.5E10, A3=4.5E11, A4=3E8, A5=8E8 mole/m³,s

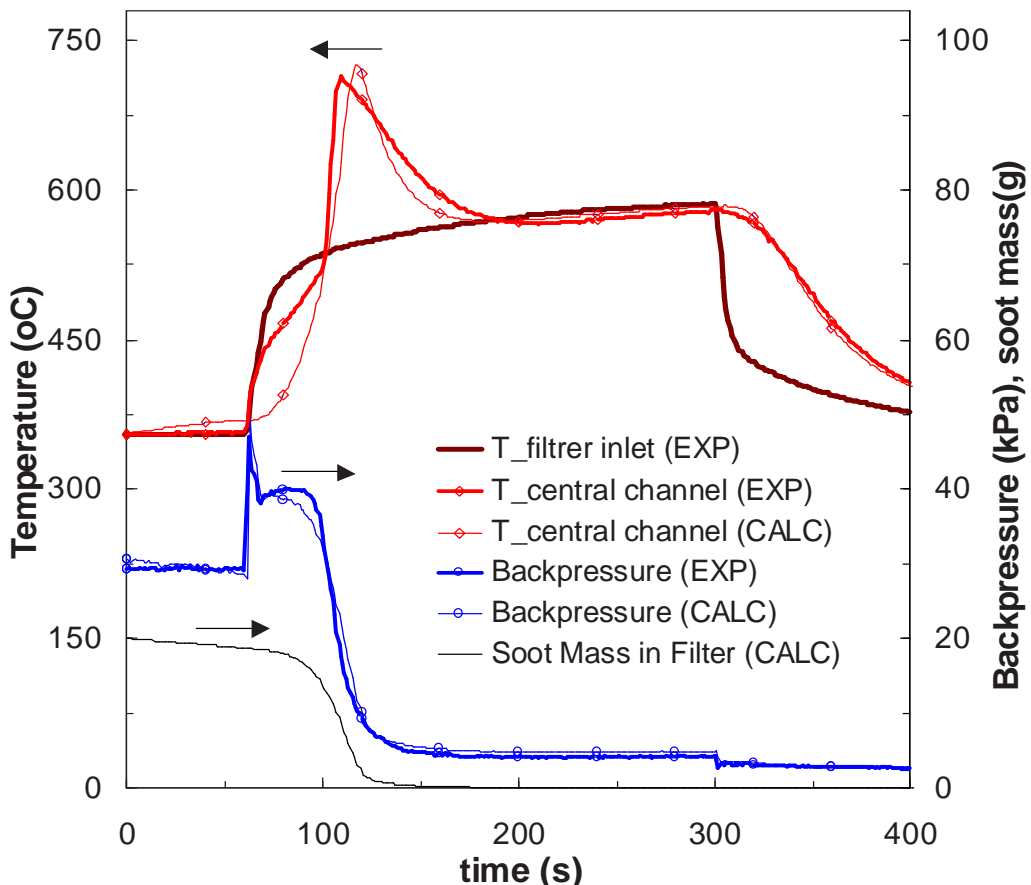


Figure 6.7: Simulation of a high soot mass loading (9g/l) filter regeneration. Measured and predicted trap temperatures near the exit of a central channel for a filter loaded with the engine running on 3000rpm, 40Nm with 25ppm Ce-doped fuel. Also measurement and prediction of filter backpressure together with soot mass prediction are presented. Computation is made with $(\rho k)_p=2.0E-13$ kg/m, activation energy values: E1=1.9E5, E2=1.5E5, E3=1.2E5, E4=0.8E5, E5=0.8E5 J/mole and frequency factor values: A1=1E13, A2=5.5E10, A3=2.5E11, A4=9E8, A5=8E8 mole/m³,s

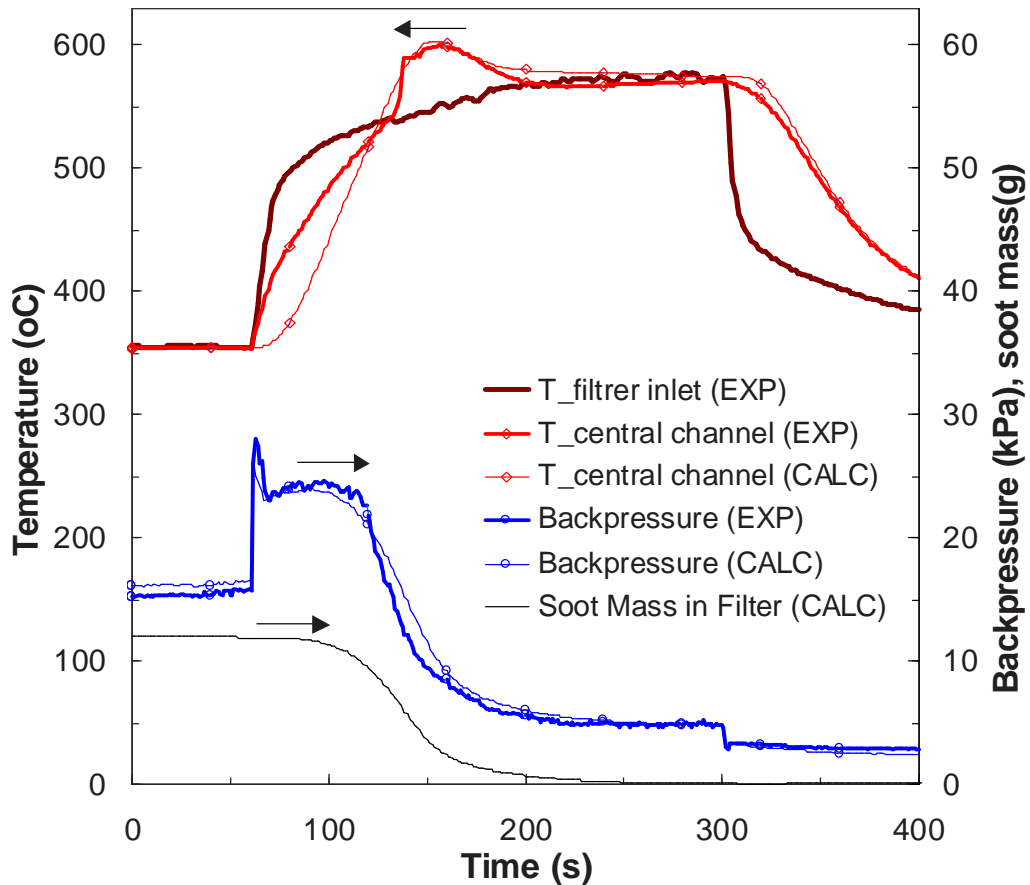


Figure 6.8: Simulation of a regeneration of a filter loaded at a low VOF operation point. Measured and predicted trap temperatures near the exit of a central channel for a medium loaded filter (6g/l) at a medium speed high load operation point (1800rpm , 90Nm) with 25ppm Ce-doped fuel resulting a low VOF content (2%) in soot. Also measurement and prediction of filter backpressure together with soot mass prediction are presented. Computation is made with $(\rho k)_p=2.6\text{E-}13 \text{ kg/m}$, activation energy values: $E_1=1.9\text{E}5$, $E_2=1.5\text{E}5$, $E_3=1.2\text{E}5$, $E_4=0.8\text{E}5$, $E_5=0.8\text{E}5 \text{ J/mole}$ and frequency factor values: $A_1=1\text{E}13$, $A_2=5.5\text{E}10$, $A_3=2.5\text{E}11$, $A_4=3\text{E}8$, $A_5=8\text{E}8 \text{ mole/m}^3\text{s}$

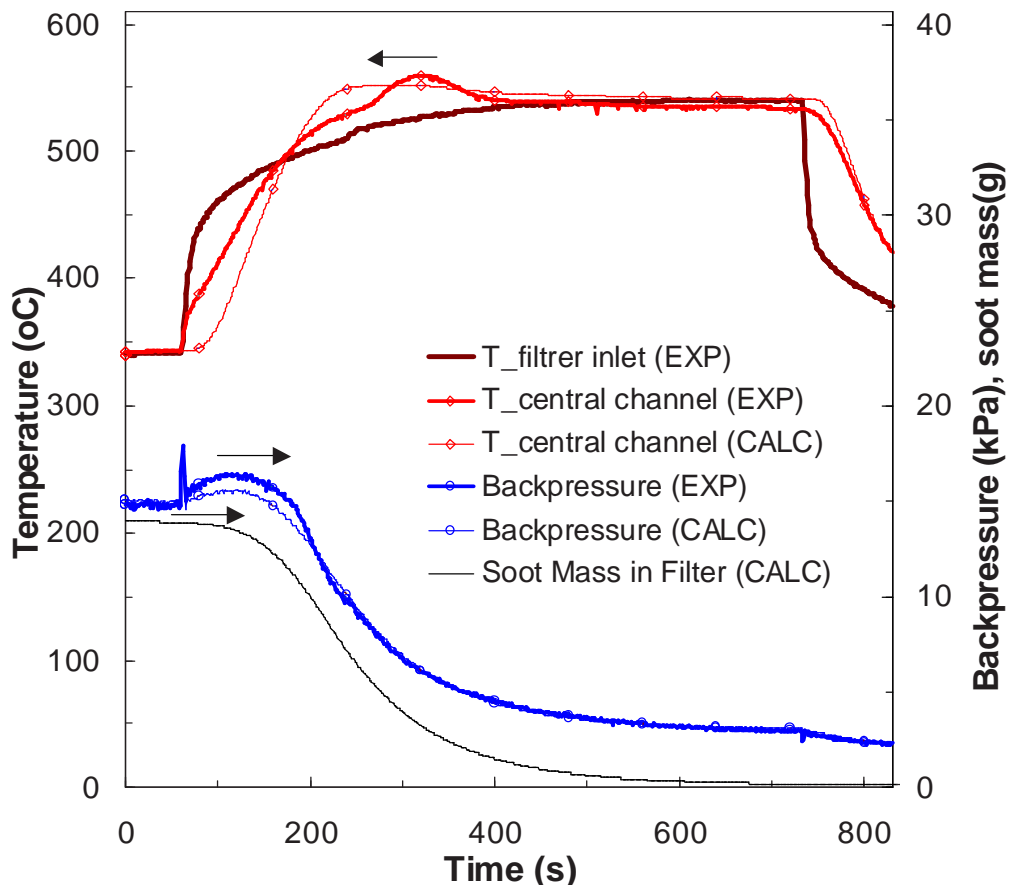


Figure 6.9: Simulation of a low mass flowrate regeneration scenario (28g/s). Measured and predicted trap temperatures near the exit of a central channel during a low mass flowrate regeneration performed at 1500rpm, 80Nm for a medium mass loaded filter at 3000rpm, 40Nm with 25ppm Ce-doped fuel. Also measurement and prediction of filter backpressure together with soot mass prediction are presented. Computation is made with $(\rho k)_p=2.2E-13$ kg/m, activation energy values: E1=1.9E5, E2=1.5E5, E3=1.2E5, E4=0.8E5, E5=0.8E5 J/mole and frequency factor values: A1=1E13, A2=5.5E10, A3=1E11, A4=2E8, A5=8E8 mole/m³s

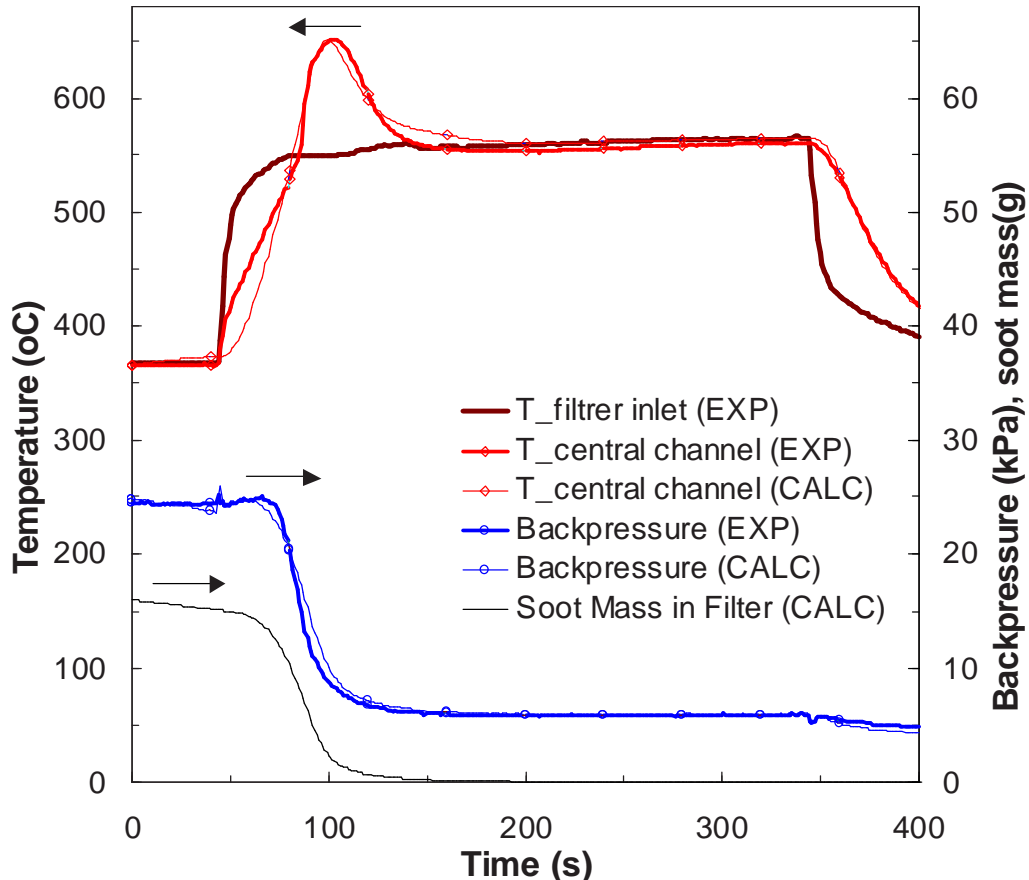


Figure 6.10: Simulation of a medium mass flowrate regeneration scenario (70g/s). Measured and predicted trap temperatures near the exit of a central channel during a low mass flowrate regeneration performed at 3000rpm, 60Nm for a medium mass loaded filter at 3000rpm, 40Nm with 25ppm Ce-doped fuel. Also measurement and prediction of filter backpressure together with soot mass prediction are presented. Computation is made with $(\rho k)_p=2.2E-13$ kg/m, activation energy values: E1=1.9E5, E2=1.5E5, E3=1.2E5, E4=0.8E5, E5=0.8E5 J/mole and frequency factor values: A1=1E13, A2=5.5E10, A3=3.5E11, A4=6E8, A5=8E8 mole/m³s

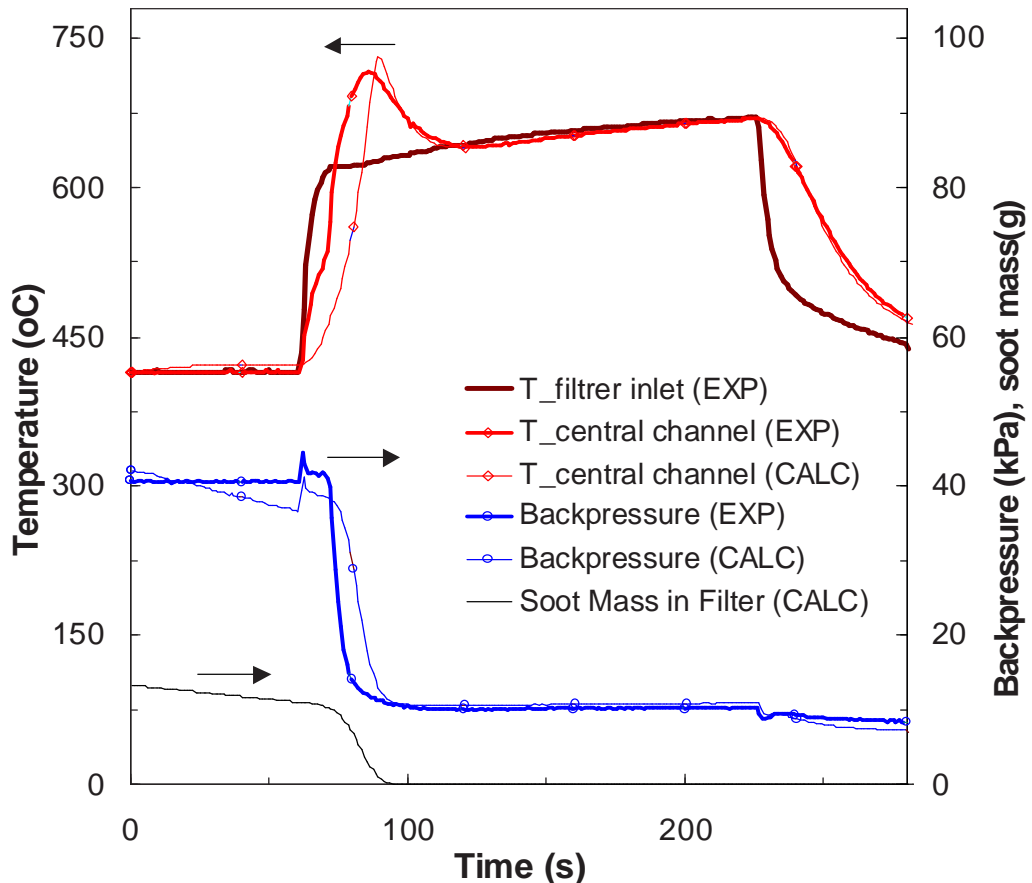


Figure 6.11: Simulation of a high mass flowrate-high temperature regeneration scenario (100g/s). Measured and predicted trap temperatures near the exit of a central channel during a high mass flowrate regeneration performed at 4000rpm, 40Nm for a medium mass loaded filter at 3000rpm, 40Nm with 25ppm Ce-doped fuel. Also measurement and prediction of filter backpressure together with soot mass prediction are presented. Computation is made with $(\rho k)_p=2.2E-13$ kg/m, activation energy values: E1=1.9E5, E2=1.5E5, E3=1.2E5, E4=0.8E5, E5=0.8E5 J/mole and frequency factor values: A1=1E13, A2=6.5E12, A3=3.5E11, A4=6E8, A5=8E8 mole/m³,s

Catalyst concentration in fuel As a first step, the case of regular soot oxidation (no catalyst in fuel) is studied. The simulation of a regeneration of a filter loaded at 3000rpm, 40Nm with the engine operating on regular (not fuel additive-doped) is presented in Figure 6.3. The values of E determined from TGA experiments produce a satisfactory prediction of the full scale process in the filter. However a certain discrepancy between the measured and the predicted filter backpressure is observed in the initial phase of regeneration. As it can be seen the model predicts a slower reduction to the pressure drop as the regeneration initiates. The reason could lie in the fact that this initial phase of the regeneration is associated with a VOF desorption process that is responsible for the rapid backpressure decrease. This situation is not predictable by the 1D pressure drop model, which considers an average soot permeability value during the whole regeneration process.

As a next step, two regeneration experiments with soot collected with 25 and 50ppm Cerium-doped fuel were performed. Starting from the simulation of the case with 25ppm Cerium doped fuel described in Figure 6.4, it should be mentioned that the fitted value of $(\rho k)_p$ was necessary to be reduced compared to the one for the soot without catalyst. It seems that the presence of catalyst inside the particulate, modifies its permeability and density characteristics.

Continuing with the simulation of the case with 50ppm Cerium doped fuel the results of Figure 6.5 indicate that the regeneration behaviour is not significantly affected by the higher fuel additive concentration. That is, the increase of catalyst concentration in fuel from 25 to 50 ppm seems not to reward with a higher catalytic effect. On the contrary, pressure drop behaviour is further affected, and a further decrease to the soot permeability is observed. Any attempt to explain these complex effects on the kinetics and pressure drop parameters of soot oxidation by Ceria must take into account the in-cylinder particulate formation mechanism that includes the injection and combustion of additive-doped fuel.

Initial soot loading The cases of 3, 6 and 9 g/ ℓ , filter soot loading were studied. The simulations of the regeneration experiments performed at 2250rpm, 60Nm for a filter loaded at 3000rpm, 40Nm with the engine operating with 25ppm doped fuel until the respective loadings are achieved are presented in Figure 6.6, Figure 6.4 (reference experiment) and Figure 6.7. The following trends are observed:

- From low-to medium-to high soot mass loading, a decrease to the $(\rho k)_p$ product is observed. Although the increase of soot layer thickness is expected to cause an increase to the soot density due to the layer compression from the exhaust flow it seems that the decrease in soot permeability is more significant. This observation is confirmed from the results of previous experimental work with single channel filters [3].
- As discussed in the previous section, higher frequency factors for the catalytic soot oxidation to CO, and, respectively, lower frequency factors for catalytic soot oxidation to CO₂ were inserted in the model to match the behaviour with higher initial soot mass in filter. The change is more severe for the 9 g/ ℓ loading, where as it can be seen in Table 6.2 where the CO/CO₂ ratio becomes about ten times higher. Any attempt to explain this behaviour must take into account the complex processes of exhaust gas oxygen diffusion through the soot layer. One could assume that in the initial phase of regeneration where the catalytic soot oxidation prevails over the thermal, the higher soot mass

makes more difficult the diffusion of exhaust gas oxygen through the deposit layer thus preventing the oxidation of Ce_2O_3 by O_2 to produce CeO_2 .

VOF content (soot accumulation condition) The effects of VOF content on the pressure drop and kinetic parameters could be assessed only indirectly, since the model considers only dry soot oxidation, without separately addressing adsorbed hydrocarbons oxidation by the catalyst. Thus, VOF oxidation kinetics must be lumped in the overall catalytic oxidation kinetics. It is known from the literature that VOF may be oxidized at temperatures as low as 200 °C and also may desorb from the particulate at higher temperatures, or even readsorb at low temperatures. Further improvements by modelling of the adsorbed hydrocarbons oxidation are currently in progress, based on the detailed study of the oxidation and sorption behavior of real diesel particulate produced by modern DI engines when run on catalyst-doped fuel [2]. The two regeneration cases considered in this validation study involve a filter loaded at 3000 rpm, 40 Nm (which is a high VOF point) and a filter loaded at 1800 rpm, 90 Nm (low VOF point). The simulations of the regenerations performed at a medium flowrate engine operation point, are presented in Figure 6.4 and Figure 6.8. Fitting of model parameters to match the experimental behaviour indicates the following trends:

- From low to high VOF content, a decrease to the value of the $(\rho k)_p$ product is observed. It seems that the VOF present in the thick particulate layer decreases the permeability of the soot layer. Furthermore secondary effects due to the adsorption–desorption processes produced from the temperature differences between the filter core and filter periphery (the VOF preferably condense on the colder outer channels of the filter) may differentiate the permeability characteristics and indicate that the mechanism is 3D.
- The lower VOF content hints to lower values for the frequency factors of catalytic soot oxidation. This could be attributed to the loss of the activity of VOF oxidation that accelerates the dry soot oxidation. According to previous experimental work for the investigation of the role of VOF to the regeneration behaviour [1], the higher soot mass is associated with a more rapid pressure drop and a higher heat release due to the higher exothermic nature of HC oxidation. On the other hand a relative increase to the frequency factor of catalytic soot oxidation to CO_2 is necessary in order to match the decreased CO produced during regeneration (the unburned hydrocarbons are oxidized by ceria mainly to CO).

6.1.4 1D modeling conclusions

The 1D DPF regeneration model that was developed in this work was applied to a systematic experimental validation procedure. The model was found capable of matching the regeneration behaviour of the DPF under the variation of soot accumulation conditions, initial soot loading and fuel additive concentrations, allowing for some variation of its parameters.

Thus, the combination of modeling with a carefully designed set of experiments as those presented herein provides insight to the operation of the DPF and indicates direction for further improvement of the model.

Specifically, this study has identified the trends of both kinetics and pressure drop models as regards the variation of soot accumulation conditions, initial soot

loading and fuel additive concentrations. Presently, these trends are not explicitly accounted for by the model. Further experimental data are required for such a task.

The model fails to match the measured behaviour of the DPF under low exhaust gas flow rates. Failure is due to the 1D nature of the model, since it is expected that, in low flow rates, non-uniformities of the flow distribution at filter inlet may significantly affect the regeneration of the DPF. This indicates that in this case a 3D approach should enhance our understanding about the variation of flow distribution at the inlet of the filter and the propagation of regeneration in general. This motivates the assessment of the 3D model that is presented in the following section under low flow rate conditions.

6.2 3D DPF model assessment

In this section, the three-dimensional DPF model is applied to a typical engine bench regeneration test. We first examine the results of the model as regards the temperature field, temperature gradient field and inlet flow field at several temporal points during the regeneration test. Then, we discuss the quality of the obtained results and the limitations of 3D modeling. Our objective is to demonstrate the capabilities and application range of the 3D model as a tool for the detailed design of diesel particulate filters.

6.2.1 Modeling results

In order to demonstrate the capacity of the 3D DPF model in the process of detailed DPF design, a simulation of the case of Figure 6.12 has been carried out. This is a low mass flow rate regeneration of the same SiC filter that was used in the 1D model validation.

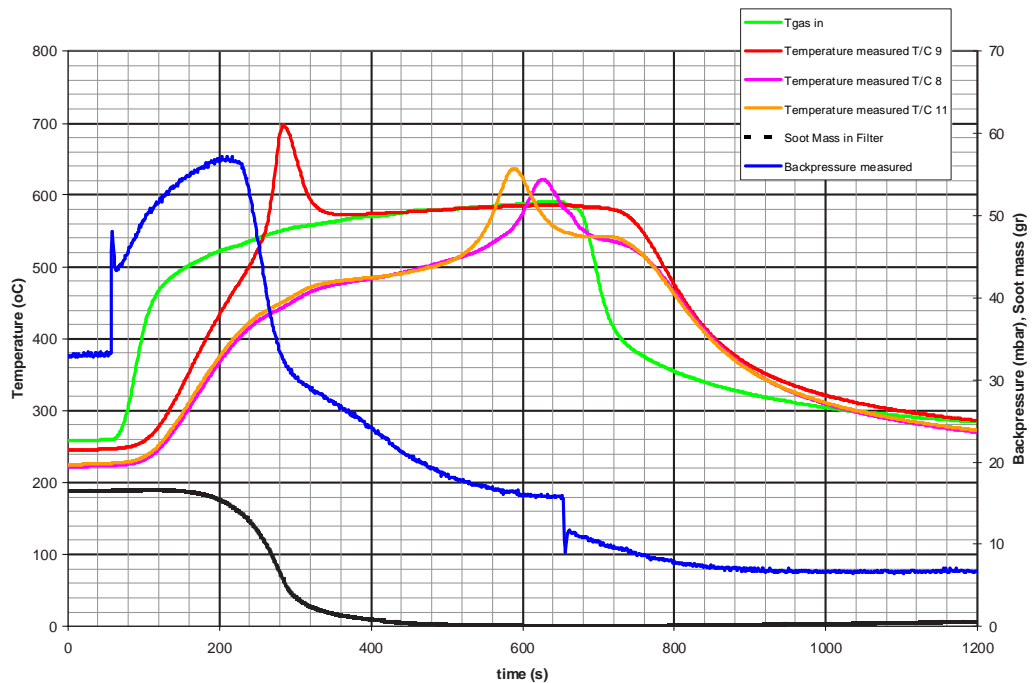
The kinetic parameters of the rate expressions that were used in this work were obtained by the validation study of the 1D DPF model. The values for the pre-exponential factor and the activation energy of each reaction is given in Table 6.3. In brief, the values of activation energies for catalytic oxidation correspond to dry soot oxidation for samples where the VOF content varies in the range between 2.5 and 8%. The pre-exponential factors were obtained by slight further tuning of the values obtained in the 1D validation study.

Furthermore, the wall permeability, soot density and soot permeability times density that were inserted in the 1D model to simulate the pressure drop behaviour of the validation experiments had the following values: Wall permeability $K=2 \cdot 10^{-3} \text{ m}^2$; Soot density $\rho_p=80 \text{ kg/m}^2$; and soot permeability times density $\rho_p K_p=2.2 \cdot 10^{-3} \text{ m}^2$.

Obviously, compared to the limited information that may be obtained by the four thermocouples of the experiment, the 3D code yields an excessive amount of information. Three-dimensional temperature fields, temperature-gradient fields for any direction and inlet flow profiles are exited by the code and may be viewed for any filter section. The model's results are examined in detail below.

Temperature field As a first step, eight snapshots of temperature fields for a section of the filter are presented in Figures 6.13 and 6.14. The elements of the canning, the insulation mat, the surrounding adhesive and the one SiC block of the

Reaction	Frequency Factor (A)	Activation Energy (E)
$C + O_2 \longrightarrow CO_2$	$1.5 \cdot 10^{13}$	190000
$C + 0.5O_2 \longrightarrow CO$	$5.0 \cdot 10^7$	150000
$C + 4CeO_2 \longrightarrow 2Ce_2O_3 + CO_2$	$8.0 \cdot 10^{10}$	120000
$C + 2CeO_2 \longrightarrow Ce_2O_3 + CO$	$5.0 \cdot 10^4$	80000
$Ce_2O_3 + 0.5O_2 \longrightarrow 2CeO_2$	$2.0 \cdot 10^{10}$	120000

Table 6.3: Kinetic parameters of the DPF model's reaction rates**Figure 6.12:** Low mass flow rate scenario employed in the 3D DPF model assessment

filter have been removed, to view compare regeneration characteristics in the center and the periphery of the filter. Regeneration starts near the filter outlet, where the maximum temperatures are also observed. It becomes apparent that the evolution of regeneration in the small periphery block is significantly different than that of a central block. Regeneration in the periphery of the filter is delayed, because of the heat losses to the ambient air. Furthermore, the adhesive that surrounds each filter block acts as insulating material, inhibiting the propagation of the heat released in central filter blocks to those in the filter periphery. Thus, the small size of the segment of the filter in the specific filter design is demonstrated to result in sustained incomplete regeneration, due to the low temperatures.

Nevertheless, the computed delay in the regeneration of the outlet blocks of the filter is significantly less than that measured. As illustrated in Figure 6.12, regeneration at the filter periphery occurs more than 5 minutes after the regeneration of the inlet block. It is beyond the capacity of the model in its current state to predict such a delay, which may thus be attributed to either phenomena that are not included in the model, or uncertainty regarding the input data of the model. More specifically:

First, the regeneration model lacks a mechanism to include the effect of the soot's VOF, which may be responsible for such a regeneration. This regeneration seems insensitive to the first regeneration occurring in the inner filter block and seems more likely connected to the gradual elevation of the inlet gas temperature. Second, the initial filter temperature and accumulated soot distributions may be significant in such a scenario, while, for the time being, the model assumes that the above distributions are uniform. Third, uncertainties regarding the thermophysical properties of the filter materials and especially the soot layer may largely influence the model's predictive ability.

Temperature gradients field The next step in the detailed study of the DPF regeneration behaviour is the study of temperature gradients. In Figure 6.15, the field of the thermal gradient magnitude is plotted for three characteristic time points. The maximum temperature gradients of the inner filter block are initially observed near the outlet of the filter, at the boundary where the plugs start. This is a consequence of the higher thermal capacity of the filter in the plug region. As the regeneration moves to the periphery of the filter, the same happens with the thermal gradients. Maximum thermal gradients of the simulation are observed at the small periphery block at the interior cement–SiC interface. Subsequently, thermal gradients gradually diminish, although their maximum values still remain at the small peripheral block of the filter.

The temperature gradient fields are employed in the computation of the thermal stress field of the filter. This process has discussed in more detail in [7]. In brief, we note that maximum thermal stresses of the order of 20 MPa have been computed in severe filter failure scenarios like that of Figure 6.16, which illustrates a sudden vehicle deceleration occurring shortly after the onset of regeneration in a heavily loaded SiC DPF. Such levels of thermal stresses are a result of excessive heat release that causes temperatures at the centre of the filter to rise to about 900 °C and, locally, presumably even higher. The thermal stresses lead to the failure of the filter material by cracking, as confirmed by full-scale experiments. Thus, the identification of high thermal stress concentrations areas like those of Figure 6.15 is very important for improvements in the detailed design of the filter.

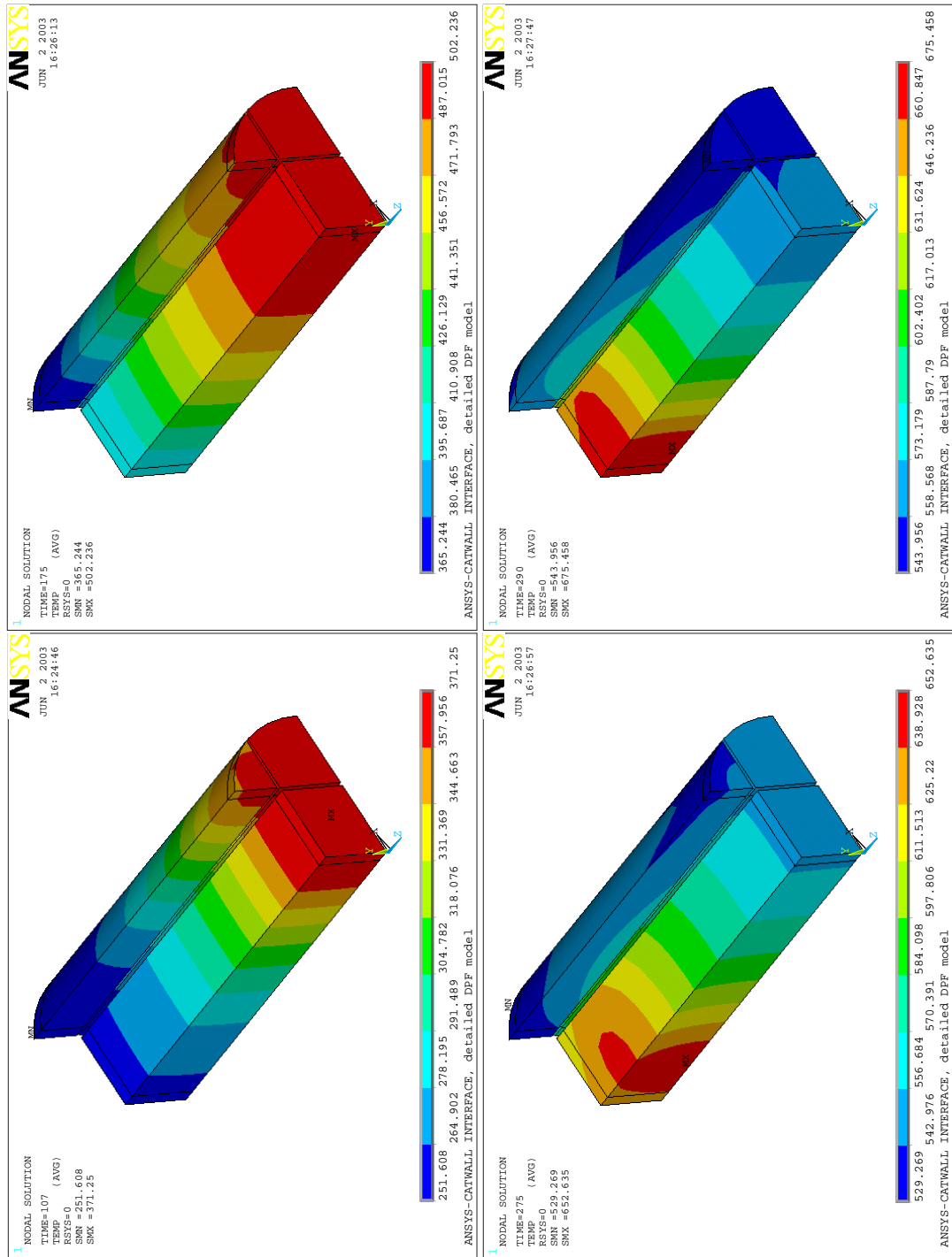


Figure 6.13: Sequence of snapshot views of the predicted temperature field of the SiC, in the interior of the DPF, at the SiC-cement boundary, at 107, 175, 275 and 290 s

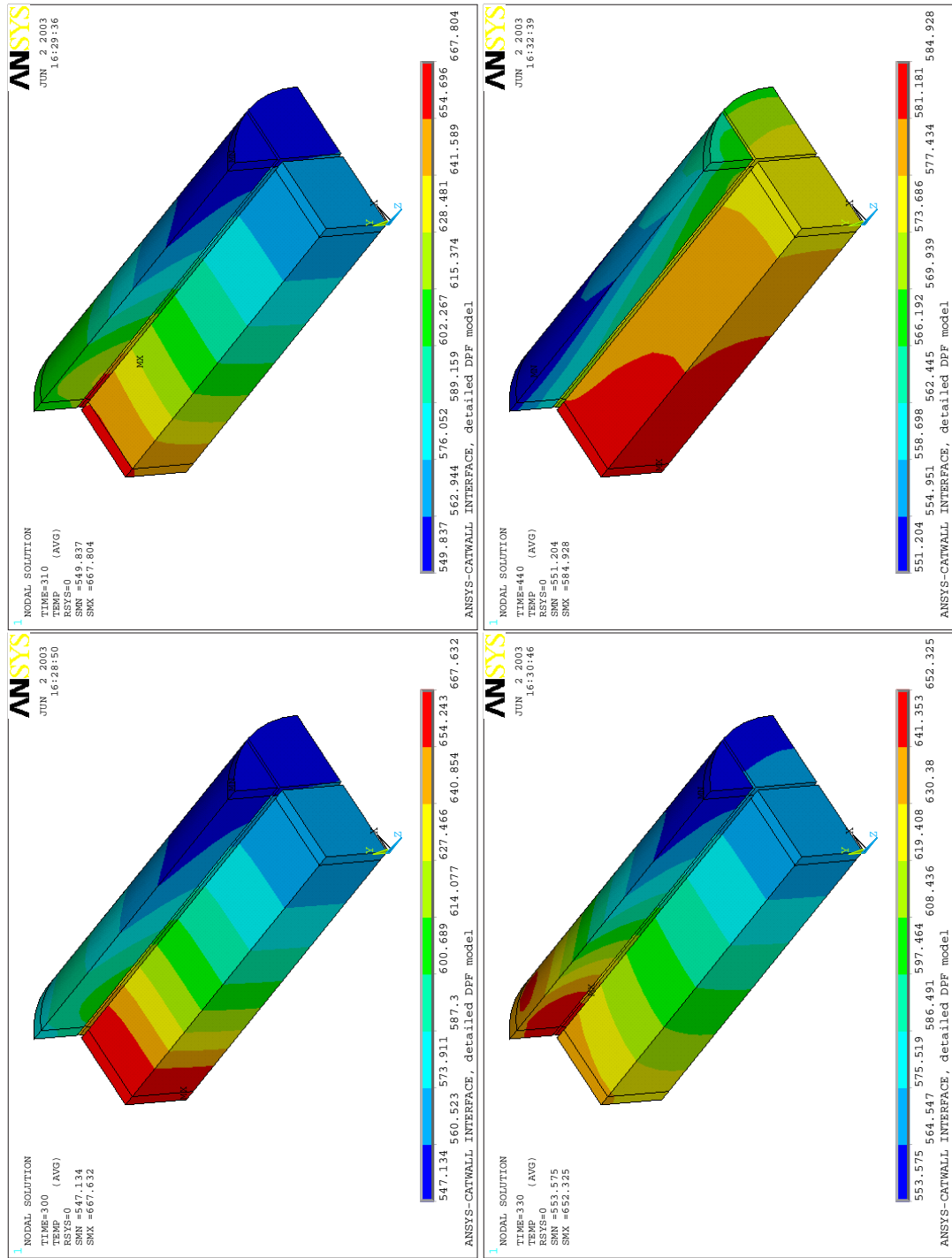


Figure 6.14: Sequence of snapshot views of the predicted temperature field of the SiC, in the interior of the DPF, at the SiC–cement boundary, at 300, 310, 330 and 440 s

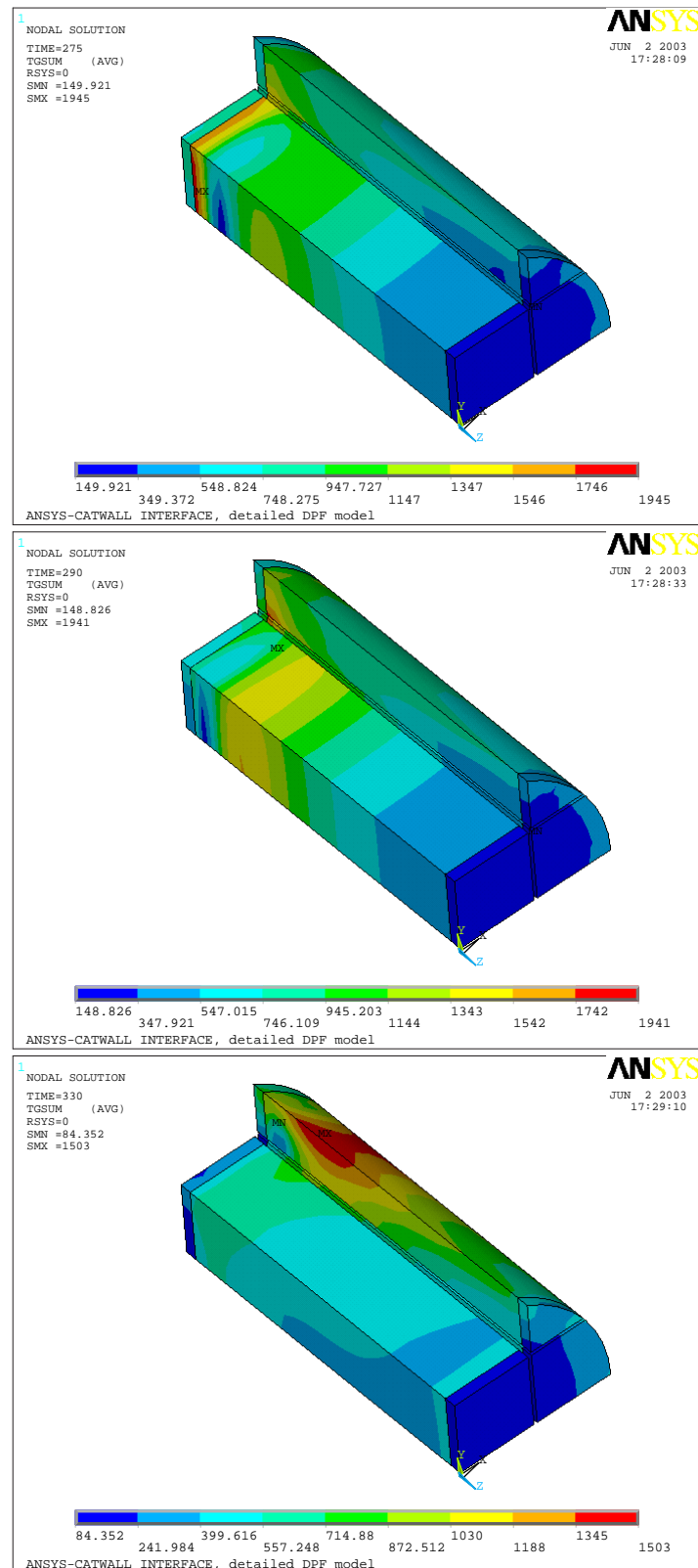


Figure 6.15: Low mass flow rate scenario employed in the 3D DPF model assessment

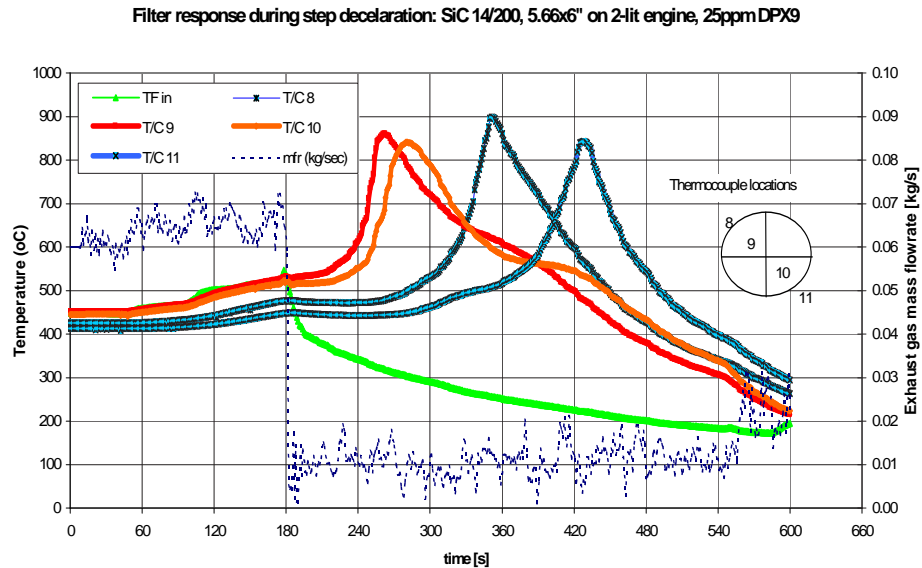


Figure 6.16: Catastrophic deceleration test with fuel additive. Initial filter soot loading: (est.) 29g. Initial engine operation at 2500 rpm–engine load 80 Nm. Filter inlet temperature 500 °C. Step decrease to 800 rpm–load 20 Nm, inlet temperature 300 °C.

Inlet flow field The third step taken in this study is the examination of the flow profiles at the inlet of the filter, as affected by the filter loading. Specifically, incomplete regenerations lead to prominent flow maldistribution, which depends on the non-uniformity of the soot layer distribution and the corresponding flow resistances. To quantify this effect, we define an index of the mass flow rate non-uniformity for each brick, as follows:

$$\gamma = \frac{\dot{m}_i}{\dot{m} \frac{A_i}{A}} = \frac{\text{flow entering the brick}}{\text{flow that would enter the brick if flow profile were uniform}} \quad (6.1)$$

The above index is unity for uniform flow. Values greater than unity imply higher mass flow rates than those expected with from a uniform inlet flow profile, and vice-versa.

In Figure 6.17, this index is plotted through the first 500s of the simulation for the four bricks that comprise the quarter of the DPF. In the beginning of the simulation, the filter is assumed uniformly loaded, therefore the non-uniformity index equals unity for all bricks. However, during the regeneration, the model predicts a significant non-uniformity of the flow. Specifically, the flow is channeled mainly through the central brick of the filter, since regeneration occurs there first. Mass flow rates through the center brick are approximately double compared to those at the filter periphery. The above results of the inlet flow distribution are aligned with the experimental findings of Stratatakis and Stamatelos [4].

A more detailed view of the non-uniformity of the inlet flow is also given in Figure 6.18, where a snapshot of the percentage of the flow entering each sector of the model is presented. It is noticeable that the model also predicts a mass flow rate profile across each filter block, which declines towards the outlet of the filter. This effect is the result of the temperature field within the filter. Temperatures decline

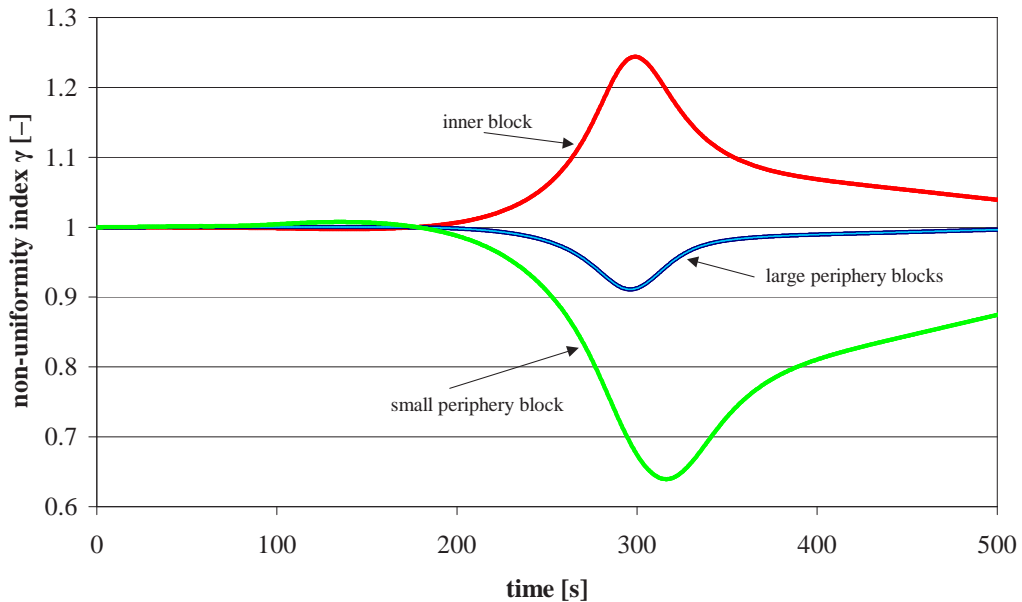


Figure 6.17: Mass flow rate non-uniformity index during the first 500 s of the simulation, for the four bricks of the filter.

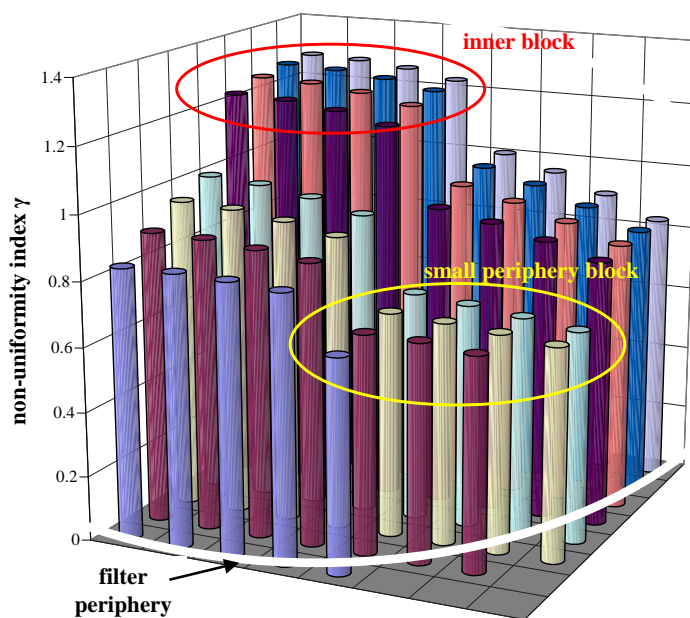


Figure 6.18: Mass flow rate non-uniformity index at 300 s of the simulation, for the sectors of the filter.

at the filter periphery owing to the losses to ambient air, and thus less soot mass is consumed and the flow resistance is higher.

The flow non-uniformity becomes milder after regeneration is propagated to the periphery of the filter. It is important to note, though, that, according to Figure 6.17, the flow profile remains non-uniform after the end of the regeneration, because of the incomplete regeneration predicted by the model. This has an impact to the total pressure drop induced by the filter, and is connected to the problem of estimating the soot load level of the filter employing pressure drop measurements.

6.2.2 Discussion

Summarizing the above, it appears that the phenomena involved in the operation of the DPF are highly complex and a formulation of a workable modeling approach is not trivial. The case study used herein was chosen in purpose to demonstrate this. The three-dimensional DPF model, accounts for the modular, anisotropic structure of the filter with great detail, and it is also enhanced with a submodel for the estimation of the effect of soot mass distribution to the inlet flow profile. Despite its increased sophistication, and despite its realistic results regarding the inlet flow profile, it is not able to predict the phasing difference between inlet and periphery regeneration onset (Figure 6.12). This leads us to the following conclusions:

First, the uncertainties associated with (a) the regenerations owing to the VOF content of the soot and (b) the thermophysical properties of the filter materials and soot deposit greatly influence the performance of the model. More work is needed related to the above directions, that may probably further enhance the reliability and the accuracy of the filter model. Nevertheless, it is speculated that the stochastic nature of such phenomena will continue to be a limiting factor of the accuracy of any model, regardless its complexity and sophistication level.

Second, the present study indicates that, even under such limitations, well-balanced engineering models have the potential to become useful tools in the design of exhaust aftertreatment systems based on diesel particulate filters. Simplified 1D models, probably with the introduction of some mechanism to include the effect of soot VOF content will give more insight especially regarding the conditions under which regenerations onset under realistic filter operation. Such improvements can lead to better tuning of the exhaust system control, reducing the risk of catastrophic uncontrolled regeneration and improving the vehicles' performance, fuel economy and drivability.

The development of a 3D regeneration model is not intended to substitute the 1D model, since the scope of each model is different. Rather, the two models should be viewed as complementary tools. As mentioned above, the application of the 3D model is based on the original tuning of the reaction kinetics performed by the 1D model for low computational cost. Furthermore, the 1D model is useful in the initial stage of the exhaust system design, where it should provide a rough view of the overall performance characteristics of the filter. The need for 3D modeling comes to the foreground in detailed DPF design and optimization studies, when local phenomena and especially thermal stress calculations are of interest.

Indeed, in its current state, and despite the acknowledged limitations, the ANSYS-CATWALL 3D DPF model already provides insight to the evolution of regeneration in the modular SiC filter and may be used for the determination of stress concentrations and the effect of critical material properties. This could be a valuable aid towards the identification of design flaws and decisive directions for

research.

What should not be expected, though, is that the advances of modeling will enable the deterministic prediction of the operation of the filter under any operating conditions and in any scale. A great many of details of the phenomena involved in the DPF regeneration will probably continue to elude us, because of their complexity and non-deterministic nature. It is most probable that the quantitative prediction of DPF operation will be possible only regarding overall characteristic quantities, such as the maximum temperature and pressure drop level. On the contrary, the prediction of detailed quantities, such as e.g. the temperature at any arbitrary point in the filter, is not expected to be other than qualitative.

Nevertheless, success for engineering modeling comes from their potential to aid the design engineer to improve and optimize the targeted systems, which does not necessarily imply a thorough understanding of the underlying phenomena, let alone their quantitative prediction. The situation seems similar with that of the catalytic converter modeling, which is being applied as a tool for the optimization of the respective exhaust aftertreatment systems, while the details of the heterogeneous catalysis phenomena remain largely obscure. Engineering DPF modeling is expected to follow a similar path of development.

6.2.3 3D modeling conclusions

- The 3D DPF regeneration model that was developed by linking a commercial FEM software with the base 1D CATWALL regeneration model was employed to simulate the behaviour of a modular SiC DPF under realistic regeneration conditions.
- The 3D model greatly extends the potential of its 1D counterpart towards the prediction of the full temperature and temperature-gradient fields within the filter, the non-uniformity of the flow and the effect of incomplete filter regenerations to the pressure drop of the filter.
- The model reveals the three-dimensional propagation of the regeneration within the filter as influenced by the filter's modular and asymmetrical structure. The accompanying effect of the soot mass distribution within the filter to the gas flow profile at the inlet is also illustrated.
- An important field of future application of the 3D model is the stress analysis and determination of stress concentrations in the detailed design of DPFs. Such an analysis may be performed by ANSYS after the evolution of the temperature field of the finite element model has been determined. Analysis of the thermal stresses of the filter under failure scenarios is expected to yield directions for the improvement of filter design, especially regarding modular SiC filter with highly anisotropic structure.
- The limitations of the model have also been illustrated. The test scenario was purposely selected to demonstrate the stochastic nature of the regenerations induced by the VOF content of the soot. The model's lack of a validated mechanism to account for it is a marked weakness of the base 1D regeneration model. The exploitation of experimental evidence regarding the VOF effect [1] is expected to assist the corresponding model development and validation this respect.

- Although the initial results presented herein are promising, it remains yet to be tested more thoroughly in this aspect, based on validation experiments scheduled for the future.
- It is concluded that the development and validation of a workable model for the DPF regeneration behaviour is not trivial, mainly because the uncertainties associated with the properties and phenomena of the studied system. Nevertheless, engineering modeling has already shown great potential for its application as an engineering tool for the optimization of DPF-based aftertreatment systems, and its accuracy and application range is expected to develop more in the future.

6.3 Summary

- The 1D DPF regeneration model that was developed in this work was applied to a systematic experimental validation procedure. The model was found capable of matching the regeneration behaviour of the DPF under the variation of soot accumulation conditions, initial soot loading and fuel additive concentrations, allowing for some variation of its parameters.
- The model failed to match the measured behaviour of the DPF under low exhaust gas flow rates. Failure is attributed to non-uniformities of the flow distribution at filter inlet that are not accounted for by the 1D model.
- Subsequently, the 3D DPF regeneration model was employed to simulate the behaviour of a modular SiC DPF under realistic regeneration conditions.
- The model revealed the three-dimensional propagation of the regeneration within the filter as influenced by the filter's modular structure and the non-uniform inlet flow profile.
- An important field of future application of the 3D model is the stress analysis and determination of stress concentrations in the detailed design of DPFs, which is expected to yield directions for the improvement of filter design.
- The test scenario was purposely selected to demonstrate the stochastic nature of the regenerations induced by the VOF content of the soot. The exploitation of experimental data on the basis of the VOF model developed in Chapter 3 is expected to further enhance the accuracy of the model.
- Although the initial results of the 3D model are promising, it remains yet to be tested more thoroughly, on the basis of validation experiments scheduled for the future.
- It is concluded that the development and validation of a workable model for the DPF regeneration behaviour is not trivial, mainly because the uncertainties associated with the properties and phenomena of the studied system. Nevertheless, engineering modeling has already shown great potential for its application as an engineering tool for the optimization of DPF-based aftertreatment systems, and its accuracy and application range is expected to develop more in the future.

References

- [1] G. A. Stratakis, G. S. Konstantas, and A. M. Stamatelos. Experimental investigation of the role of soot volatile organic fraction in the regeneration of diesel filters. *Proc Instn Mech Engrs, Part D: J. Automobile Engineering*, 217:307–317, 2003.
- [2] G. A. Stratakis and A. M. Stamatelos. Thermogravimetric analysis of soot emitted by a modern diesel engine run on catalyst-doped fuel. *Combustion and Flame*, 132:157–169, 2003.
- [3] G. A. Stratakis, D. L. Psarianos, and A. M. Stamatelos. Experimental investigation of the pressure drop in porous ceramic diesel particulate filters. *Proc Instn Mech Engrs, Part D: J. Automobile Engineering*, 216:773–784, 2002.
- [4] G. A. Stratakis and A. M. Stamatelos. Flow distribution effects in the loading and catalytic regeneration of diesel particulate filters. *Proc Instn Mech Engrs, Part D: J. Automobile Engineering*, 2003. (*Submitted*).
- [5] S. C. Sorenson, J. W. Hoj, and P. Stobbe. Flow characteristics of SiC diesel particulate filter materials. *SAE paper 940236*, 1994.
- [6] H. Aoki, A. Asano, K. Kurazono, K. Kobashi, and H. Sami. Numerical simulation model for the regeneration process of a wall-flow monolith diesel particulate filter. *SAE paper 930364*, 1993.
- [7] G. N. Pontikakis, A. M. Stamatelos, K. Bakasis, and N. Aravas. 3-D catalytic regeneration and stress modeling of diesel particulate filters using ABAQUS FEM software. *SAE paper 2001-01-1017*, 2002.

Chapter 7

From computational cores to engineering tools

In the previous chapters, we have developed two models for the monolithic catalytic converter and the diesel particulate filter respectively. For the catalytic converter model, two different kinetic submodels were formulated, which describe the chemical phenomena occurring in two different washcoat formulations, used for the three-way catalytic converter and diesel oxidation catalyst respectively. The reaction rates embodied in the kinetic submodels necessitate the estimation of a kinetic parameters set, a task that was accomplished by coupling the catalytic converter model with an optimization procedure that uses a custom performance measure and a genetic algorithm.

Subsequently, it was demonstrated that the models are capable of describing the operation of the catalytic converter and the diesel particulate filter respectively in a quantitative manner, so that they may be employed by the design engineer as computational tools in the process of exhaust aftertreatment systems analysis and design.

In this chapter, we attempt to demonstrate that the power and capabilities of the models that have been developed herein stems from their design principles, which are consistently oriented towards building tools for the automotive engineer that can be used for the design and analysis of exhaust aftertreatment systems.

Specifically, we first attempt to identify the primary industry requirements for any model that is to be used for CAE design of automotive powertrain components. Then, the scope and scientific disciplines of the models employed in the design of powertrain components are discussed, and a classification of three major modeling levels is postulated. It is recognized that a different modeling paradigm is connected to each modeling level. Therefore, we subsequently suggest a set of design concepts and requirements that embody the modeling paradigm for the exhaust aftertreatment devices, and address the requirements of the automotive industry. If this modeling paradigm is combined with an implementation that is oriented towards versatility and ease of use, the result should be the transformation of a computational core to a real engineering tool, which is of benefit to both the developer of the model and its final user.

7.1 Industry requirements

A primary objective of the automotive industry is to build fast-to-market and right-first-time, cost-effective exhaust lines that will enable the vehicle to succeed in the legislated driving cycle tests. Because of the increasingly stringent emission standards, we observe a trend towards more complicated exhaust lines. Their successful design obliges the designers to study the exhaust line as a system, comprising of the engine, exhaust piping, exhaust aftertreatment devices and control.

Because of the complexities involved in the operation of its components, such a system presents significant difficulties as regards its successful design and optimization. Relying solely on experimental testing of different system configurations implies elevated cost and design time. Therefore, exhaust systems engineering could be significantly benefited by the incorporation of computer-aided engineering (CAE) practices in the design of exhaust lines, which is currently under way in the automotive industry.

The automotive industry has already been applying CAE methodologies in the design process of most automotive components and subsystems [1]. Nevertheless, this has not been the case with the exhaust line, because of the lack of reliable models oriented to engineering usage. A bottleneck here has always been the modeling of aftertreatment devices. Currently, an indicative wish-list of the automotive industry for an ideal modeling tool of the kind seems to be the following:

- *Reliability.* It should be crosschecked and validated thoroughly in real world case studies before conclusions and design decisions can be drawn using it.
- *Speed.* It should run reasonably fast with common computer equipment so that it can be tested, adjusted and used within the time and cost constraints of the automotive industry.
- *Versatility.* It should be easy to modify and apply to different system configurations, in order to enable their assessment and tuning.
- *Ease of use.* It should be easy to validate and use by automotive engineers who are not modeling experts.
- *Minimum input data.* It should require input data that may be acquired by a minimum number of routine experiments, in order to keep cost low and to prevent input data uncertainty and errors.

The above requirements are connected to a modeling paradigm which has been established by models that have been adopted by the automotive industry for the design and optimization of automotive components other than the catalytic converters. A comparison of modeling practices for such automotive applications hints to a rough classification of models, which is useful for the understanding of the capacity, applicability and the pre-requisites of different models depending on the system under study.

7.2 Comparative discussion of various modeling levels

Historical evolution of modeling in the automotive powertrain design date back to the sixties. Figure 7.1 summarizes the evolution of the various levels of computer-

MODEL APPLICATIONS IN POWERTRAIN DESIGN (1960–today)

Level	1	2	3
Scope	Mechanical + Dynamic computations in components	Heat transfer + Thermal stress computation	Combustion, Gas exchange processes, exhaust system gas dynamics, catalytic exhaust after-treatment
Models employed	FEM, Lumped Parameter Models	FEM, 0-D models of engine cycle	CFD, reacting flow codes, 1D to 3D
Disciplines involved in the models	Mechanics, Rigid body dynamics	Engine cycle Thermodynamics, heat transfer, thermoelasticity	Turbulent flows, Turbulent premixed and diffusion flames, laminar flows + heterogeneous catalysis, Compressible flows

DETAILS OF LEVEL 3 MODELING SUB-CATEGORIES

Level	3a	3b	3c	3d
Scope	Gas exchange processes, cooling system	Combustion in cylinder	Catalytic exhaust after-treatment	Exhaust system gas dynamics
Models employed	CFD	CFD + reactive flows modeling	1D reacting flow modeling	1D acoustic modeling
Disciplines involved in the models	Turbulent flows	Turbulent flows + homogeneous reaction kinetics	Laminar flows + heterogeneous reaction kinetics	Compressible flows

Figure 7.1: Modeling levels of automotive powertrain components

aided engineering applications in the design of automotive powertrain components during the last 40 years. Modeling practices have gradually progressed from simple to more complicated components and processes. We may roughly divide three levels of modeling, with different objectives and requirements, explained below.

- **Level 1 modeling.** The first applications dealt with stress fields computations on simple components like the connecting rod or crankshaft, with the objective to support the mechanical design of the studied system. The introduction of finite element methods for such calculations severely reduced the heavy dependence on unknown stress concentration factors, that should be determined by extensive experimental effort, which was not directly transferable to different designs.

Thus, the finite elements methods first introduced modeling and CAE practices in the automotive industry during the seventies and through their success, established a paradigm for applications of modeling in other fields of automotive design. We refer to this modeling paradigm as Level 1 modeling. Its primary characteristics are that it supports mechanical design, requiring only geometrical data and material properties of the system under study.

Level 1 component models have been evolved during the last years into vehicular powertrain systems models that can be used in powertrain system design, development, and analysis. In-house computer models of vehicle systems are now routinely used by automobile manufacturers as a tool to estimate fuel economy and performance [2]. Programs of this type allow a broad spectrum of users within these companies to access these programs and acquire knowl-

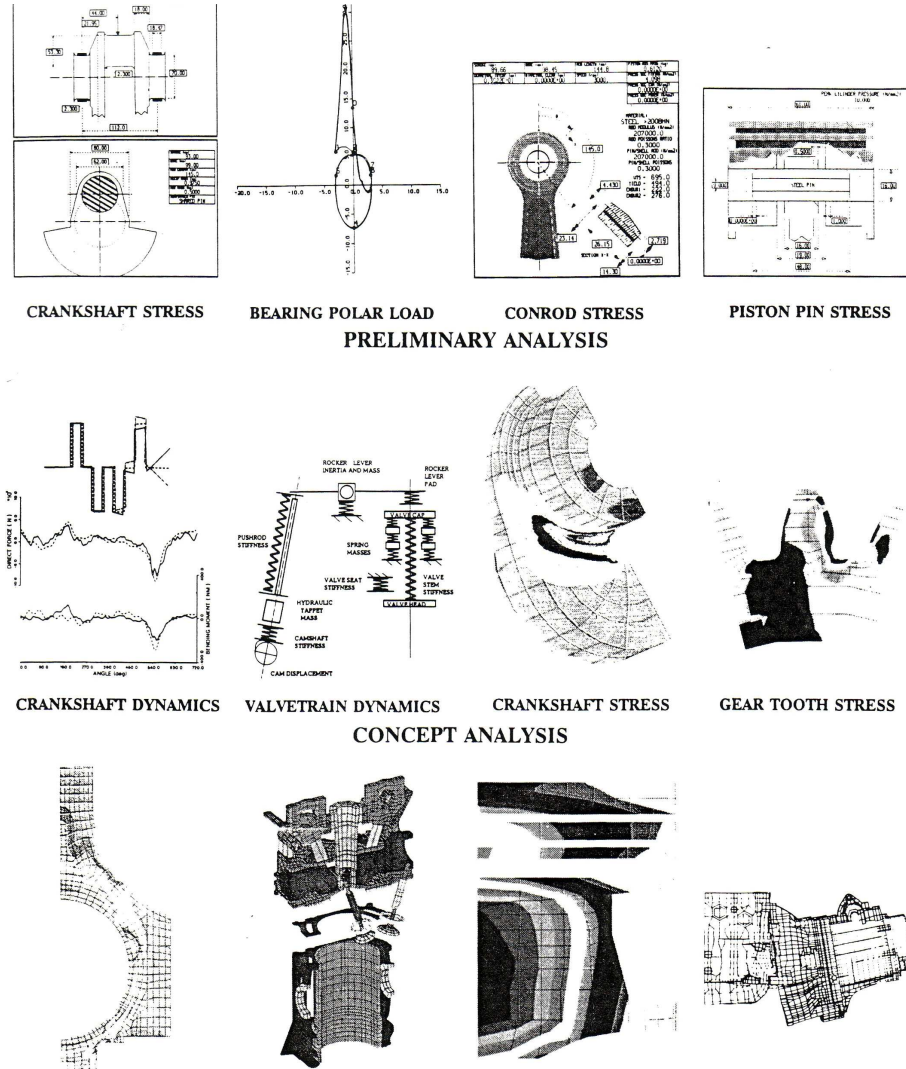


Figure 7.2: CAE applications in the design of automotive powertrain components. Adapted from Sandford and Jones [1]

edge of general vehicle performance data in a relatively short time and at a low cost without the difficulties of performing actual vehicle tests. In recent years, these and other similar programs have been refined to improve their fidelity and accuracy. More detailed CFD models have been included to provide predictions of air flow around and under the hood of the simulated vehicles, as well as for cooling flows. Structural dynamics programs have come a long way in recent years so that expensive crash tests can now be simulated with reasonable fidelity on supercomputers. Again, in all of these instances the simulations do not entirely replace experimentation, but experimentation now plays a very important role in tuning or calibrating these simulation programs. Company products-specific knowledge and knowhow acquired during the years are invested in these in-house software packages.

- **Level 2 modeling.** The extension of modeling practices to include computations of components directly in contact with fluids — like combustion gases or cooling system fluids (piston, cylinder head, valves, cylinder liners) — necessitated the modeling of the engine cycle. Zero-dimensional modeling, already being developed during the late sixties, was fully exploited during the late seventies. In this thermodynamic approach, a simplified (tunable) phenomenologic combustion law was employed along with certain tunable combustion chamber and cooling system heat transfer correlations.

Such modeling practices date back to the ‘70s and introduced a more complicated modeling approach, which we call Level 2 modeling. The objective at this level was to supply thermal boundary conditions for the computation of the temperature and thermal-mechanical stress fields which again supported the mechanical design at the above-mentioned components. Figure 7.2, adapted from Sandford & Jones [1], presents typical Level 1 and 2 applications in the design of automotive powertrain systems.

- **Level 3 modeling.** During the ‘80s, the advent of CFD brought new dimensions in powertrain design. In this case, the objective was to support the combustion chamber design, combustion optimization, emissions reduction, cooling system optimization, exhaust gas dynamics etc. CFD modeling made clear that modeling of complex, chemically reacting flows was tractable.

In this category of models, the augmentation or diminishing of chemical and transport phenomena that are involved in the corresponding processes are central to the design of the respective components. The mechanical design of the system is here of lower priority.

Applications in this field fall into four broad categories:

- *Level 3a.* Turbulent flows, primarily met in gas exchange processes and the cooling system of the engine. CFD is commonly applied to solve such problems.
- *Level 3b.* Chemically reacting turbulent flows with homogeneous (gaseous phase) reactions. This is mainly the case for the design of the combustion chamber of the engine towards efficiency maximization and emission reduction. It necessitates CFD computations coupled with modeling of chemical reactions under certain simplifying assumptions. For example,

in the case of DI diesel combustion, flamelet modeling allows the application of comprehensive chemical mechanisms, which include all relevant chemical combustion processes that occur during autoignition, the burnout in the partially premixed phase, the transmission to diffusion burning and the formation of NOx and particulates. Separating the numerical effort associated with the resolution of the small chemical time and length scales from the CFD computation of the engine cycle, the resulting 1D unsteady set of PDEs is advantageously solved online with the 3D CFD code [3]. The advent of efficient parallel processors enables the application of LES methods with hybrid grids in the CFD simulation of SI engine cycle processes[4]. In order to be effective, these complicated and demanding modeling approaches are supported by advanced experimental studies [5]. Up to the late nineties, the total simulation time for a complete engine cycle was of the order of weeks to months, however, recent progress with rapid template-based meshers and parallel flow solvers and post-processors, reduced the total time to a few days [6].

- *Level 3c.* Laminar flow with heterogeneous catalytic reactions. This case corresponds to the modeling of various reactors for the exhaust aftertreatment and reduction of emissions. The modeling approaches for the catalytic converter and diesel particulate filters presented in this work fall into this category. Because of the laminar flow, the corresponding computations are simpler here but focus moves to the accurate prediction of the effects of extremely complicated heterogeneous reactions and sorption phenomena.
- *Level 3d.* 3D compressible, pulsating flows, which are met in the modeling of the inlet and exhaust manifold and the piping design regarding cylinder interaction, and the modeling of engine valves and turbocharging components.

Despite the considerable developments in the application of CAE in powertrain design during the last 40 years, the paradigm in this area remains that of the '70s (Level 1). The characteristics of the models presented previously (Section 7.1) mainly originate from this paradigm. For this reason, in most cases the design engineer expects that the model will save him a lot of experiments without requiring any substantial input from his experience or any experimental data, except from geometrical data or data regarding material properties.

Only recently the industry begins to assimilate a new paradigm corresponding to Level 2, where the chemical and transport phenomena involved in the operation of the components enter the process of mechanical design as boundary conditions of the respective models. At this level, chemical and transport phenomena are recognized as playing a significant role, but they are modeled in a phenomenological and thus simplified way (e.g. Wiebe function of fuel burning rate or Woschni correlation for in-cylinder heat transfer). Usually, it is expected that complications arising from 3D effects and transient conditions may be averaged and a simplified approach is adequate.

Level 3 modeling focuses primarily on the chemical and transport phenomena occurring in the components under study. A part of this phenomena are modeled in more detailed by use of CFD computations. However, another part, and especially that involving complex reactions coupled with heat and mass transfer is

extremely complex (turbulent premixed or diffusion flames). Moreover, there exists another part for which no integrated and validated computational framework is yet established. This is especially the case for the modeling of exhaust aftertreatment components that has been the aim of this study.

In particular, within the aftertreatment devices dealt with in this work, there is lack of fundamental understanding of the processes involved in the case of heterogeneous catalytic reactions, physical and chemical adsorption-desorption processes, filtration and formation of particle layers (cake filtration) or dendrites (deep-bed filtration). In other words, the most dominant phenomena that are involved in the operation of exhaust aftertreatment devices are only marginally understood qualitatively and usually there is no well established quantitative theory.

The reason for this situation is twofold. First, the inherent complexity of these phenomena is very high and insight in the underlying processes is very difficult to attain, usually necessitating very accurate measurements and complicated measurements. As an example, we should bear in mind that the exact path of the heterogeneous catalytic reactions in the various washcoats is practically intractable, despite the numerous chemical studies, because of the complexity of the phenomena as well as the rapid change of washcoat technology.

Second, the exhaust aftertreatment devices operate under highly transient and even unknown conditions. The experimenter's lack of ability to measure the hydrocarbon mixture of the exhaust gas—especially as the content of the mixture changes transiently according to engine operation—is a characteristic example of this case. Most importantly, laboratory studies are often invalidated under real-world operating conditions, where unforeseen interactions emerge and cause significant deviation from laboratory operation. A typical example in this regard is the inhibition or poisoning of catalytic converter reaction rates because of the presence of exhaust gas species absent in the laboratory setup.

The modeling efforts at this level generally view the chemical and diffusion phenomena through simplified phenomenological laws. Such laws are based on whatever fundamental insight is provided by scientific disciplines but have various drawbacks and in no case may be considered as a substitute for the lack of integrated theory. Heterogeneous rate expressions or foam filter filtration efficiency expressions are typical in this regard. The most common issues that are introduced by the use of phenomenological laws are the following:

- The accuracy of such laws depends greatly on several parameters which are not *a priori* known and should be experimentally estimated. The development of the genetic algorithm optimization methodology described in Chapter 4 addresses exactly this issue in the case of catalytic converter reaction rates.
- Such phenomenological laws are valid mainly in the range of conditions under which they were derived. This implies that their usefulness is usually limited. On the other hand, the Voltz kinetic rate expressions are a classic example of phenomenological law that is valid—or, at least, workable—outside the range of conditions for which it was originally developed.

Summarizing, the fundamental phenomena occurring in the devices studied in Level 3c modeling that has received our focus herein are obscure, may not be easily viewed under an integrated theoretical framework and do not accept a straightforward quantitative description. Thus, when formulating the system of differential

equations that usually comprise the mathematical model, the engineer is usually found in a position where several terms of the equations are of unknown value, or even of unknown form.

This situation should be contrasted with the Level 1 modeling problems, where a theoretical framework exists (e.g. continuity equations, elasticity theory etc.) and has been thoroughly validated. In this case, the modeling difficulties are of mathematical nature only, that is, the remaining difficulty is to solve the mathematical model accurately and efficiently.

Nevertheless, the engineer that attempts to model exhaust aftertreatment systems (Level 3) is expected by the automotive industry to comply with requirements that correspond to a completely different modeling paradigm (Level 1), where a general theory enables far more accurate and consistent computations.

This extrapolation of the Level 1 modeling paradigm to problems that belong to the Level 3 modeling paradigm is unfortunate and cannot yield acceptable results. The applicability of such an engineering model depends heavily on (a) realistic phenomenological laws that embody the intuition gained by more fundamental research and (b) high quality input data for the accurate and non-ambiguous determination of tunable parameters of the model. Both of the above points are expected to be input to the developer of such a model and no model formulation may compensate for their absense and, in fact, are the cornerstones for the whole development and utilization process of a engineering model.

It appears that a new modeling paradigm should evolve that is pertinent for the development and application of Level 3c engineering models. Below, we attempt to roughly shape such a paradigm, by summarizing the major design concepts and requirements that, in our view, should be followed to accomplish this task. This paradigm has dominated the design and development of the models that have been presented in this work.

7.3 Design concepts and requirements

In order to build engineering models that belong to modeling Level 3c, the lack of theoretical background should be always in mind. Here, we argue for a bottom-up design, where a simple model is designed and implemented first and then scaled up to meet the accuracy required by real-world applications. Such a model should be always backed by proper data. The industry's requirements (Section 7.1) should be always born in mind, as well as the fact that Level 1 models are now widely adopted by the automotive industry because they managed to fulfill these requirements. The concepts that guided the design and development of the models of the present work are detailed below:

Objectives and application range. The model's objectives and targeted application range should be kept realistic and be always judged in connection with the quality of the key phenomenological laws incorporated in the model. The idea here is that the accuracy provided by the model is influenced by the fundamental limitations of any fundamental phenomenological laws. The pressure drop submodel of the diesel particulate filter (Section 3.3) and the rate expressions of the oxygen storage reactions of the three-way catalytic converter (Section 2.3) are typical examples in this regard.

Computational cost. The model should be built with computational efficiency in mind. This is an important industry requirement per se, but the model should be fast for yet another reason: Such models have to be linked with an optimization procedure for the estimation of unknown parameters introduced by the phenomenological laws embodied in the model. The case of the catalytic converter indicates that the accurate estimation of tunable parameters may greatly enhance the predictive power of the model. Model simplicity can be valuable in this regard, because it may enable analytical solutions that substitute numerical methods and offer much higher computational speed. The oxygen storage submodel of the 3WCC (Section 2.3.1) and the regeneration model of the DPF (Section 3.4) are good examples in this case.

Data availability and cost. Industry requirements usually also specify that the model's input data should be kept to a minimum and be available from simple routine experiments. It should be kept in mind, though, that the accuracy of model's prediction is greatly influenced by the quality of such data, especially of those that the model is very sensitive to. A corrupt oxygen measurement for the three-way catalytic converter renders any modeling attempt vain, regardless of the model, because the input oxygen is central to the operation of this device. Mathematical tools for the quality assurance of input data should be extremely helpful. This has not been addressed in this work but it is a field of rapid development by other members of the Laboratory of Thermodynamics and Thermal Engines [7].

Model sophistication. Increasing model sophistication involves increasing degrees of freedom of the model's behaviour. In concept, this implies the ability of the model to account for phenomena that are neglected in simpler models (e.g. three- vs. one-dimensional heat transfer for the diesel particulate filter, more inclusive reactions scheme etc).

Nevertheless, higher model sophistication does not guarantee more accuracy, unless it is done in a thoughtful way and it is coupled by higher quality input data that are needed by more sophisticated models. Characteristic examples of the above assertion is the incorporation of diffusion effects in the 3WCC model and the extension of the DPF model to account for 3D heat transfer.

In the first case, the incorporation of diffusion equations was believed to enhance model prediction, which did not happen. Moreover, the diffusion model expanded the set of tunable parameters of the model. Diffusion effects had to be discarded and real increase of the model's results was attained with the improvement of the oxygen storage submodel.

In the second case, the 3D reactor model of the DPF was indeed necessary because of the 3D evolution of the regeneration, which in its turn was attributed to the interaction between trap loading and flow field within and at the inlet of the trap. Although the 3D model provides additional insight to the regeneration process of the DPF, the 1D model is not rendered obsolete. On the contrary, the 3D model should prove its real predictive power only with conjunction with detailed, 3D measurements of the flow field at the filter's inlet [8].

From our viewpoint, if the above points are met, a realistic engineering model can be developed that should be useful by the design engineer, despite the limitations introduced by the lack of a coherent theoretical background of the fundamental phenomena incorporated in the model. Although the predictive accuracy of such a

model may be lower than that usually expected by e.g. a FEM methodology, and although the input data will probably require more accurate measurements, it should serve as a valuable tool in the design process of modern exhaust aftertreatment systems.

7.4 From computational cores to engineering tools

The application of the above design principles should establish a realistic engineering model. Nevertheless, this may well remain a powerful but hard to use computational core. Engineering models are perceived as tools for the design engineer, who is their target user. Therefore, effort should be eventually oriented towards the development of a software product. As such, it should fulfill the two requirements of the automotive industry that have not been discussed so far, namely *versatility* and *ease of use*.

The importance of these two requirements has been already pointed out with the comparison between ABAQUS–CATWALL and ANSYS–CATWALL interfaces (Section 3.6.2). Although both shared the same operating concept and are in principle equivalent, the ABAQUS–CATWALL lacked the versatility and ease of use that characterize the ANSYS–CATWALL interface, in the sense that the engineer-user can vary the filter geometry and the element meshing in a simple and automatated manner. This suggests that, at their present status of development, only the more advanced implementation approaches the requirements of an engineering tool. It is not a coincidence that the more advance interface of ANSYS–CATWALL has been developed with motivation by an industrial partner.

Furthermore, both the catalytic converter model (CATRAN) and the 1D variant of the DPF model have been also interfaced with the MATLAB/Simulink environment, and this was also motivated by another industrial partner. This work allowed the models to be integrated to an existing framework of modeling tools that the industry employs for the calculation of the rest of the components of the exhaust system. The base MATLAB/Simulink environment is demonstrated in Figure 7.3, while some typical output of the model is presented in Figure 7.4.

As another example, an important part of the NO_x storage catalyst modeling job is carried out in the Simulink environment, because of the role of this modeling in the development of virtual supervisors that advise the engine control unit when it is necessary to regenerate the NO_x trap (regeneration is effected by operation of the engine at slightly rich A/F for 2 seconds, employing the produced excess of reducing agents in the reduction of NO_x stored in the storage component of the washcoat during the prevailing lean operation of the vehicle [9, 10]). Interfacing to a data acquisition environment (e.g. LabVIEW) is additionally necessary when specialized experiments are conducted to support and check the controller – supervisor design.

An example of the complex situation that must be studied by the exhaust system design engineer, is schematically illustrated in Figure 7.5. A more detailed study of the catalytic converter should go to 3D modeling of the monolith. This could, in principle, be accomplished in a manner similar to the ANSYS interfacing. However, in this case, flow maldistribution phenomena are even more pronounced than with the diesel filter (see Figure 7.3, left). Thus, the interfacing to a CFD code would be necessary in this case. The specific CFD modelling could not, in practice, consider the channel flow, because this is a phenomenon of different length scale. It should

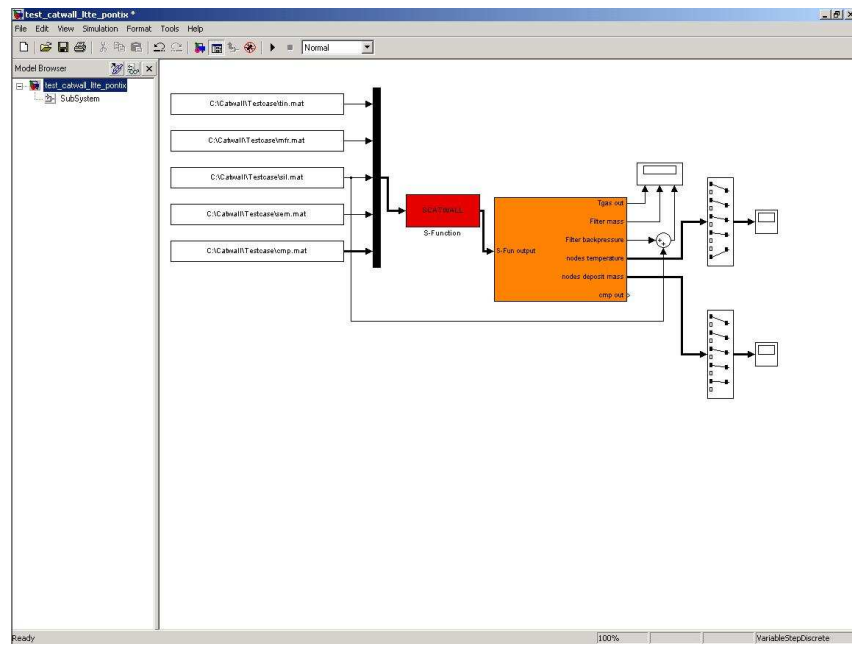


Figure 7.3: MATLAB/Simulink environment for the 1D CATWALL model – Base environment

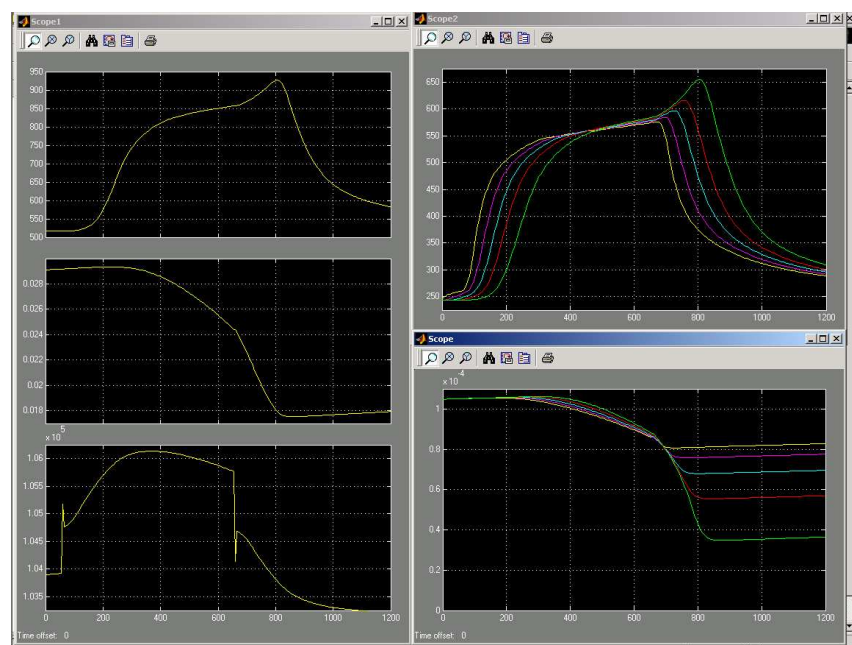


Figure 7.4: MATLAB/Simulink environment for the 1D CATWALL model – Typical output

Exhaust Aftertreatment Physical Parameters

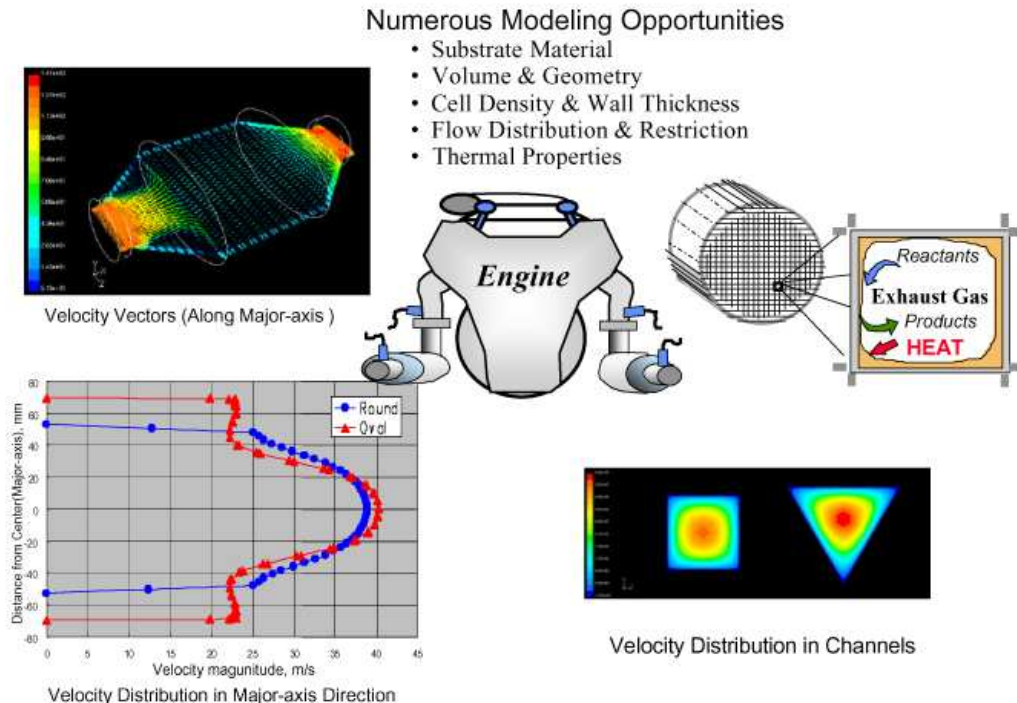


Figure 7.5: Exhaust aftertreatment physical parameters. Adapted from [12]

focus on the diffuser modeling, and address the monolith by some type of interfacing with CATRAN. This is a realistic approach, because the velocity distribution in the rectangular channels of the monolith (see the right side of the Figure), can be adequately addressed by the 1D approach of CATRAN code. If the purpose and scope of modeling is not properly assessed, modeling may lose focus and result in overly complex models that still fail to account for important degrees of freedom of the system. The 3D modeling of the converter, coupled with CFD in the channel but without accounting for diffuser modeling and flow maldistribution [11] is, from our viewpoint a typical example of this unbalanced and excessively complex modeling.

Versatility and user-friendliness can also be of great benefit during the development process of the model per se. This has been the case with the pre- and post-processing of data which was required by both the catalytic converter and the DPF model. Pre- and post-processing Visual Basic macros that were developed by other LTTE members had a significant impact on the development and validation of the core models. First, the preparation of the input data of the models was automated, which eliminated many common errors during the data pre-processing and increased confidence to the modeling results. Second, the focus was moved to the evaluation of modeling results and more time was spared for it. This eased the validation of the models and allowed their rapid improvement.

The models that are developed in academia usually remain in the status of a computational core. To transform this core into an engineering tool, time and effort should also be invested towards consistency, flexibility and user-friendliness. Our experience has shown that the interaction with the industry and the development of models oriented to evolve to engineering tools, will significantly benefit their

development process, their applicability and their potential audience.

The evolution of an engineering software tool usually presupposes an adequate incubation time period. In the case of the models presented herein, for example, about a dozen certified and about as many casual users exist today, spread in 5 companies worldwide (total for catalytic converter and diesel filter models of various categories). This is still a small number to allow us acquire significant feedback. Moreover, the nature of catalytic exhaust after-treatment systems design as critical R&D area requires a strict confidentiality to be followed in the application. Most partners choose to continue investing on these tools after completion of the transfer procedure, by in-house customization and further development. This means that although we receive positive feedback regarding the validity of our approach and usefulness of our software, we are informed on the performance of our models only in a limited number of cases (usually the ones published by our partners in the frame of their publication strategy). The largest source of information for improving our modeling, stems from our own Lab's experimental validation studies, and to an equivalent extent, also from our partners' experimental studies that are supplied to us as input for case studies assigned to the Laboratory of Thermodynamics and Thermal Engines.

Our experience indicates that a new Paradigm is emerging regarding the computer-aided design and optimization of exhaust aftertreatment systems. This could be visualized in the form of the flowchart of Figure 7.6. The concept design is based on the analysis of test data, that are related to a specific engineering design problem (in our case, the design of an exhaust after-treatment system). Mathematical modeling is employed in the setting up of a computational model that could address the engineering problem in a realistic (sufficiently accurate and feasible) way. This should take into account the control system design, that is always a major factor. When one moves from the concept to the detailed design, a number of important factors must be weaved around the core of the computational tool (that is based on the mathematical model). An important part is the selection of a valid kinetic scheme and the development of a computer aided parameter estimation tool. These are addressed in detail in the present work. Further, important building blocks in a valid detailed design methodology, comprise: The adaptation of the tool to multiple environments that could be necessary for a system's approach (see above). The development of an automated preprocessing and post-processing procedure. Last but not least, the development of a complete methodology for quality assurance of test data.

Finally, the integrated detailed design process should be interfaced to a rapid prototyping process, that is specific to the exhaust systems. This process does not present any special difficulties, and currently comprises an exhaust piping part (today based on welded parts), a converter canistering part, (well adapted by the exhaust systems manufacturers) and a catalytic converter washcoating part (well standardized by the catalytic converter industry). As already discussed, the bottleneck in the complete design process lies in the successful prediction of the system's performance, and this is where this work is intended to support further progress.

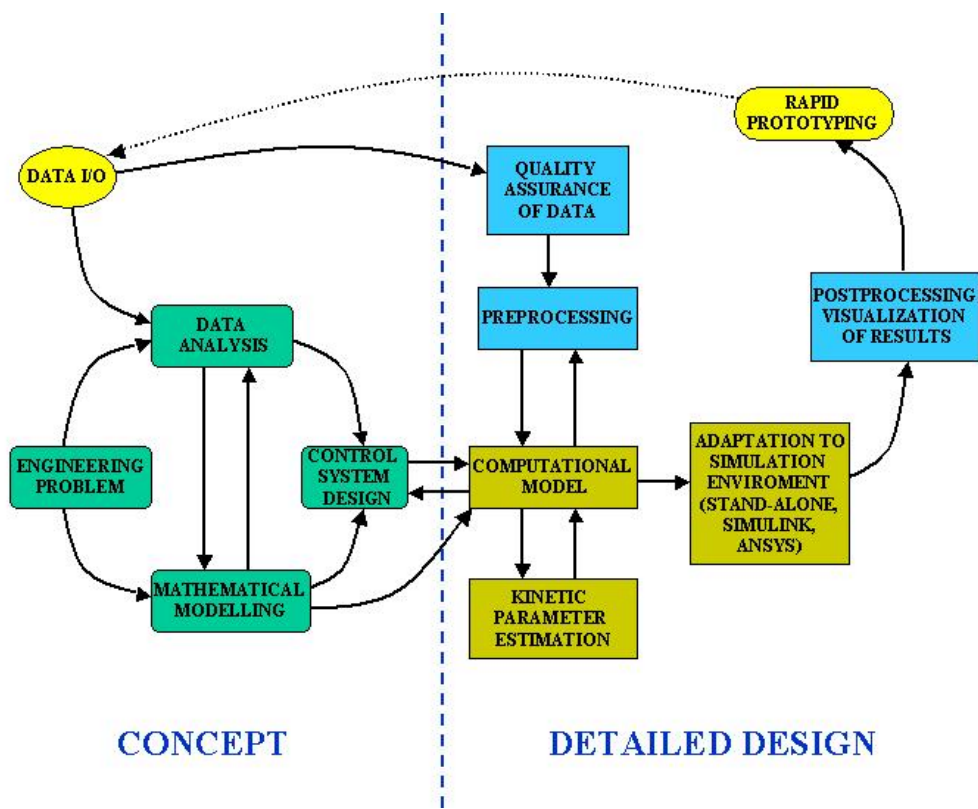


Figure 7.6: An emerging paradigm for exhaust aftertreatment systems engineering modeling

References

- [1] M. H. Sandford and R. D. Jones. Powerplant systems and the role of cae – part 1 exhaust systems. *SAE paper 920396*, 1992.
- [2] Z. J. Rubin, S. A. Munns, and J. J. Moskwa. The Development of Vehicular Powertrain System Modeling Methodologies: Philosophy and Implementation. *SAE paper 971089*, 1997.
- [3] H. Barths, C. Antoni, and N. Peters. Three-Dimensional Simulation of Pollutant Formation in a DI Diesel Engine Using Multiple Interactive Flamelets. *SAE paper 982459*, 1998.
- [4] N. Sinha, P. A. Cavallo, A. Hosangadi, R. A. Lee, H. Affes, and D. Chu. Efficient CFD Simulations for In-Cylinder Flows Using Hybrid Grids. *SAE paper 1999-01-1184*, 1999.
- [5] S. J. Lacher, L. Fan, B. Backer, J. K. Martin, R. Reitz, J. Yang, and R. Anderson. In-Cylinder Mixing Rate Measurements and CFD Analyses. *SAE paper 1999-01-1110*, 1999.
- [6] H. Jasak, J. Y. Luo, B. Kaludercic, A. D. Gosman, H. Echtle, Z. Liang, F. Wirbeleit, M. Wierse, S. Rips, A. Werner, G. Fernstrom, and A. Karlsson. Rapid CFD simulation of internal combustion engines. *SAE paper 1999-01-1185*, 1999.
- [7] G. Konstantas and A. M. Stamatelos. Quality assurance of exhaust emissions test data. *Proc. Instn Mech Engrs, Part D*, 2003. (*Submitted*).
- [8] G. A. Stratakis and A. M. Stamatelos. Flow distribution effects in the loading and catalytic regeneration of diesel particulate filters. *Proc Instn Mech Engrs, Part D: J. Automobile Engineering*, 2003. (*Submitted*).
- [9] M. S. Brogan, R. J. Brisley, A. P. Walker, D. E. Webster, W. Boegner, N. P. Fekete, M. Krämer, B. Krutzsch, and D. Voigtländer. Evaluation of NOx Storage Catalysts as an Effective System for NOx Removal from the Exhaust Gas of Leanburn Gasoline Engines. *SAE paper 952490*, 1995.
- [10] N. Fekete, R. Kemmler, D. Voigtländer, B. Krutzsch, E. Zimmer, G. Wenninger, W. Strehlau, J. A. A. van den Tillaart, J. Leyer, E. S. Lox, and W. Müller. Evaluation of nox storage catalysts for lean burn gasoline fueled passenger cars. *SAE paper 970746*, 1997.
- [11] J. Braun, T. Hauber, H. Többen, J. Windmann, P. Zacke, D. Chatterjee, C. Correa, O. Deutchmann, L. Maier, S. Tischer, and J. Warnatz. Three-dimensional simulation of the transient behaviour of a three-way catalytic converter. *SAE paper 2002-01-0065*, 2002.
- [12] F. Ament. Emissions Controls and Aftertreatment – Full System Modeling. In *D.O.E. Crosscut Workshop on Lean Emissions Reduction Simulation*, Knoxville, TN, U.S.A., 2001.

Appendix A

The problem of diffusion–reaction in the washcoat

We present here some work done on the problem of coupled diffusion and reaction of chemical species in the washcoat of the automotive catalytic converter. We have been seeking approximate analytical expressions that account for diffusion and simultaneous reaction of more than one species. Ideally, these expressions should have been derived by approximately solving a simplified system of mass balance equations for diffusion–reaction. The target has been to avoid numerical computations of the complete mass balances. We formulate the simplified version of the problem but no solution is provided; this remains an open issue.

A.1 General

The washcoat of the three-way catalytic converter (3WCC) may be viewed as a flat plate, of thickness δ (Figure A.1). One side of the plate lies on the ceramic substrate of the converter. The other side is exposed to the exhaust gas. From the exhaust gas, species diffuse in the washcoat, where they react with each other, because of the presence of precious metal catalysts. Thus, a concentration profile establishes within the boundary layer of the flow and the washcoat of the three-way catalytic converter.

The effect of the boundary layer is usually taken into account in 3WCC models but, more often than not, the washcoat diffusion effect is neglected. Our objective is to estimate this effect quantitatively and incorporate it in our transient, one-dimensional 3WCC model.

This can be done by solving the mass balance equations for diffusion and reaction in the washcoat. Since these mass balances are systems of nonlinear differential equations, we have to solve them numerically. However, we want to *avoid* incorporating numerical computations that significantly increase the computational power needed by our 3WCC model.

A.2 Reaction rates

Initially, we briefly review the reactions that occur in the washcoat of the three-way catalytic converter. We present all rate expressions in a form that is convenient for

the formulation of the mass balances for the problem of diffusion.

In the context of the diffusion–reaction problem, we neglect hydrogen oxidation owing to its limited significance compared to the rest of the redox reactions. We thus consider the reactions of CO & HC oxidation, NO reduction and oxygen storage.

Except from the CO–NO reaction, the rates of all other redox reactions are in the form:

$$r = \frac{Ae^{-E/R_g T} c_A c_B}{G_1} \quad (\text{A.1})$$

where c_A and c_B are the concentrations of reactions A and B and G is an inhibition factor that may be a function of temperature and several species concentrations. In this work, we use the inhibition factor of Voltz et al. [1]:

$$G_1 = T(1 + K_1 c_{CO} + K_2 c_{THC})^2(1 + K_3 c_{CO}^2 c_{THC}^2)(1 + K_4 c_{NO}^{0.7}) \quad (\text{A.2})$$

All reactions taken into account in the reaction–diffusion problem along with their rate expressions in the form of eq. A.1 are summarized in Table A.1.

The effective diffusivity D_{eff} is also needed in the calculations that follow. It is a measure of the rate that a species diffuses in a porous medium (here, the washcoat). Hayes et al. [2] recommend the use of the parallel pore model for an alumina washcoat. According to this model, the effective diffusivity of the washcoat is given by:

$$D_{\text{eff}} = \frac{\varepsilon D}{\tau}$$

In the above equation, ε is the overall porosity of the washcoat; τ is the tortuosity factor that can be viewed as an adjustable parameter; and D is a diffusivity that is a combination of bulk and Knudsen diffusivities:

$$\frac{1}{D} = \frac{1}{D_b} + \frac{1}{D_K}$$

It can be shown that bulk diffusivity is negligible and D is approximately equal to the Knudsen diffusivity:

$$D \approx D_K = 48.5 d_p \sqrt{\frac{T}{10^3 M}}$$

where T is the temperature in [K], d_p is the pore diameter in [m] and M is the molecular weight of the diffusing species in [kg/m³].

The effective diffusivity is, in principle, different for each species but the values should not differ greatly. To simplify the equations, we assume that *the effective diffusivity of all species is the same*.

A.3 CO oxidation by O₂ in stoichiometric conditions

In Chapter 2 we have formulated the problem of diffusion and reaction (decomposition) of a single species A . The reaction rate was assumed first order ($r = kc_A$) and the diffusion isothermal. The solution has been first given by Thiele [3].

If we raise the assumption that the O₂ concentration is in excess, then its profile within the washcoat may not be considered uniform. We have to write two mass

Reaction	Rate expression
<i>Oxidation reactions</i>	
1 2CO + O ₂ —→ 2CO ₂	$r_1 = \frac{A_1 e^{-E_1/R_g T} c_{CO} c_{O_2}}{G_1}$
2 2H ₂ + O ₂ —→ 2H ₂ O	$r_2 = \frac{A_2 e^{-E_2/R_g T} c_{H_2} c_{O_2}}{G_1}$
3 CH _{1.8} (fast) + 1.4O ₂ —→ —→ CO ₂ + 0.9H ₂ O	$r_3 = \frac{A_3 e^{-E_3/R_g T} c_{HCf} c_{O_2}}{G_1}$
4 CH _{1.8} (slow) + 1.4O ₂ —→ —→ CO ₂ + 0.9H ₂ O	$r_4 = \frac{A_4 e^{-E_4/R_g T} c_{HCs} c_{O_2}}{G_1}$
<i>NO reduction</i>	
5 2CO + 2NO —→ 2CO ₂ + N ₂	$r_5 = A_5 e^{-E_5/R_g T} c_{CO} c_{NO}$
<i>Oxygen storage</i>	
6 2Ce ₂ O ₃ + O ₂ —→ 4CeO ₂	$r_6 = A_6 e^{-E_6/R_g T} c_{O_2} (1 - \psi)$
7 2Ce ₂ O ₃ + 2NO —→ 4CeO ₂ + N ₂	$r_7 = A_7 e^{-E_7/R_g T} c_{NO} (1 - \psi)$
8 CO + 2CeO ₂ —→ Ce ₂ O ₃ + CO ₂	$r_8 = A_8 e^{-E_8/R_g T} c_{CO} \psi$
9 CH _{1.8} (fast) + 3.8CeO ₂ —→ —→ 1.9Ce ₂ O ₃ + CO ₂ + 0.9H ₂ O	$r_9 = A_9 e^{-E_9/R_g T} c_{HCf} \psi$
10 CH _{1.8} (slow) + 3.8CeO ₂ —→ —→ 1.9Ce ₂ O ₃ + CO ₂ + 0.9H ₂ O	$r_{10} = A_{10} e^{-E_{10}/R_g T} c_{HCs} \psi$

Table A.1: Reactions and rate expressions in the three-way catalytic converter in the context of the problem of diffusion–reaction in the washcoat

balances, for both CO and O₂, taking care of the stoichiometry:

$$D_{\text{eff}} \frac{d^2 y^{CO}}{dx^2} - \frac{\bar{k}}{G_1} y^{CO} y^{O_2} = 0 \quad (\text{A.3a})$$

$$D_{\text{eff}} \frac{d^2 y^{O_2}}{dx^2} - \frac{1}{2} \frac{\bar{k}}{G_1} y^{CO} y^{O_2} = 0 \quad (\text{A.3b})$$

This system of equations must be solved for the profiles of y^{CO} and y^{O_2} under the same boundary conditions as the previous problem, that is:

$$\begin{aligned} \text{At } x = 0 : \quad & y^i(x = 0) = y_0^i = \text{constant} \\ \text{At } x = \delta : \quad & \left. \frac{dy^i}{dx} \right|_{x=\delta} = 0 \quad \text{for } i = \text{CO, O}_2. \end{aligned} \quad (\text{A.4})$$

Subtracting equations (A.3a) and (A.3b), we get

$$\frac{d^2 y^{CO}}{dx^2} = 2 \frac{d^2 y^{O_2}}{dx^2} \quad (\text{A.5})$$

$$\frac{dy^{CO}}{dx} = 2 \frac{dy^{O_2}}{dx} + C_1 \quad (\text{A.6})$$

$$y^{CO} = 2y^{O_2} + C_1 x + C_2 \quad (\text{A.7})$$

Applying the boundary conditions, for $x = \delta$, we have:

$$\left. \frac{dy^{CO}}{dx} \right|_{x=\delta} = \left. \frac{dy^{O_2}}{dx} \right|_{x=\delta} = 0 \Rightarrow C_1 = 0$$

and for $x = 0$, we have:

$$\begin{cases} y^{CO}(x = 0) = y_0^{CO} \\ y^{O_2}(x = 0) = y_0^{HC} \end{cases} \Rightarrow C_2 = y_0^{CO} - 2y_0^{O_2}$$

Substituting to equations (A.5)–(A.7) the values for C_1 and C_2 , we get:

$$\frac{d^2 y^{CO}}{dx^2} = 2 \frac{d^2 y^{O_2}}{dx^2} \quad (\text{A.8})$$

$$\frac{dy^{CO}}{dx} = 2 \frac{dy^{O_2}}{dx} \quad (\text{A.9})$$

$$y^{CO} - y_0^{CO} = 2(y^{O_2} - y_0^{O_2}) \quad (\text{A.10})$$

Equation (A.10) may be substituted in the mass balance for CO, eqn (A.3a) so that we get one differential equation, with y^{CO} being the only unknown:

$$D_{\text{eff}} \frac{d^2 y^{CO}}{dx^2} = \frac{\bar{k}}{G_1} y^{CO} \left[\frac{1}{2} y^{CO} + \left(y_0^{O_2} - \frac{1}{2} y_0^{CO} \right) \right] \quad (\text{A.11})$$

We solve numerically for $y^{CO}(x)$. We first want to check if the inhibition term is significant. Therefore, we solve two cases—neglecting and taking into account the influence of G_1 .

A.3.1 Neglecting G_1

If we neglect the influence of G_1 , eqn (A.11) becomes:

$$D_{\text{eff}} \frac{d^2 y^{CO}}{dx^2} = \bar{k} y^{CO} \left[\frac{1}{2} y^{CO} + \left(y_0^{O_2} - \frac{1}{2} y_0^{CO} \right) \right] \quad (\text{A.12})$$

To solve this numerically we first develop an expression for y'_{CO} and a limit for y_δ .

An expression for y'_{CO}

Defining $K = \phi^2/\delta^2 = \bar{k}/D_{\text{eff}}$, $\Delta y_0 = y_0^{O_2} - \frac{1}{2}y_0^{CO}$, $p = y'$ and dropping the ‘CO’ superscripts for simplicity of notation, we have:

$$\left. \begin{array}{l} p' = Ky\left(\frac{1}{2}y + \Delta y_0\right) \\ p = y' \end{array} \right\} \Rightarrow \left. \begin{array}{l} p' = \frac{1}{2}Ky^2 + Ky\Delta y_0 \\ p = y' \end{array} \right\}$$

We multiply the two equations and integrate:

$$pp' = \frac{1}{2}Ky^2y' + Ky\Delta y_0 \Rightarrow \frac{d}{dx} \left[\frac{p^2}{2} - K\frac{y^3}{6} - K\Delta y_0 \frac{y^2}{2} \right] = 0$$

We get:

$$y' = -\sqrt{\frac{1}{3}Ky^3 + K\Delta y_0 y^2 + C}$$

For $x = \delta$, $y' = 0$ and $y = y_\delta$, thus:

$$C = -\frac{1}{3}Ky_\delta^3 - K\Delta y_0 y_\delta^2$$

and we have an expression of y' as a function of y_δ :

$$y' = -\sqrt{\frac{1}{3}K(y^3 - y_\delta^3) + K\Delta y_0(y^2 - y_\delta^2)} \quad (\text{A.13})$$

or

$$y' = -\sqrt{K(y - y_\delta)} \sqrt{\frac{1}{3}(y^2 + yy_\delta + y_\delta^2) + \Delta y_0(y + y_\delta)}$$

A limit for y_δ

The term $\frac{1}{2}y^{CO} + (y_0^{O_2} - \frac{1}{2}y_0^{CO})$ of eqn (A.11) must be positive, because it is equal to the oxygen concentration:

$$\frac{1}{2}y^{CO} + (y_0^{O_2} - \frac{1}{2}y_0^{CO}) = y^{O_2} \geq 0$$

The above inequality is satisfied automatically in case that $y_0^{CO} \leq 2y_0^{O_2}$, but provides a limit in case that $y_0^{CO} \geq 2y_0^{O_2}$. Since it is valid for every y^{CO} , it is also valid for $y^{CO}(x = \delta) = y_\delta^{CO}$. Thus,

$$y_\delta^{CO} \geq -2(y_0^{O_2} - \frac{1}{2}y_0^{CO}) = -2\Delta y_0 \quad (\text{A.14})$$

We use the above inequality to limit the range of values of y_δ that we guess during the numerical solution of the problem, which follows immediately.

Numerical solution

The solution of equation (A.11) is obtained numerically. We solve the boundary value problem by a shooting method. The algorithm is presented in Figure A.2. It

guesses the value of y_δ using eqn (A.13) to estimate y'_0 . Then, we solve the initial value problem:

$$\left. \begin{array}{l} p' = Ky\left(\frac{1}{2}y + \Delta y_0\right) \\ y' = p \end{array} \right\}$$

with initial conditions:

$$\begin{aligned} p'(x=0) &= y'|_{x=0} = y'_0 \\ y(x=0) &= y_0 \end{aligned}$$

This problem is solved with a fourth order Runge-Kutta scheme. We establish convergence by checking the boundary condition at $x = \delta$. If it is satisfied ($y'_\delta = 0$), the solution has converged. Otherwise, we correct our guess for y_δ and thus our guess for y'_0 . The values of y_δ that we guess must always satisfy equation (A.14).

A.3.2 Taking into account G_1

If we take into account the influence of G_1 , we first notice that, because $y^{HC} = y^{NO} = 0$, G_1 reduces to:

$$G_1 = (1 + k_1 y^{CO})^2 \quad (\text{A.15})$$

Thus, eqn (A.11) becomes:

$$D_{\text{eff}} \frac{d^2 y^{CO}}{dx^2} = \frac{\bar{k}}{(1 + k_1 y^{CO})^2} y^{CO} \left[\frac{1}{2} y^{CO} + \left(y_0^{O_2} - \frac{1}{2} y_0^{CO} \right) \right] \quad (\text{A.16})$$

Again, we substitute $K = \bar{k}/D_{\text{eff}}$, $\Delta y_0 = y_0^{O_2} - \frac{1}{2} y_0^{CO}$ and $p = y'$, drop the ‘CO’ subscripts, and multiply both sides of eqn (A.16) with p . We get:

$$\left. \begin{array}{l} p' = \frac{1}{2} K \frac{y^2}{(1 + k_1 y)^2} + K \Delta y_0 \frac{y}{(1 + k_1 y)^2} \\ p = y' \end{array} \right\} \Rightarrow \left. \begin{array}{l} pp' = \frac{1}{2} K \frac{y^2 y'}{(1 + k_1 y)^2} + K \Delta y_0 \frac{yy'}{(1 + k_1 y)^2} \\ p = y' \end{array} \right\}$$

Integration gives:

$$\begin{aligned} y' = - & \left\{ K \left[\frac{1}{k_1^2} y - \frac{1}{k_1^3 (1 + k_1 y)} - \frac{2}{k_1^3} \ln(1 + k_1 y) \right] \right. \\ & \left. + 2K \Delta y_0 \left[\frac{1}{k_1^2 (1 + k_1 y)} + \frac{1}{k_1^2} \ln(1 + k_1 y) \right] + C \right\}^{\frac{1}{2}} \end{aligned}$$

We apply the boundary condition at $x = \delta$ to find the constant of integration C . We finally obtain an expression for y' which corresponds to eqn (A.13) but this time has been developed taking into account the effect of the inhibition term G_1 :

$$y' = -\sqrt{K(u_1 - u_2 - u_3) + 2K \Delta y_0(u_4 + u_5)} \quad (\text{A.17})$$

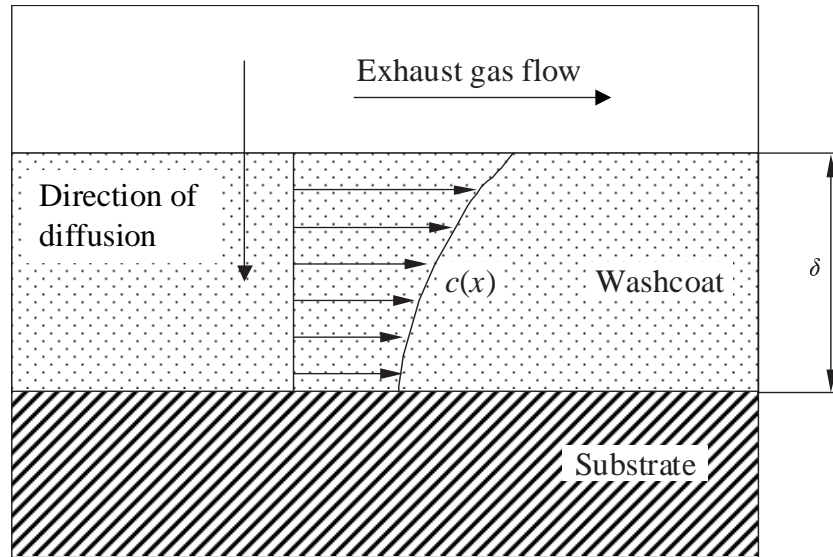


Figure A.1: Washcoat of the three-way catalytic converter.

Require: Initial guess for y_δ

while not converged **do**

$$\text{Estimate } y'_0: y'_0 = -\sqrt{\frac{1}{3}K(y_0^3 - y_\delta^3) + K\Delta y_0(y_0^2 - y_\delta^2)}$$

Solve the initial value problem:

$$\left. \begin{array}{l} p' = Ky\left(\frac{1}{2}y + \Delta y_0\right) \\ y' = p \end{array} \right\} \text{with i.c.:} \quad \begin{array}{l} p'(x=0) = y'|_{x=0} = y'_0 \\ y(x=0) = y_0 \end{array}$$

if $p(x = \delta) \approx 0$ **then**

Converged; exit

else if $p(x = \delta) < 0$ **then**

Increase y_δ

else if $p(x = \delta) > 0$ **then**

Decrease y_δ

end if

end while

Figure A.2: Algorithm for numerical solution of the problem of CO+O₂ oxidation near stoichiometry

where:

$$\begin{aligned} u_1 &= \frac{1}{k_1^2}y - \frac{1}{k_1^2}y_\delta \\ u_2 &= \frac{1}{k_1^3(1+k_1y)} - \frac{1}{k_1^3(1+k_1y_\delta)} \\ u_3 &= \frac{2}{k_1^3}\ln(1+k_1y) - \frac{2}{k_1^3}\ln(1+k_1y_\delta) \\ u_4 &= \frac{1}{k_1^2(1+k_1y)} - \frac{1}{k_1^2(1+k_1y_\delta)} \\ u_5 &= \frac{1}{k_1^2}\ln(1+k_1y) - \frac{1}{k_1^2}\ln(1+k_1y_\delta) \end{aligned}$$

To solve numerically for the profile of $y(x)$, we use eqn (A.17) in the algorithm of Figure A.2 to get an estimate for y' , and we solve the initial value problem:

$$\left. \begin{aligned} p' &= \frac{1}{2}K \frac{y^2}{(1+k_1y)^2} + K\Delta y_0 \frac{y}{(1+k_1y)^2} \\ y' &= p \end{aligned} \right\}$$

with initial conditions:

$$\begin{aligned} p'(x=0) &= y'|_{x=0} = y'_0 \\ y(x=0) &= y_0 \end{aligned}$$

Again, the solution is obtained with a fourth-order Runge-Kutta scheme. The check for convergence remains unchanged.

A.3.3 Results

Having developed the solution of the

The effectiveness factor depends on the Thiele modulus (ϕ), the excess of O₂ or CO (Δy_0) and the inhibition term G_1 .

If the inhibition term G_1 is taken into account (in general: if it is assumed that the reaction rate is not first-order), the effectiveness factor changes with CO in a manner consistent with that shown on the paper of Zygourakis and Aris [4] (Figure A.3).

The effectiveness factor for the NEDC cycle was also computed employing the inlet concentrations of CO and O₂, the inlet temperature T and diffusion data from Hayes et al. [2]. Of course, the kinetics for CO oxidation play an important role; we give two examples for values of the pre-exponential factor: $A = 10^{11}$ and $A = 10^{14}$ (Figures A.4 and A.5).

Apparently, the discrepancy between the values of the effectiveness factor that were computed neglecting and taking into account the inhibition term G_1 . Thus, it does not seem acceptable to neglect the inhibition term. This greatly complicates the equations of the CO–HC–O₂ system, which is the next step towards a full model of diffusion in the catalytic converter washcoat.

A.4 Simultaneous oxidation of CO and HC by O₂

The next step is to examine the problem of simultaneous diffusion of CO, HC and O₂ in the washcoat. This is done in order to illustrate the complications involved

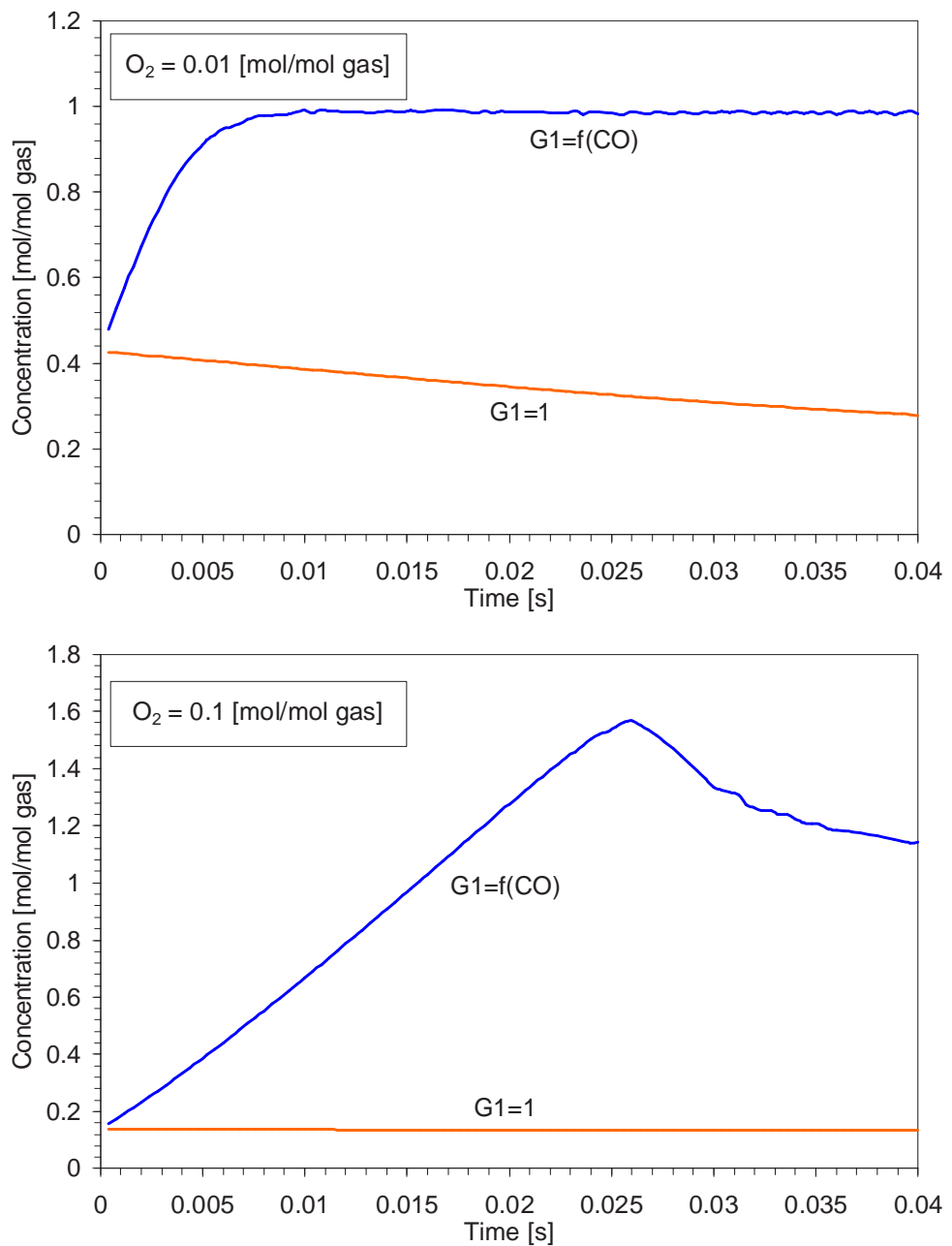


Figure A.3: Effectiveness factor as a function of CO concentration, for $y^{O_2} = 0.01$ and $y^{O_2} = 0.1$ ($A = 10^{11}$).

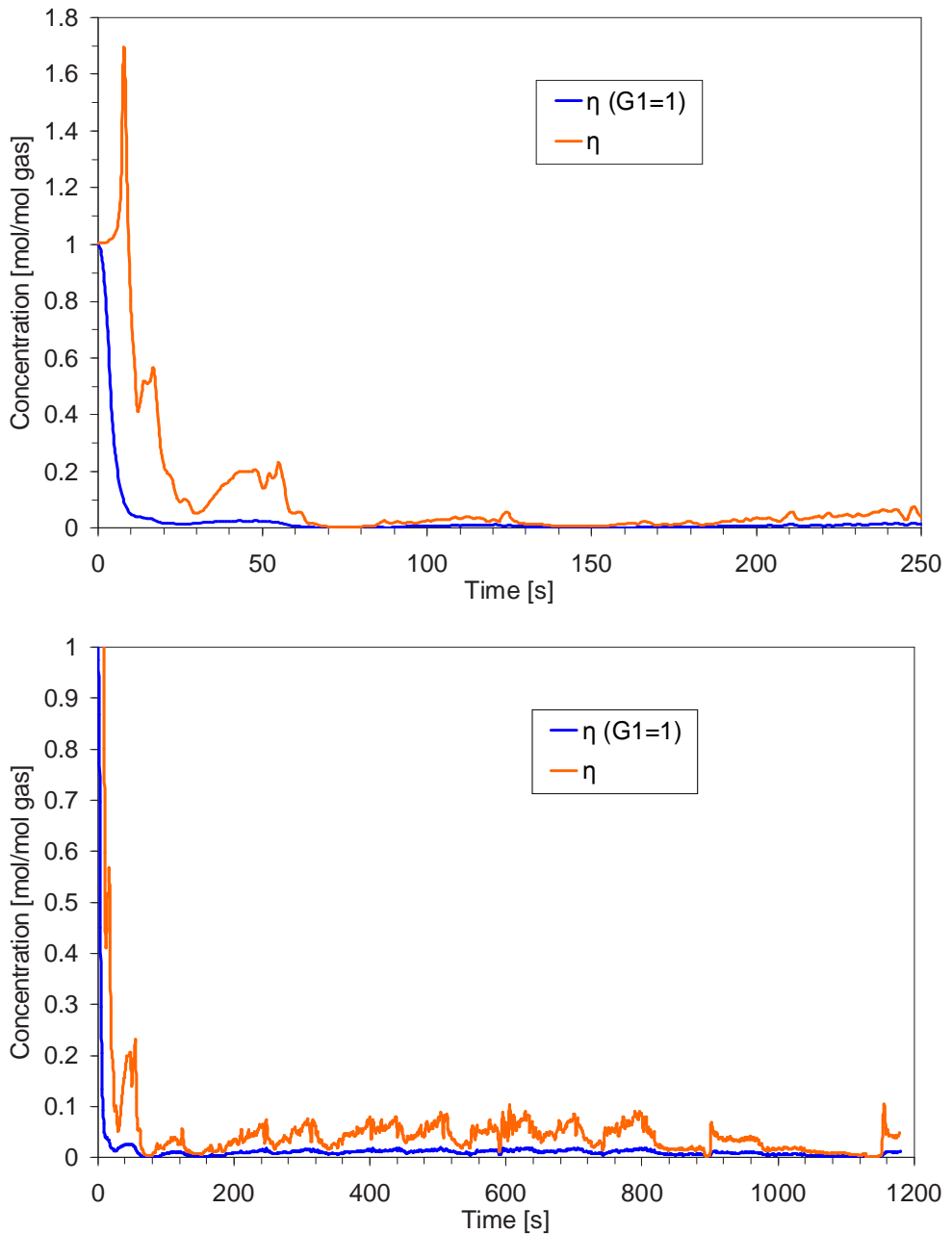


Figure A.4: Effectiveness factor during the NEDC cycle, $A = 10^{14}$

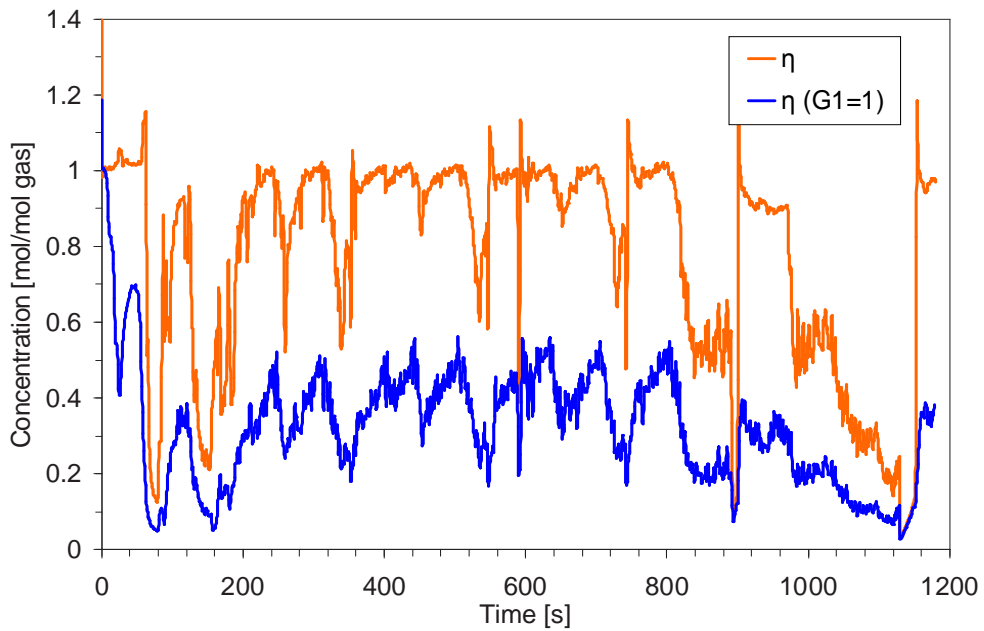
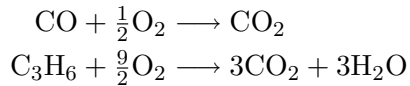


Figure A.5: Effectiveness factor during the NEDC cycle, $A = 10^{11}$

when adding one more species to the system under study.

For simplicity, we will assume that the hydrocarbon being oxidized is C₃H₆. In this case O₂ oxidizes CO and HC according to the reactions:



The mass balances for this problem are:

$$D_{\text{eff}} \frac{d^2 y^{\text{CO}}}{dx^2} = \frac{\bar{k}_1}{G_1} y^{\text{CO}} y^{\text{O}_2} \quad (\text{A.18a})$$

$$D_{\text{eff}} \frac{d^2 y^{\text{HC}}}{dx^2} = \frac{\bar{k}_2}{G_1} y^{\text{HC}} y^{\text{O}_2} \quad (\text{A.18b})$$

$$D_{\text{eff}} \frac{d^2 y^{\text{O}_2}}{dx^2} = \frac{1}{2} \frac{\bar{k}_1}{G_1} y^{\text{CO}} y^{\text{O}_2} + \frac{9}{2} \frac{\bar{k}_2}{G_1} y^{\text{HC}} y^{\text{O}_2} \quad (\text{A.18c})$$

This system of equations must be solved for the concentration profiles $y^{\text{CO}}(x)$, $y^{\text{HC}}(x)$ and $y^{\text{O}_2}(x)$, with the boundary conditions:

$$\begin{aligned} \text{At } x = 0 : \quad y^i(x = 0) &= y_0^i = \text{constant} \\ \text{At } x = \delta : \quad \left. \frac{dy^i}{dx} \right|_{x=\delta} &= 0 \quad \text{for } i = \text{CO, HC, O}_2. \end{aligned} \quad (\text{A.19})$$

We deal with the problem similarly to the previous section. Substituting

eqn (A.18a) and (A.18b) in (A.18c), we have:

$$\frac{d^2y^{O_2}}{dx^2} = \frac{1}{2} \frac{d^2y^{CO}}{dx^2} + \frac{9}{2} \frac{d^2y^{HC}}{dx^2} \quad (\text{A.20})$$

$$\frac{dy^{O_2}}{dx} = \frac{1}{2} \frac{dy^{CO}}{dx} + \frac{9}{2} \frac{dy^{HC}}{dx} + C_1 \quad (\text{A.21})$$

$$y^{O_2} = \frac{1}{2}y^{CO} + \frac{9}{2}y^{HC} + C_1x + C_2 \quad (\text{A.22})$$

Applying the boundary conditions, for $x = \delta$, we have:

$$\left. \frac{dy^{CO}}{dx} \right|_{x=\delta} = \left. \frac{dy^{O_2}}{dx} \right|_{x=\delta} = \left. \frac{dy^{HC}}{dx} \right|_{x=\delta} = 0 \Rightarrow C_1 = 0$$

and for $x = 0$, we have:

$$\left. \begin{aligned} y^{CO}(x=0) &= y_0^{CO} \\ y^{O_2}(x=0) &= y_0^{O_2} \\ y^{HC}(x=0) &= y_0^{HC} \end{aligned} \right\} \Rightarrow C_2 = y_0^{O_2} - \frac{1}{2}y_0^{CO} - \frac{9}{2}y_0^{HC}$$

Substituting to equations (A.20)–(A.22) the values for C_1 and C_2 , we get:

$$\frac{d^2y^{O_2}}{dx^2} = \frac{1}{2} \frac{d^2y^{CO}}{dx^2} + \frac{9}{2} \frac{d^2y^{HC}}{dx^2} \quad (\text{A.23})$$

$$\frac{dy^{O_2}}{dx} = \frac{1}{2} \frac{dy^{CO}}{dx} + \frac{9}{2} \frac{dy^{HC}}{dx} \quad (\text{A.24})$$

$$y^{O_2} - y_0^{O_2} = \frac{1}{2}(y^{CO} - y_0^{CO}) + \frac{9}{2}(y^{HC} - y_0^{HC}) \quad (\text{A.25})$$

Equation (A.25) may be substituted in the mass balances for CO and HC, eqns (A.18a) and (A.18b), so that we get a system of two differential equations, with y^{CO} and y^{HC} being the unknowns:

$$D_{\text{eff}} \frac{d^2y^{CO}}{dx^2} = \frac{\bar{k}_1}{G_1} y^{CO} \left[\frac{1}{2}y^{CO} + \frac{9}{2}y^{HC} + \left(y_0^{O_2} - \frac{1}{2}y_0^{CO} - \frac{9}{2}y_0^{HC} \right) \right] \quad (\text{A.26a})$$

$$D_{\text{eff}} \frac{d^2y^{HC}}{dx^2} = \frac{\bar{k}_2}{G_1} y^{HC} \left[\frac{1}{2}y^{CO} + \frac{9}{2}y^{HC} + \left(y_0^{O_2} - \frac{1}{2}y_0^{CO} - \frac{9}{2}y_0^{HC} \right) \right] \quad (\text{A.26b})$$

The above system is a boundary value problem that must be solved numerically. Evidently, the solution of this problem is much more complicated than the solution of the single CO-O₂ system. Furthermore, the addition of all reactions of the 3WCC reaction scheme would

A.5 Conclusions

The problem of diffusion and simultaneous reaction between CO and O₂ in the catalytic converter washcoat under stoichiometric conditions has been studied. It has been shown that, under realistic conditions of operation, the Voltz inhibition term of the reaction rate may not be neglected. The study is consistent with the characteristic diffusion behaviour as reported by Zygourakis and Aris [4].

The findings of these work showed that the problem is difficult to handle in a simplified way. It is most probable that a complicated numerical solution of the mass balances of the diffusing-reacting species in the washcoat should be developed, if the effect of diffusion is worth accounting for in an engineering catalytic converter model.

The process of investigating the influence of diffusion was discontinued as soon as the improved model with the parameter estimation methodology was proved capable of predicting the transient behaviour of the 3WCC under the real-world conditions of the PML case study with remarkable accuracy.

The above achievement of the model implies that the effect of diffusion is not observable in the overall efficiency of the 3WCC under the conditions met in the legislation tests. The above results are communicated to the few researchers that assumed in the past an important role of diffusion in this process.

The diffusion problem nevertheless remains open, and may become significant in the case of ultra-low thin-walled substrates (900 and 1200 cpsi substrates).

References

- [1] S. E. Voltz, C. R. Morgan, D. Liederman, and S. M. Jacob. Kinetic study of carbon monoxide and propylene oxidation on platinum catalysts. *Industrial Engineering Chemistry — Product Research and Development*, 12:294, 1973.
- [2] R. E. Hayes, S. T. Kolaczkowski, P. K. C. Li, and S. Awdry. Evaluating the effective diffusivity of methane in the washcoat of a honeycomb monolith. *Applied Catalysis B: Environmental*, 25:93–104, 2000.
- [3] E. W Thiele. Relation between catalytic activity and size of particle. *Ind. Eng. Chem*, 31(11):916, 1939. [Citation Classic. *Current Contents/Engineering, Technology & Applied Sciences*, 10(2):10, 1979.].
- [4] K. Zygourakis and R. Aris. Multiple oxidation reactions and diffusion in the catalytic layer of monolith reactors. *Chemical Engineering Science*, 38(5):733–744, 1983.

CURRICULUM VITAE

Personal Data

Date of birth 17th May 1975 in Thessaloniki
Parents Nikolaos Pontikakis and Evangelia, born Maloudi
Civil status Single

Education

- 1993 – 1998 Diploma of Mechanical Engineering,
Aristotle University of Thessaloniki.
- 1999 – 2003: PhD candidate,
Laboratory of Thermodynamics and Thermal Engines,
Mechanical and Industrial Engineering Dept.
University of Thessaly.
- 2001 – 2003: Reserve Officer,
Greek Army, Technical Staff
- 1998 – now: Production Engineer,
EXTHERM Co. – Heating, Ventilating
and Air Conditioning Systems, Thessaloniki

Publications

- A. M. Stamatelos, G. C. Koltsakis, I.P. Candydas and G. N. Pontikakis: Computer Aided Engineering in the Development of Diesel Exhaust Aftertreatment Systems. *SAE paper 1999-01-0458*, 1999.
- A. M. Stamatelos, G. C. Koltsakis, I.P. Candydas and G. N. Pontikakis: Computer Aided Engineering in Diesel Exhaust Aftertreatment Systems Design. *Proc. Inst. Mech. Engrs., Part D, Journal of Automobile Engineering*, 213, 1999.
- G. N. Pontikakis, G. C. Koltsakis, A. M. Stamatelos, R. Noirot, Y. Agliany, H. Colas, P. Versaevel: Experimental and Modeling Study on Zeolite Catalysts for Diesel Engines. *CAPOC V, Fifth International Congress on Catalysis and Automotive Pollution Control*, Brussels, April 2000.
- G. N. Pontikakis, G. C. Koltsakis, A. M. Stamatelos, R. Noirot, Y. Agliany, H. Colas, P. Versaevel: Experimental and Modeling Study on Zeolite Catalysts for Diesel Engines. *Topics in Catalysis*, 16:329–335, 2001.
- G. N. Pontikakis, G. C. Koltsakis and A. M. Stamatelos: A Mathematical Model for the Dynamic Particulate Filtration in Diesel Foam Filters. *Particulate Science and Technology: An International Journal*, 17(3):179–200, 1999.

- G. N. Pontikakis, G. C. Koltsakis and A. M. Stamatelos: Dynamic Filtration Modeling in Foam Filters for Diesel Exhaust. *Chemical Engineering Communications* 188:21–46, 2001.
- G. Pontikakis and A. Stamatelos: Mathematical Modeling of Catalytic Exhaust Systems for EURO-3 and EURO-4 Emissions Standards. *Proc. Inst. Mech. Engrs., Part D, Journal of Automobile Engineering*, 215:1005–1015, 2001.
- G. Pontikakis, A. Stamatelos, K. Bakasis and N. Aravas. 3-D Catalytic Regeneration and Stress Modeling of Diesel Particulate Filters by ABAQUS FEM Software. *SAE paper 2001-01-1017*, 2001
- G. Pontikakis, C. Papadimitriou and A. Stamatelos: Kinetic Parameter Estimation by Standard Optimization Methods in Catalytic Converter Modeling. *In press, Chemical Engineering Communications*, 2003.
- G. N. Pontikakis, G. Konstantas and A. M. Stamatelos: Three-Way Catalytic Converter Modelling as a Modern Engineering Design Tool. *Submitted, ASME Transactions, Journal of Engineering for Gas Turbines and Power*, 2002.
- G. N. Pontikakis and A. M. Stamatelos. Identification of Catalytic Converter Kinetic Model Using a Genetic Algorithm Approach. *Submitted, ASME Transactions, Journal of Dynamic Systems, Measurement & Control*, 2003.
- G. A. Stratakis, G. N. Pontikakis and A. M. Stamatelos. Experimental Validation of a Fuel Additive Assisted Regeneration Model in SiC Diesel Filters. *Submitted, American Institute of Chemical Engineers Journal*, 2003.
- G. N. Pontikakis and A. M. Stamatelos. 3-D Catalytic Regeneration Modeling of Diesel Particulate Filters. *Submitted, Combustion and Flame*, 2003.

Participation in Research Programmes ---

- Catalytic Trap for Diesel Particulate Control (CATATRAP).
Research engineer. Funding: European Commission
- Development and Experimental Validation of Computational Tools for Exhaust Aftertreatment Systems Design Optimization.
Research engineer. Funding: PSA Peugeot Citroën.
- Software Development and Validation for 1D and 3D Modeling of Diesel Filters.
Research engineer. Funding: IBIDEN Co. Ltd.
- The Modeling of Automotive Catalytic Converters for Gasoline- and Diesel-fuelled Vehicles.
Research engineer. Funding: dmc² division of Degussa-Hüls A.G.